Characterization of the Behavior of High Volume Fly Ash Concrete

by

Kevin Paul Keith

A thesis submitted to the Graduate Faculty of
Auburn University
in partial fulfillment of the
requirements for the Degree of
Master of Science

Auburn, Alabama
December 12, 2011

Keywords: high volume fly ash concrete, fly ash, hydration development, calorimetry, setting times, compressive strength development

Approved by

Anton K. Schindler, Chair, Associate Professor of Civil Engineering
Robert W. Barnes, James J. Mallett Associate Professor of Civil Engineering
James S. Davidson, Associate Professor of Civil Engineering

Abstract

Fly ash is commonly used as a supplementary cementitious material (SCM) in the production of portland cement concrete. Concrete produced with high fly ash replacement levels is considered high volume fly ash (HVFA) concrete. HVFA concrete has many benefits, including reduced concrete production cost, reduced greenhouse gas emissions, and improved sustainability. Despite the advantages, there are several barriers that limit the use of HVFA concrete. One of the main limitations to the increased usage of HVFA concrete is the lack of contractor and transportation agency familiarity with the setting time and strength development of these concrete mixtures.

For this research, a laboratory testing program was developed to examine the effect of fly ash type, fly ash dosage, cement chemical composition, and environmental conditions on the hydration development, setting times, and compressive strength development of HVFA concrete. Results from semi-adiabatic calorimetry were used to develop a hydration model for HVFA concrete. Finally, the ConcreteWorks software program was used to predict the in-place performance of selected HVFA concrete mixtures when placed in various transportation structures. It is concluded that HVFA concrete may be produced to have comparable setting times and early-age compressive strength development to conventional portland cement concrete when used for transportation infrastructure.

Acknowledgements

First, I would like to thank Dr. Anton Schindler for his guidance and instruction throughout this research project and my graduate career. I would also like to thank concrete lab manager Billy Wilson for the guidance he provided over the past few years. Fellow graduate students, Ben Byard and Ruddy Thompson, as well as all undergraduate research assistants deserve special thanks for all of the hard work they provided during the laboratory testing portion of this project. Without all of their help, this research would not have been possible. I must also thank my parents, Larry and Jamie Keith, my sister, Kelsey, and the Fore family for the love and support they have given me. Finally, I would like to thank my wife, Ashley. Without her love, support and patience, this would not have been possible.

I must also thank the producers which supplied the raw materials for the duration of this project. I am very appreciative of the generous support offered by W.R. Grace & Co., LaFarge North America, Headwaters Resources, Boral, and ProAsh. I would like to thank Dr. Weiss from Purdue University, the National Institute of Standards and Technology (NIST), and the National Ready Mix Concrete Association (NRMCA) for their collaboration on this project. Finally, I would like to thank the Federal Highway Administration (FHA) for funding this research project.

Table of Contents

List of Tables

List of Figures

Chapter 1

Introduction

1.1 Background

Fly ash is one of the by-products of the combustion of coal in electric power generating plants. For over 65 years, fly ash has been widely used as a supplementary cementitious material (SCM) for the production of portland cement concrete in the United States. Typically, fly ash replacement levels for the production of portland cement concrete have been limited to roughly 25% by weight of the total cementitious system due to concerns about in-place performance and constructability (Obla et al. 2003).

Increased fly ash replacement levels in the production of portland cement concrete have economical, environmental, and performance benefits. The economical and environmental benefits associated with high volume fly ash (HVFA) concrete include reduced concrete production cost, reduced greenhouse gas emissions, and improved sustainability. Additionally, some of the performance benefits associated with high fly ash replacement levels in portland cement concrete include reduced water demand, improved long-term compressive strength, and reduced in-place concrete temperatures.

Cement is the most expensive material used in the production of portland cement concrete. According to the American Coal Ash Association (2011), the cost of one ton of ASTM C 618 (2005) fly ash is typically half the price of one ton of portland cement. Therefore, the production cost for concrete can be reduced by replacing a portion of

cement with less expensive fly ash. HVFA concrete may be produced with significant cost savings when compared to conventional portland cement concrete.

During the production of portland cement, carbon dioxide (CO_2) is released due to the combustion of carbon-based fuels and the calcination of limestone (Chen and Juenger 2009). For each ton of portland cement clinker that is produced, approximately one ton of the greenhouse gas carbon dioxide (CO_2) is released (Greer et al. 2004). A reduction in CO_2 emissions may be achieved by reducing the demand for portland cement with the increased use of HVFA concrete. An increase in the average fly ash replacement level would result in less portland cement required for concrete production, and ultimately less CO_2 emissions resulting from cement manufacture.

The use of HVFA concrete could also improve the sustainability of the concrete industry. According to the American Coal Ash Association (ACAA) coal combustion product (CCP) survey, approximately 63 million tons of fly ash were produced in 2009. Of the 63 million tons produced, 9.8 million tons were used beneficially for concrete production. For all industries, nearly 25 million tons were used beneficially, accounting for 39.2% of all fly ash produced (ACAA 2011). If the fly ash is not recycled for beneficial use, it is most often disposed of in landfills. The ACAA estimates that each ton of recycled fly ash is the space equivalent of 455 days worth of solid waste in a landfill (2009). If the average fly ash replacement level is increased, less landfill space will be required. The use of HVFA concrete also improves the sustainability of the concrete industry by reducing the amount of virgin materials consumed during the production of portland cement.

In addition to the economic and environmental advantages presented above, HVFA concrete may be produced to have improved performance characteristics when compared to conventional portland cement concrete. First, the water demand required for a given workability can be reduced when fly ash is used as a partial cement replacement. Malhotra and Jiang (2000) found that concrete proportioned with 55% fly ash can experience up to 20% reduction in water demand. In addition to the reduction in water-demand, HVFA concrete generally exhibits improved late-age compressive strength results when compared to conventional portland cement concrete (ACI 232.R 2003). The improvements in late-age compressive strength results for HVFA concrete are dependent on the duration of moist curing. Finally, high fly ash replacement levels may be used to decrease the maximum in-place temperature development for mass concrete elements. Langley et al. (1992) reported that the peak temperature rise of a 3.05 x 3.05 x 3.05 meter block was reduced by 52 °F when a 55% dosage of Class F fly ash was used. The maximum in-place temperature development is important when considering the susceptibility of mass concrete elements to delayed ettringite formation (DEF).

Despite the advantages associated with the use of HVFA concrete, there are several barriers which limit its use. One of the main barriers to the increased use of HVFA concrete is the concern over retarded set times, especially when high fly ash dosages are specified or cold curing conditions are encountered. Retarded set times can cause undesirable delays to concrete finishing operations. Similarly, there are concerns over the low early-age compressive strength development of HVFA concrete. Low early-age compressive strengths can require extended curing times, which can delay formwork removal and negatively impact construction sequencing. Finally, there are concerns that

material incompatibilities between fly ash, chemical admixtures, and cement may arise when high-calcium Class C fly ashes are specified in high dosages (Spiratos et al. 2003). Due to these barriers, contractors and transportation agencies are often reluctant to specify HVFA concrete for transportation structures.

1.2 Research Objectives

The main goal of this research was to evaluate the in-place performance of HVFA concrete when used in various transportation structures. The results from this research are aimed at providing guidance to contractors, concrete producers, and transportation agencies when specifying HVFA concrete for use in transportation infrastructure.

Auburn University, Purdue University, the National Institute of Standards and Technology (NIST), and the National Ready Mix Concrete Association (NRMCA) all worked together to address the limitations associated with HVFA concrete. One of the main limitations to the increased usage of HVFA concrete is the lack of prediction models for the in-place performance of HVFA concrete. Despite the advantages offered by HVFA concrete, there is a lack of knowledge concerning the in-place temperature development, setting times, and compressive strength development of concrete mixtures proportioned with high fly ash replacement levels. Auburn University was tasked with addressing these limitations. The primary objectives of the research conducted by Auburn University were

- Perform laboratory testing to quantify the effect of fly ash type, fly ash dosage, cement chemical composition, and curing temperature on the

hydration, setting, and compressive strength development of HVFA concrete mixtures,

- Develop a HVFA concrete hydration model, and
- Develop prediction methods to quantify the effect of fly ash type, fly ash dosage, and curing conditions on the maximum in-place concrete temperature, time to initial set, and compressive strength development of HVFA concrete placed in selected transportation structures.

1.3 Research Methodology

To effectively characterize the behavior of HVFA concrete, a three-stage research plan was developed. First, a laboratory testing program was conducted. For the laboratory testing program, two control mixtures and HVFA concrete mixtures with 35% and 50% fly ash dosages were produced. Four fly ash sources, two Class C and two Class F, were selected for laboratory testing to represent the range of fly ash chemical compositions available to the concrete industry in the United States. Also, two cement sources with different chemical compositions were tested. A total of 16 HVFA concrete mixtures were developed based on all combinations of fly ash dosage, fly ash type, and cement source. Each concrete mixture was produced at three batching temperatures (40 °F, 73 °F, and 105 °F). Semi-adiabatic calorimetry, penetration resistance testing, and compressive strength testing were conducted for all mixtures to investigate the effect of fly ash dosage, fly ash type, cement chemical composition, and curing temperature on the hydration development, setting times, and compressive strength development of HVFA concrete.

Second, a hydration model for HVFA concrete was developed. The hydration model was developed based on semi-adiabatic calorimetry testing results obtained from the laboratory testing phase. The purpose of the HVFA concrete hydration model is to provide an efficient and reliable means of estimating the hydration parameters of HVFA concrete for concrete producers and transportation agencies.

Finally, an evaluation of the in-place performance of HVFA concrete was completed based on the results obtained from the laboratory testing program and hydration model development. The ConcreteWorks software program was used to develop in-place temperature profiles for HVFA concrete placed under varying placement conditions. The in-place temperature profiles were then used to estimate the in-place temperature development, initial setting times, and compressive strength development of HVFA concretes placed in various transportation structures.

1.4 Document Organization

An overview of past research relating to HVFA concrete as well as the test methods used for this research project is presented in Chapter 2. That chapter opens with an introduction, which details the origin of fly ash. Following the introduction, the physical and chemical properties of fly ash are presented along with a brief review of the cement hydration and pozzolanic reactions. Semi-adiabatic calorimetry and isothermal calorimetry are also introduced as a means to measure the progress of hydration.

After the review of fly ash material properties, HVFA concrete is introduced. In this section, the mixture proportioning of HVFA concrete is reviewed along with the effects that high fly ash dosages have on concrete fresh and hardened properties. Since

one of the major limitations to the increased use of HVFA concrete is the lack of prediction methods for setting and strength prediction, an introduction to the hydration equation and the equivalent age maturity method, as they relate to hydration modeling, is presented.

In Chapter 3, the overall laboratory testing program is reviewed. Material properties for all aggregate, cement, and fly ash sources used for the project are presented. Also, the concrete production method used throughout the project is detailed. Finally, an overview of all testing procedures and apparatus is detailed. Sample preparation and curing methods, if applicable, for each of the test methods are introduced.

Sample results from each of the test methods are presented in Chapter 4. Chapter 4 includes results from fresh concrete testing, setting time by penetration resistance testing, isothermal and semi-adiabatic calorimetry, and compressive strength testing.

The HVFA concrete hydration model is presented in Chapter 5. First, the modeling approach is outlined. Next, a hydration model for cementitious materials from previous research is reviewed. The database of hydration parameters that were used to develop the HVFA concrete hydration model is detailed. Finally, the HVFA concrete hydration model developed for this project is presented.

The in-place performance of selected HVFA concrete mixtures was evaluated with the use of the ConcreteWorks software program. This analysis was completed to provide guidance to concrete producers and transportation agencies for prediction of the maximum in-place concrete temperature, time to initial set, and compressive strength development of HVFA concrete. The analysis considers a range of concrete placement temperatures and concrete element types (column, bridge deck, and pavement). In

Chapter 6, the modeling approach and baseline conditions are introduced. Also, sample results from the analysis are presented. Finally, the analysis results are presented and discussed.

Conclusions and recommendations related to the use of HVFA concrete in transportation structures are presented in Chapter 7. Appendices A through F follow Chapter 7. Appendix A contains results from fresh concrete property testing for each concrete mixture. Results from penetration resistance testing, isothermal and semi-adiabatic calorimetry, and compressive strength testing for each concrete mixture are presented in Appendices B, C, and D, respectively. The inputs and outputs used for development of the HVFA concrete hydration model are presented in Appendix E. Finally, in-place temperature profiles that were generated with the ConcreteWorks software program are presented in Appendix F.

Chapter 2

Literature Review

2.1 Introduction

Fly ash is commonly used as a supplementary cementitious material (SCM) in the production of portland cement concrete. Due to concerns relating to constructability and performance, fly ash replacement levels have been limited to roughly 25% by weight of cementitious material. In recent years, however, research has indicated that higher fly ash replacement levels may be used. In this chapter, technical information relating to the development and use of high volume fly ash (HVFA) concrete will be introduced.

Topics in this chapter include the origin and properties of fly ash, cement and fly ash hydration reactions, HVFA concrete mixture proportioning, HVFA concrete fresh properties, and HVFA concrete hardened properties. Also, hydration modeling will be introduced along with a discussion of the equivalent age maturity method.

2.2 Origin and Properties of Fly Ash

2.2.1 Fly Ash Production

Coal combustion products (CCPs) are the by-products of the combustion of pulverized coal in electric power generating plants. Fly ash, bottom ash, boiler slag, and flue gas desulferized gypsum are all recognized as CCPs. According to the American Coal Ash Association, 134.7 million tons of CCPs were produced in 2009, 63 million tons of which were fly ash (ACAA 2011).

Fly ash is commonly used as a SCM in the production of portland cement concrete. ACI 116 (2000) defines fly ash as "the finely divided residue that results from the combustion of ground or powdered coal and is transported by flue gases from the combustion zone to the particle removal system."

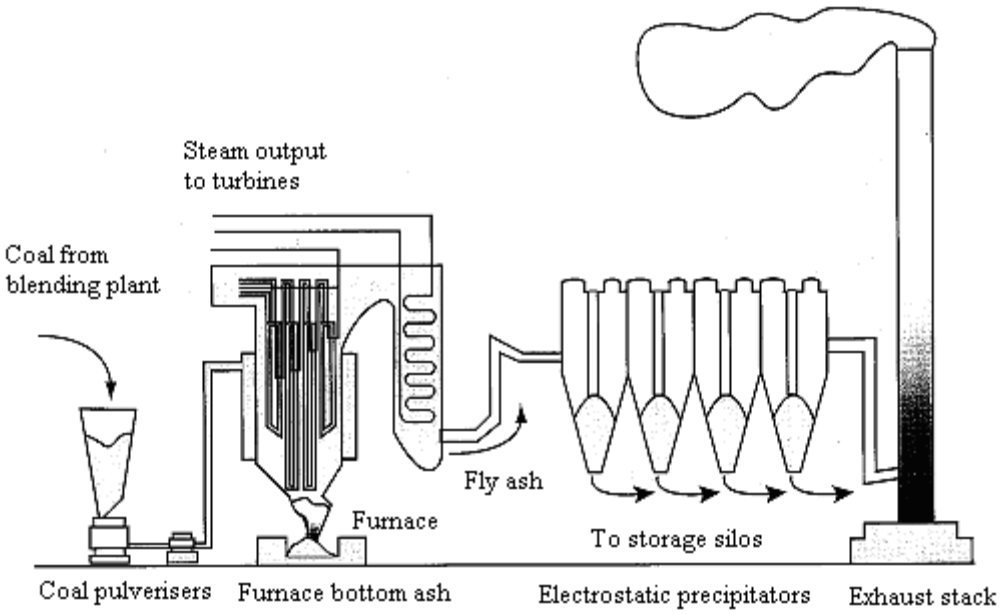

Figure 2.1: Fly ash production (Sear 2001)

A schematic layout of a coal-fired electrical generating station is presented in Figure 2.1. The production of fly ash begins when the coal is pulverized and sent to the burning zone of the furnace. In the furnace, the coal combusts and temperatures up to approximately 2700 °F (1485 °C) are produced. At this high temperature, the non-combustible inorganic materials liquefy and form molten droplets. The inorganic materials include quartz, calcite, gypsum, pyrite, feldspar, and clay minerals. The flue gases then carry these droplets away from the combustion chamber and they begin to cool. The spherical, glassy particles that are formed during cooling are termed fly ash (ACI 232.2R 2003).

Fly ash is removed from the flue gases by either mechanical or electrostatic precipitators. A typical electrostatic precipitator collection process is illustrated in Figure 2.2. When collected with electrostatic precipitators, the fly ash particle size and density vary from one hopper to the next. With mechanical precipitators, however, the fly ash is separated in sequential precipitator hoppers according to particle size and density. Regardless of the removal system, the fineness, density, and carbon content may vary from hopper to hopper. Therefore, fly ash from all hoppers is combined before storage to create a consistent, homogenous material (ACI 232.2R 2003).

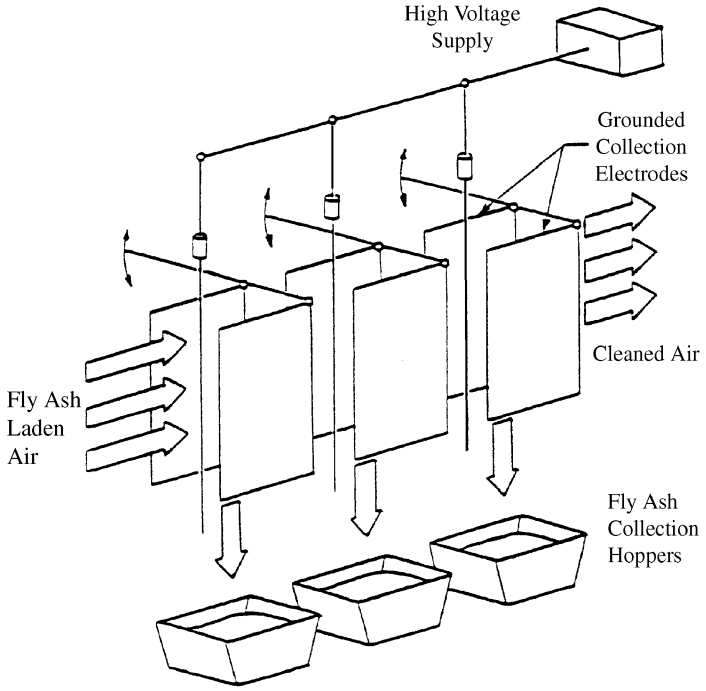

Figure 2.2: Electrostatic precipitator (ACI 232.2R 2003)

2.2.2 Chemical Composition of Fly Ash

In the United States, fly ash may be separated into two classes: Class C and Class F. Fly ash is categorized by chemical composition into one of the two classes in accordance with ASTM C 618 (2005) as follows:

Class F: $SiO_2 + Al_2O_3 + Fe_2O_3 \geq 70\%$

Class C: $SiO_2 + Al_2O_3 + Fe_2O_3 \geq 50\%$.

Class F fly ash is the byproduct of burning anthracite and bituminous coals. Class C fly ash, however, results from the combustion of lignite and sub-bituminous coals (Mehta and Monteiro 2006). Class C fly ashes have higher calcium oxide (CaO) contents than Class F ashes because the sum of SiO_2, Al_2O_3, and Fe_2O_3 may be significantly less than the 70% minimum limit stated for Class F ashes (ACI 232.2R 2003). Although Class F fly ash is strictly pozzolanic in behavior, Class C fly ash has both pozzolanic and cementitious properties because much of the calcium is in the form of reactive crystalline compounds such as tricalcium aluminate (C_3A), calcium sulfate ($C\overline{S}$) and tetracalcium trialuminate sulfate ($C_4A_3\overline{S}$) (Mehta and Monteiro 2006). In addition to differing CaO contents, Class C and Class F ashes typically differ in their unburned carbon content. Class F fly ashes generally have higher contents of residual carbon (Mindess, Young, and Darwin 2003). The chemical composition of fly ash has a direct influence on both the fresh and hardened properties of the concrete in which it is used.

2.2.3 Physical Properties of Fly Ash

Similar to the chemical composition, the physical properties of fly ash, such as particle size, particle shape, fineness, and density, directly influence both the fresh and hardened properties of the concrete in which it is used. Fly ash particle size and shape are dependent on the coal source, degree of pulverization before burning, combustion environment, and type of collection system used (ACI 232.2R 2003). Fly ash particles

are spherical in shape, glassy and may be hollow (cenospheres) or solid (plerospheres). A micrograph showing fly ash particles is presented in Figure 2.3.

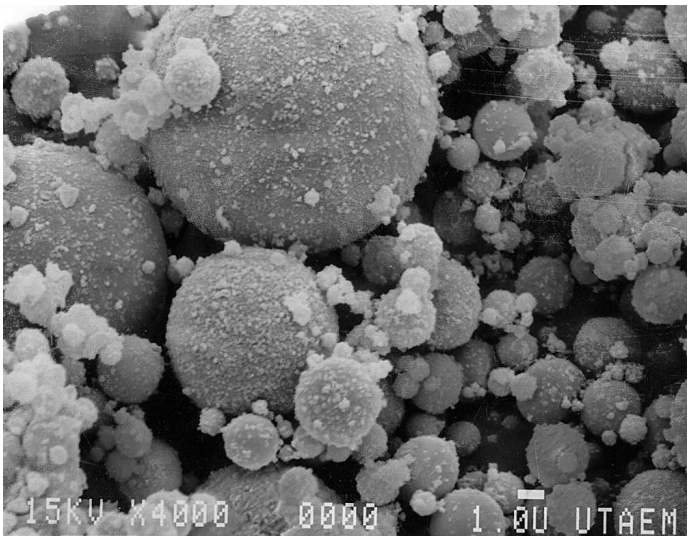

Figure 2.3: Micrograph of fly ash particles (ACI 232.2R 2003)

Fly ash particles typically vary between < 1 μm and 100 μm in diameter (Mehta and Monteiro 2006). A comparison of the particle size distribution of fly ash to that of portland cement and silica fume is shown in Figure 2.4. ASTM C 618 dictates that fly ash used in concrete should not have more than 34% of the fly ash particles retained on the 45 μm sieve (ASTM C 618 2005).

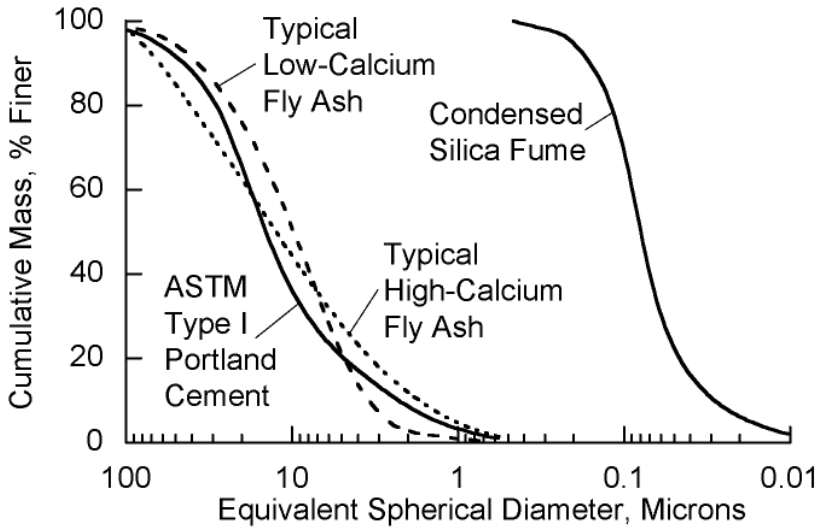

Figure 2.4: Fly ash particle size distribution (Mehta and Monteiro 2006)

Typically, fly ash specific gravities fall between 2.2 and 2.8 (Luke 1961). ASTM Class C fly ashes have higher specific gravity values than Class F ashes. The higher specific gravities of Class C ashes correspond to a higher amount of fine particles and fewer cenospheres. The lower specific gravity values for Class F ashes result from higher unburned carbon contents (ACI 232.2R 2003). The particle shape and size, particle size distribution, and specific gravity of fly ash all directly influence the water demand for a given concrete mixture, which, in turn, affects both fresh and hardened properties of the concrete being produced.

2.3 Hydration of Cementitious Materials

2.3.1 Portland Cement Hydration

The hydration of portland cement is important because this process yields hydration products that possess setting and hardening characteristics. Cement hydration products also serve to bind the fine and coarse aggregate (Mehta and Monteiro 2006).

The hydration process is directly influenced by the chemical composition and fineness of the cement. Portland cement is composed of four main Bogue compounds: tricalcium silicate (C_3S), dicalcium silicate (C_2S), tricalcium aluminate (C_3A), and tetracalcium aluminoferrite (C_4AF) (Mehta and Monteiro 2006). The hydration of portland cement may be divided into two main processes: hydration of the aluminates (C_3A and C_4AF) and hydration of the calcium silicates (C_3S and C_2S).

When water is first added to portland cement, C_3A immediately begins to hydrate and produce ettringite, a calcium sulfoaluminate hydrate, while releasing a significant amount of heat (Mehta and Monteiro 2006). The hydration of C_3A is presented in Reaction 2.1.

$$C_3A + \text{Gypsum} + H_2O \rightarrow \text{Ettringite} + 1350\ J/g \qquad \textbf{Reaction 2.1}$$

Ettringite, a needle-like hydration product, is only stable when sulfates are present in solution. Therefore, gypsum is added during the production of portland cement as a source of sulfate to help regulate the hydration of C_3A. As ettringite is produced, the reaction of the remaining C_3A is slowed, resulting in the dormant period in which concrete may be placed. After all of the sulfates in solution (gypsum) have been consumed, ettringite becomes unstable. The ettringite is then converted to monosulfate hydrate (MSH) as C_3A begins to hydrate again rapidly, as shown in Reaction 2.2 (Mehta and Monteiro 2006).

$$\text{Ettringite} + C_3A + H_2O \rightarrow \text{MSH} + 0\ J/g \qquad \textbf{Reaction 2.2}$$

The hydration of the calcium silicates occurs at a much slower rate than C_3A according to Reactions 2.3 and 2.4.

$C_3S + H_2O \rightarrow C\text{-}S\text{-}H + 3CH + 500$ J/g **Reaction 2.3**

$C_2S + H_2O \rightarrow C\text{-}S\text{-}H + CH + 260$ J/g **Reaction 2.4**

The silicate hydration reactions result in the formation of two hydration products: calcium silicate hydrate (C-S-H) and calcium hydroxide (CH). C-S-H is the largest contributor to strength in hydrated cement paste. Calcium hydroxide, however, is weak and soluble (Mehta and Monteiro 2006).

The cement hydration reaction is exothermic, meaning heat is released as hydration progresses. The amount of heat released as portland cement hydrates is referred to as the heat of hydration and can serve as an indication of the progress of the overall hydration process. The overall cement hydration process (combined hydration of silicates and aluminates) can be divided into five separate phases as shown by Figure 2.5.

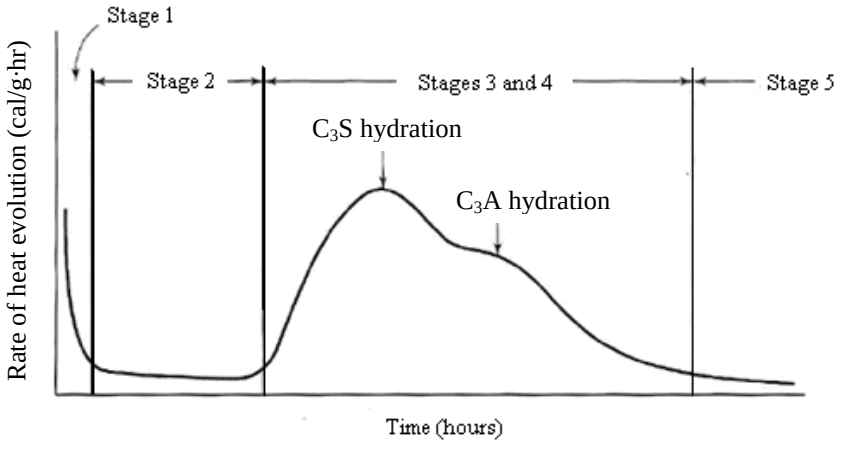

Figure 2.5: Portland cement hydration rate of heat evolution (Mindess, Young, and Darwin 2003)

During Stage 1, high heat evolution occurs as the portland cement hydrates rapidly. This initial peak is followed by the dormant period (Stage 2). During this time, very little heat is evolved and concrete remains in a plastic state, allowing it to be placed. The dormant period is followed by Stages 3 and 4, the acceleration and post-acceleration periods. During these stages, C_3S and C_3A rapidly hydrate again as illustrated by their individual peaks. The rate of heat evolution gradually decreases in Stage 4 until it reaches a steady state at Stage 5 (Mindess, Young, and Darwin 2003).

2.3.2 Portland Cement and Fly Ash Hydration

2.3.2.1 Pozzolanic Reaction

When fly ash is used in concrete as a supplementary cementing material (SCM), it reacts with the alkalis and calcium hydroxide (CH) within the hydrating cement paste to form calcium silicate hydrates (C-S-H) and calcium aluminate hydrates (ACI 232.2R 2003). Fly ash particles react with CH to form C-S-H, as shown by Reaction 2.5 (Mehta and Monteiro 2006).

Fly Ash + CH + water → C-S-H **Reaction 2.5**

Reaction 2.5 is referred to as the pozzolanic reaction. The fly ash will continue to react with CH to produce C-S-H until either all of the CH is consumed within the pore fluid, or there is no more mixing water available (ACI 232.2R 2003). In addition to the pozzolanic reaction, Class C fly ash may also react with the alkalis present in concrete to form calcium aluminate hydrates. Both of these reactions are dependent upon the

breakdown of the glassy structure of the fly ash by hydroxide ions and the heat generated in early stages of hydration of the hydraulic cement (Philleo 1991).

The pozzolanic reaction is important because it serves to convert the weak, soluble CH into the much stronger C-S-H hydration product, thereby increasing the durability of the hydrated cement paste. Also, the pozzolanic reaction occurs at a slow rate and releases little heat of hydration in comparison to the cementitious reactions (Mehta and Monteiro 2006).

2.3.2.2 Temperature Effects

The hydration of portland cement is temperature dependent. Generally, an increase in hydration temperature results in an accelerated hydration reaction. Figure 2.6 shows hydration development for five mortar specimens of the same w/c ratio (w/c = 0.50) cured at isothermal temperatures of 5, 12.5, 20, 35 and 50 °C (Kjellsen and Detwiler 1992).

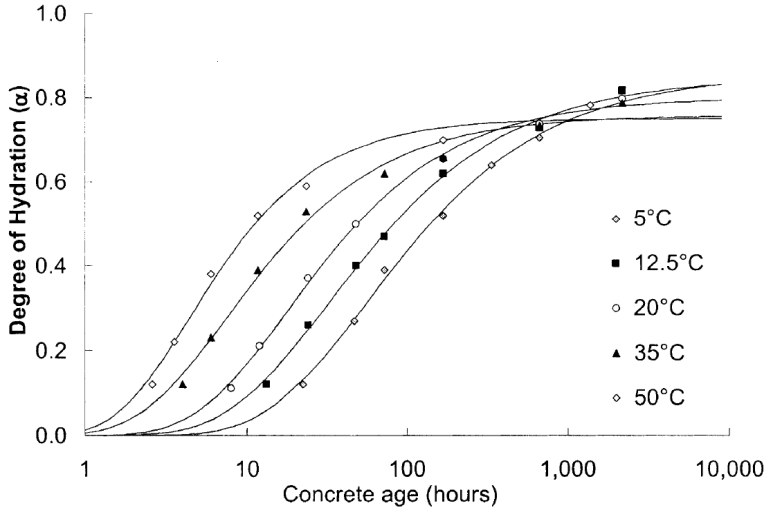

Figure 2.6: Effect of curing temperature on degree of hydration (Kjellsen and Detwiler 1992)

The figure illustrates that higher curing temperatures result in an increased rate of hydration. Similarly, as the curing temperature decreases, the rate of hydration slows. The effect of curing temperature on hydration development will be discussed in more detail in Section 2.6 when the degree of hydration formulation is introduced.

2.4 Calorimetry

2.4.1 Isothermal Calorimetry

The heat of hydration of a sample of paste, mortar, or concrete may be used as an indication of its degree of hydration (Powers and Brownyard 1948). One of the main methods used to measure heat of hydration is isothermal calorimetry. Isothermal calorimetry, also referred to as conduction calorimetry, is the measure of the heat of hydration of a sample that is maintained at a constant temperature (Poole et al. 2007). The useful duration of isothermal testing results varies from approximately 2 to 7 days depending on the sample size and testing temperature. After the first few days of testing, the hydration process begins to slow and the amount of liberated heat decreases. At this time, the error within the testing set-up may be similar in magnitude to the heat released by the sample (Poole et al. 2007). Results from isothermal calorimetry testing are useful in determining the temperature sensitivity (activation energy) of a given concrete mixture. An example of isothermal calorimetry results obtained for mortar samples for this project (with and without fly ash replacement) is shown in Figure 2.7. It can be seen in this figure that the rate of heat evolution is dependent on the cementitious system. In this figure, the results were normalized per gram of cementitious material.

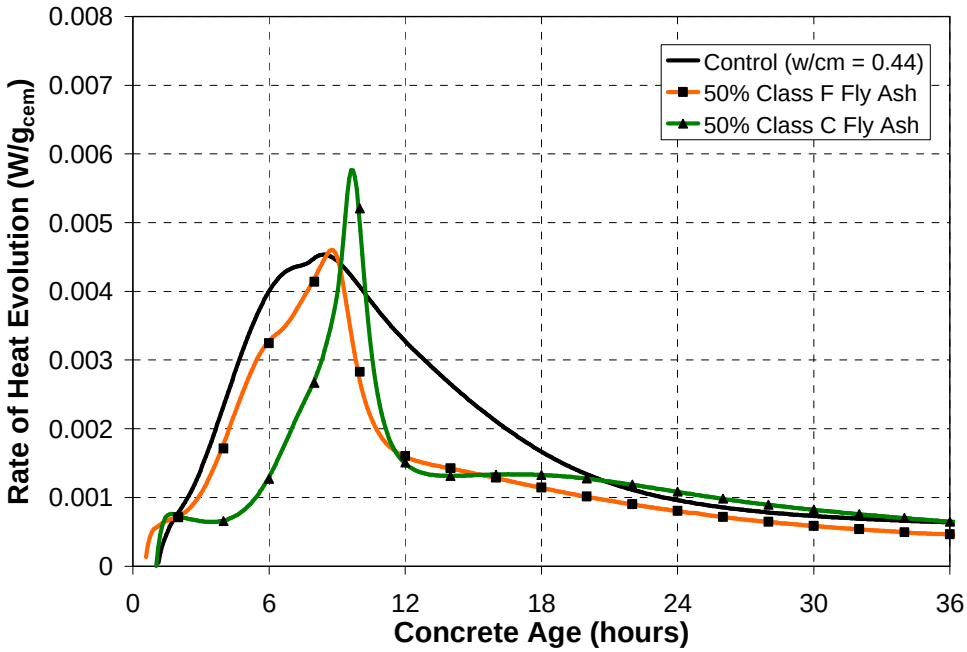

Figure 2.7: Sample isothermal calorimetry results

2.4.2 Semi-Adiabatic Calorimetry

Another method commonly used to measure the heat of hydration of a concrete sample is adiabatic calorimetry. Adiabatic calorimetry is based on the principle that at any time during testing, the temperature of the sample surroundings will be equal to the temperature of the concrete (RILEM TC 119 1997). Since it is very difficult to provide a test set-up in which there is no heat exchange to or from the testing environment, semi-adiabatic calorimetry (SAC) was developed (NRMCA 2PE004 2009). During semi-adiabatic calorimetry testing, a small amount of heat loss from the test set-up is expected to occur. These device specific losses are recorded and used to estimate a fully-adiabatic temperature profile. The fully-adiabatic profile must also account for the effect that the temperature difference between fully adiabatic and semi-adiabatic conditions has on the rate of hydration of the sample (Schindler and Folliard 2005). An example of heat of

hydration data for concrete produced with 15%, 25% and 35% Class F fly ash collected from a semi-adiabatic calorimeter is presented in Figure 2.8.

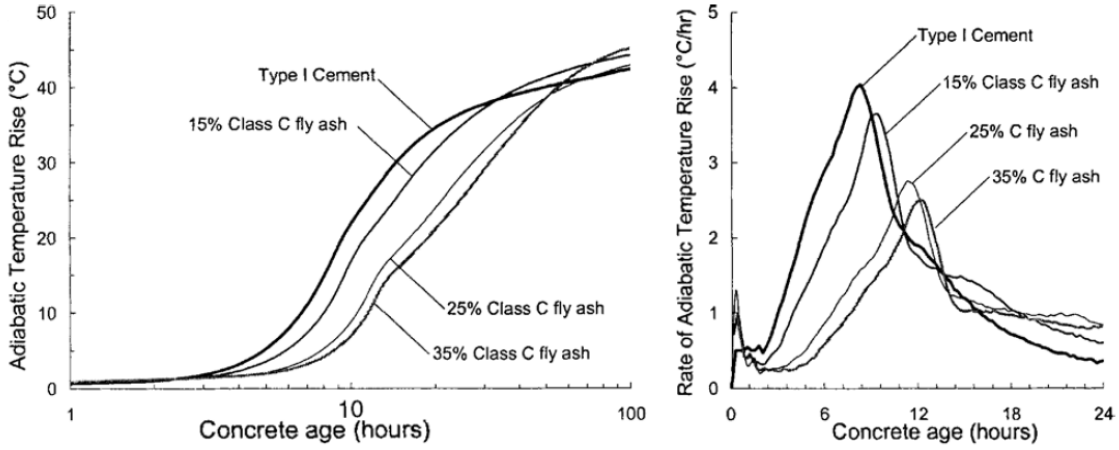

Figure 2.8: Sample SAC curves (Schindler and Folliard 2005)

2.5 High Volume Fly Ash Concrete

Due to the economic and environmental benefits discussed in Chapter 1, higher fly ash replacement levels have been pursued for concrete production. Malhotra and Mehta (2002) define HVFA concrete according to the following characteristics:

- Minimum of 50% fly ash by mass of cementitious materials.
- Water content less than 130 kg/m^3 (219 lb/yd^3).
- Cement content of no more than 200 kg/m^3 (337 lb/yd^3).
- Mandatory use of high-range water-reducing admixtures for concrete mixtures with a specified compressive strength of 30 MPa (4400 psi) or higher, slumps greater than 150 mm (6 in.) and water-to-cementitious materials ratio of the order of 0.30.

- Mandatory use of an air-entraining admixture for concrete exposed to freezing and thawing environments.

2.5.1 HVFA Mixture Proportions

2.5.1.1 Fly Ash Replacement Level

When fly ash is used as a supplementary cementitious material (SCM), the optimum replacement level is affected by the following factors: class of fly ash, chemical composition of cement, use of chemical admixtures, placement conditions, strength requirements, and curing conditions (Prusinski et al. 1993). Therefore, the optimum replacement level should be investigated for each concrete application.

Obla et al. (2003) recommend that fly ash contents for structural concrete be selected based on the concrete application. Under this approach, structural concrete may be categorized based on the finishing requirements. Table 2.1 presents recommended fly ash replacement levels based on concrete application assuming an average daily temperature of 68 °F. Also, it is assumed that temperatures will be higher during placement and curing. Note that the recommended fly ash contents presented in Table 2.1 should be tested with local materials to ensure compatability.

Table 2.1: Fly ash replacement based on concrete application (Obla et al. 2003)

Classification	Use	Fly Ash Content (%)	Critical Factors
A. No Finishing	Columns, walls, beams, precast (750 psi [5.2 MPa] by 14 to 16 hrs)	40 to 50%	Early strengths should be met with materials to be used in the job under site conditions.
	Precast and prestressed (3000 to 6000 psi [21 to 41 MPa] by 16 hrs)	20 to 30%	
	Some foundations, drilled piers, and mud mats (no early strength)	40 to 50%	
B. Needs Finishing	Slabs-on-ground, foundations, concrete pavements, tilt-up walls, suspended slabs, SOG subjected to early loading, SOG post-tensioned, slabs on metal deck, and toppings	40 to 50% (if broom finished)	Cast trial slabs to understand bleed and setting properties of HVFA concrete. May have to use measures to control plastic shrinkage cracking.
		25 to 50% (if trowel finished)	

For each classification, the recommended fly ash contents are separated based on the concrete application. Under the "No Finishing" classification, precast and prestressed elements have the lowest fly ash content due to required high early-age strength. Concrete for cast-in-place elements such as columns, walls, and beams, however, may be proportioned with higher fly ash contents. At 40 – 50% replacement levels, however, the w/cm ratio must be lowered to achieve adequate strength for form removal. Also, high-range water-reducing admixtures may be required to provide adequate workability. Concrete for foundations, on the other hand, may be proportioned with high fly ash contents without altering the w/cm ratio because low early-age strength and delayed setting times are typically not a concern for this application (Obla et al. 2003).

Obla et al. (2003) classify slabs-on-ground, pavements, tilt-up walls, suspended slabs, and other flatwork as concrete that requires finishing. For these applications, the

recommended fly ash contents vary according to the type of finish. When trowel finished, the recommended fly ash content varies from 25 – 50%, based on set time requirements, fly ash source, and use of chemical admixtures (Obla et al. 2003). It should be noted that ACI 318 (2008) places a limit on the maximum fly ash content at 25% when the concrete element is exposed to deicing chemicals.

2.5.1.2 Water-to-Cementitious Materials Ratio

The water-cement (w/c) ratio is defined as the mass of water divided by the mass of cement. Similarly, the water-cementitious material (w/cm) ratio is defined as the mass of water divided by the mass of cementitious materials (cement plus SCMs). Abrams (1919) reported that concrete compressive strength is inversely proportional to the water-cement ratio. Popovics (1986) determined that concrete produced with fly ash also followed Abrams' law. Since compressive strength is one of the most common measures used to determine concrete quality, selection of a proper w/cm ratio is crucial. It should be noted, however, that concrete produced with the same w/cm ratio may experience differences in strength due to differences in aggregate properties, types and sources of cementitious materials, use of chemical admixtures, entrained air contents, and curing conditions (Mindess, Young, and Darwin 2003).

When proportioning HVFA concrete, a low w/cm ratio is necessary. During research conducted at CANMET, Bilodeau et al. (2001) determined that for HVFA concrete, "the proportion of fly ash should be as high as possible and the water-cementitious materials ratio as low as possible to provide adequate early-age strength and durability." Furthermore, Bilodeau et al. (2001) recommend that HVFA concrete should

not be produced with a w/cm ratio above 0.35 unless durability is not a concern. High-range water-reducing admixtures are typically required to maintain adequate workability at low w/cm ratios.

2.5.1.3 Chemical Admixtures

2.5.1.3.1 Accelerating Admixtures

ASTM C 494 (2005) Type C accelerating admixtures are defined as "an admixture that accelerates the setting and early-age strength development of concrete." Accelerators are often used during winter months to offset the effects that cold placement temperatures have on the rate of hydration and strength gain. Similarly, accelerating admixtures are commonly used in HVFA concrete to counteract the retarding effects that high fly ash contents have on the hydration process.

Accelerating admixtures shorten set times by increasing the rate of hydration of C_3S. The induction period is typically shortened, and the rate of hydration during Stages 3 and 4 (Figure 2.5) is increased (Mindess, Young, and Darwin 2003). With the correct accelerator dosage, set times and early-age strength development for HVFA concrete can be made comparable to conventional concrete.

2.5.1.3.2 High-Range Water-Reducing Admixtures

ASTM C 494 (2005) Type F and G high-range water-reducing admixtures (a.k.a. superplasticizers) are admixtures that reduce "the amount of mixing water required to produce a concrete of a given consistency by 12% or greater." High-range water-reducing admixtures (HRWRA) are commonly used in HVFA concrete to ensure

adequate workability at the low w/cm ratios required for adequate early-age strength. Popovics (1993) reported that the effectiveness of HRWRA in HVFA concrete is dependent on the type and dosage of the admixture and the chemical composition of the cementitious material used in the concrete.

Superplasticizers are surfactants which achieve reductions in water demand by dispersing the cement grains in the mixing water. Cement and fly ash particles carry residual charges on their surface. When adjacent particles have opposite charges, they flocculate and adsorb mixing water onto their surface. Therefore, less mixing water is available to reduce the viscosity of the paste (Mindess, Young, and Darwin 2003). Superplasticizers act to neutralize the surface charges of the cement and fly ash particles, causing the particles to repel each other and free up the mixing water.

2.5.2 Effects of High Volume Fly Ash on Fresh Concrete

2.5.2.1 Workability and Water Demand

Mindess, Young and Darwin (2003) define workability as "the amount of mechanical work, or energy, required to produce full compaction of a concrete without segregation." The workability of fresh concrete is often measured by determining the slump according to ASTM C 143 (2005). Workability is affected by: water content, mixture proportions, aggregate type, concrete temperature, cement characteristics, use of chemical admixtures and use of SCMs (Mindess, Young, and Darwin 2003).

The use of fly ash as cement replacement generally reduces the water demand required for a given workability. Thomas (2007) approximates that each 10% of fly ash replacement should provide at least 3% water reduction. Figure 2.9 illustrates the

combined effect of fly ash fineness and replacement level on the water demand for concrete proportioned to have equal slump (Owens 1979).

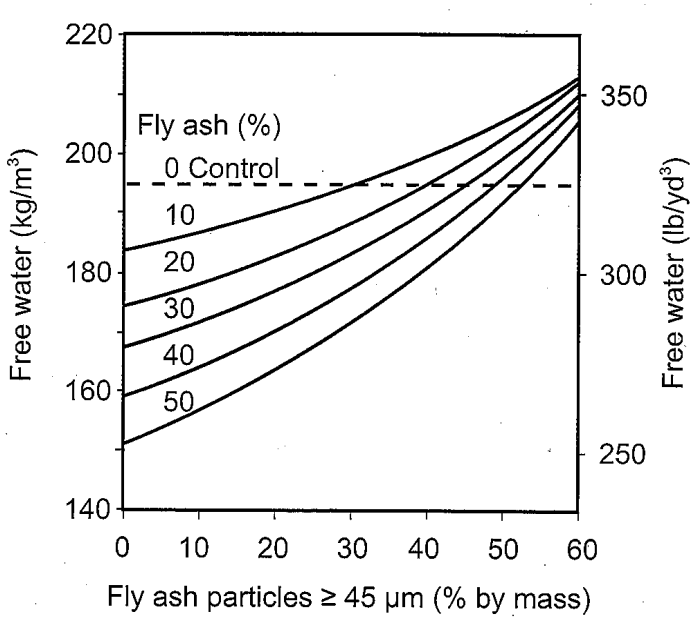

Figure 2.9: Fly ash fineness and replacement level effect on water demand (Owens 1979)

Malhotra and Jiang (2000) found similar results to Owens, with a maximum decrease in water demand of approximately 20%. Malhotra and Jiang investigated eight different fly ash sources with varying chemical compositions and fineness. All mixtures were produced with a 55% fly ash replacement level and w/cm ratios from 0.34 to 0.39. No air-entraining admixtures were used. The following table presents the water reduction (%) results obtained for each of the fly ash sources investigated.

Table 2.2: Reduction in water demand for HVFA concrete (Malhotra and Jiang 2000)

Mixture No.	Fly Ash Source	*w/cm*	Water Reduction (%)
F0	None	0.43	-
F1	Point Tupper	0.38	11.2
F2	Lingan	0.39	8.8
F3	Sundance	0.37	14.1
F4	Forestburg	0.35	17.6
F5	Thunder Bay	0.34	18.8
F6	Belledune	0.38	9.4
F7	Belews Creek	0.38	10.6
F8	Coal Creek	0.34	19.4

Mehta (2004) states that the reductions in water demand may be attributed to three mechanisms. First, the fine fly ash particles prevent cement flocculation. Also, since the fly ash particles have a smooth, spherical surface (illustrated in Figure 2.3), interparticle friction is reduced. Finally, the reduction in water demand may be attributed to more efficient particle packing within the paste (Mehta 2004). Based on the results, it is apparent that fly ash may be used as a water-reducing SCM at high replacement levels.

2.5.2.2 Bleeding

Bleeding is defined as the "upward movement of water after concrete has been consolidated, but before it has set" (Mindess, Young, and Darwin 2003). As the aggregates settle after placement, some of the mixing water is displaced and is forced to the surface. ASTM C 232 (2007) is the standard test method for determining the total bleeding capacity as well as the rate of bleeding for a fresh concrete sample.

In 1986, Gebler and Klieger performed research to quantify the effect that fly ash has on the bleeding capacity of concrete. Results from this research are summarized in Table 2.3. All fly ash concrete had a cementitious material content of 517 lb/yd^3 and fly

ash was proportioned with a 25% by mass replacement level. Gebler and Klieger (1986) verified that fly ash reduces the bleeding capacity of concrete. They also found that concretes proportioned with Class C ashes generally exhibited less bleed water than those proportioned with Class F ashes. The bleeding capacity of a concrete mixture is directly related to the water demand. Therefore, bleeding is typically reduced in HVFA concrete mixtures due to the low water contents required for adequate workability (Gebler and Klieger 1986).

Table 2.3: Effect of fly ash on bleeding (Gebler and Klieger 1986)

Test Mixtures		**Bleeding**	
Fly Ash		**%**	**ml/cm^2 of surface**
Identification	**Class of Fly Ash**		
A	C	0.22	0.007
B	F	1.11	0.036
C	F	1.61	0.053
D	F	1.88	0.067
E	F	1.18	0.035
F	C	0.13	0.004
G	C	0.89	0.028
H	F	0.58	0.022
I	C	0.12	0.004
J	F	1.48	0.051
Average:			
Class C		0.34	0.011
Class F		1.31	0.044
Control Mixtures:			
517 pcy		1.75	0.059
474 pcy		2.42	0.080

Low bleed water combined with extended initial set times can make HVFA concrete susceptible to plastic shrinkage cracking. Plastic shrinkage occurs when rate of

loss of water from the concrete surface exceeds the rate at which bleed water is generated. Plastic shrinkage cracking occurs when the tensile stress at the concrete surface due to shrinkage exceeds the concrete strength (Mehta and Monteiro 2006). If plastic shrinkage cracking is a concern, the guidelines set forth by ACI 305 (1999), titled *Hot Weather Concreting*, should be followed to reduce evaporation from the plastic concrete surface. ACI 305 (1999) states that evaporation from the plastic concrete surface may be reduced by the use of wind breaks, fog sprays, evaporation retarders, and impervious sheeting.

2.5.2.3 Air Entrainment

Concrete is susceptible to damage from freezing and thawing cycles when in a saturated or near-saturated condition. Air-entraining admixtures (AEA) are used to provide resistance to this damage by creating a small, well-distributed air-void system within the concrete. Air-entraining admixtures contain surfactants, which are molecules with a hydrophilic head and hydrophobic tail. Surfactants concentrate at the water-air interface and reduce the surface tension of the water to allow for the formation of small, stabilized bubbles (Mindess, Young, and Darwin 2003).

For HVFA concrete, the amount of air-entraining admixture required to produce the target air content may vary considerably. Class C fly ashes may reduce the required AEA dosage due to water-soluble alkalis in the fly ash (Pistilli 1983). The use of low-calcium, Class F fly ashes, however, typically requires increases in AEAs due to their high levels of unburned carbon (Thomas 2007). The unburned carbon reduces the effectiveness of the AEA by absorbing the air-entraining admixture. The loss on ignition

(LOI) is an indirect measure of the amount of unburned carbon for a fly ash source, and is often used as a predictor for the AEA dosage requirement. Research conducted by Folliard et al. (2007) suggests that a direct correlation cannot be made between LOI and AEA dosage requirement due to variability in the burning process of power generating plants. In recent years, many power generating plants have installed low NO_x burners to comply with environmental quality standards. Folliard et al. (2007) reported that measurement of the surface area of fly ash by Brunauer, Emmet, and Teller (BET) nitrogen absorption analysis is a better indicator of AEA demand.

According to Gebler and Klieger (1983), fly ashes that require a larger AEA dosage exhibit an increased rate of air loss when compared to a control concrete with no fly ash replacement and a similar w/cm ratio. Based on research findings, fly ash-AEA compatibility should be investigated on a case-by-case basis for HVFA concrete.

2.5.2.4 Setting Time

Mehta and Monteiro (2006) define setting of concrete as "the onset of solidification in a fresh concrete mixture." Initial set defines the time at which fresh concrete can no longer be properly mixed and placed, whereas final set defines the beginning of the development of mechanical properties (Mindess, Young and Darwin 2003). Set times for HVFA concrete are influenced by the following factors: class and quantity of fly ash, type and quantity of cement, environmental conditions, concrete temperature, use of chemical admixtures, and water-to-cementitious materials ratio (Mehta and Monteiro 2006). Initial and final set times are determined according to ASTM C 403 (2006), *Standard Test Method for Time of Setting of Concrete Mixtures by*

Penetration Resistance. Initial and final set times as determined according to ASTM C 403 are illustrated in Figure 2.10.

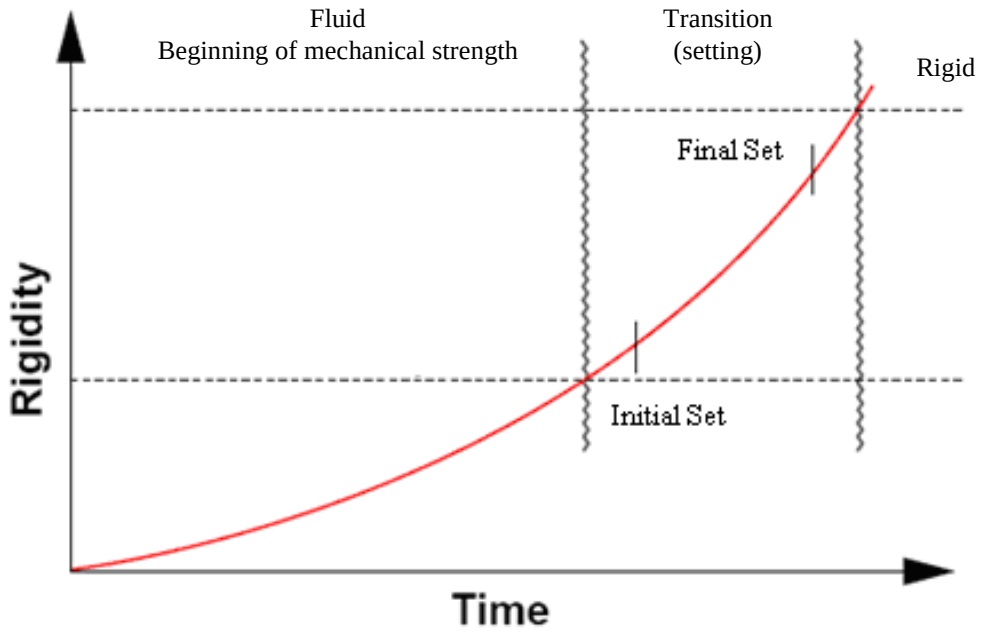

Figure 2.10: Setting and hardening of concrete (Mindess, Young, and Darwin 2003)

Ravina and Mehta (1986) performed a study on the fresh concrete properties of concrete produced with fly ash contents of 35, 42 and 50% by weight of cementitious materials. For this study, four fly ash sources were investigated, two Class F and two Class C. The chemical compositions for each of the four fly ash sources are shown in Table 2.4.

Table 2.4: Chemical composition of fly ashes for Ravina and Mehta (1986)

Item	ASTM Class F		ASTM Class C	
	No. 1	No. 2	No. 3	No. 4
SiO_2 (%)	52.2	68.4	45.8	39.5
Al_2O_3 (%)	27.4	17.2	22.3	19.5
Fe_2O_3 (%)	9.2	3.7	7.4	5.7
CaO (%)	4.4	5.6	19.0	24.7
MgO (%)	1.0	1.6	5.0	3.4
SO_3 (%)	0.45	0.52	1.60	1.80
Na_2O (%)	0.12	0.99	0.33	1.56
K_2O (%)	0.68	0.44	0.19	0.21
Loss on Ignition (%)	3.50	0.30	0.20	0.21
Specific Gravity	2.31	2.30	2.46	2.58

A summary of the penetration resistance data from this study for each of the fly ash sources detailed above at a replacement level of 35% by mass of total cementitious material is shown in Table 2.5. The setting results for the reference control concrete (no fly ash replacement) are also presented for comparison.

Table 2.5: Setting of concrete mixtures with 35% fly ash (Ravina and Mehta 1986)

Setting Time (hr:min)	Control	Fly Ash 1	Fly Ash 2	Fly Ash 3	Fly Ash 4
Initial Set	5:40	6:00	6:15	8:20	7:10
Final Set	8:40	9:40	10:15	11:30	10:25
Delay of Initial Set	----	0:20	0:35	2:40	1:30
Delay of Final Set	----	1:00	1:35	2:50	1:45

Ravina and Mehta (1986) reported initial set time delays of 20 minutes to 4 hours and 20 minutes and final set time delays of 1 hour to 5 hours and 15 minutes when compared to the control concrete depending on the fly ash type and dosage. ASTM Class C fly ashes resulted in longer set times when compared to equivalent concrete mixtures prepared with Class F fly ashes. Also, the delay in set times increased with higher fly ash replacement levels. This research, indicates that HVFA concretes exhibit delayed set times when compared to a control mixture with no fly ash replacement and a similar w/cm ratio.

As discussed in Section 2.3, tricalcium aluminate, C_3A, begins to hydrate rapidly when water is first added to a concrete mixture. The rate of C_3A hydration is highly dependent on the presence of sulfate ions in the hydrating cement paste. When the sulfate content is increased, the rate of C_3A hydration is slowed. Ravina and Mehta (1986) report that the delayed setting times for the concrete mixtures incorporating Class C fly ashes can be attributed to their higher sulfate contents.

Eren et al. (1995) performed research to quantify the effect of curing temperature on setting times of HVFA concrete and slag cement concrete. The results for HVFA concrete proportioned with 50% Class F fly ash are shown in Figure 2.11. It is shown that setting times are temperature dependent. Set times decrease with an increase in curing temperature and increase with a decrease in curing temperature. During cold weather, the rate of hydration is slowed, and high fly ash replacement levels can cause significant delays in initial and final set times. During hot weather, however, the retardation caused by fly ash may be beneficial.

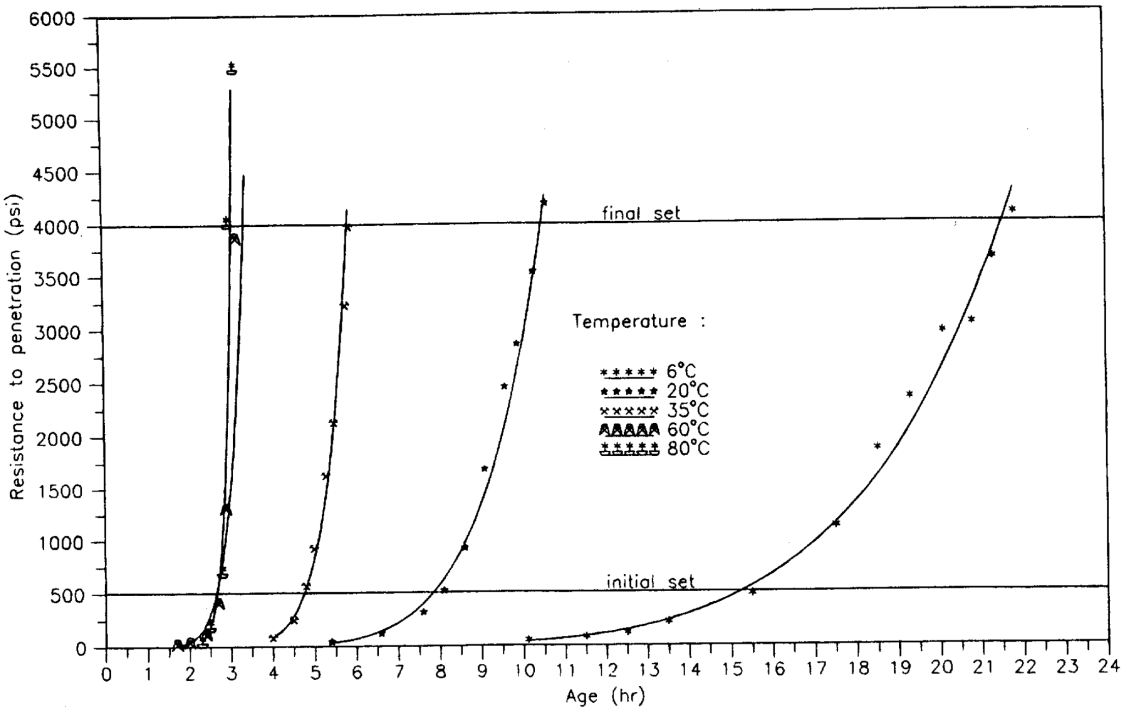

Figure 2.11: Effect of curing temperature on HVFA concrete setting times (Eren et al. 1995)

2.5.2.5 Heat of Hydration

As discussed in Section 2.3, the hydration of cement is an exothermic process. When fly ash is used to replace cement in portland cement concrete, the rate of heat development and overall heat of hydration is altered. In some cases, the total heat of hydration is reduced, which can be very beneficial in mass concrete construction. During mass concrete pours, the maximum temperature rise for concrete containing fly ash will depend on the chemical composition of the fly ash, replacement level, and concrete temperature at placement (Thomas 2007).

Langley et al. (1992) performed research to quantify the effect that high fly ash dosages have on the temperature rise for concrete. For their study, three 3.05 x 3.05 x

3.05 meter concrete blocks were cast and the temperature rise was monitored with embedded thermocouples. Langley et al. (1992) reported that the temperature rise caused by the hydration of HVFA concrete may be significantly reduced. When the cementitious materials content was held constant, it was found that the peak temperature of the block cast incorporating concrete with 55% Class F fly ash replacement was reduced by 29°C (52°F). When the total cementitious materials content was reduced and fly ash was incorporated, a reduction of 53°C (95°F) was achieved (Langley et al. 1992).

Similar research was conducted by Bisaillon et al. (1994). The results from this study are shown in Table 2.5. The fly ash selected for this research had a CaO content of 2%. Bisaillon et al. (1994) also reported decreases in peak in-place temperature when monitoring the temperature rise of large concrete monoliths (2.5 x 3.0 x 4.0 meter blocks) cast with fly ash replacement levels ranging from 56 to 62%.

Table 2.6: Temperature rise of HVFA concrete monoliths (Bisaillon et al. 1994)

Mix	**Cement kg/m^3 (lb/yd^3)**	**Class F Fly Ash kg/m^3 (lb/yd^3)**	**w/cm**	**Max. Temp °C (°F)**	**Time to Max (hour)**
1	365 (600) Type I	-	0.45	68 (154)	29
2	125 (211) Type I	155 (261)	0.46	44 (111)	53
3	170 (287) Type I	220 (370)	0.29	54 (129)	57
4	330 (556) Type II	-	0.50	55 (131)	75
5	125 (211) Type I	155 (261)	0.41	47 (117)	98

The rate of temperature development and maximum temperature rise for HVFA concrete is dependent on the chemical composition of the fly ash. Thomas et al. (1995) performed an isothermal calorimetry study on cement-fly ash pastes with CaO contents ranging from 2.6% to 27.1%. The results from this study are illustrated in Figure 2.12.

From this study, it was determined that as the CaO content of the fly ash increases, the rate of temperature development also increases.

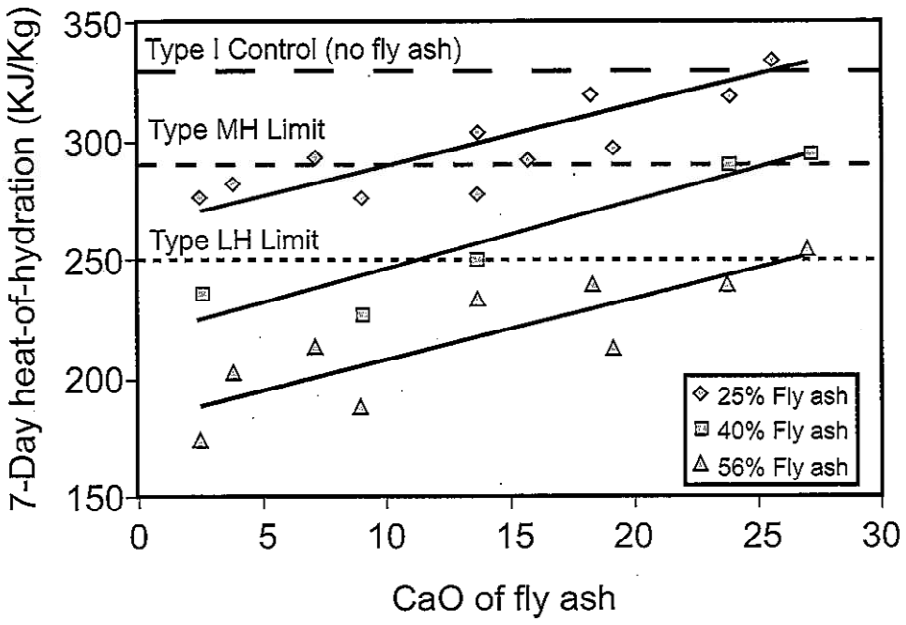

Figure 2.12: Influence of fly ash CaO content on heat of hydration (Thomas et al. 1995)

The heat contribution of fly ash to the overall heat of hydration of a concrete sample will be discussed in further detail in Section 2.6 when the degree of hydration formulation is introduced.

2.5.3 Effects of High Volume Fly Ash on Hardened Concrete Properties

2.5.3.1 Compressive Strength Development and Curing Requirements

The rate of strength gain for HVFA concrete is affected by the chemical composition of the fly ash, the type of cement used, and the concrete mixture proportions (EPRI CS-3314). Generally, as the fly ash dosage increases (for a given w/cm ratio),

early-age compressive strength decreases. At later ages, however, the compressive strength may be improved with increased fly ash replacement. The increase in strength gain at later ages can be attributed to the pozzolanic activity of the fly ash, and will only be achieved if the concrete is kept moist (ACI 232.R 2003). Moisture is required for the pozzolanic reaction to convert CH to C-S-H. Berry and Malhotra (1980) report that the strength gain at later ages will continue to increase and will result in higher later-age strengths than would be achieved with an increase in cement content. The general effect of fly ash dosage (Class F) on concrete compressive strength development is shown in Figure 2.13. In Figure 2.13, it is shown that as the fly ash dosage is increased, the rate of strength development at early ages decreases. At later ages, however, the compressive strength increases with an increase in fly ash dosage.

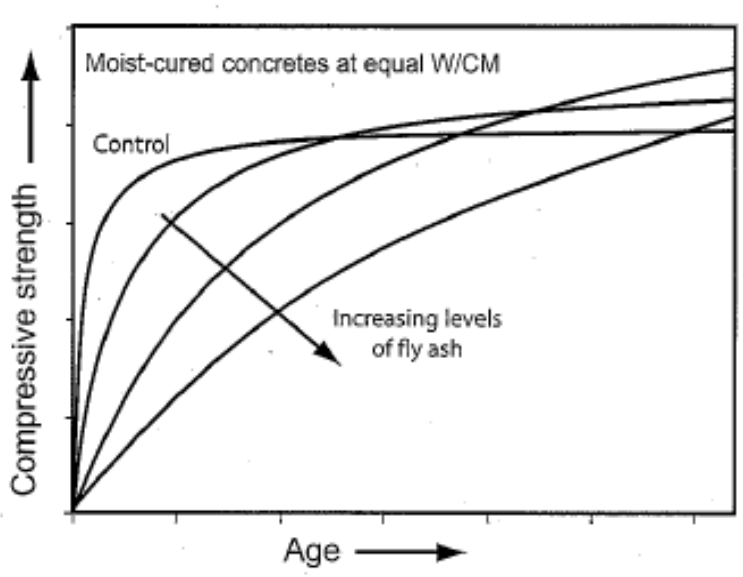

Figure 2.13: Effect of Class F fly ash on concrete compressive strength (Thomas 2007)

Class C fly ashes exhibit a higher rate of reaction at early ages than Class F ashes (Smith et al. 1982). Typically, the early-age strength for HVFA concrete will increase with increasing fly ash CaO content. However, some Class C ashes may not exhibit the increased later-age strength gain found with Class F ashes (ACI 232.R 2003).

The late-age strength gains for HVFA concrete are dependent on the duration of moist curing. Langley et al. (1989) performed a study to quantify the effect of curing duration on the development of compressive strength for concrete proportioned with 56% fly ash by weight of total cementitious materials. The results from this study are shown in Figure 2.14.

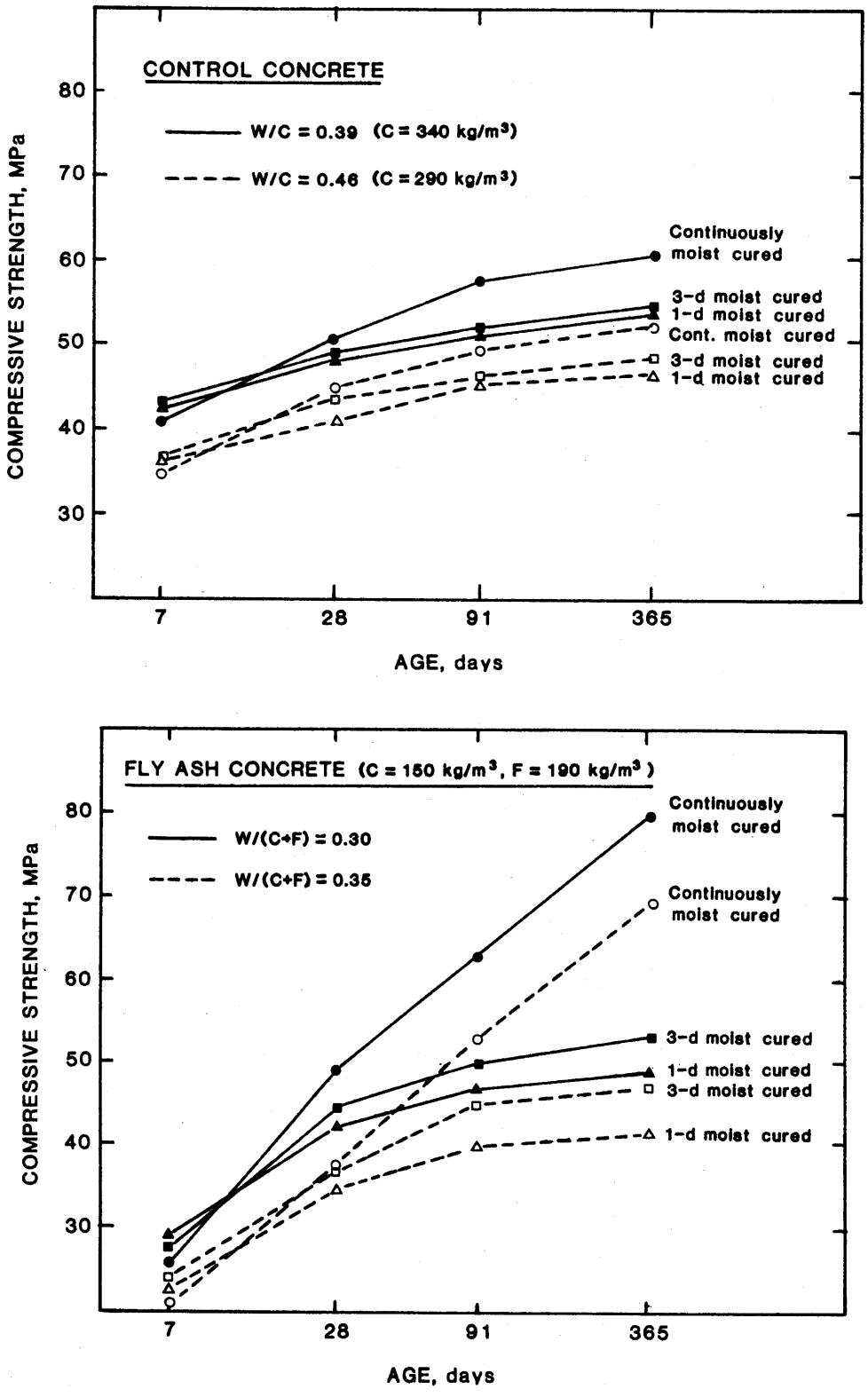

Figure 2.14: Effect of curing temperature on HVFA concrete compressive strength development (Langley et al. 1989)

As shown in Figure 2.14, HVFA concrete benefits greatly from increased moist-curing duration. When continuously moist-cured, the HVFA concrete continues to gain strength at testing ages up to 365 days. Langley et al. (1989) determined that HVFA concrete may not require extended curing periods in the field, however, because comparable compressive strengths at 28 days were achieved with only 3 days of moist-curing. Also, in large structural elements, the long-term strength development of interior concrete will not be affected as severely by drying as the 6 in. x 12 in. test cylinders used for laboratory testing (Langley et al. 1989).

2.6 Hydration Modeling

2.6.1 Degree of Hydration

Degree of hydration (α) is used to quantify the progress of the hydration reactions between cementitious materials and water contained in a concrete sample. The degree of hydration varies with time. At an α of 0, no reactions have occurred. The maximum value of α is 1, representing a state of complete hydration (RILEM CEA 42 1981). It should be noted, however, that a degree of hydration of 1 may never be reached because not all cementitious material will hydrate (Mills 1966). Figure 2.15 shows a typical degree of hydration versus concrete age plot.

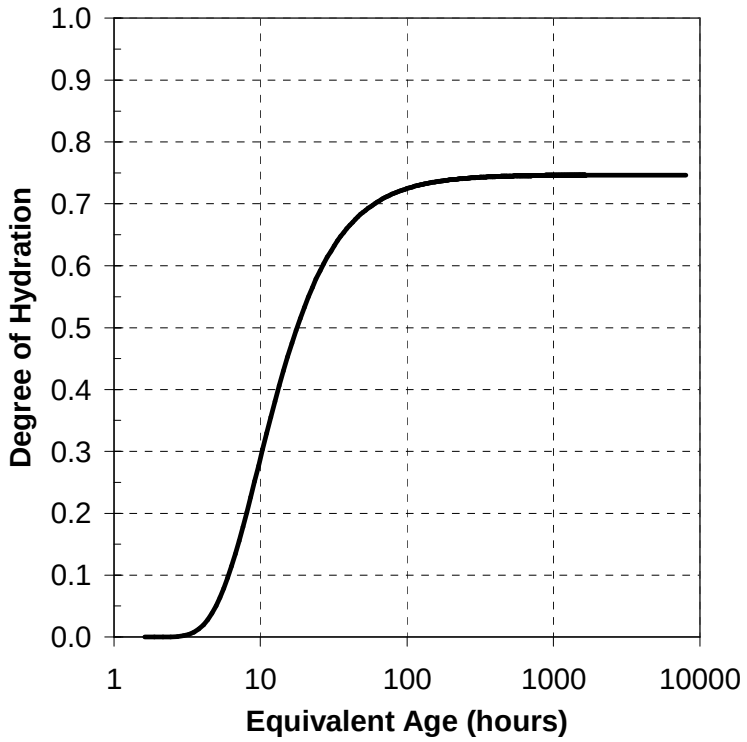

Figure 2.15: Plot of degree of hydration versus concrete age

2.6.1.1 Degree of Hydration Formulas

The degree of hydration for a concrete mixture may be determined experimentally by either direct or indirect methods. The International Union of Laboratories and Experts in Construction Materials, Systems, and Structures (RILEM) defines a direct method for calculating degree of hydration based on determining the quantity of hydration products formed. The RILEM CEA 42 (1981) definition for degree of hydration is presented in Equation 2.2:

$$\alpha(t) = \frac{C(t)}{C} \qquad \textbf{Equation 2.2}$$

where:

$\alpha(t)$ = degree of hydration at time t,

$C(t)$ = quantity of hydrated cement at time t, and

C = original quantity of cement.

According to RILEM CEA 42 (1981), it is "almost impossible to make a direct determination of the quantity of cement gel formed or the quantity of hydrated cement." Therefore, the degree of hydration is most often determined by indirect methods. One indirect method for determining α is by analysis of the chemically bound water within the hydrating cement paste. Powers and Brownyard (1948) reported that a relationship exists between the amount of chemically bound water within the paste and the quantity of cement gel formed. Also, Powers and Brownyard found that portland cement will bind approximately 25% by weight of water at complete hydration. Based on these findings, the following formulation of degree of hydration was presented.

$$\alpha(t) = \frac{w_n(t)}{0.25 \cdot C} \qquad \textbf{Equation 2.3}$$

where:

$\alpha(t)$ = degree of hydration at time t,

$w_n(t)$ = quantity of bound water at time t, and

C = original quantity of cement.

For this formulation, the quantity of bound water, w_n, is defined as "the quantity of water which is emitted from a dried (105°C) specimen when it is subjected to ignition (1050°C)" (Byfors 1980).

Another indirect method for determining the degree of hydration is based on measuring the heat of hydration of the cement paste. Powers and Brownyard (1948)

found that the quantity of bound water is directly proportional to the quantity of heat developed during hydration. Therefore the degree of hydration may be determined by dividing the heat developed at a given time by the theoretical total quantity of heat available within the cementitious system. The degree of hydration formulation based on heat of hydration is as follows (Powers and Brownyard 1948):

$$\alpha(t) = \frac{H(t)}{H_T} \qquad \textbf{Equation 2.4}$$

where:

$\alpha(t)$ = degree of hydration at time t,

$H(t)$ = quantity of heat developed at time t, and

H_T = quantity of heat developed at complete hydration.

The quantity of heat generated at a given time, *H(t)*, may be determined by the following methods: adiabatic calorimetry, isothermal calorimetry or measurement of the heat of solution. Isothermal calorimetry and semi-adiabatic calorimetry were introduced in Sections 2.4.1 and 2.4.2, respectively. Due to unreliability of heat of solution measurements, calorimetry methods are preferred (RILEM CEA 42 1981).

The formulation given above also requires determination of H_T, the total quantity of heat available within the cementitious system. H_T accounts for heat generated by both portland cement and SCMs at 100% hydration. The ultimate heat of hydration for a concrete mixture, H_T, can be quantified as follows (Schindler and Folliard 2005):

$$H_T = H_u \cdot C_c \qquad \textbf{Equation 2.5}$$

where:

H_T = ultimate heat of hydration of the concrete (J/m^3),

H_u = total heat of hydration of cementitious materials (J/g), and

C_c = cementitious materials content (g/m^3).

The total heat of hydration of the cementitious system includes heat contribution from both portland cement and SCMs. Schindler and Folliard (2005) proposed the following approximation for the total heat of hydration of the cementitious materials:

$$H_u = H_{cem} \cdot p_{cem} + 461 \cdot p_{slag} + p_{FA} \cdot h_{FA} \qquad \textbf{Equation 2.6}$$

where:

H_u = total heat of hydration of cementitious materials hydration (J/g),

H_{cem} = total heat of hydration of cement (J/g),

p_{cem} = cement weight ratio in terms of total cementitious content,

p_{slag} = slag weight ratio in terms of total cementitious content,

p_{FA} = fly ash weight ratio in terms of total cementitious content, and

h_{FA} = heat of hydration of fly ash (J/g).

2.6.1.1.1 Portland Cement Heat Contribution

As seen in the formulation for H_u, the heat of hydration contribution from portland cement and fly ash must be determined. Since each portland cement compound has a unique heat of hydration, the total heat of hydration of cement at complete hydration, H_{cem}, may be calculated as follows (Bogue 1947):

$$H_{cem} = 500 \cdot p_{C3S} + 260 \cdot p_{C2S} + 866 \cdot p_{C3A} + 420 \cdot p_{C4AF} + 624 \cdot p_{SO3} + 1186 \cdot p_{FreeCaO} + 850 \cdot p_{MgO} \qquad \textbf{Equation 2.7}$$

where:

H_{cem} = total heat of hydration of cement (J/g) and

p_i = weight ratio of *i*-th compound in terms of total cement content.

2.6.1.1.2 Fly Ash Heat Contribution

To calculate the total heat available within the cementitious system, the heat contribution from fly ash must be determined. Since the cementitious nature of a fly ash is correlated with its CaO content, fly ash heat of hydration is calculated based on CaO content. Kishi et al. (1995) proposed a value of 209 kJ/kg for fly ash with a CaO content of 8.8%. Schindler and Folliard (2005) expanded the formulation for fly ash heat of hydration based on semi-adiabatic test results obtained during the development of a general hydration model for cementitous materials. The formulation for fly ash heat of hydration proposed by Schindler and Folliard (2005) is as follows:

$$h_{FA} = 1800 \cdot p_{FA\text{-}CaO} \qquad \textbf{Equation 2.8}$$

where:

h_{FA} = total heat of hydration of fly ash (J/g) and

$p_{FA\text{-}CaO}$ = fly ash CaO weight ratio in terms of total fly ash content.

In 2009, Ge and Wang modified the formulation proposed by Schindler and Folliard based on semi-adiabatic calorimetry test results obtained from concrete mixtures containing 15, 30, 45 and 60% fly ash by weight of cementitious materials. The fly ash sources investigated in this study had CaO contents ranging from 1.51% to 27.11%. The formulation proposed by Ge and Wang (2009) is as follows:

$h_{FA} = 15.9 \cdot (p_{FACaO} \text{ x } 100) + 74.3$ **Equation 2.9**

where:

h_{FA} = total heat of hydration of fly ash (J/g) and

p_{FACaO} = fly ash CaO weight ratio in terms of total fly ash content.

2.6.1.2 Ultimate Degree of Hydration

Unless the water-cement ratio is extremely high, complete hydration will not occur ($\alpha = 1.0$). After investigation of the hydration of a wide range of cementitious materials, Mills (1966) concluded that "most, if not all, cement paste hydration stops before the cement is totally consumed." Mills determined that the ultimate degree of hydration is strongly influenced by the water-cement ratio. Based on this study, Mills developed the following equation as an approximation for the ultimate degree of hydration.

$$\alpha_u = \frac{1.031 \cdot w/c}{0.194 + w/c}$$ **Equation 2.10**

where:

α_u = ultimate degree of hydration

w/c = water-cement ratio by weight.

The ultimate degree of hydration formulation proposed by Mills does not take into account the use of SCMs. Therefore, Schindler and Folliard (2005) expanded Mills model:

$$\alpha_u = \frac{1.031 \cdot w/c}{0.194 + w/c} + 0.5 \cdot p_{FA} + 0.3 \cdot p_{SLAG} \leq 1.0 \qquad \textbf{Equation 2.11}$$

where:

α_u = ultimate degree of hydration

w/c = water-cement ratio by weight

p_{FA} = weight ratio of fly ash in terms of total cement content

p_{SLAG} = weight ratio of GGBF slag in terms of total cement content.

In Section 2.3.2.2, it was shown that the rate of hydration is affected by curing temperature. The ultimate degree of hydration, however, is independent of curing temperature (Kjellsen and Detwiler 1992). The influence of curing temperature on ultimate degree of hydration is shown in Figure 2.6. The difference in ultimate degree of hydration for the samples cured at 5 °C and 50 °C is approximately 2%.

2.6.1.3 Hydration Equation

After collecting data for the degree of hydration development of a concrete sample, the data may be represented by a best-fit mathematical model. Friesleben, Hansen, and Pederson (1984) developed a three-parameter exponential equation to represent the heat development of a portland cement concrete sample. In 2002, Hansen and Pane modified the original equation to represent the development of degree of hydration versus time:

$$\alpha(t) = \alpha_u \cdot \exp\left(-\left(\frac{\tau}{t}\right)^{\beta}\right) \qquad \textbf{Equation 2.12}$$

where:

$\alpha(t)$ = degree of hydration at time t

α_u = ultimate degree of hydration

τ = hydration time parameter

β = hydration shape parameter, and

t = concrete age or equivalent age.

2.6.2 Equivalent Age Maturity Method

The development of mechanical properties and hydration for a given concrete mixture is a function of its age and curing temperature history. Therefore, it is difficult to accurately estimate the in-place concrete strength based on strength data that have been obtained under standard laboratory conditions. The maturity method was developed to predict concrete behavior at any given time based on the measured temperature history of a concrete sample (Carino 2004). With the maturity method, a maturity function is used to convert the chronological age of a concrete cured at any temperature to an equivalent age for a specimen cured at a reference temperature (Schindler 2004).

In 1977, Friesleben, Hansen and Pederson introduced the maturity function presented in Equation 2.13. This function is based on the Arrhenius equation and is commonly called the equivalent age maturity method (ASTM C 1074 2004). ASTM C 1074 (2004) defines equivalent age as the amount of time at a specified temperature required to produce a maturity equal to the maturity reached by a curing period at temperatures other than the specified reference temperature. The Arrhenius method maturity function is typically evaluated using a reference temperature, T_R, of 73 °F (23 °C) in the United States or 68 °F (20 °C) in Europe.

$$t_e = \sum e^{\frac{-E}{R}\left(\frac{1}{T_c}-\frac{1}{T_R}\right)}\Delta t \qquad \textbf{Equation 2.13}$$

where:

t_e = equivalent age at the reference curing temperature (hours),

T_C = average temperature of concrete during time interval Δt (K),

T_R = reference temperature (K),

E = activation energy (J/mol), and

R = universal gas constant, 8.3144 J/ (mol K).

2.6.2.1 Activation Energy

The activation energy used in the Arrhenius equation defines the temperature sensitivity of the concrete mixture (Carino 2004). When the difference between the curing and reference temperatures increases, it is important that an accurate estimate of the activation energy is used so that reliable estimates of the in-place concrete strength and hydration development are achieved.

Friesleben, Hansen and Pederson (1977) recommend the following values for activation energy when estimating the development of mechanical properties:

E = 33,500 J/mol for T ≥ 20 °C

E = 33,500 + 1470 (20 – T) for T < 20 °C.

ASTM C 1074 (2004) also provides guidance on the selection of appropriate activation energy values based on the cement type used. For a Type I cement with no chemical admixtures, an activation energy of 40,000 to 45,000 J/mol is suggested (ASTM C 1074 2004). Since activation energy values are highly dependent on mixture proportions and

the use of chemical admixtures, Annex A of ASTM C 1074 (2004) provides an experimental procedure to determine more accurate activation energy values.

The maturity method may also be used to predict hydration development. The method for determining activation energy values outlined in ASTM C 1074 (2004), the *Standard Practice for Estimating Concrete Strength by the Maturity Method*, is suitable for strength prediction. When predicting hydration progress, however, Schindler (2004) and Poole et al. (2007) determined that isothermal calorimetry data, rather than mortar cube compressive strength results, provides a more accurate estimate of the activation energy.

Schindler (2004) proposed the following formulation for estimating the activation energy for a given concrete mixture based on the chemical composition and fineness of the cement, as well as the presence of supplementary cementitious materials:

$$E = 22{,}100 \cdot f_E \cdot p_{C3A}^{0.30} \cdot p_{C4AF}^{0.25} \cdot \text{Blaine}^{0.35} \qquad \textbf{Equation 2.14}$$

where:

E = activation energy (J/mol),

f_E = activation energy factor to account for use of SCMs,

p_{C3A} = weight ratio of C_3A in terms of total cement content,

p_{C4AF} = weight ratio of C_4AF in terms of total cement content, and

Blaine = Blaine specific surface area of cement (m^2/kg).

The activation energy modification factor, f_E, is calculated as follows:

$$f_E = 1 - 1.05 \cdot p_{FA} \cdot (1 - p_{FACaO}/0.40) + 0.40 \cdot p_{SLAG} \qquad \textbf{Equation 2.15}$$

where:

f_E = activation energy factor to account for use of SCMs,

p_{FA} = weight ratio of fly ash replacement,

p_{FACaO} = weight ratio of CaO content for fly ash, and

p_{SLAG} = weight ratio of GGBF slag replacement.

2.6.2.2 Application of Maturity Method

2.6.2.2.1 Compressive Strength Prediction

After determining the activation energy for a given concrete mixture, the equivalent age for a test specimen may be calculated at any time based on the recorded temperature history using Equation 2.14. As long as the concrete has been properly placed, consolidated and cured, this equivalent age can then be used to help estimate the in-place concrete strength. When comparing concrete strength based on equivalent age, rather than real age, inaccurate correlations due to differing temperature histories may be avoided, as illustrated by Figure 2.16. Accurate prediction of the in-place concrete strength is crucial for planning construction operations such as form removal and application of post-tensioning forces (Carino 2004).

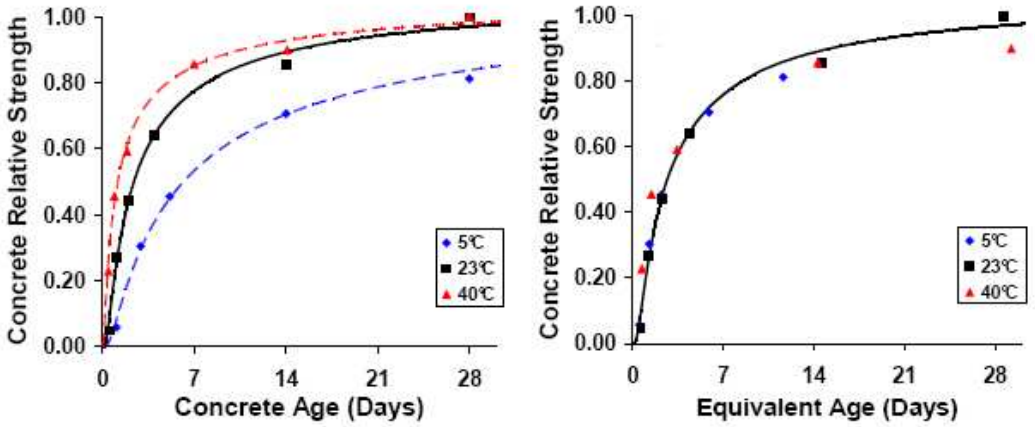

Figure 2.16: Comparison of compressive strength versus real concrete age and equivalent age for samples cured at different temperatures (Weakley 2010)

Application of the maturity method for strength prediction requires two phases: laboratory testing and field measurement of in-place temperature history. The laboratory testing phase requires two types of testing. First, the temperature sensitivity (activation energy) of the concrete mixture must be selected or determined as discussed in Section 2.6.2.1. Second, the strength-maturity relationship for the mixture must be determined by plotting the compressive strength of laboratory-cured concrete cylinders against the equivalent age at the time of testing (Carino 2004).

Friesleben, Hansen, and Pederson (1985) proposed that the strength-maturity relationship should be similar to the heat of hydration versus equivalent age relationship. This strength-maturity relationship is as follows:

$$S(M) = S_u \cdot \exp\left(-\left(\frac{\tau}{M}\right)^a\right)$$ **Equation 2.16**

where:

S(M) = strength at maturity M,

S_u = ultimate strength,

τ = characteristic time constant,

M = maturity index, and

a = shape parameter.

The ultimate strength, time constant, and shape parameter are unique for each concrete mixture. Regression analysis is used to fit Equation 2.16 to the compressive strength versus equivalent age data. After determining the strength-maturity relationship, in-place concrete strengths may be estimated based on recorded in-place concrete temperatures.

2.6.2.2.2 Setting Prediction

The maturity method may be used to account for the effect of temperature on concrete setting times. Initial and final set times are defined based on penetration resistance of a wet-sieved mortar sample according to ASTM C 403 (2006). Pinto and Hover (1999) performed research to determine the effect of curing temperature on setting time as determined by penetration resistance. Although the initial and final set times at each curing temperature varied significantly, the calculated equivalent ages did not, as shown in Figure 2.17. This was also confirmed by Wade et al. (2010), Weakley (2010)

and Pinto and Schindler (2010). From this research, it was determined that initial and final set times are primarily influenced by the hydration of the cementitious material. The setting times may be estimated for a given mixture at varying placement conditions if the apparent activation energy, temperature history, and equivalent ages at setting are known.

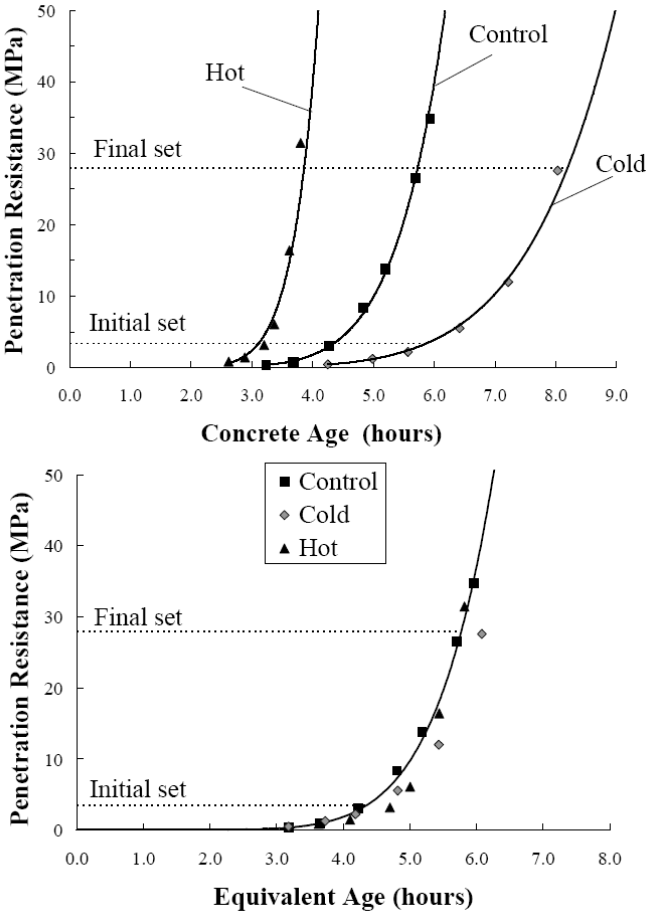

Figure 2.17: Concrete setting versus equivalent age (Wade et al. 2010)

2.7 HVFA Concrete and Sustainability

2.7.1 LEED Construction

In an effort to promote more energy-efficient and environmentally friendly construction practices, the U.S. Green Building Council instituted the Leadership in Energy and Environmental Design (LEED) program. The LEED certification system is credit-based. Under the LEED designation, construction projects are awarded credits based on performance in the following categories: Sustainable Sites, Water Efficiency, Energy and Atmosphere, Materials and Resources, Indoor Environmental Quality, and Innovation and Design Process. Based on the number of credits awarded, construction projects may be LEED certified as follows:

- LEED Certified 26 – 32 credits
- LEED Silver 33 – 38 credits
- LEED Gold 39 – 51 credits
- LEED Platinum 52 – 70 credits.

The LEED system defines fly ash as an "environmentally free post-industrial recycled material." When used in concrete, fly ash contributes to the recycled material content of the structure. Requirements for the Materials and Resources, and Innovation and Design Process categories may be fulfilled when HVFA concrete is specified for a construction project (ACI 232.2R 2003).

2.7.2 Greenroads

Similar to the LEED certification system, the Greenroads Rating System is used to rate the sustainability achieved in roadway construction projects. Greenroads is a "voluntary third-party rating system" that helps quantify the sustainable attributes of roadway and bridge projects (Muench et al. 2011). The Greenroads rating system was developed jointly by the University of Washington, CH2M Hill, and various industry groups and consultants. Currently, the Greenroads Rating System only considers the pavement system and does not consider transportation structures such as bridges, tunnels, walls, etc. (Muench et al. 2011).

There are several project requirements that must be met in order to be considered a Greenroad. Greenroad projects must also earn voluntary credits in the following categories: environment and water, access and equity, construction activities, materials and resources, and pavement technologies (Muench et al. 2011). Voluntary credits are tied to a number of points (1 to 5) based on the impact that the credit has on the sustainability of the project. Based on the project requirements and the total points achieved through voluntary credits, projects may be Greenroads certified as follows:

- Certified All project requirements plus 32 – 42 credit points
- Silver All project requirements plus 45 – 53 credit points
- Gold All project requirements plus 54 – 63 credit points
- Evergreen All project requirements plus 64 or more credit points.

Currently, the use of HVFA concrete for pavement systems may earn credits in the following Materials and Resources categories: MR-4 Recycled Materials and MR-5

Regional Materials. The Greenroads manual and information for all credits are documented at http://www.greenroads.us.

2.8 Summary

In this chapter, the use of fly ash as an SCM for portland cement concrete is reviewed. Technical information relating to the development and use of HVFA concrete is also presented. The key points from this chapter are summarized below.

The origin and properties of fly ash may be summarized as follows:

- Fly ash is a by-product of the combustion of ground or powdered coal in electrical power generating plants.
- Fly ash is classified as either Class C or Class F according to ASTM C618 (2005). Class C fly ash typically contains 15-40% CaO and is both cementitious and pozzolanic in nature. Class F fly ash typically contains less than 10% CaO, is strictly pozzolanic in nature, and has higher contents of unburned carbon. The chemical composition of the ash is a function of the coal source.
- Fly ash particles are spherical in shape. Fly ash particle size and shape are a function of the coal source, degree of pulverization before burning, combustion environment, and collection system (ACI 232.2R 2003).

Cement and fly ash hydration reactions may be summarized as follows:

- The cement hydration reaction is an exothermic process that is directly influenced by the chemical composition of the cement. Cement

hydration may be divided into two main processes: hydration of aluminates and the hydration of the calcium silicates.

- The silicate hydration reactions result in the formation of calcium silicate hydrate (C-S-H) and calcium hydroxide (CH). CH is weak and soluble.
- The pozzolanic reaction converts CH into C-S-H in the presence of water. Therefore, the durability of the hydrating cement paste is increased.
- Both the cement hydration reaction and the pozzolanic reaction are temperature dependent. An increase in hydration temperature typically results in an accelerated hydration reaction.

HVFA concrete has been defined as concrete with at least 50% fly ash by mass of cementitious materials (Malhotra and Mehta 2002). When proportioning HVFA concrete, the following concepts must be considered:

- The optimum fly ash replacement level is affected by many factors including fly ash and cement chemical composition, use of chemical admixtures, environmental conditions, strength requirements, and curing conditions.
- Low w/cm ratios are necessary to achieve adequate early-age compressive strength.
- High fly ash replacement levels retard the rate of hydration at early ages. ASTM C 494 (2005) Type C accelerating admixtures are typically used

to offset this effect and make HVFA concrete setting times comparable to conventional concrete.

- ASTM C 494 (2005) Type F and G high-range water-reducing admixtures are used in HVFA concrete to ensure adequate workability despite the low w/cm ratios required for early-age strength.

The effects of high fly ash dosage on selected fresh and hardened concrete properties may be summarized as follows:

- The use of fly ash generally reduces the water demand required for a given workability. The reduction in water demand may be attributed to the following: fly ash particles help prevent cement flocculation, reduce interparticle friction, and improve particle packing within the hydrating cement paste (Mehta 2004).
- Bleeding is typically reduced for HVFA concrete mixtures due to low water contents. Due to low bleed water and extended setting times, HVFA concrete mixtures are susceptible to plastic shrinkage cracking.
- The effectiveness of air-entraining admixtures is reduced when used in HVFA concrete because the admixture may be absorbed by the unburned carbon.
- HVFA concretes exhibit delayed setting times when compared to a control concrete with no fly ash replacement. HVFA concrete proportioned with Class C fly ashes generally exhibit longer set times

than those proportioned with Class F ashes due to the higher sulfate content of Class C ashes.

- When fly ash is used as a cement replacement, the rate of heat development and overall heat of hydration will be altered. Fly ash contribution to the overall heat of hydration is a function of the CaO content of the ash.
- Generally, as the fly ash dosage increases, early-age compressive strength values decrease. If adequate moisture is supplied, compressive strength at later ages may be higher for HVFA concrete when compared to a control concrete with no fly ash replacement. Moisture is required for fly ash to convert CH to C-S-H.

Finally, the concept of heat of hydration and the degree of hydration formulation is discussed in this chapter. Typically, the heat of hydration of a concrete mixture is decreased when fly ash is used as a cement replacement. The application of degree of hydration formulation will be discussed in further detail in Chapter 5 when the hydration model for HVFA concrete is developed. The equivalent age maturity method accounts for the effect of curing temperature on concrete setting times and compressive strength development.

Chapter 3

Laboratory Testing Program

The main objective of this research project was to provide guidance for the increased use of HVFA concrete in transportation structures. To accomplish this objective, a laboratory testing program was conducted to characterize the behavior of HVFA concrete mixtures. This chapter provides an overview of this testing program as well as discussion on raw material properties, concrete mixture proportions, concrete production, curing methods, and testing methods.

3.1 Overview of Testing Program

The main focus of this research was to expand the use of HVFA concrete by providing guidance on mixture proportioning, compressive strength development, setting time prediction, and in-place temperature development prediction to both concrete producers and transportation agencies. To accomplish this goal, a laboratory testing program was developed to quantify the effect that an increased volume fraction of fly ash has on the overall rate of hydration, setting times, and compressive strength development for a given concrete mixture at various temperatures.

Since the rate of hydration is dependent on the chemical composition of the cementitious system, two portland cement sources and four fly ash sources were investigated. The two portland cement sources varied in their alkali content, expressed as equivalent Na_2O. The "high-alkali" cement (HA) had a total alkali content of 1.04%,

whereas the “low-alkali” (LA) source had a total alkali content that ranged from of 0.53% to 0.57% based on the shipment. The four fly ash sources varied in their calcium oxide (CaO) contents, ranging from approximately 1% to 28%. Two Class C and two Class F fly ashes were selected to examine the effect that the fly ash chemical composition has on the hydration behavior and temperature sensitivity of the concrete mixture. Since the CaO content of a fly ash is largely a function of the coal source being burned, the range of CaO contents that were investigated represent the variety of fly ash sources available in the United States.

Twenty individual concrete mixtures were evaluated to examine the effect that increased volume fraction of fly ash, variation in fly ash CaO content, variation in cement alkali content, and changes in w/cm ratio have on the rate of hydration, setting behavior, compressive strength development, and temperature development of a concrete sample. Two control mixtures at w/cm ratios of 0.42 and 0.44 were completed for each cement source. The resulting four control mixtures were proportioned without the use of fly ash in the cementitious system to serve as a baseline for comparison purposes. These mixtures are representative of concrete that is commonly used in bridge deck applications in Alabama. In addition to the two control mixtures for each cement source, two concrete mixtures were completed for each fly ash source at 35% and 50% fly ash replacement by volume (w/cm ratios of 0.39 and 0.34 respectively). The fly ash mixtures were completed for each combination of cement and fly ash source leading to a total of sixteen separate HVFA concrete mixtures. In total, twenty concrete mixtures were investigated. Table 3.1 summarizes the concrete mixtures based on their w/cm ratio, cement source, and fly ash dosage.

Table 3.1: Mixture summary for each fly ash source

Cement Source	w/cm	Fly Ash Dosage
Low-Alkali Cement	0.42	0%
	0.44	0%
	0.39	35%
	0.34	50%
High-Alkali Cement	0.42	0%
	0.44	0%
	0.39	35%
	0.34	50%

The combined effect of temperature and fly ash replacement on the rate of hydration was also investigated. Therefore, each of the twenty concrete mixtures was batched at the following three temperatures: 40 °F, 73 °F, and 105 °F (5 °C, 23 °C, and 40 °C). The hot (105 °F) and cold (40 °F) batching temperatures were selected to simulate the extreme upper and lower limits associated with concreting during the summer and winter months. By completing a mixture at all three temperatures, the temperature sensitivity of that particular mixture could be quantified.

The laboratory testing program may be separated into the following two phases:

1. Phase I: Hydration and setting time study, and
2. Phase II: Study of compressive strength development.

During Phase I, the temperature sensitivity of each mixture was determined by calculating the activation energy (E). This was achieved by performing isothermal calorimetry on wet-sieved mortar samples for each mixture at the three batching temperatures (40 °F, 73 °F, and 105 °F). The initial and final setting times were also determined according to ASTM C 403 (2008) for each batch to quantify the effect of

mixing temperature on setting times. The equivalent ages for the initial and final setting times from each of the three batching temperatures were also calculated. Also during Phase I, semi-adiabatic calorimetry (SAC) testing was performed for each room temperature (73 °F) batch to determine the heat of hydration development of the HVFA concrete mixtures. SAC was also used to characterize the hydration development of each mixture through calculation of the hydration parameters: τ (time parameter), β (shape parameter), and α_u (ultimate degree of hydration). The results from Phase I (calculated activation energies and semi-adiabatic test results) were used to develop a hydration model for prediction of the hydration parameters (τ, β and α_u) for HVFA concrete mixtures.

Phase II consisted of compressive strength testing for each concrete mixture batched at room temperature. For each mixture, a strength-maturity relationship was determined using the activation energy calculated in Phase I along with the measured temperature history of the specimens and their recorded compressive strengths. In addition to developing strength-maturity relationships for all mixtures, quality-control cylinders were prepared from each hot and cold batch. The quality-control cylinders were tested at 28 days and compared to the room temperature results for that batch to ensure that the concrete was produced consistently at all three batching temperatures.

After developing the HVFA concrete hydration model, the results from Phases I and II were combined to evaluate the in-place performance of HVFA concrete when placed in selected transportation structures. The ConcreteWorks software program was used to estimate in-place temperature profiles for HVFA concrete mixtures placed under varying placement conditions. The placement conditions were varied by environmental

conditions and concrete element type. Based on the in-place temperature profiles, the maximum in-place temperature, time to reach initial set, and compressive strength development could be determined for each HVFA concrete mixture. Using these results, the effect of fly ash dosage, fly ash type, placement conditions, and concrete element type on the in-place performance of HVFA concrete could be evaluated. The results from the ConcreteWorks analysis were designed to provide guidance on mixture proportioning and fly ash selection for HVFA concrete. A review of these results will be detailed in Chapter 6. An overview of the testing program described previously is presented in Figure 3.1.

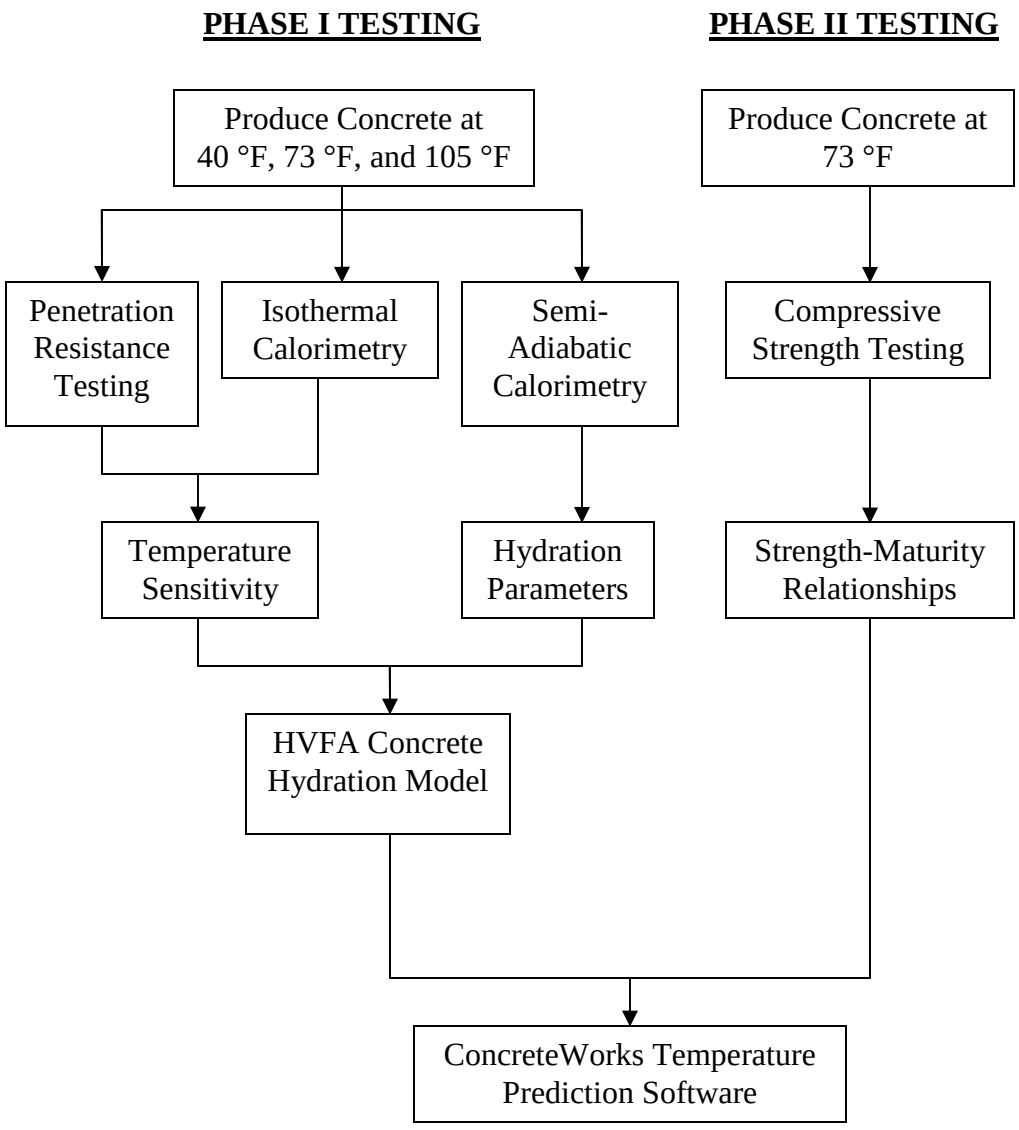

Figure 3.1: Testing program overview

3.2 Mixture Proportions

Twenty different concrete mixtures (two control mixtures and eight fly ash mixtures per cement source) were used to quantify the effect of fly ash CaO content, fly ash dosage, and cement alkali content on the hydration and temperature development,

setting times, and strength development of HVFA concrete. The nomenclature used for both the control and fly ash concrete mixtures throughout this thesis is shown below:

Control:

Mix ID	w/c Ratio	Cement Source	Fresh Concrete Temperature
↑	↑	↑	↑
CTRL	0.42	Low-alkali (LA)	73 °F (Room)
	0.44	High-alkali (HA)	40 °F (Cold)
			105 °F (Hot)

Example: **CTRL44 – LA – 73F**, represents the control concrete mixture with a w/c ratio equal to 0.44 batched at 73 °F.

Fly Ash:

Cement Source	Fly Ash Dosage	CaO Content	Fresh Concrete Temperature
↑	↑	↑	↑
Low-alkali (LA)	35%	1%	73 °F
High-alkali (HA)	50%	15%	40 °F
		24%	105 °F
		28%	

Example: **LA – 35FA – 15% - 40F**, represents the HVFA concrete mixture with a 35% dosage of the 15% CaO fly ash batched at 40 °F.

The control mixture selected for this research has similar proportions to concrete routinely used for bridge deck applications. To evaluate the effect of fly ash type, fly ash dosage, and cement alkali content on hydration development, each of the HVFA concrete mixtures were proportioned by only changing the variable under consideration. Water-

reducing admixture dosages were adjusted per mix to control workability. A target slump range of 2 to 7 in. was selected for all room temperature mixtures. A mid-range water-reducing admixture was used for all control mixtures. Due to low w/cm ratios, a high-range water-reducing (HRWR) admixture was used to provide adequate workability for all HVFA concrete mixtures.

Research conducted by Ravina and Mehta (1986) indicates that concrete proportioned with high fly ash dosages will experience delayed set times when compared to a control concrete with no fly ash replacement. Results from this research are presented in Section 2.5.2.4. Based on these results, an accelerating admixture was used for all HVFA concrete mixtures. The accelerating admixture dosages were selected with the goal of producing HVFA concrete mixtures that possess similar setting times to the control mixtures. The admixture supplier (W.R. Grace) recommended that accelerating admixture dosages of 15 oz/cwt and 30 oz/cwt be used for the 35% and 50% fly ash mixtures, respectively.

When proportioning HVFA concrete, Bilodeau et al. (2001) report that "the proportion of fly ash should be as high as possible and the water-cementitious materials ratio as low as possible to provide adequate early-age strength and durability." A preliminary mortar cube study was conducted to determine the w/cm ratios required to provide adequate early age strength (4 to 7 days) for the 35% and 50% fly ash mixtures. For this study, 2 in. mortar cubes were prepared with varying w/cm ratios for each fly ash dosage. The cubes were tested for compressive strength according to ASTM C 109 (2007). Based on the results from this study, it was determined that the w/cm ratios should be 0.34 and 0.39 for the 50% and 35% fly ash mixtures, respectively.

All of the fly ash mixtures were proportioned to have the same paste volume as the control mixes; therefore, small adjustments were made to the fine aggregate proportions due to variations in the specific gravities of the fly ash sources. The adjustments made to the fine aggregate volumes were considered negligible. Mixture proportions for each of the twenty mixtures are given in Table 3.2. All batch weights for the aggregate are given at a saturated surface-dry (SSD) state. Also, the HRWR admixture dosages are given for both LA cement and HA cement mixtures. The LA cement dosages are given first, followed by the HA cement dosages in parentheses for each mixture.

Table 3.2: Mixture proportions

Item	CTRL42	CTRL44	35FA-1%	35FA-15%	35FA-24%	35FA-28%	50FA-1%	50FA-15%	50FA-24%	50FA-28%
Water (lb/yd^3)	260	266	239	243	247	246	217	223	227	228
Cement (lb/yd^3)	620	603	445	438	434	431	378	369	363	360
Fly Ash (lb/yd^3)	-	-	166	185	195	200	260	289	303	310
Coarse Aggregate (lb/yd^3)	1920	1920	1920	1920	1920	1920	1920	1920	1920	1920
Fine Aggregate (lb/yd^3)	1210	1210	1199	1198	1198	1198	1182	1180	1179	1181
Water-Reducing Admixture (oz/cwt)	6 (9)	4 (9)	3 (9)	1 (2)	0 (1)	1 (2)	4 (6)	2 (5.5)	4 (5)	1 (2)
Accelerating Admixture (oz/cwt)	-	-	15				30			
w/cm	0.42	0.44	0.39				0.34			
Fly Ash Dosage (by Volume)	-	-	35%				50%			

Note: No mixtures are air-entrained. Water-reducing admixture dosages were adjusted to produce target slump of 2 to 7 in. Water-reducing admixture dosages presented in parentheses represent dosages used for HA cement mixtures.

3.3 Raw Material Properties

To eliminate variations during testing due to differences in material properties, a single source of each material was used for the full duration of laboratory testing. The source and properties of the portland cement, fly ash, aggregates, and admixtures are discussed in the following sections.

3.3.1 Portland Cement

As was discussed previously, two cement sources with different total alkali contents were used during this research. The Type I/II "low-alkali" (LA) cement used for concrete testing was supplied by Lafarge North America from their Sugar Creek, Missouri plant. The Type I "high-alkali" (HA) cement, however, was supplied by W.R. Grace. The chemical compounds for each cement were computed according to ASTM C114 (2006) by an outside laboratory. The free lime content and Blaine fineness values were supplied by the producers. The Lafarge cement was received in two separate shipments corresponding to two separate production periods, denoted LA Cement (1) and LA Cement (2). A summary of the chemical composition for each cement as received from the independent laboratory is shown in Table 3.3.

Table 3.3: Cement properties

Parameter	HA Cement	LA Cement (1)	LA Cement (2)
Tricalcium Silicate, C_3S (%)	52.51	56.33	60.40
Dicalcium Silicate, C_2S (%)	15.73	15.24	11.80
Tricalcium Aluminate, C_3A (%)	12.45	8.15	7.70
Tetracalcium Aluminoferrite, C_4AF (%)	6.43	8.95	9.04
Free CaO (%)	0.58	1.35	1.35
Sulfur Trioxide, SO_3 (%)	3.84	3.15	2.99
Magnesium Oxide, MgO (%)	2.63	1.62	2.04
Equivalent Alkali, Na_2O_{eq} (%)	1.04	0.53	0.57
Blaine Fineness (m^2/kg)	369	396	396

3.3.2 Fly Ash

Four fly ash sources, two Class C and two Class F, were selected for testing. These fly ash sources were selected from across the United States to capture the range of fly ashes available to the concrete industry. For this project, the four sources were differentiated based on their calcium oxide (CaO) content. Table 3.4 lists the four fly ash sources and identifies the supplier and location of the coal-fired power-generation plant.

Table 3.4: Fly ash source information

Fly Ash ID	Supplier	Plant Name	Location
FA-28	Headwaters Resources	Burlington	Burlington, New Jersey
FA-24	Lafarge North America	Muskogee	Fort Gibson, Oklahoma
FA-15	Boral	Big Brown	Fairfield, Texas
FA-1	ProAsh	Brandon Shores	Baltimore, Maryland

The four fly ash sources have varying chemical compositions based on the type of coal burned during their production. The chemical analysis results and specific gravity values for each of the fly ash sources as received from an independent laboratory are presented in Table 3.5. All testing was completed according to ASTM C 311 (2006).

Table 3.5: Fly ash properties

Parameter	FA-28	FA-24	FA-15	FA-1
Calcium Oxide, CaO (%)	27.08	23.07	15.34	1.01
Silicon Dioxide, SiO_2 (%)	35.64	39.17	51.61	59.56
Aluminum Oxide, Al_2O_3 (%)	15.88	18.48	20.16	27.30
Iron Oxide, Fe_2O_3 (%)	6.47	7.06	4.83	5.02
Magnesium Oxide, MgO (%)	6.45	5.04	3.05	1.06
Sulfur Trioxide, SO_3 (%)	2.14	1.24	0.71	0.05
Sodium Oxide, Na_2O (%)	2.19	1.56	0.88	0.42
Potassium Oxide, K_2O (%)	0.42	0.66	0.90	2.53
Equivalent Alkali, Na_2O_{eq} (%)	2.47	1.99	1.47	2.08
Loss on Ignition (%)	0.35	0.17	0.23	0.17
Specific Gravity	2.71	2.63	2.47	2.17

3.3.3 Aggregate

The fine aggregate used for this project was natural siliceous river sand. This sand was acquired from the Shorter Sand and Gravel Pit located in Mt. Meigs, Alabama. At the beginning of the testing program, samples were taken from both the coarse and fine aggregate sources to determine the aggregate gradation, bulk specific gravity, and absorption capacity per ASTM C 136 (2006) and ASTM C 128 (2007). The gradation for

the Shorter sand as well as the upper and lower gradation limits as specified in ASTM C 33 (2003) are presented in Figure 3.2.

The coarse aggregate selected for this project was a No. 67 river gravel. This aggregate was also acquired from the Shorter Sand and Gravel Pit in Mt. Meigs, Alabama. Similar to the fine aggregate, the gradation, bulk specific gravity, and absorption capacity for this aggregate source was determined at the beginning of the laboratory testing period. The coarse aggregate gradation as well as the upper and lower limits for a No. 67 gradation according to ASTM C 33 (2003) are presented in Figure 3.3. Both aggregates met the gradation requirements of ASTM C 33. The bulk specific gravity and absorption capacity values determined for each aggregate are presented in Table 3.6.

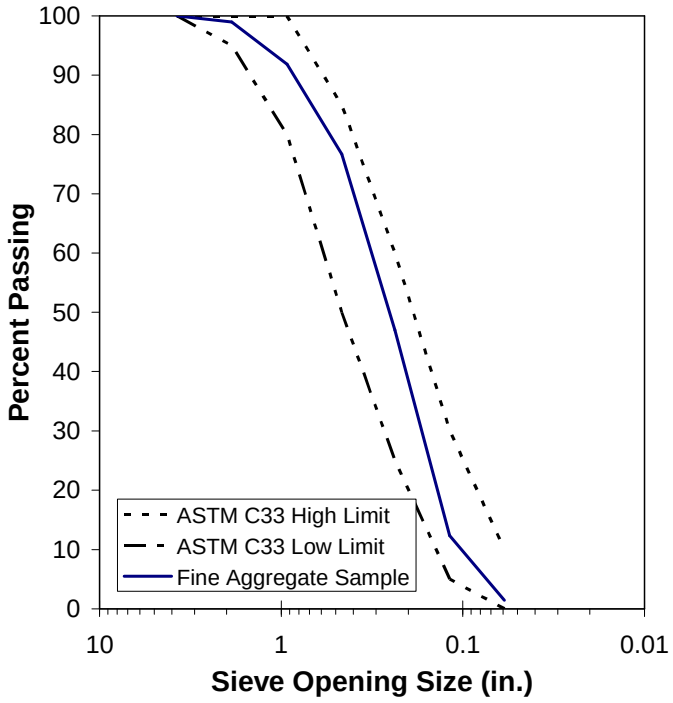

Figure 3.2: Fine aggregate gradation

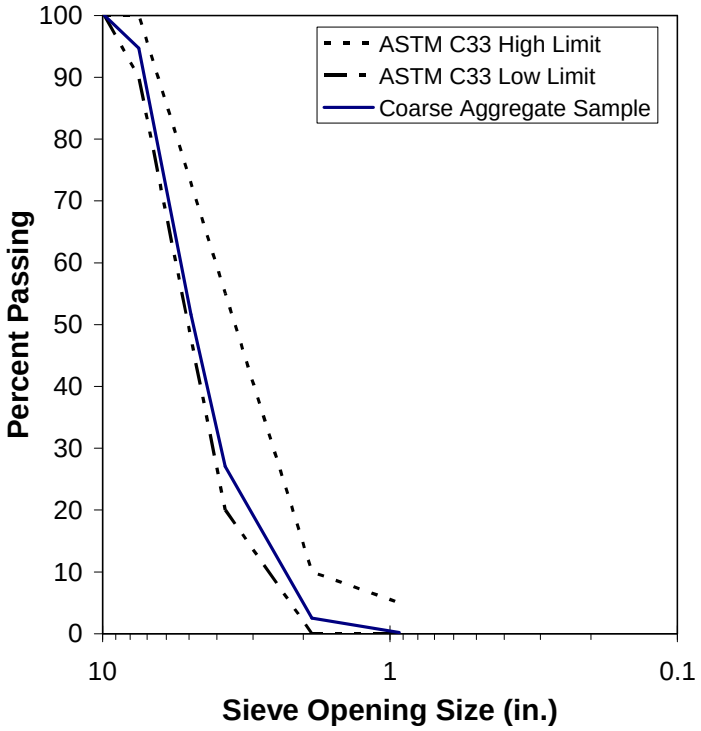

Figure 3.3: Coarse aggregate gradation

Table 3.6: Bulk specific gravity and absorption capacity values for aggregates

Material	Bulk Specific Gravity	Absorption Capacity (%)
No. 67 River Gravel	2.64	0.52
Natural Siliceous River Sand	2.61	0.41

3.3.4 Chemical Admixtures

Water-reducing admixtures were used during the laboratory testing to help control the workability of both the control and fly ash mixtures. A mid-range water-reducing admixture was used for all control concrete mixtures, whereas a high-range water-reducing (HRWR) admixture was used for all HVFA concrete mixtures. Also, an accelerating admixture was used for all HVFA concrete mixtures with the goal of producing HVFA concrete with set times comparable to the control mixtures. All

admixtures were supplied by W.R. Grace. The combined use of the specific HRWR admixture and accelerating admixture was recommended by W.R. Grace.

For the control mixtures, ADVA 140M was used to achieve adequate workability. The use of this admixture was required due to the selected w/cm ratios as well as the lack of entrained air. ADVA 140M is classified according to ASTM C 494 (2005) as a Type A and Type F chemical admixture. For this research, the dosage levels used correspond to a mid-range water-reducing admixture. The ADVA 140M dosages for each control mixture are shown in Table 3.2.

For the 35% and 50% fly ash dosage mixtures, both a HRWR admixture, Advacast 575, and an accelerating admixture, Daraset HES, were used. Advacast 575 is a polycarboxylate-based Type F chemical admixture. The Advacast 575 dosages for each fly ash mixture are given in Table 3.2.

Daraset HES meets the requirements of ASTM C 494 as a Type C chemical admixture, and was used to increase the rate of hydration for the HVFA mixtures. Daraset HES is a non-corrosive, non-chloride admixture. The accelerator dosages were kept constant at 15 oz/cwt for all 35% fly ash mixtures and 30 oz/cwt for all 50% fly ash mixtures, regardless of the batching temperature.

For this research, no air-entraining admixtures were used due to their temperature-dependent behavior and possible incompatibility with low-calcium fly ash sources.

3.4 Concrete Production

For each of the concrete mixtures, a 3.5 ft^3 (0.099 m^3) batch was produced at room temperature (73 °F). From each room temperature batch, cylinders were cast for

compressive strength and semi-adiabatic calorimetry testing. Also, mortar was wet-sieved to provide setting test and isothermal calorimetry samples. In addition to the batches produced at room temperature, a 1.5 ft^3 (0.042 m^3) batch was produced for each mixture at both the hot and cold batching temperatures. For each of these batches, mortar was wet-sieved to provide setting and isothermal calorimetry samples. Quality control cylinders were also cast for each hot and cold batch. The batching and mixing procedures described in the following sections were followed for each concrete mixture that was produced to provide for consistent, reproducible results.

3.4.1 Batching

All materials were batched approximately one day before concrete production. At this time, the batch weights were approximated and all necessary materials were stored in 5-gallon buckets. Tight-fitting lids were placed on each bucket to prevent moisture-loss during storage. For the room temperature batches, the materials were left in the ambient conditions of an air-conditioned laboratory, approximately 73° F (23° C) until moisture corrections were completed. For the hot and cold batches, however, the materials were stored in an insulated temperature-controlled environmental chamber. The environmental chamber was used to simulate hot and cold weather concreting conditions. To counteract the effect of mixing at ambient conditions, the materials for the hot and cold batches were over-heated and over-cooled to achieve the desired fresh concrete temperatures of 105 and 40 °F, respectively. For the hot batches, the environmental chamber was set to 120° F (49 °C), whereas, it was set to 32 °F (0° C) for the cold batches. Images of the

environmental chamber and temperature control unit used for the duration of this project are presented in Figure 3.4.

Figure 3.4: Environmental chamber used for all hot and cold testing

Moisture corrections were completed according to ASTM C 566 (1997) for all batches on the morning of mixing. Representative samples for both the fine and coarse aggregate were weighed, heated until all moisture was removed, and re-weighed to determine the moisture content to be used for determination of final batch weights. After completing the moisture corrections, the batch weights were adjusted and chemical admixtures were batched.

3.4.2 Mixing Procedure

For each batch, the concrete mixing procedure set forth in ASTM C 192 (2007) was followed. All room temperature batches were completed using a mixer with a total volume of 12 ft^3 (0.34 m^3). The hot and cold batches, however, were completed with a concrete mixture with a total volume of 6 ft^3 (0.17 m^3). The two mixers are shown in Figure 3.5.

Figure 3.5: Concrete mixers

Before mixing, a mixture of fine aggregate, cement, and water was used to "butter" the concrete mixer. This "butter" was proportioned at approximately 2:1 fine aggregate to cement. Water was added until the inside of the mixer was evenly coated. All excess mortar was then removed before the materials were added.

After "buttering" the mixer, all aggregate was added by alternating between coarse and fine aggregate buckets. After adding all aggregate, approximately 80 % of the

mixing water was added, and the mixer was started. For the HVFA concrete mixes, the accelerating admixture was added with 80 % of the water. After approximately two minutes of mixing, the mixer was stopped and all cementitious material, remaining admixtures, and the final 20 % of water was added. At this point, the concrete was mixed for three minutes. After three minutes of mixing, the concrete was allowed to rest for three minutes. Following the rest period, the concrete was mixed for an additional two minutes. In order to reduce heat loss or gain during the mixing process, a lid was used to cover the mixer during all mixing phases. At the end of the "three-three-two" mixing sequence, concrete fresh properties were measured. If the concrete was deemed adequate, the necessary samples were obtained and testing was completed.

3.5 Testing Methods

As was described earlier, the testing for this project was broken into two phases. In the first testing phase, the activation energy was calculated for each mixture based on isothermal calorimetry results collected at each of the three batching temperatures. Also, initial and final set times were determined for each batch and the equivalent age corresponding to the initial and final set times were calculated. Finally, SAC testing was completed to characterize hydration development for each concrete mixture.

Phase II consisted of developing strength-maturity relationships for each of the mixtures. To do this, the activation energies from Phase I were used along with the recorded temperature history of the cured compressive strength specimens. The following sections describe the test apparatus and procedure that were followed to complete the requirements of Test Phases I and II.

3.5.1 Fresh Concrete Properties Testing

For each batch, the following fresh concrete tests were performed:

- slump ASTM C 143 (2008),
- unit weight ASTM C 138 (2008),
- temperature ASTM C 1064 (2008), and
- air content ASTM C 231 (2004).

Fresh concrete testing was performed immediately following the mixing procedure described previously. For all batches, the tests were performed under the laboratory ambient conditions. After performing each of the fresh tests noted above, samples for penetration resistance testing, isothermal calorimetry, semi-adiabatic calorimetry, and compressive strength testing were collected.

3.5.2 Penetration Resistance Testing

Initial and final set times for each batch were determined by penetration resistance testing according to ASTM C 403 (2006). According to ASTM C 403, penetration resistance results are to be obtained using an upright penetrometer and a standard set of proctor needles. The testing apparatus and sample mortar can used throughout this project can be seen in Figure 3.6. The mortar sampling can used for the duration of this project was aluminum with a tight-fitting lid. The sampling can dimensions were 7.5 in. (190.5 mm) in diameter and 6 in. (152.4 mm) in height.

Mortar was wet-sieved for the sampling can samples immediately after the fresh concrete testing was completed. The concrete was sieved through a No. 4 sieve (4.75 mm) with the aid of a vibrating table. When the sampling can was full, the mortar was

consolidated with a vibrating table, and temperature recording was started with a maturity meter and Type T thermocouple wire. Although sieving for all mixture temperatures was completed in the ambient conditions of the lab, all hot and cold batch setting tests were conducted in the environmental chamber set to their respective batching temperature. Penetration measurements were recorded according to the specifications of ASTM C 403.

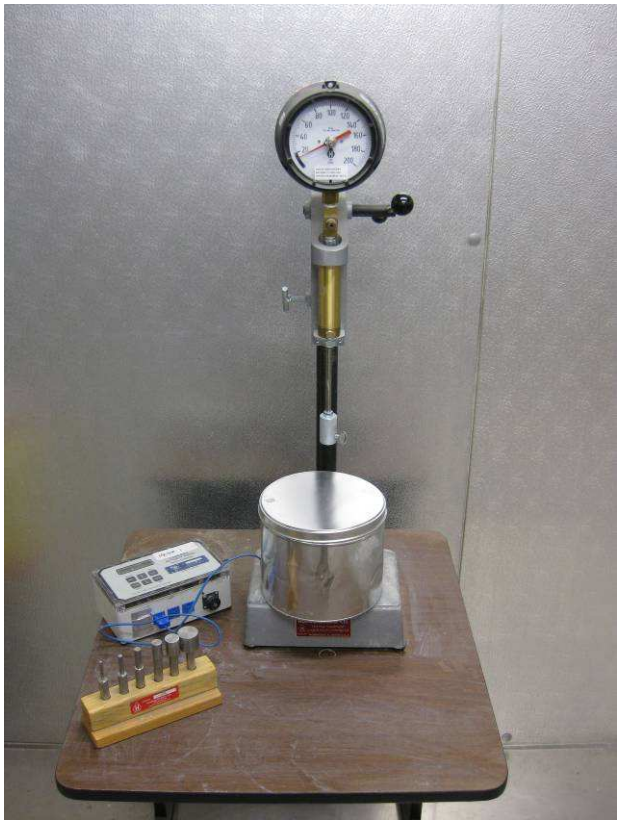

Figure 3.6: Penetrometer with mortar sample for set time determination

The maturity meter shown in Figure 3.6 was used to record the mortar temperatures throughout penetration resistance testing. The maturity meter recorded the mortar temperature at 30-minute increments for the duration of setting testing. A wooden dowel was fastened vertically inside each container to support the thermocouple wire as seen in Figure 3.7. With the recorded temperature history of the mortar samples, the

initial and final set times could be converted to equivalent age, and the best-fit activation energy could be back-calculated.

Figure 3.7: Mortar set can and thermocouple set-up

3.5.3 Isothermal Calorimetry

In addition to wet-sieving mortar for the penetration resistance testing, mortar samples for each batch were also collected for isothermal calorimetry testing. Isothermal calorimetry was used to calculate the activation energy for each of the mixtures. For isothermal calorimetry testing, the mortar sample was allowed to hydrate under a constant temperature. The heat required to maintain this temperature was then recorded.

For this project, the AdiaCal TC unit manufactured by W.R Grace and Company was used for all isothermal calorimetry. The AdiaCal TC unit has eight separate cells for testing. This unit can be seen in Figure 3.8.

The isothermal calorimeter was set to the appropriate batching temperature approximately 24 hours before testing so that it could reach equilibrium. Similar to the set test samples, the mortar samples for isothermal calorimetry were wet-sieved through a

No. 4 sieve (4.75 mm) immediately following fresh concrete testing. The mortar was placed in 2 in. (5 cm.) diameter plastic containers and weighed as quickly as possible to reduce the amount of heat lost or gained. After weighing, the sample was placed in the calorimeter and the data acquisition for that cell was started. All samples were tested for 72-94 hours, depending on mixing temperature, to ensure that all significant hydration was captured.

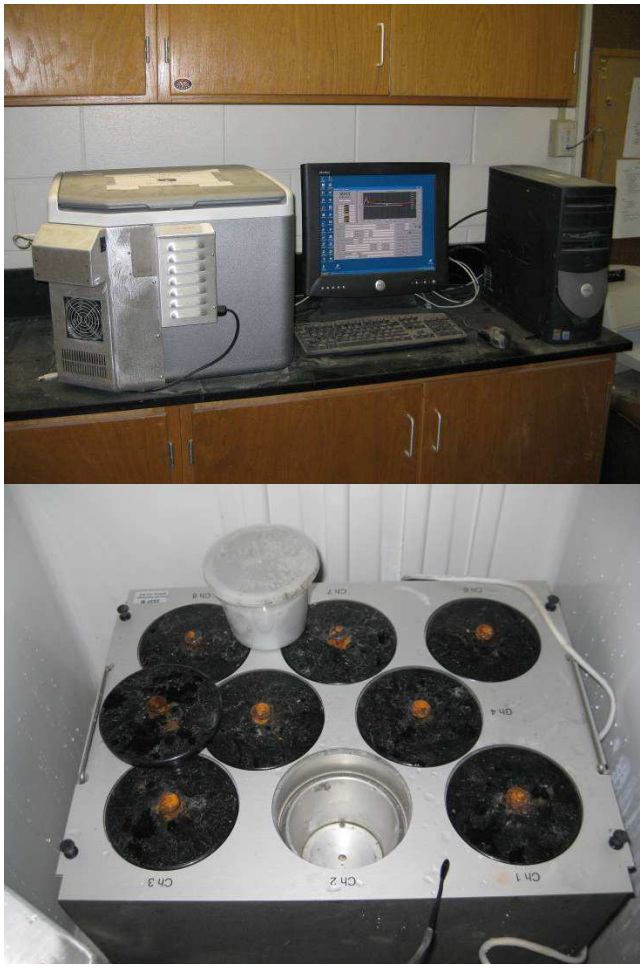

Figure 3.8: Adiacal TC isothermal calorimeter

3.5.4 Semi-Adiabatic Calorimetry

Semi-adiabatic calorimetry (SAC) testing was completed for each batch to measure the heat of hydration. Based on the SAC testing results, the hydration parameters could be calculated for each mixture. The following paragraphs provide a brief description of the calorimeter used for all SAC testing.

Calorimeter I is shown in Figure 3.9. This calorimeter is referred to as an iQdrum device and is manufactured by Digital Site Systems, located in Pennsylvania. The iQdrum calorimeter accommodates one concrete sample (4x8 or 6x12 cylinder). For this project, 6x12 cylinders were used for all iQdrum testing. The sample is insulated on all sides. Each of the three iQdrum calorimeters that were used during testing was calibrated to determine correction factors to be applied during data analysis.

Figure 3.9: Calorimeter I – iQdrum

Temperature measurements were recorded by inserting a Type T thermocouple directly into the concrete sample, as shown in Figure 3.10. The thermocouple was covered with a plastic sleeve before inserting it into the concrete to allow for easy removal at the end of testing and ultimately extend the life of the thermocouple sensor. A flux sensor and ambient temperature sensor are located within the unit and take recordings at the same interval as the thermocouple. A sampling rate of 15 min. was selected.

Figure 3.10: iQdrum sample

Approximately 24 hours before mixing, the calorimeter was opened and previous samples were removed to allow the device to reach equilibrium with the surrounding laboratory environment. When testing the hot and cold batches, an "equilibrium" sample that had been conditioned to the batching temperature in the environmental chamber was placed in the calorimeter approximately one hour before testing to allow the device to be as close to the fresh concrete temperature as possible. SAC testing was conducted for at least five days after mixing. For each batch, the cylinders for semi-adiabatic testing were

cast and placed within the calorimeters as quickly as possible to minimize the amount of heat loss or gain from the specimen.

3.5.5 Compressive Strength Testing and Curing Methods

After measuring the fresh concrete properties and preparing samples for calorimetry and penetration resistance testing, cylinders were cast for compressive strength testing according to ASTM C 192 (2007). Cylinders were consolidated by rodding unless the slump was less than 1 in. (25 mm). For concrete in which the slump was less than 1 in. (25 mm), cylinders were consolidated with the use of the vibrating table. After finishing was complete, each cylinder was capped with a plastic lid to protect against moisture loss. The cylinders were left undisturbed in the laboratory for the first 24 hours.

Approximately 24 hours after mixing, the cylinders were de-molded, labeled, and transported to the moist-curing room. The moist-curing room was kept at a constant temperature of 73 °F (23 °C) and 100% relative humidity.

For each of the room temperature batches, twenty-five 4x8 cylinders were cast for compressive strength testing. Also, one cylinder was cast from each room temperature batch to collect temperature versus time data for the duration of curing. These data were collected with the use of a maturity meter with a thermocouple embedded within the center of the cylinder. The cylinders for all room temperature batches were moist-cured until testing. Compressive strength testing was completed at the following concrete ages: 12 hours, 1 day, 2 days, 4 days, 7 days, 14 days, 28 days, and 56 days. At each test age, three cylinders were tested for compressive strength according to ASTM C 39 (2004).

The compressive strength testing results and recorded cylinder temperature histories were used to develop strength-maturity relationships for each concrete mixture.

For each of the hot and cold batches, three quality control 4x8 cylinders were cast. These cylinders were continuously moist-cured until testing at 28 days. All compressive strength testing was conducted according to ASTM C 39 (2004).

Chapter 4

Presentation of Results

In this chapter, results from the laboratory testing program described in Chapter 3 are presented and reviewed. First, the fresh concrete properties are presented for all room temperature (73 °F) batches. After reviewing the fresh concrete properties, the results from Phases I and II are presented. The results from Phases I and II are applied in Chapters 5 and 6 for the development of the HVFA concrete hydration model and evaluation of the in-place performance of HVFA concrete. A summary of all data collected for each concrete mixture at each of the three batching temperatures may be found in Appendices A through D. The nomenclature used in the remainder of this document is consistent with the description provided in Section 3.2.

4.1 Fresh Concrete Properties

Standard fresh concrete properties (slump, air content, and unit weight) were determined for each batch of concrete immediately following the mixing procedure outlined in Section 3.4.2. The fresh concrete testing results are presented in Figures 4.1 through 4.6 for all 73 °F batches.

All room temperature (73 °F) concrete mixtures were produced with a target slump range of 2 in. to 7 in. The slump results for 73 °F low-alkali (LA) cement and high alkali (HA) cement batches are presented in Figures 4.1 and 4.2, respectively.

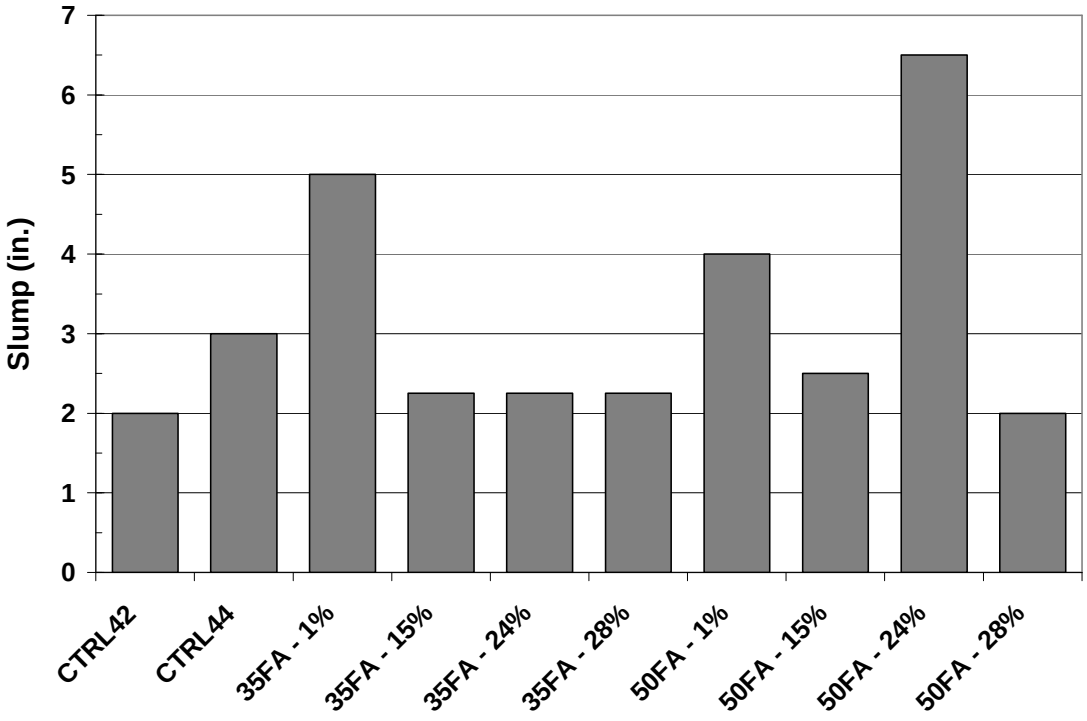

Figure 4.1: LA cement – 73 °F slump results

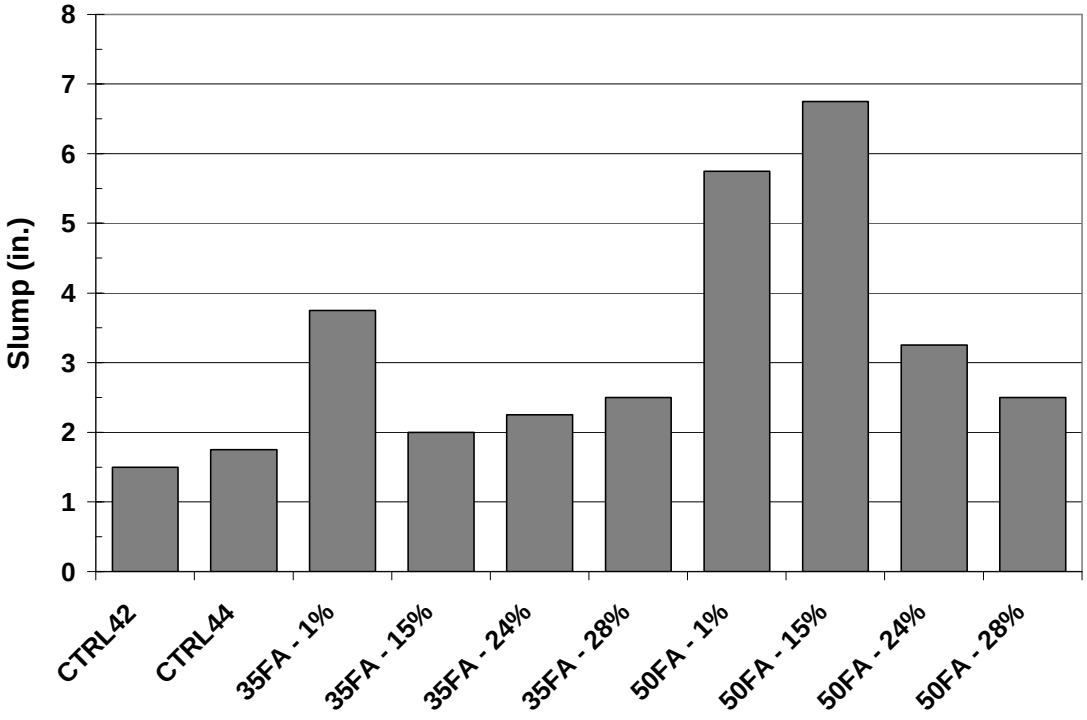

Figure 4.218: HA cement – 73 °F slump results

In Figures 4.1 and 4.2, it is shown that all room temperature batches had slumps within the desired range, with the exception of the following two mixtures: CTRL42-HA and CTRL44-HA. The concrete for these batches exhibited acceptable workability, despite the slump results being lower than the desired minimum. When batching each mixture at the hot (105 °F) and cold (40 °F) temperatures, the admixture dosages were kept constant. Therefore, variations in slump due to mixing temperature were observed. For all mixtures, the slump decreased with an increase in mixing temperature and increased with a decrease in mixing temperature. The slump results for all hot and cold batches are summarized in Appendix A. When producing concrete cylinders for mixtures with slump results less than one inch, consolidation was achieved by vibration rather than rodding, per ASTM C 192 (2007).

The air content and unit weight were determined for each concrete batch according to ASTM C 138 (2008). The results for all 73 °F batches are presented in Figures 4.3 through 4.6. For this project, no air-entraining admixtures were used due to their temperature-dependent behavior and possible incompatibilities with low-calcium fly ashes. The design air content for all mixtures was 2%. This air content was determined based on the No. 67 river gravel used as coarse aggregate. All 73 °F batches had air contents ranging between 2.5 and 3.5%. Similar to the slump results, variations in air content and unit weight occurred according to mixing temperature. Both slump and air content increased with a decrease in mixing temperature. The air content and unit weight results for all hot and cold batches are summarized in Appendix A.

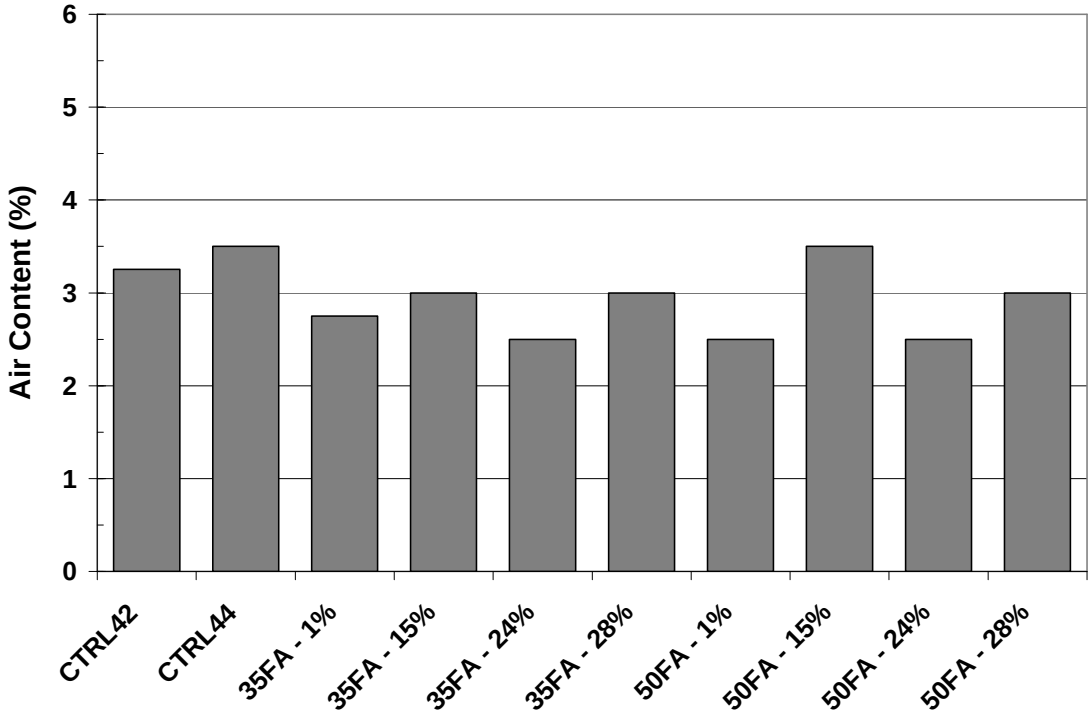

Figure 4.3: LA cement – 73 °F air content results

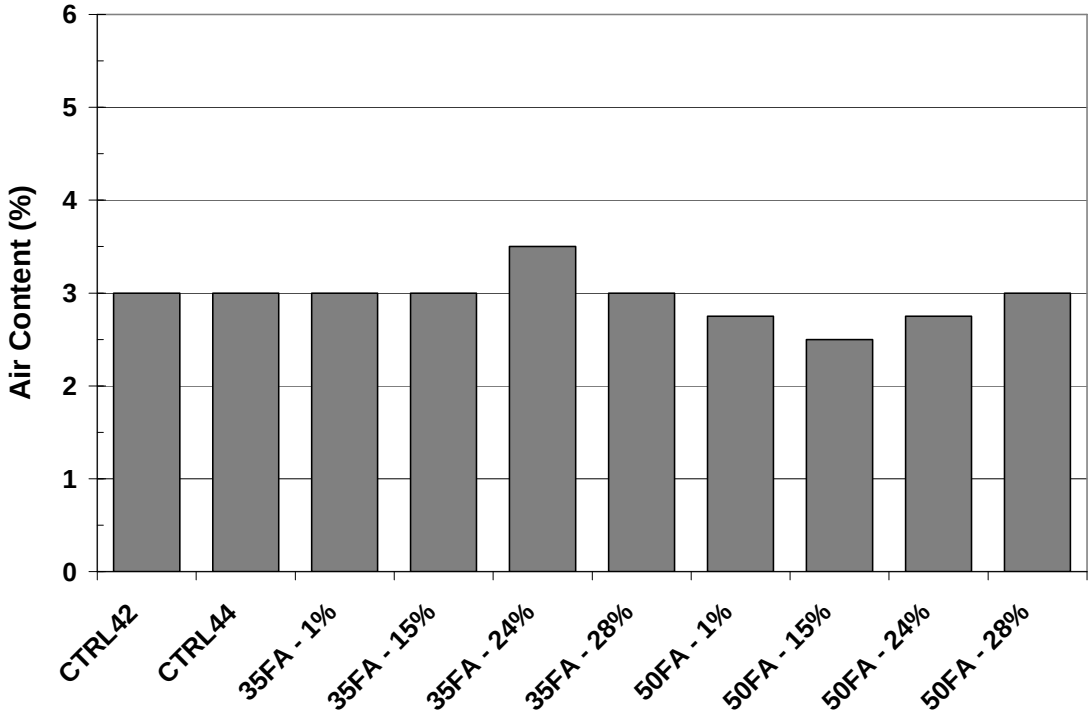

Figure 4.4: HA cement – 73 °F air content results

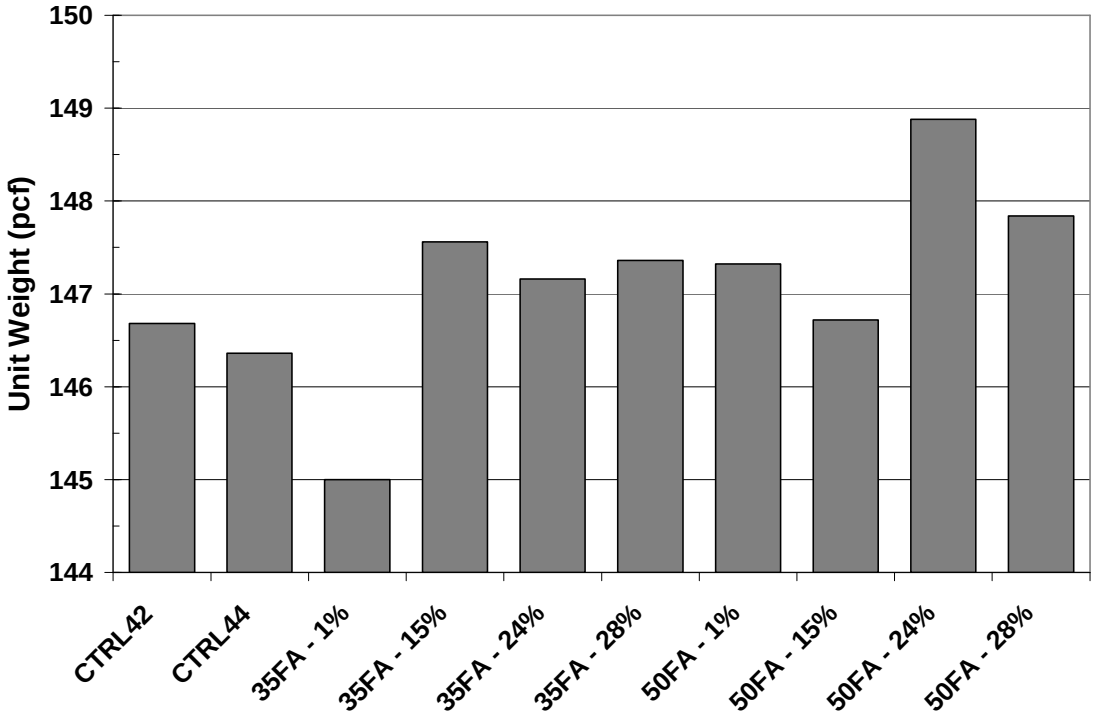

Figure 4.5: LA cement – 73 °F unit weight results

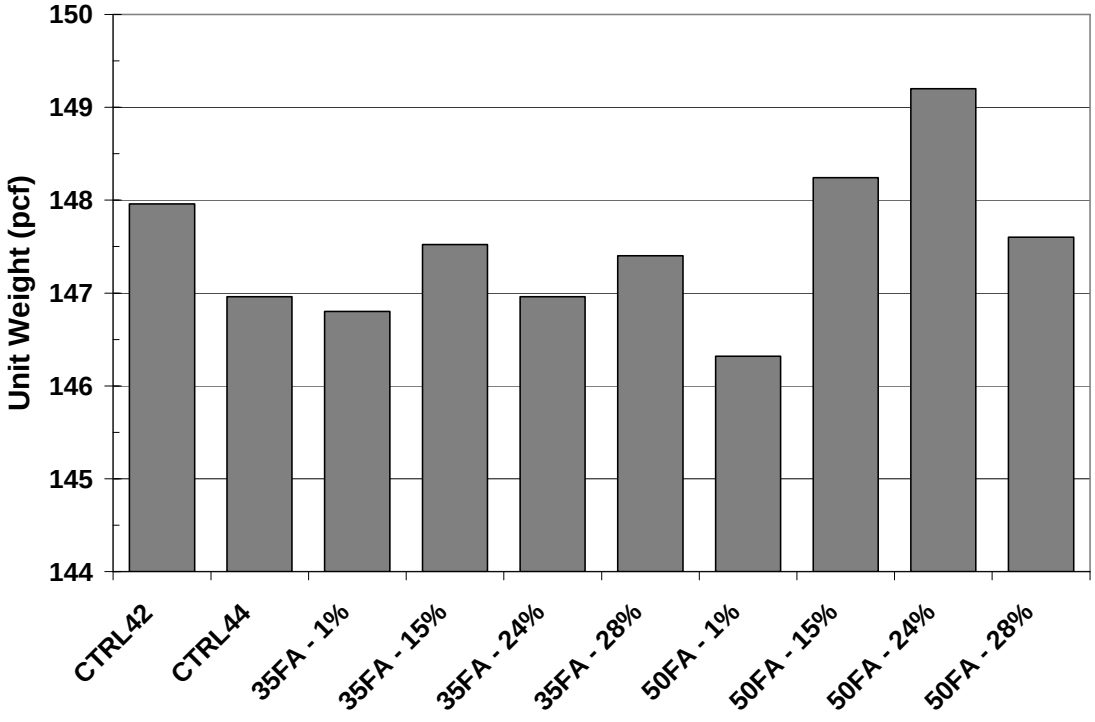

Figure 4.6: HA Cement – 73 °F unit weight results

4.2 Phase I Testing Results

4.2.1 Set Times from Penetration Resistance Testing

Initial and final set times were determined for all concrete batches according to ASTM C 403 (2006). As described in Section 3.5.2, a mortar sample was wet-sieved from the fresh concrete immediately following fresh concrete testing, and penetration resistance testing was completed at the respective mixing temperatures. A maturity meter was used to record the mortar temperature for the duration of the test. According to ASTM C 403 (2006), initial set and final set are defined as the times when the penetration resistance is equal to 500 psi and 4000 psi, respectively. To determine the initial and final set times for each concrete mixture, the penetration resistance data were plotted versus concrete age. Regression analysis was then performed to fit a power function to the data, as per ASTM C 403 (2006).

In the following four sections, the effect of fly ash dosage, fly ash CaO content, cement alkali content, and mixing temperature on the setting times of HVFA concretes will be investigated. For all penetration resistance plots presented in this chapter, the solid lines represent the best-fit power curves obtained from regression analysis. Also, data markers are used to differentiate between the mixtures, and do not represent actual test points, unless otherwise indicated.

4.2.1.1 Effect of Fly Ash Dosage on Set Time

In Figures 4.7 and 4.8, penetration resistance plots are presented for all 73 °F batches completed with the LA and HA cement sources, respectively.

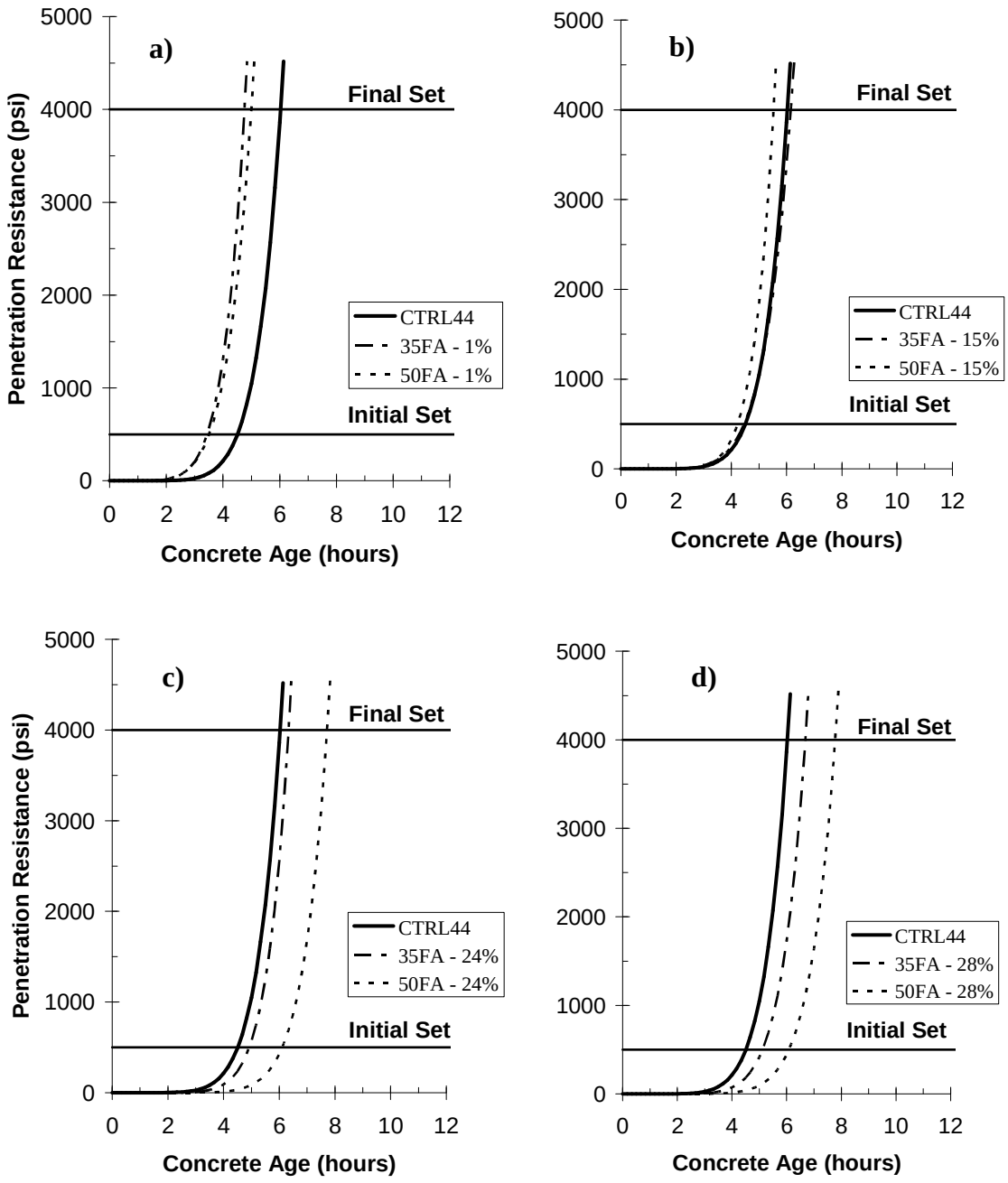

Figure 4.7: Effect of fly ash dosage on set times for a) LA-1%, b) LA-15%, c) LA-24% and d) LA-28% mixtures (73 °F)

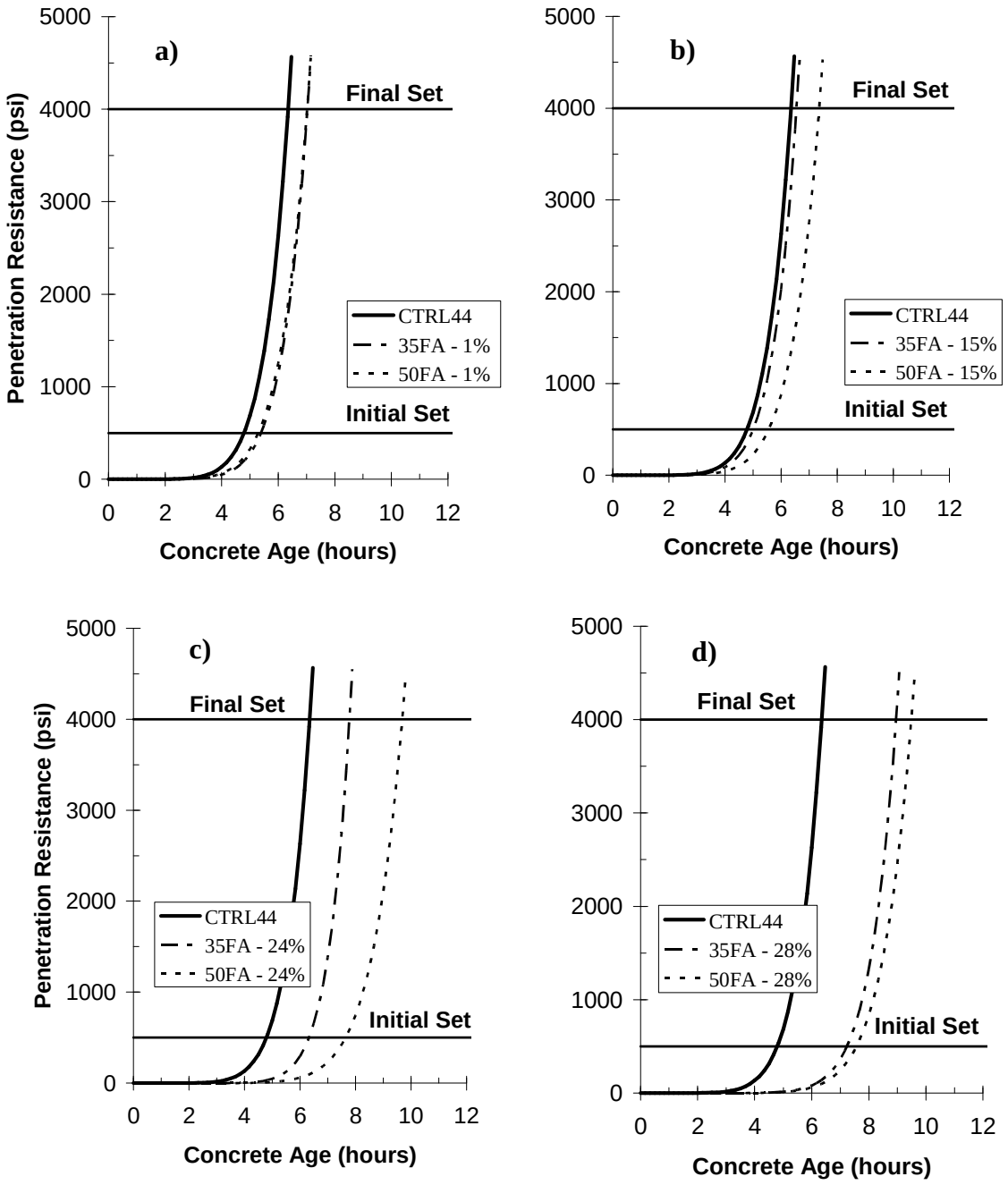

Figure 4.8: Effect of fly ash dosage on set times for a) HA-1%, b) HA-15%, c) HA-24%, and d) HA-28% mixtures (73 °F)

From Figures 4.7 and 4.8, it can be seen that an *increase in fly ash dosage* resulted in delayed initial and final set times for all mixtures proportioned with both the Class C and Class F fly ash sources, except for the LA cement concrete mixtures proportioned with the 15% CaO fly ash source. It should be noted, that the accelerating admixture dosage was doubled for the 50% fly ash mixtures (30 oz/cwt) when compared to the 35% fly ash mixture dosages (15 oz/cwt). Also, the w/cm ratio was not constant for all mixtures. Therefore, the effect of fly ash dosage alone on concrete setting time could not be completely isolated. The setting test results for all concrete mixtures batched at 73 °F are summarized in Table 4.1. It is shown that the HVFA concrete proportioned with low-calcium Class F ashes generally have similar, if not accelerated, set times when compared to the control mixtures for each cement source.

Table 4.1: Summary of initial and final set times for all 73 °F mixtures

Mixture	LA Cement		HA Cement	
	Initial Set (hours)	Final Set (hours)	Initial Set (hours)	Final Set (hours)
CTRL42	4.33	5.71	4.78	6.12
CTRL44	4.51	6.03	4.79	6.35
35FA - 1%	3.44	4.76	5.40	7.03
35FA - 15%	4.46	6.16	4.01	6.55
35FA - 24%	4.93	6.34	6.32	7.78
35FA - 28%	5.12	6.68	7.23	8.96
50FA - 1%	3.51	5.00	5.30	7.00
50FA - 15%	4.23	5.53	5.63	7.45
50FA - 24%	6.11	7.72	7.64	9.68
50FA - 28%	6.08	7.78	7.57	9.49

4.2.1.2 Effect of Fly Ash CaO Content on Set Time

As was discussed in Section 2.5.2.4, the initial and final set times for HVFA concrete will be delayed as the fly ash CaO content is increased. HVFA concrete mixtures proportioned with a Class C fly ash will exhibit longer set times when compared to a similar concrete proportioned with a Class F fly ash. In Figure 4.9, penetration resistance data for ASTM C 403 (2006) are presented for all 73 °F concrete batches.

From Figure 4.9, it is shown that as the fly ash CaO content increases for a given dosage, the set times are delayed. From Table 4.1, it is shown that this trend was consistent for all HVFA concrete mixtures tested with the exception of the HA–35FA–15% mixture. According to Ravina and Mehta (1986), the rate of C_3A hydration is highly dependent on the presence of sulfate ions in solution. The sulfate contents for the fly ashes were 0.05% for FA-1, 0.71% for FA-15, 1.24% for FA-24, and 2.14% for FA-28. Therefore, the increased set time delays observed for concrete proportioned with Class C fly ashes may be attributed to the higher sulfate contents of these ashes.

4.2.1.3 Effect of Cement Alkali Content on Set Time

The setting times of HVFA concretes are also influenced by the alkali content of the cement. For this project, two cement sources were investigated: one low alkali (LA) source and one high alkali (HA) source. The chemical composition of each cement source is presented in Table 3.3. The effect of cement alkali content on set times is shown in Figure 4.9 and Table 4.1. Set times were delayed for all HVFA concrete mixtures proportioned with the HA cement source when compared to the same mixture

produced with the LA cement source. The delay in final set times ranged from 0.39 hours (35FA-15%) to 2.39 hours (50FA-1%).

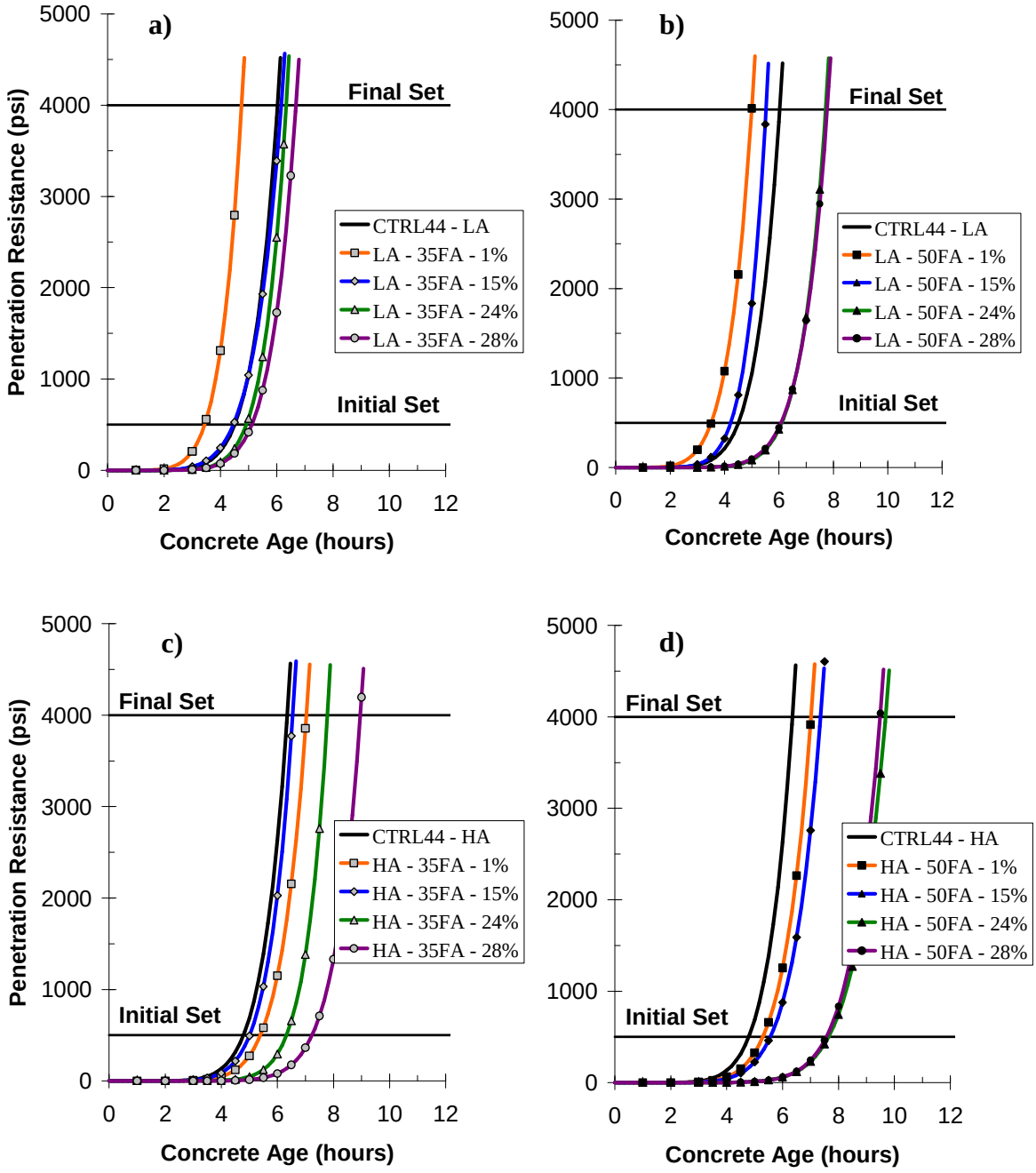

Figure 4.9: 73 °F Setting test results for a) LA-35FA, b) LA-50FA, c) HA-35FA and d) HA-50FA mixtures

4.2.1.4 Effect of Curing Temperature on Set Time

The effect of curing temperature on concrete setting time is illustrated in Figure 4.10 for four selected HVFA concrete mixtures. In this figure, the data markers represent penetration resistance measurements taken during testing. For this project, set times were accelerated for all hot batches (105 °F) and delayed for all cold batches (40 °F), when compared to the room temperature (73 °F) results. As discussed in Section 2.3.2.2, the rate of hydration is temperature dependent. At high curing temperatures, the rate of hydration is increased, and initial and final setting times are accelerated. Similarly, curing at low temperatures decreases the rate of hydration and set times are delayed.

The temperature history was measured for each mortar sample during penetration resistance testing with a maturity meter and thermocouple set-up, as shown in Figure 3.6. An example of a recorded mortar temperature history is shown in Figure 4.11. The data markers shown in the mortar temperature history are used to distinguish between data series and do not represent actual data points.

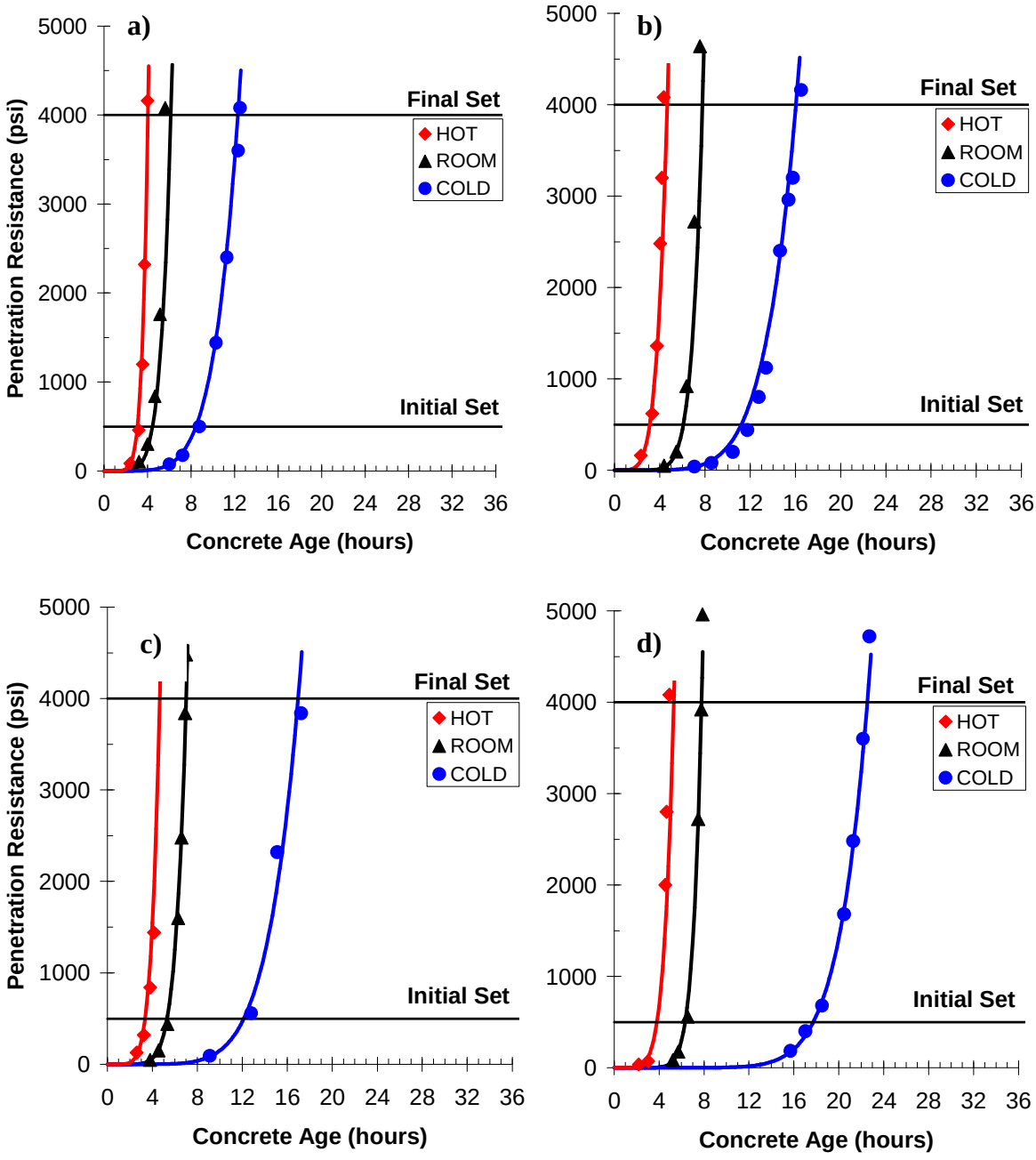

Figure 4.10: Effect of temperature on HVFA concrete set times for a) LA-35FA-15%, b) LA-50FA-28%, c) HA-50FA-1% and d) HA-35FA-24%

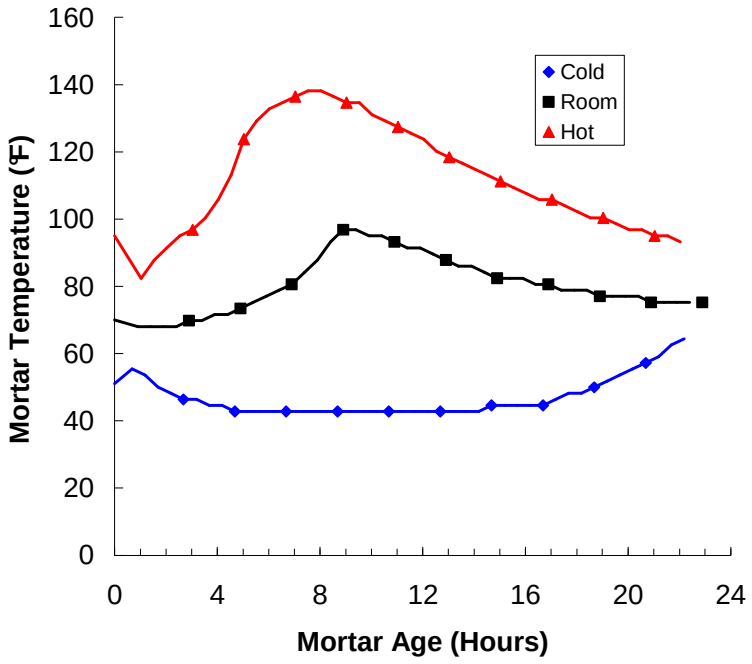

Figure 4.11: Sample mortar temperature history (LA-35FA-28%)

Since the mortar was sieved at room temperature for all batches, all hot batch samples experienced heat loss and cold batch samples experienced heat gain during the sieving process. To account for this effect, linear interpolation was used between the measured fresh concrete temperature and the first recorded mortar temperature for all batches. The recorded temperature history for each mortar sample was used to calculate the equivalent age for initial and final set. Pinto and Hover (1999), Schindler (2004), and Weakley (2010) reported that although set times will vary according to curing temperature, the calculated equivalent ages for these set times will not. Therefore, initial and final set times may be estimated for various placement conditions if the activation energy of the mixture, equivalent age at setting, and concrete temperature history are known. Based on this research, best-fit activation energies were calculated for each

mixture based on the setting results obtained for the hot, room, and cold batches. The best-fit activation energies from penetration resistance testing are presented in Section 4.2.2 alongside the activation energies calculated from isothermal calorimetry results. Penetration resistance versus equivalent age results for the LA-35FA-15% and HA-50FA-1% mixtures are presented in Figure 4.12. The best-fit activation energy is also presented for each mixture. The equivalent ages at initial set calculated using the procedure outlined above are used to estimate the in-place setting times of HVFA concretes with the ConcreteWorks temperature prediction software. The results from this analysis are presented in Chapter 6.

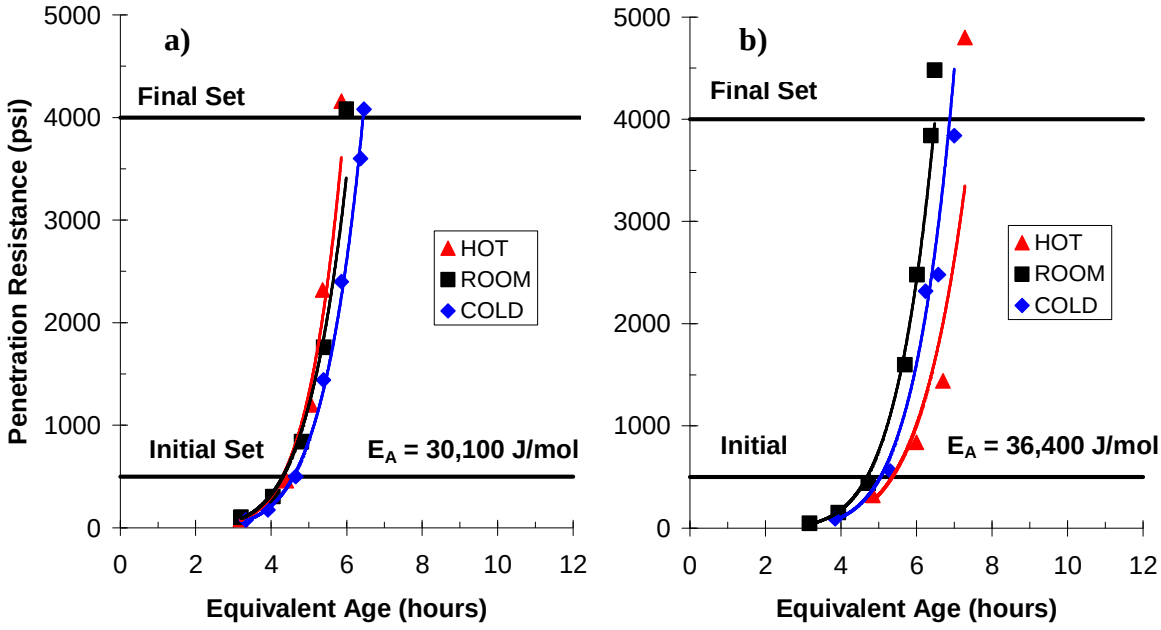

Figure 4.12: Penetration resistance versus equivalent age results for: a) LA-35FA-15% and b) HA-50FA-1% concrete mixtures

4.2.1.5 Setting Test Results Summary

As can be seen in Figures 4.7 through 4.10, fly ash dosage, fly ash CaO content, cement alkali content, and curing temperature all effect the time of setting for HVFA concrete mixtures. Setting times are delayed when the fly ash dosage is increased, for a similar w/cm ratio. Similarly, setting times are also delayed when the fly ash CaO content increases or the alkali content of the cement increases. Finally, setting times for HVFA concrete mixtures are temperature dependent. A decrease in curing temperature can cause significant set time delays, especially when high-calcium, Class C fly ashes are used at high dosages.

4.2.2 Isothermal Calorimetry Results

Mortar samples were wet-sieved from each concrete batch for isothermal calorimetry testing. Isothermal calorimetry results are given in Figures 4.13 and 4.14 (rate of heat evolution) for all 73 °F batches. Each isothermal calorimetry sample was tested for 72 hours to ensure that all significant hydration was captured. The results were normalized per gram of cementitious material (g_{cem}).

a)

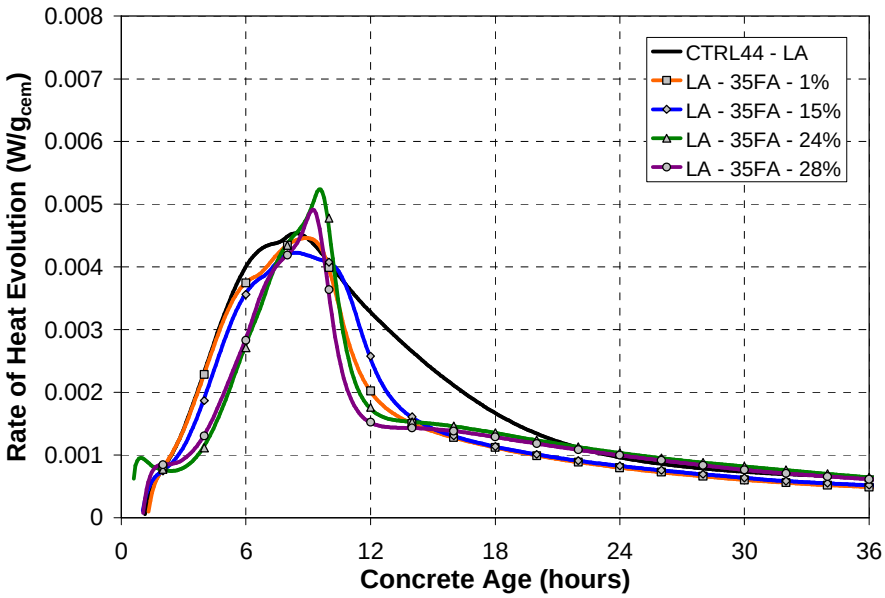

b)

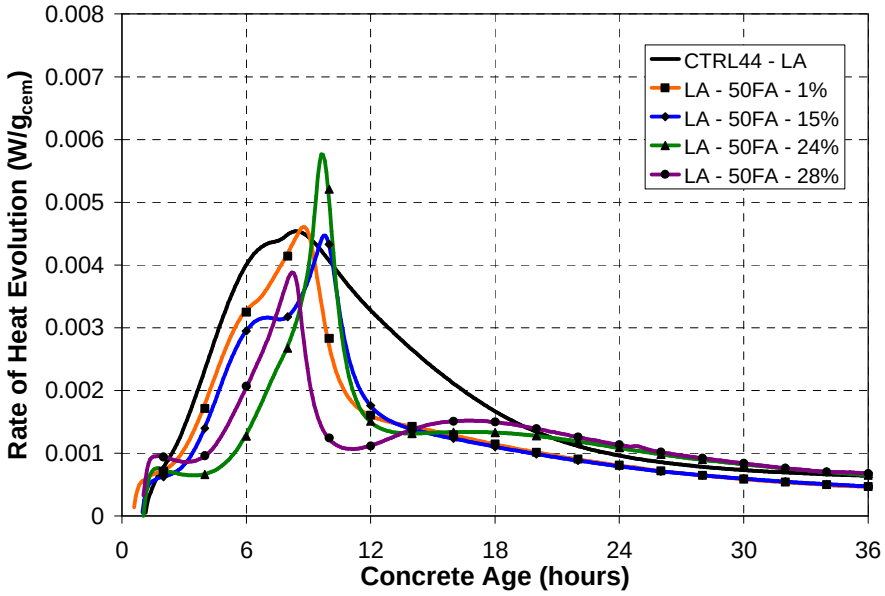

Figure 4.13: Rate of heat evolution for a) LA-35FA and b) LA-50FA mixtures

a)

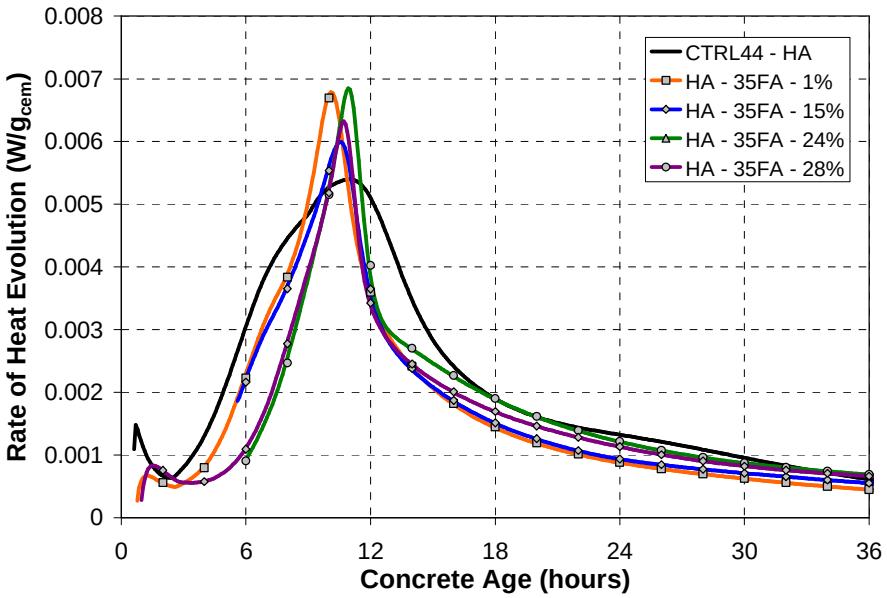

b)

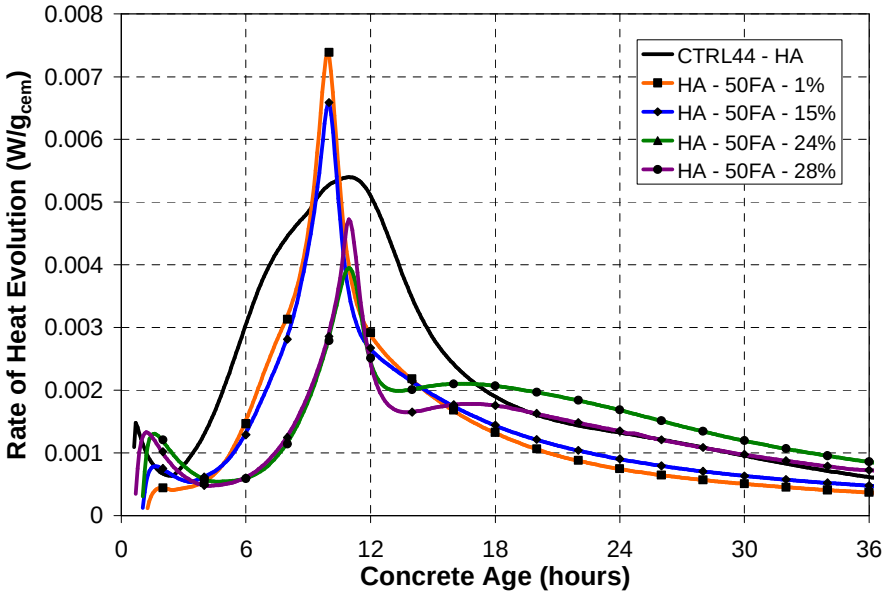

Figure 4.14: Rate of heat evolution for a) HA-35FA and b) HA-50FA mixtures

Based on Figures 4.13 and 4.14, the rate of heat evolution for a mortar sample is dependent upon fly ash dosage, fly ash CaO content, cement chemical composition, w/cm ratio, and the use of chemical admixtures. In Figure 4.15, the effect of curing temperature on the rate of heat evolution is illustrated for selected HVFA concrete

mixtures. The results in Figure 4.15 indicate that the rate of heat evolution varies significantly based on the curing temperature. Isothermal calorimetry results for all concrete mixtures are presented in Appendix C.

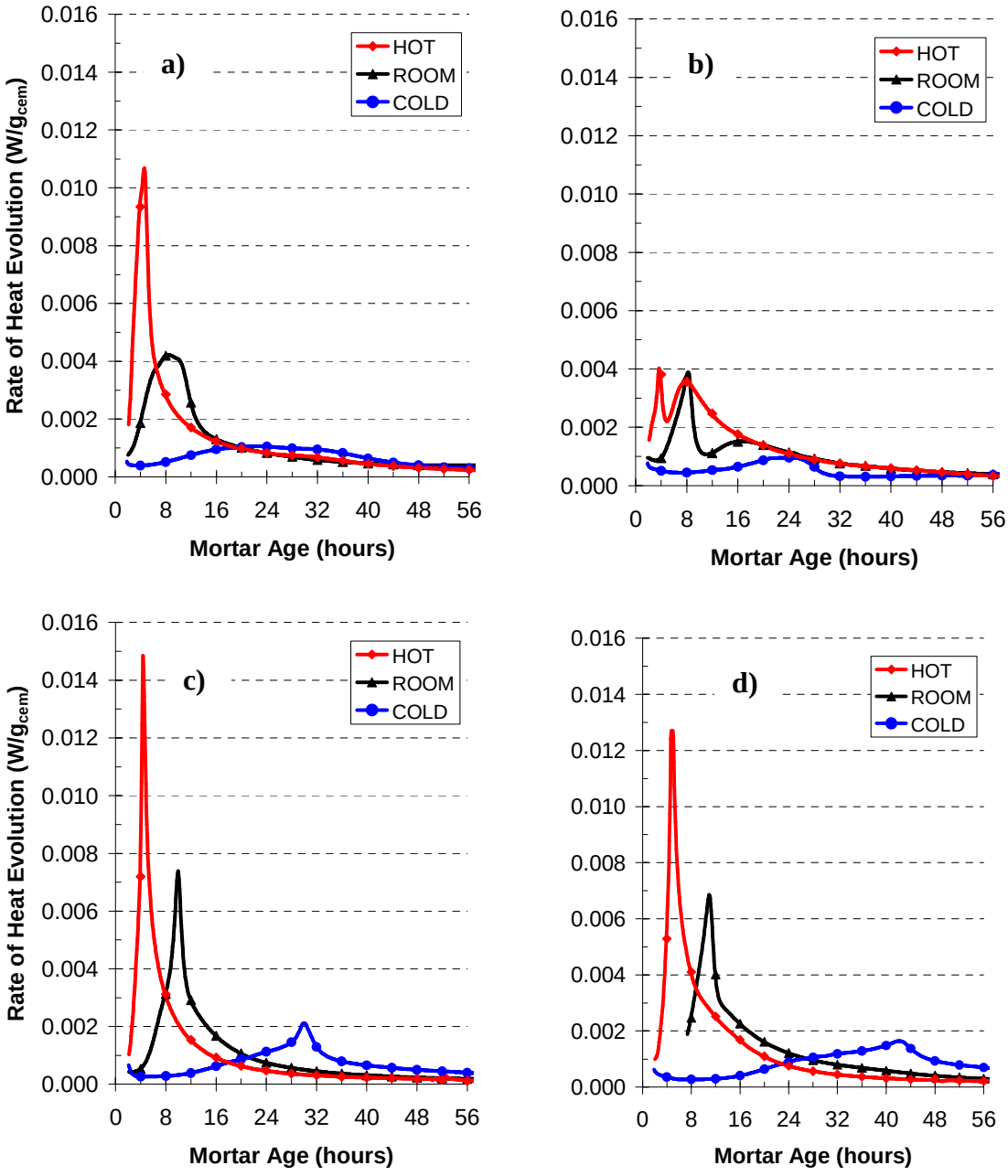

Figure 4.15: Rate of heat evolution for a) LA-35FA-15%, b) LA-50FA-28%, c) HA-50FA-1% and d) HA-35FA-24%

The temperature sensitivity of a concrete mixture is represented by its activation energy. The activation energy is used in the equivalent age maturity method to convert concrete properties determined at a reference temperature to any other curing temperature. As discussed in Section 2.6.2, the equivalent age maturity method proposed by Friesleben, Hansen, and Pederson (1977) is based on the Arrhenius rate theory for chemical reactions. Schindler (2004) determined that there is a link between the hydration time parameter (τ) and the Arrhenius rate constant (k). The activation energy was determined for each concrete mixture according to the procedure outlined in the following paragraphs.

To determine the activation energy for each concrete mixture, isothermal calorimetry was performed on sieved mortar samples from the hot, cold, and room temperature batches. At each mixing temperature, the degree of hydration equation (Equation 2.12) was fit to the isothermal calorimetry data. Schindler (2004) determined that the hydration shape parameter (β) and the ultimate degree of hydration (α_u) are independent of curing temperature; therefore, they were treated as constants for each mixture. The hydration time parameter (τ) was the only variable that changed according to curing temperature.

After determining τ for each curing temperature, an Arrhenius plot (ln(k) vs. 1/T) was developed for each mixture. Activation energies were calculated for each concrete mixture by multiplying the negative slope of the best-fit line through the Arrhenius data by the universal gas constant, R (ASTM C 1074 2004; Carino 2004). Arrhenius rate plots and calculated activation energies are presented in Figure 4.16 for selected HVFA concrete mixtures.

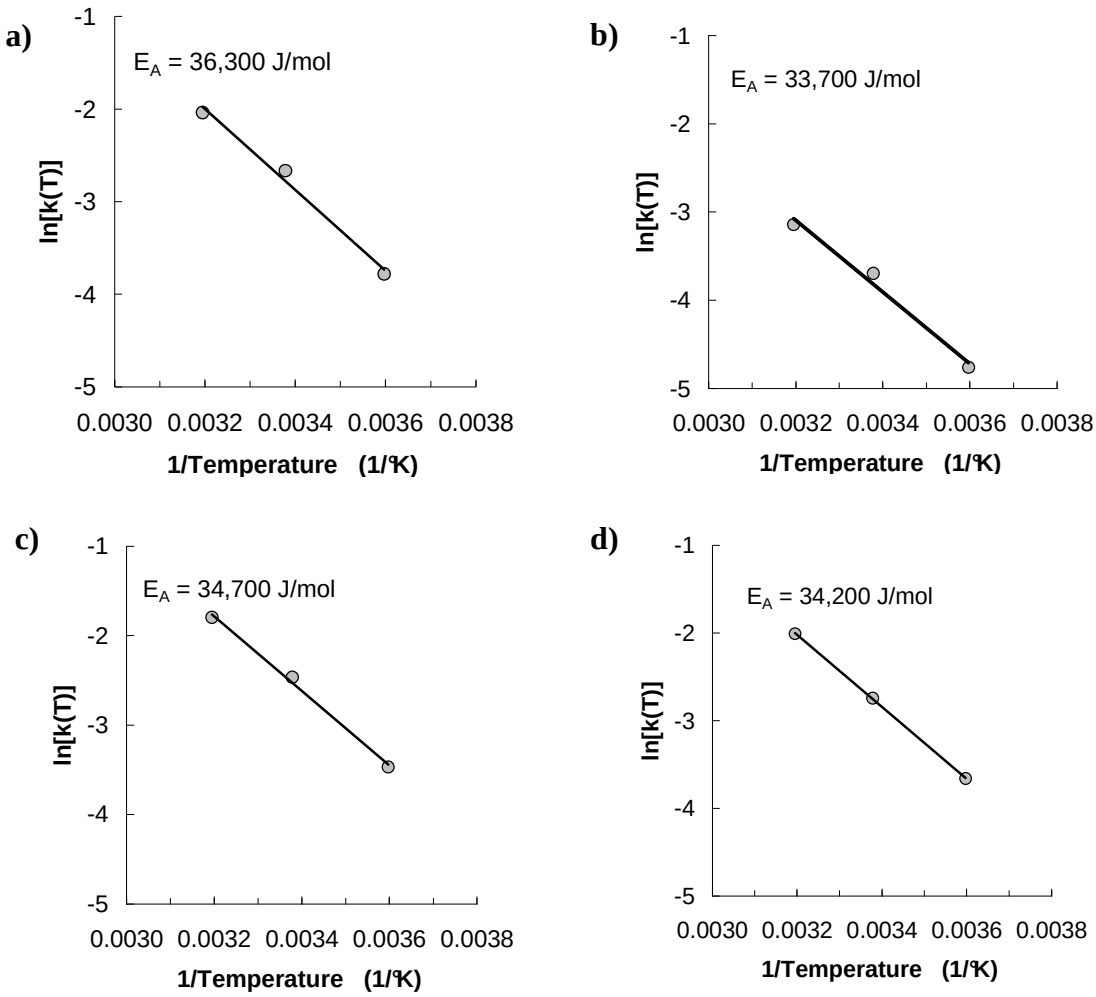

Figure 4.16: Arrhenius rate plots for a) LA-35FA-15%, b) LA-50FA-28%, c) HA-50FA-1% and d) HA-35FA-24%

A summary of all activation energies calculated from both isothermal calorimetry and penetration resistance testing are given in Tables 4.2 and 4.3 for the LA and HA cement sources, respectively. Also, the percent difference between the activation energy calculated from each test method is presented for each concrete mixture. The activation energy values calculated from isothermal calorimetry were used for development of the HVFA concrete hydration model. The HVFA concrete hydration model is developed,

presented and discussed in Chapter 5. All activation energies were determined to the nearest 100 J/mol.

In Tables 4.2 and 4.3, it is shown that the activation energies calculated from penetration resistance data compare well to those obtained from isothermal calorimetry testing. Only three mixtures had a percent difference between the two activation energy values greater than 20%. The activation energy values calculated from isothermal calorimetry for the LA cement mixtures ranged from 28,300 J/mol (35FA-1%) to 36,300 J/mol (35FA-15%). Similarly, the activation energy values for the HA cement mixtures ranged from 28,400 J/mol (35FA-28%) to 34,800 J/mol (35FA-1%). No consistent trends in activation energies could be established based on fly ash dosage or fly ash type for the HVFA concrete mixtures.

Table 4.2: LA cement mixtures activation energy summary

Mixture	Isothermal Calorimetry Activation Energy, E (J/mol)	Penetration Resistance Activation Energy, E (J/mol)	Percent Difference (%)
CTRL42	32,500	30,400	6.7
CTRL44	33,500	30,100	10.7
35FA-1%	28,300	32,600	14.1
35FA-15%	36,300	30,100	18.7
35FA-24%	32,600	31,200	4.4
35FA-28%	35,700	31,200	13.5
50FA-1%	29,600	22,800	26
50FA-15%	30,300	29,200	3.7
50FA-24%	29,900	30,000	0.3
50FA-28%	33,700	33,300	1.2

Table 4.3: HA cement mixtures activation energy summary

Mixture	Isothermal Calorimetry Activation Energy, E (J/mol)	Penetration Resistance Activation Energy, E (J/mol)	Percent Difference (%)
CTRL42	38,000	37,600	1.1
CTRL44	35,600	35,400	0.6
35FA - 1%	34,800	36,300	3.4
35FA - 15%	32,000	38,300	17.9
35FA - 24%	34,200	37,300	8.7
35FA - 28%	28,400	34,400	19.1
50FA - 1%	34,700	36,400	4.8
50FA - 15%	33,500	39,900	17.4
50FA - 24%	30,800	45,000	45
50FA - 28%	28,400	42,500	32

4.2.3 Semi-Adiabatic Calorimetry Results

Semi-adiabatic calorimetry (SAC) testing was conducted for all mixtures batched at 73 °F to characterize the hydration development of HVFA concrete. All SAC testing was conducted with the use of an iQdrum device, as described in Section 3.5.4. Testing was conducted for 120 hours to ensure that the concrete sample had hydrated sufficiently. Temperature measurements were recorded every fifteen minutes.

The results from SAC testing were used to develop a database of best-fit hydration parameters to be used for generation of the HVFA concrete hydration model. A summary of the best-fit hydration parameters from SAC testing is presented in Chapter 5. In the following sections, the effect of fly ash dosage and fly ash CaO content on the temperature development of HVFA concrete mixtures is examined.

4.2.3.1 Effect of Fly Ash Dosage on Heat of Hydration

Heat generation per volume of concrete (MJ/m^3) plots for all 73 °F LA cement and HA cement concrete mixtures are presented in Figures 4.17 and 4.18, respectively. The heat generation plots were calculated by multiplying the measured heat of hydration of the sample by the cementitious material content of that particular concrete mixture. For both cement sources, an increase in fly ash dosage resulted in a decreased heat of hydration and less heat generated per volume of concrete, with the exception of the LA-15% and LA-28% concrete mixtures. For these mixtures, the heat generation was approximately equal for both fly ash dosages.

For the HA cement, Class F fly ash concrete mixtures, the 50% fly ash dosage resulted in significant reductions in heat generation (10 – 38 MJ/m^3) when compared to the control (CTRL44–HA). The significant reduction in heat generation of the HVFA mixtures proportioned with the Class F fly ashes agree with past research, as described in Section 2.5.2.5. Langley et al. (1992) reported that the peak in-place temperatures of 3.05 x 3.05 x 3.05 meter concrete blocks were reduced by 52 °F when a 55% dosage of Class F fly ash was used.

When compared to the control concrete results, the HVFA concrete mixtures proportioned with the Class F fly ashes (FA-1 and FA-15) generated less heat even at a high dosage and low w/cm ratio. The HVFA concrete mixtures proportioned with the Class C fly ashes (FA-24 and FA-28) were shown to have similar heat generation results to the control concrete. It should be noted that the w/cm ratio was not constant for the 35 and 50% fly ash dosage mixtures. Generally, the heat of hydration increases according to a decrease in w/cm ratio. Since the w/cm ratio was not constant for all mixtures, the

effect of fly ash dosage alone on the temperature development could not be completely isolated.

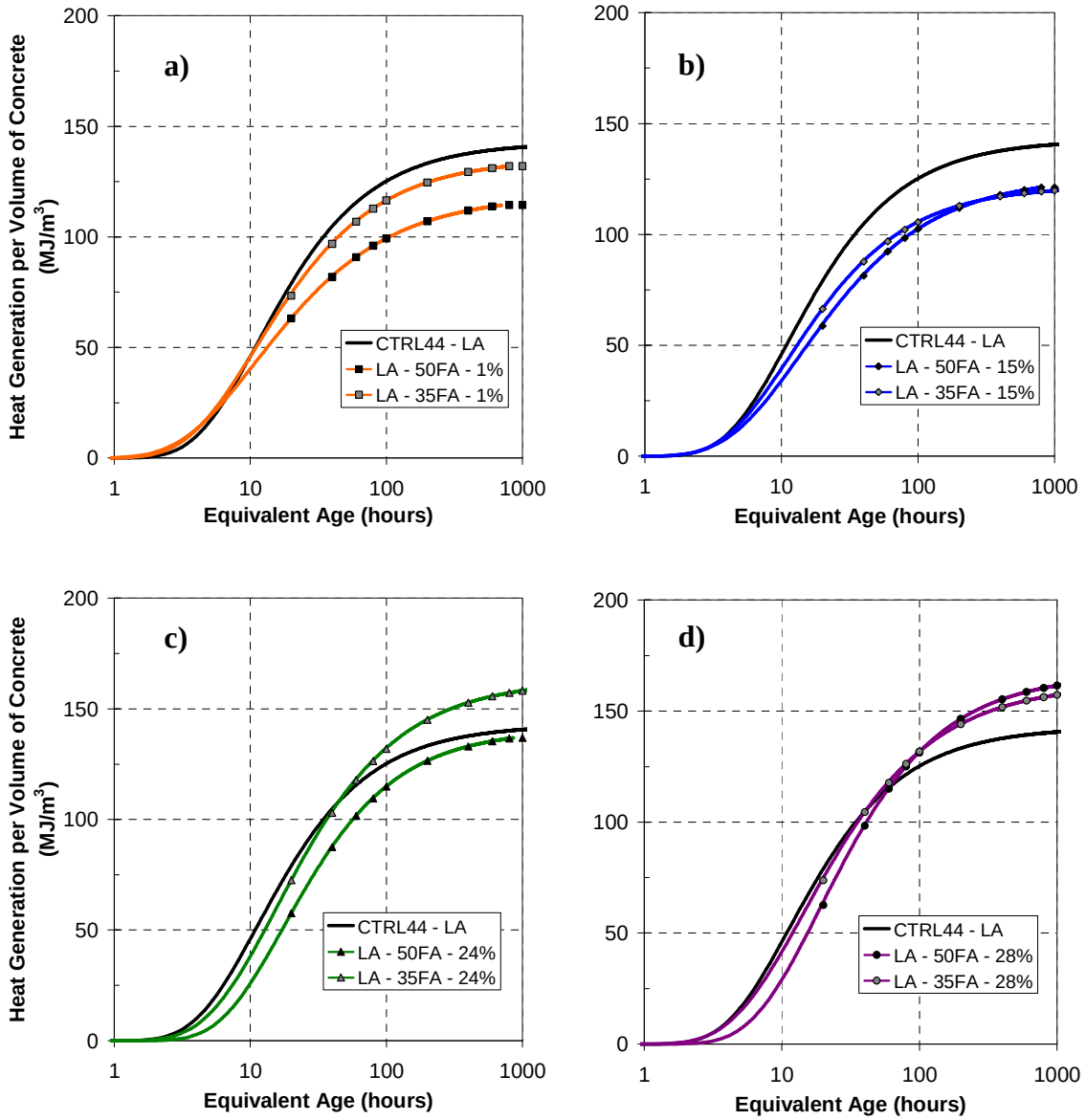

Figure 4.17: Heat generation per volume of concrete for a) LA-1%, b) LA-15%, c) LA-24% and d) LA-28% concrete mixtures (1 MJ/m^3 = 0.725 $kBTU/yd^3$)

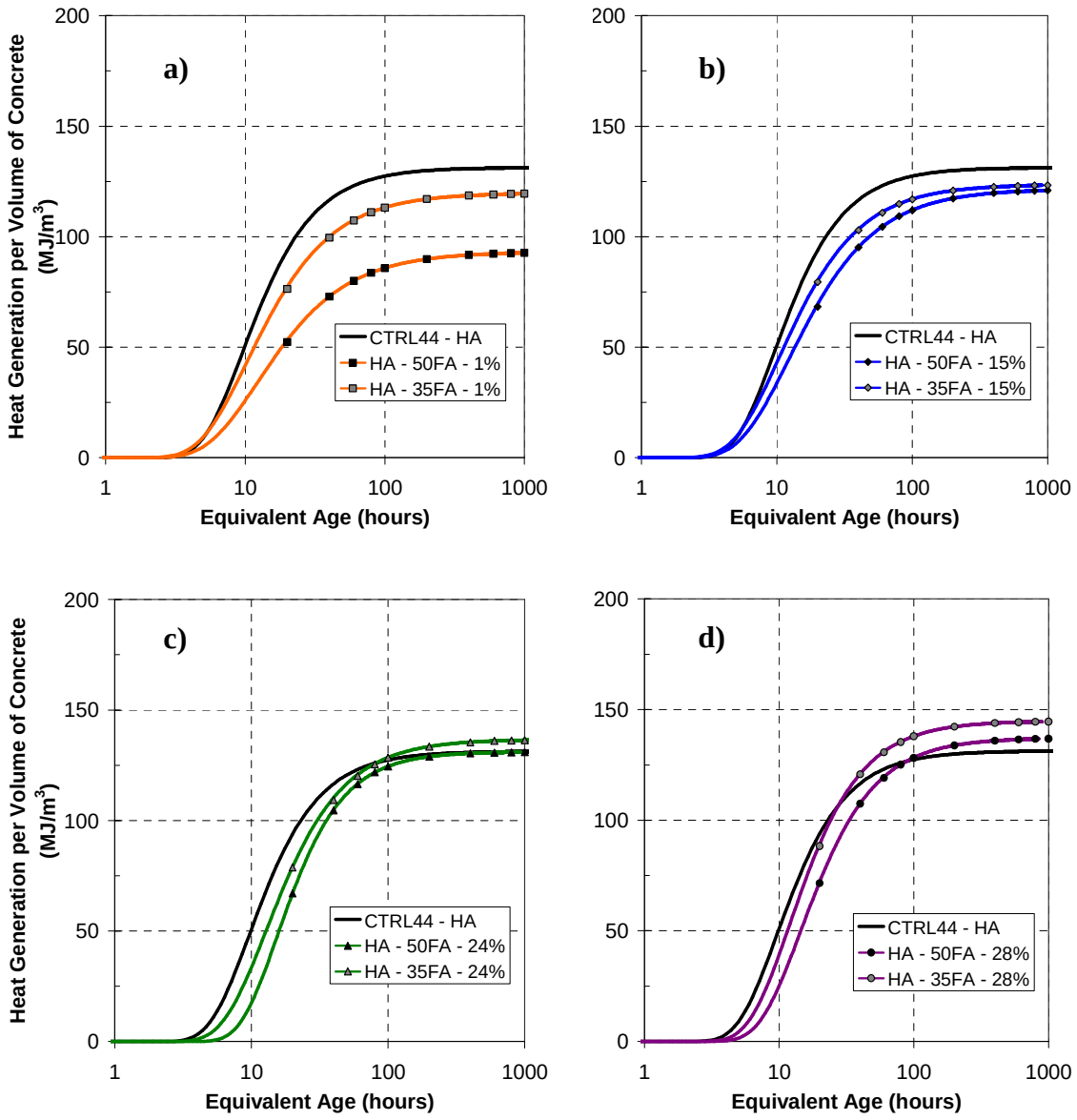

Figure 4.18: Heat generation per volume of concrete for a) HA-1%, b) HA-15%, c) HA-24% and d) HA-28% concrete mixtures (1 MJ/m^3 = 0.725 kBTU/yd^3)

4.2.3.2 Effect of Fly Ash CaO Content on Heat of Hydration

As presented in Section 2.5.2.5, the rate of temperature development and maximum temperature rise for HVFA concrete is dependent on the chemical composition of the fly ash. The effect of fly ash CaO content on the heat generation of HVFA

concrete is presented in Figure 4.19 for the HA cement concrete mixtures (35% and 50% fly ash dosages). In this figure, it is shown that as the fly ash CaO content is increased for a given dosage, the heat generation per volume of concrete also increases. The same trend was found for all LA cement concrete mixtures.

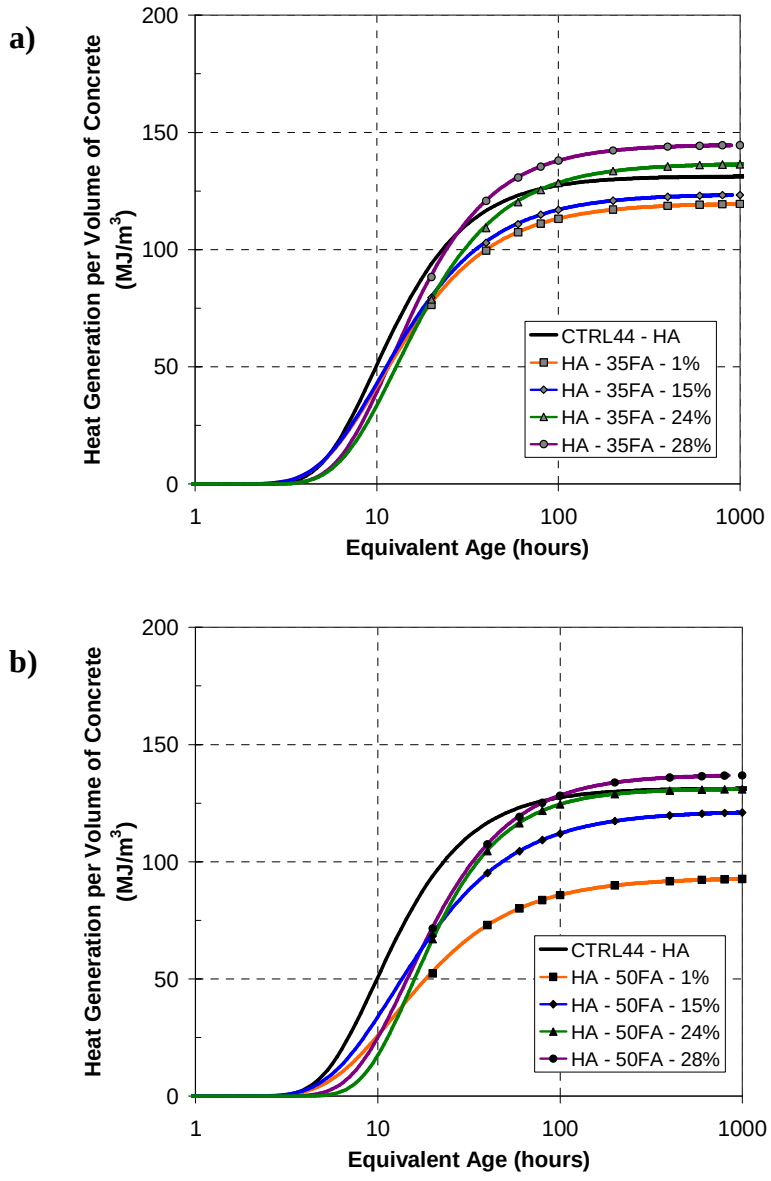

Figure 4.19: Effect of fly ash CaO content on heat generation for a) HA-35FA and b) HA-50FA concrete mixtures

4.2.3.3 Semi-Adiabatic Calorimetry Testing Summary

As shown in Figures 4.17 through 4.19, fly ash dosage, fly ash CaO content, and cement alkali content each have an effect on the heat generation of HVFA concrete. As the fly ash dosage is increased, the heat generated by the concrete mixture will decrease. It was also shown that an increase in the fly ash CaO content (for a given fly ash dosage), results in more heat generated per volume of concrete. The results from SAC testing are discussed in further detail in Chapter 5 when the HVFA concrete hydration model is developed. In that chapter, a review of the degree of hydration formulation is completed. and the best-fit hydration parameters (τ, β, and α_u) that were calculated for each mixture are presented.

4.3 Phase II Testing Results

4.3.1 Compressive Strength Testing

Immediately following fresh concrete testing, cylinders were cast from each room temperature batch for compressive strength testing. The cylinders were continuously moist-cured and tested according to ASTM C 39 (2004) based on the schedule outlined in Section 3.5.5. A maturity meter was used to record the temperature history of one cylinder from each batch. With the recorded compressive strengths and temperature history, strength-maturity relationships were developed for each mixture.

In addition to developing the strength-maturity relationship for all room temperature batches, quality-control (QC) cylinders were cast from each hot and cold batch. The QC cylinders were tested after 28 days of moist-curing. A summary of strength-maturity relationship parameters and compressive strength quality-control

testing results for each mixture are presented in Appendix C. In the following sections, the effect of fly ash dosage, fly ash CaO content, and cement alkali content on the compressive strength development of HVFA concrete are reviewed.

4.3.1.1 Effect of Fly Ash Dosage on Compressive Strength

One of the main limitations of HVFA concrete is low early-age strength values. Therefore, HVFA concrete is proportioned with low w/cm ratios to counter its reduced rate of early-age compressive strength development (Malhotra and Mehta 2002). For this project, HVFA concrete mixtures were proportioned with w/cm ratios of 0.39 and 0.34 for 50% and 35% fly ash dosages, respectively. Compressive strength testing results (moist-cured specimens) for all LA and HA cement concrete mixtures are presented in Figures 4.20 and 4.21, respectively. In each figure, each data point represents an average of three test results for that age.

From the figures, it can be seen that both the 35% and 50% fly ash mixtures were proportioned to have comparable compressive strengths to the control mixtures at early ages. At four days, all mixtures (LA and HA cement) had compressive strength values within 15% of the CTRL44 strength. The results in Figures 4.20 and 4.21 also indicate that the HVFA concrete mixtures continue to gain strength at late ages due to the moist-curing conditions. In comparison, the control mixtures had negligible compressive strength gain after 28 days.

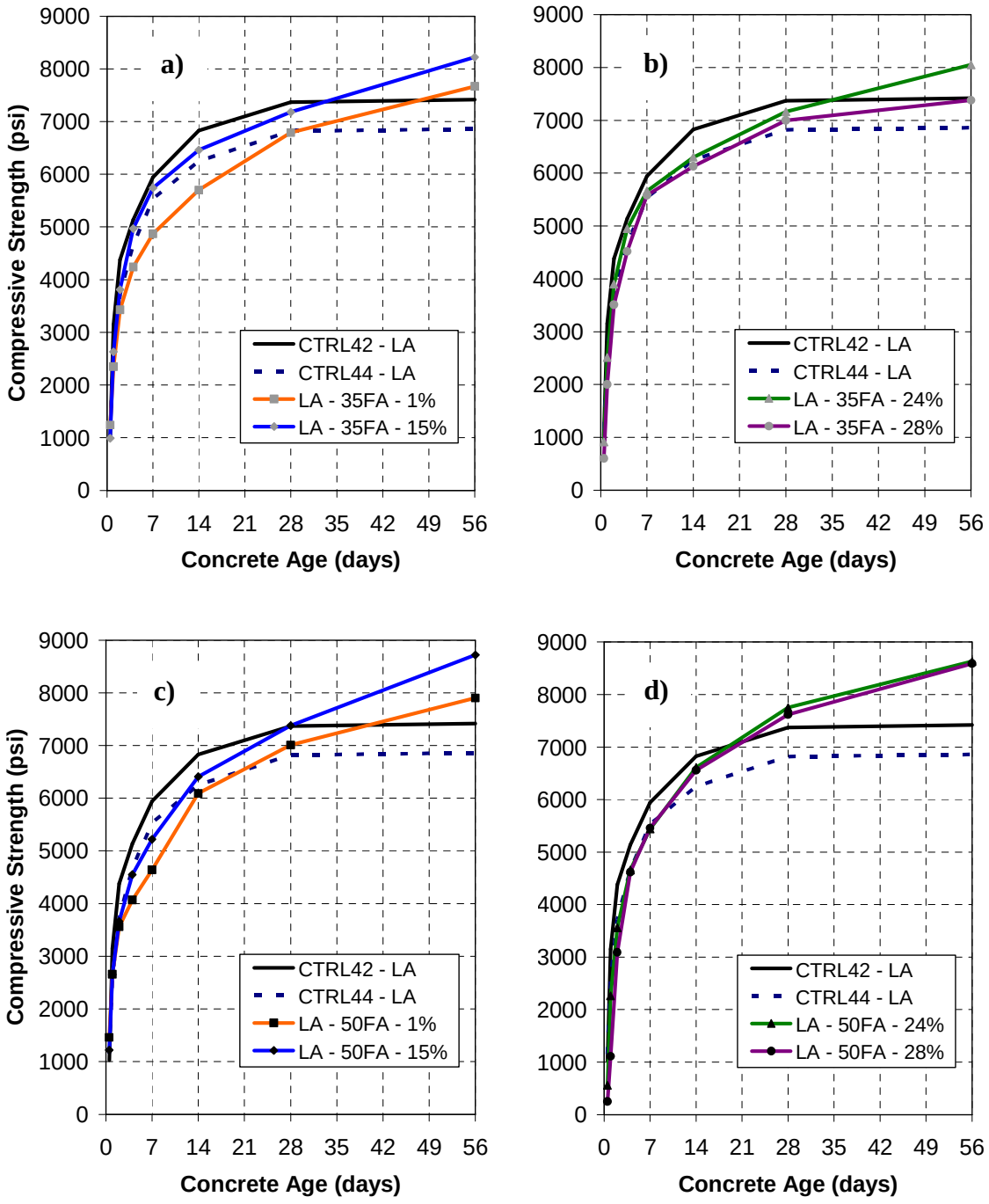

Figure 4.20: Compressive strength testing results for a) LA-35FA-Class F, b) LA-35FA-Class C, c) LA-50FA-Class F, and d) LA-50FA-Class C mixtures

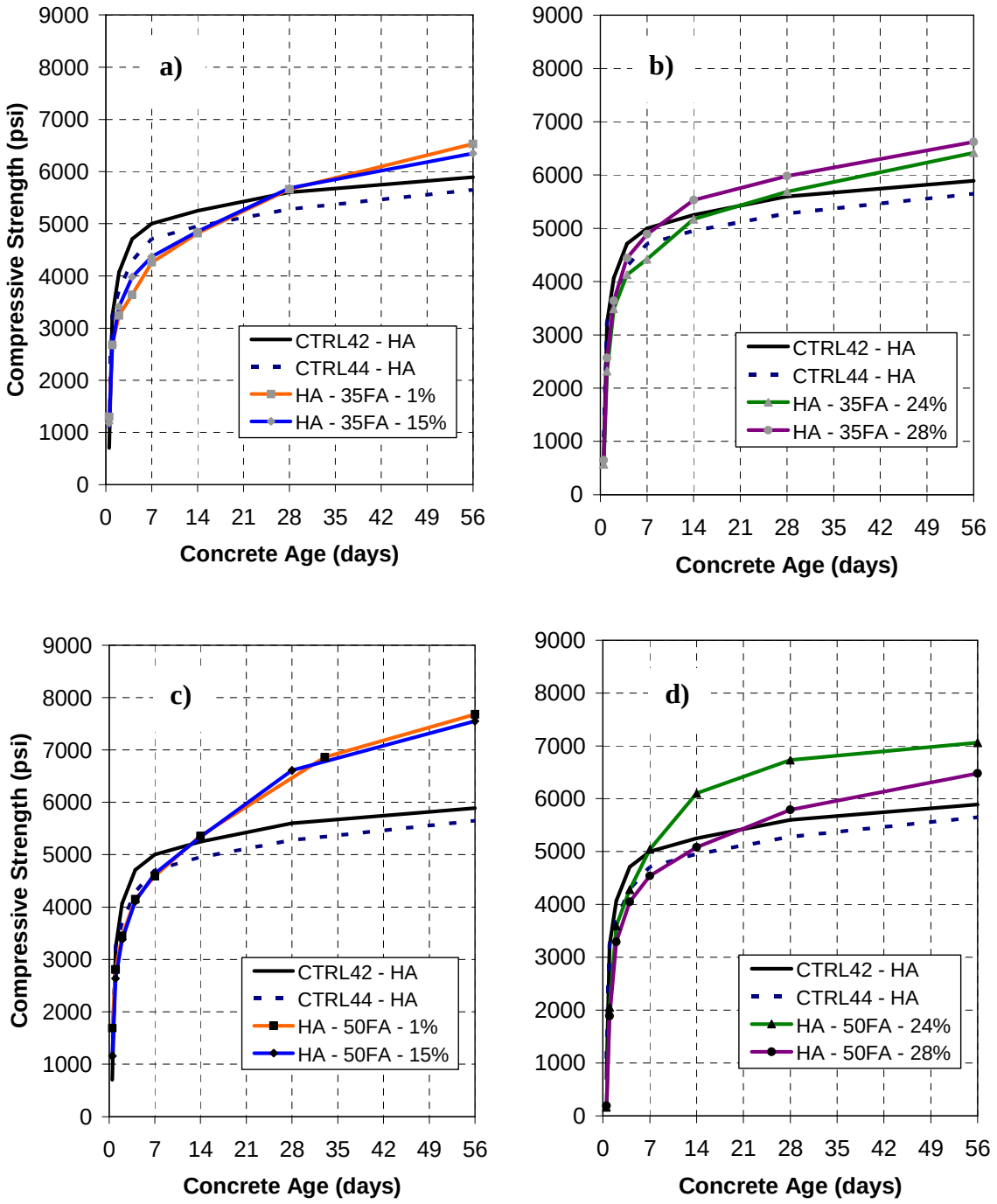

Figure 4.21: Compressive strength testing results for a) HA-35FA-Class F, b) HA-35FA-Class C, c) HA-50FA-Class F, and d) HA-50FA-Class C mixtures

Generally, an increase in fly ash dosage for a given w/cm ratio will result in a decreased rate of compressive strength development at early ages. At later ages, however, the compressive strength may be increased with high fly ash dosages when compared to a control concrete with no fly ash replacement (Thomas 2007). This improvement in late-age compressive strength for HVFA concrete will only be achieved if adequate moisture is supplied. The moisture is required for the pozzolanic reaction to convert CH to C-S-H (ACI 232.R 2003).

4.3.1.2 Effect of Fly Ash CaO Content on Compressive Strength

In Figures 4.20 and 4.21, it is shown that the HVFA concrete mixtures proportioned with the 1% CaO Class F fly ash had the lowest rate of early-age strength development for both cement sources. In Figure 4.22, the general effect of fly ash CaO content on the compressive strength development of HVFA concrete is illustrated. It is shown that the HVFA concrete proportioned with the Class C fly ash exhibits a higher rate of reaction at early ages when compared to the Class F fly ash mixture. This effect is amplified when the fly ash dosage is increased from 35% to 50%. For the 50% fly ash dosage mixtures, the compressive strength of the Class F fly ash mixture surpasses the Class C fly ash mixture results at approximately 33 days. After this point, the HA-50FA-1% mixture continues to gain strength, whereas the strength development of the HA-50FA-24% mixture slows. The high rate of strength gain at late ages for HVFA concrete proportioned with low-calcium Class F fly ashes is due to the increased pozzolanic activity of these ashes. The improvement in late-age strength for HVFA is dependent on

curing conditions because moisture is required for the pozzolanic reaction to convert CH to C-S-H (ACI 232.R 2003).

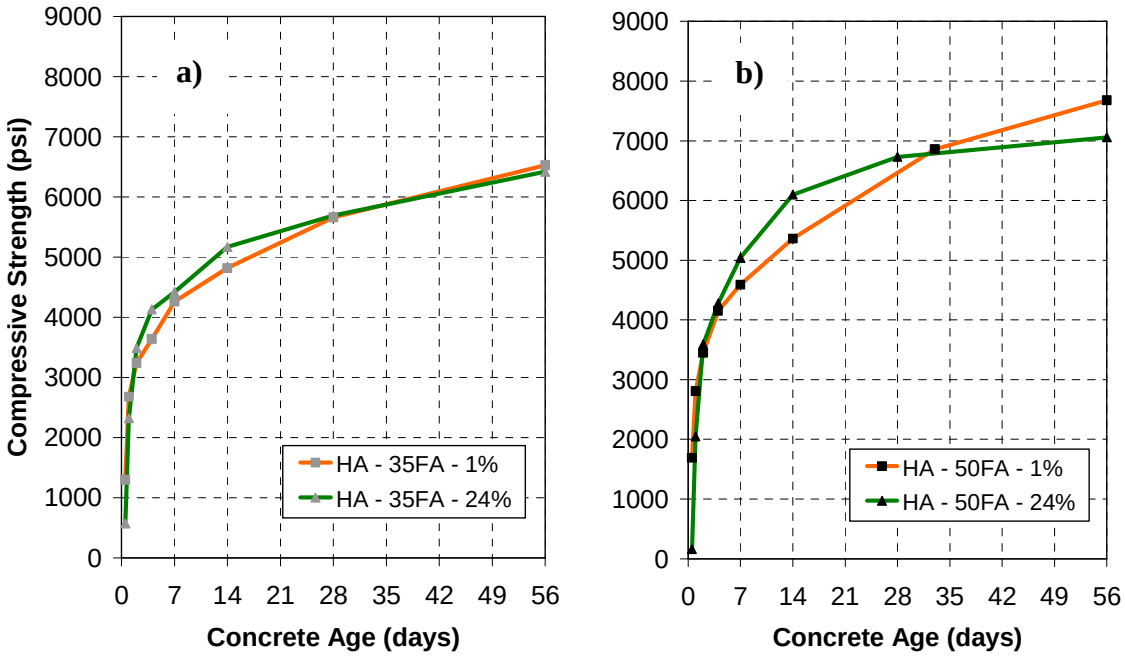

Figure 4.22: Effect of fly ash CaO content on compressive strength development of a) HA-35FA and b) HA-50FA mixtures

4.3.1.3 Effect of Cement Alkali Content on Compressive Strength

The compressive strength development of HVFA concrete is also influenced by the alkali content of the cement. In Figures 4.20 and 4.21, it is shown that the compressive strengths were decreased at 4 days and beyond for all HVFA concrete mixtures proportioned with the HA cement source when compared to the LA cement source. The average percent reduction in the compressive strength results for the 35% and 50% fly ash dosage concrete mixtures are, 12.6% and 18.3%, respectively. Jawed

and Skalny (1978) reported cements with a high alkali content will generally exhibit higher strengths at early ages, but lower strengths at 28 days and beyond.

4.3.1.4 Compressive Strength Testing Summary

As shown in Figures 4.20, 4.21 and 4.22, the rate of strength development for HVFA concrete is dependent on the w/cm ratio, fly ash dosage, fly ash chemical composition and cement chemical composition. Generally, an increase in fly ash dosage will result in lowered early-age compressive strengths. This effect may be offset; however, if HVFA concrete is proportioned with a low w/cm ratio and HRWR admixtures are used to control workability. The compressive strength testing results presented were used to develop a unique strength-maturity relationship for each mixture. The strength-maturity relationships for each mixture were later used to evaluate the in-place compressive strength development of HVFA concrete in transportation structures, which is described in Chapter 6.

4.4 Summary

In this chapter, sample results from each of the test methods outlined in Chapter 3 are presented and discussed. Fresh concrete properties of all 20 concrete mixtures at each of the three mixing temperatures are presented. Setting test results are examined for selected mixtures and trends are identified. Results from isothermal calorimetry testing are presented to illustrate the effect of curing temperature on the rate of hydration of HVFA concrete mixtures. Sample semi-adiabatic calorimetry results from room temperature batches are presented to illustrate the effect that the use of fly ash has on

temperature development. Finally, compressive strength testing results for all mixtures are presented and reviewed.

The key findings of the work covered in this chapter can be summarized as follows:

- All batches of concrete were deemed acceptable based on fresh concrete testing. It was found that slump and air content varied considerably when mixtures were batched at the hot and cold temperatures.
- Curing temperature has a significant impact on both the setting time of HVFA concrete and the rate of isothermal heat development. The setting time delays due to lowered curing temperature are largest when high-calcium, Class C fly ashes are used at high dosages.
- Fly ash dosage, fly ash CaO content, and cement alkali content were all found to have a significant effect on the setting time, rate of isothermal heat development, heat of hydration, and rate of compressive strength development of HVFA concrete mixtures.

The key points listed above were applied in the development of the HVFA concrete hydration model and the evaluation of the in-place performance of HVFA concrete. The processes are described in Chapters 5 and 6.

Chapter 5

Development of HVFA Concrete Hydration Model

In Chapter 4, the laboratory testing results from Phases I and II are presented and discussed. The activation energies from isothermal calorimetry testing and hydration development data from semi-adiabatic calorimetry testing were used to develop a hydration model for concrete proportioned with high fly ash dosages. In this chapter, the modeling approach and software are introduced. Next, the calibration database used for the development of the hydration model is presented. After presenting the modeling approach and calibration database, the HVFA concrete hydration model is presented, along with an evaluation of the model. Finally, a summary is presented for significance and use of the final model.

5.1 Modeling Approach

As discussed in Section 2.6.1.3, Hansen and Pane (2002) developed the following equation to represent the degree of hydration development versus time for a concrete sample:

$$\alpha(t) = \alpha_u \cdot \exp\left(-\left(\frac{\tau}{t}\right)^{\beta}\right) \qquad \textbf{Equation 5.1}$$

where:

$\alpha\ (t)$ = degree of hydration at time t,

α_u = ultimate degree of hydration,

τ = hydration time parameter,

β = hydration shape parameter, and

t = concrete age or equivalent age.

The equation presented above describes the S-shaped degree of hydration development in terms of the hydration time parameter (τ), hydration shape parameter (β), and ultimate degree of hydration (α_u). The hydration time parameter (τ) is expressed in terms of hours, and it represents the start of the acceleration phase of the hydration development. The hydration shape parameter (β) is unitless, and it describes the rate (slope) of the hydration development. Finally, the ultimate degree of hydration (α_u) represents the maximum degree of hydration that may be achieved. The mixture-specific hydration parameters (τ, β, and α_u) are back-calculated by fitting Equation 5.1 to the degree of hydration versus time results obtained from semi-adiabatic calorimetry (SAC) testing. The effect of an increase to each of the hydration parameters to the shape of the overall hydration development are summarized in Figures 5.1a, 5.1b, and 5.1c. An example of the degree of hydration equation fitted to sample SAC testing results is presented in Figure 5.1d.

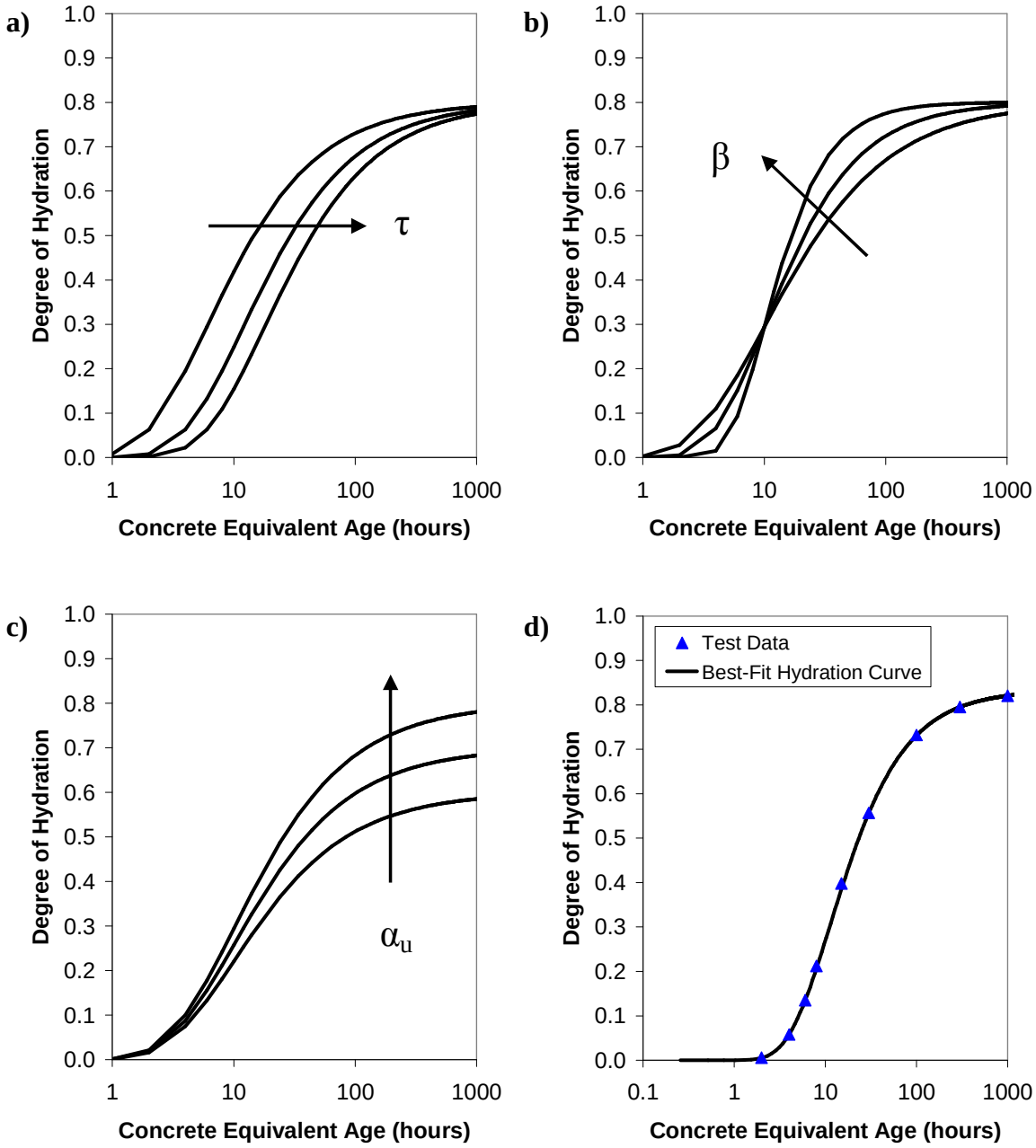

Figure 5.1: Effect of changes to: a) hydration time parameter, b) hydration shape parameter, and c) ultimate degree of hydration on the overall hydration development and d) example of hydration equation fitted to SAC testing results

The hydration model for HVFA concrete was developed with the use of multivariate regression analysis. To complete this analysis, SAS Version 9.2 was used. This software is distributed by SAS Institute Inc. located in Cary, North Carolina. The multivariate regression analysis was completed in three steps: identification of the most significant variables, development of model, and evaluation of goodness of fit.

The first step in developing the HVFA concrete hydration model was to identify the most significant variables for individually predicting both the hydration time parameter (τ) and the hydration shape parameter (β). The chemical and physical properties of the cements, fly ash chemical compositions, and fly ash dosages were taken as explanatory variables and the τ and β parameters were taken as the response variables for each mixture. Interactions between the variables were also considered. Since the cement and fly ash chemical properties are not independent of each other, a correlation matrix was constructed for all variables. From the correlation matrix, variable dependence could be tested for simultaneous use in the model. In this step, the explanatory variables to be used in the final model were selected. Also, initial estimates of the coefficients for the nonlinear regression model were calculated by statistical means.

After identifying the most significant variables, the HVFA concrete hydration model could be developed. In this step, the chemical and physical properties of the cements, fly ash chemical compositions, and fly ash dosages were taken as independent variables and the degree of hydration values from semi-adiabatic testing were taken as the response variables for each mixture. Nonlinear regression analysis was used to determine the best-fit statistical values for each of the independent variables.

After developing the degree of hydration model, it could be evaluated for goodness of fit. The goodness of fit was evaluated by determining the coefficient of determination (r^2) and the standard deviation of the absolute error (S_j). Also, residual plots for each of the independent variables were created. One of the underlying assumptions of linear regression analysis is homogeneity of variance. Residual plots were used to identify if this assumption was met. A high r^2, low S_j and random distribution of unexplained error indicate that the model explains most of the variability contained within the data set.

It was determined that the data could be best modeled by a nonlinear relationship, as documented by Schindler and Folliard (2005). To transform the data set into a linear relationship, the natural logarithm of both the independent and response variables was taken. By doing this, the data set could be analyzed by a multivariate linear regression analysis, and a power function could be fit to the response variables. An example of this transformation is presented in Equations 5.2 and 5.3. In Equation 5.2, two independent parameters, x_1 and x_2 are shown to have a nonlinear relationship to the response variable y (Barnes 1994).

$$y = (x_1)^{c_1} \cdot (x_2)^{c_2} \cdot e^{c_3} \qquad \textbf{Equation 5.2}$$

where:

y = response variable,

x_i = independent variables, and

c_i = regression constants.

By taking the natural logarithm of both sides of Equation 5.2, the equation is transformed into a two parameter multivariate linear model, as presented in Equation 5.3.

When comparing Equations 5.2 and 5.3, it is shown that the linear model is obtained by taking the natural logarithm of the response and independent variables: $Y = \ln(y)$, $X_1 = \ln(x_1)$ and $X_2 = \ln(x_2)$ (Barnes 1994).

$$\ln(y) = \ln((x_1)^{c_1} \cdot (x_2)^{c_2} \cdot e^{c_3})$$

$$\ln(y) = \ln(x_1)^{c_1} + \ln(x_2)^{c_2} + \ln e^{c_3}$$

$$\ln(y) = c_1 \cdot \ln(x_1) + c_2 \cdot \ln(x_2) + c_3$$

$$Y = c_1 \cdot X_1 + c_2 \cdot X_2 + c_3 \qquad \textbf{Equation 5.3}$$

5.2 Calibration Database

The first step in developing the hydration model for HVFA concrete involved creating a calibration database which included both the independent variables and response variables for each concrete mixture. The independent variables selected for the calibration database included the chemical and physical properties of the cements, the fly ash chemical compositions, the fly ash dosages, and the w/cm ratios for each mixture used to develop this model. This information is presented in Tables 3.3, 3.5, and 3.2, for each of the twenty concrete mixtures completed for this project.

5.2.1 Semi-Adiabatic Test Data

For each concrete mixture, the hydration shape parameter (β), hydration time parameter (τ), and ultimate degree of hydration (α_u) were selected as the response variables. The hydration parameters for each concrete mixture were obtained from semi-adiabatic calorimetry (SAC) testing. All SAC testing was conducted with the use of an iQdrum device as described in Section 3.5.4. A summary of the best-fit hydration

parameters for all twenty concrete mixtures (LA and HA cement sources) is presented in Table 5.1. The activation energies presented in this table were calculated from isothermal calorimetry test results obtained from three curing temperatures, as described in Section 4.2.2.

Table 5.1: Best-fit hydration parameters from SAC testing

Mixture Description	E (J/mol)	Hydration Parameters			H_u (J/g)
		β	τ (hours)	α_u	
CTRL42-LA	32,500	0.966	10.44	0.812	466
CTRL44-LA	33,500	0.937	11.41	0.833	479
LA-35-1	28,300	0.856	10.94	0.990	377
LA-35-15	36,300	0.895	11.44	0.762	433
LA-35-24	32,600	0.844	15.53	0.917	476
LA-35-28	35,700	0.814	14.60	0.874	496
LA-50-1	29,600	0.778	11.08	0.990	314
LA-50-15	30,300	0.803	13.96	0.805	401
LA-50-24	29,900	0.925	17.68	0.767	464
LA-50-28	33,700	0.870	19.00	0.849	494
CTRL42-HA	38,000	1.468	9.68	0.728	462
CTRL44-HA	35,600	1.500	9.66	0.747	491
HA-35-1	34,800	1.272	10.42	0.872	379
HA-35-15	32,000	1.281	10.43	0.769	435
HA-35-24	34,200	1.355	12.84	0.767	478
HA-35-28	28,400	1.431	12.05	0.777	498
HA-50-1	34,700	1.230	11.43	0.866	322
HA-50-15	33,500	1.193	12.31	0.764	408
HA-50-24	30,800	1.590	15.55	0.705	471
HA-50-28	28,400	1.403	14.60	0.689	501

The total heat of hydration (H_u) for each concrete mixture is presented in Table 5.1. The total heat of hydration accounts for heat generated by portland cement and SCMs, as presented in Equation 2.7. The portland cement heat contribution was calculated for each cement according to Equation 2.8.

As discussed in Chapter 2, the heat contribution of fly ash is calculated based on the fly ash CaO content. There are several recommendations for calculating fly ash heat contribution from past research. Kishi and Maekawa (1995) recommended a heat of hydration of 209 J/g for a fly ash with a CaO content of 8.8% based on SAC testing results. Schindler and Folliard (2005) proposed that the fly ash heat contribution should be calculated according to Equation 5.4. Finally, Ge and Wang (2009) proposed the relationship presented in Equations 5.5.

$h_{FA} = 1800 \cdot p_{FA\text{-}CaO}$ **Equation 5.4**

$h_{FA} = 15.9 \cdot (p_{FACaO} \times 100) + 74.3$ **Equation 5.5**

where:

h_{FA} = total heat of hydration of fly ash (J/g) and

$p_{FA\text{-}CaO}$ = fly ash CaO weight ratio in terms of total fly ash content.

A plot of fly ash heat contribution versus fly ash CaO content for the results presented by Kishi and Maekawa (1995), Schindler and Folliard (2005), and Ge and Wang (1999) are presented in Figure 5.2.

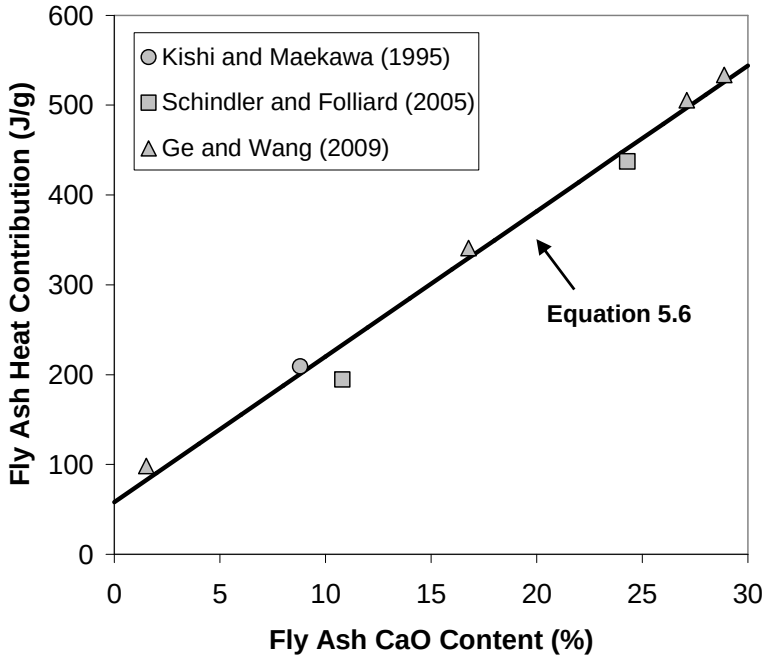

Figure 5.2: Fly ash heat contribution versus fly ash CaO content

Based on all past research, the best-fit expression for fly ash heat of hydration versus fly ash CaO content is presented below. This expression was used to calculate the heat of hydration of the fly ash used for this research.

$$h_{FA} = 16.2 \cdot (p_{FACaO} \times 100) + 58 \qquad \textbf{Equation 5.6}$$

where:

h_{FA} = total heat of hydration of fly ash (J/g), and

p_{FACaO} = fly ash CaO weight ratio in terms of total fly ash content.

5.2.2 Supplemental Data from Past Research

Schindler and Folliard (2005) created a model to predict the hydration development for concrete incorporating supplementary cementitious materials (fly ash and slag). To develop their model, two fly ash sources, one Class C and one Class F, and

three Type I cement sources were investigated. The fly ash dosages varied from 15% to 45% by volume of cementitious materials. SAC testing results from Schindler and Folliard's study were incorporated to expand the calibration database for this project.

The physical and chemical properties of the cementitious materials from the research conducted by Schindler and Folliard are presented in Table 5.2. From this table, it is shown that the Class C fly ash investigated by Schindler and Folliard has a similar CaO content to the FA-24 Class C fly ash evaluated for this research. The CaO content of the Class F ash, however, does not coincide with either of the Class F sources included in this research. The three cement sources identified varied slightly in their chemical composition and were all commonly available in Texas at the time of Schindler and Folliard's research.

Table 5.2: Chemical and physical properties of cementitious materials used by Schindler and Folliard (2005)

Parameter	Type I Portland Cement			Fly Ash	
	A	B	C	Class C	Class F
Silicon Dioxide, SiO_2 (%)	19.9	20.9	20.1	35.6	54.1
Aluminum Oxide, Al_2O_3 (%)	5.7	5	5.3	21.4	26.2
Iron Oxide, Fe_2O_3 (%)	2.9	1.8	3.2	5.6	3
Calcium Oxide, CaO (%)	63.6	65.4	65.5	24.3	10.8
Free CaO (%)	2.9	1	0.8	-	-
Magnesium Oxide, MgO (%)	1.3	1.4	0.6	4.8	2.4
Equivalent Alkalies (%)	0.69	0.52	0.67	1.4	0.3
Sulfur Trioxide, SO_3 (%)	3.5	2.9	3.3	1.2	0.3
Loss on Ignition (%)	1.9	1.44	1.2	0.3	0.1
Tricalcium Silicate, C_3S (%)	57	63	64	-	-
Dicalcium Silicate, C_2S (%)	14	12	9	-	-
Tricalcium Aluminate, C_3A (%)	10	10	8	-	-
Tetracalcium Aluminoferrite, C_4AF (%)	8	6	10	-	-
Blaine Value (m^2/kg)	358	354	367	-	-
Specific Gravity	-	-	-	2.75	2.33

SAC testing was used to characterize the hydration development for each of the mixtures investigated by Schindler and Folliard. The best-fit hydration parameters and w/cm ratios for each of the mixtures are presented in Table 5.3. The fly ash dosages, indicated in Table 5.3 under mixture description, were computed on a volume basis. Finally, the activation energies presented were calculated using Equation 2.15.

Table 5.3: Best-fit hydration parameters from SAC Testing for mixtures from Schindler and Folliard (2005)

Cement Source	Mixture Description	w/cm	E (J/mol)	Hydration Parameters			H_u (J/g)
				β	τ (hours)	α_u	
A	Type I Cement	0.37	46,000	0.905	13.69	0.689	477
A	15% Class C fly ash	0.37	43,100	0.874	13.81	0.713	471
A	25% Class C fly ash	0.38	41,300	0.772	23.28	0.793	468
A	35% Class C fly ash	0.38	39,400	0.716	29.43	0.893	464
A	45% Class C fly ash	0.39	37,500	0.724	36.66	0.849	460
A	15% Class F fly ash	0.38	40,700	0.825	15.97	0.797	444
A	25% Class F fly ash	0.39	37,200	0.786	18.30	0.831	421
A	35% Class F fly ash	0.40	33,700	0.809	19.08	0.838	396
A	45% Class F fly ash	0.41	30,100	0.774	21.73	0.894	370
B	Type I Cement	0.50	42,000	0.719	16.88	0.887	513
C	Type I Cement	0.50	46,300	0.727	16.32	0.882	492

5.3 Hydration Model Development

After assembling the calibration database, the hydration model for concrete proportioned with high fly ash replacement levels was developed. The first step in developing this model involved reviewing the hydration model for cementitious materials developed by Schindler and Folliard (2005). After reviewing this model, a "cement-only" hydration study was completed based on eight control concrete mixtures with no fly ash replacement. By completing this step, the most significant variables for cement

hydration based on present-day cement manufacturing processes were identified. Finally, the hydration model for concrete proportioned with high volume fly ash replacement was developed. Each of the three steps is explained in the following sections.

5.3.1 Hydration Model Developed by Schindler and Folliard (2005)

Schindler and Folliard (2005) used multivariate regression analysis to develop a hydration model for concrete incorporating cementitious materials. This model was developed from a database including SAC testing results from thirteen mixtures prepared by Schindler and Folliard and heat of hydration data for twenty cement sources from research conducted by Lerch and Ford (1948). The Lerch and Ford data set is one of the most comprehensive resources for heat of hydration data for United States cement sources. This data set includes heat of hydration test results for eight Type I cements, five Type II cements, three Type III, three Type IV cements, and one Type V cement. Based on this expanded database, Schindler and Folliard developed the following models for β and τ:

$$\beta = 181.4 \cdot p_{C3A}^{0.146} \cdot p_{C3S}^{0.227} \cdot Blaine^{-0.535} \cdot p_{SO3}^{0.558} \cdot \exp(-0.647 \cdot p_{SLAG}) \quad \textbf{Equation 5.7}$$

$$\tau = 66.78 \cdot p_{C3A}^{-0.154} \cdot p_{C3S}^{-0.401} \cdot Blaine^{-0.804} \cdot p_{SO3}^{-0.758} \cdot \exp(2.187 \cdot p_{SLAG} + 9.50 \cdot p_{FA} \cdot p_{FA\text{-}CaO}) \quad \textbf{Equation 5.8}$$

where:

p_{C3A} = weight ratio of C_3A in terms of total cement content,

p_{C3S} = weight ratio of C_3S in terms of total cement content,

$Blaine$ = cement Blaine value (m^2/kg),

p_{SO3} = weight ratio of SO_3 in terms of total cement content,

p_{SLAG} = weight ratio of GGBF slag in terms of total cementitious content,

p_{FA} = weight ratio of fly ash in terms of total cementitious content, and

$p_{FA\text{-}CaO}$ = weight ratio of fly ash CaO in terms of total fly ash content.

The ultimate degree of hydration model developed by Schindler and Folliard is presented in Equation 5.9. This model was based on the model developed by Mills (1966). From this model, complete hydration will never be achieved, but an increase in ultimate degree of hydration will be achieved when SCMs are used.

$$\alpha_u = \frac{1.031 \cdot w/cm}{0.194 + w/cm} + 0.50 \cdot p_{FA} + 0.30 \cdot p_{SLAG} \leq 1.0 \qquad \textbf{Equation 5.9}$$

where:

α_u = ultimate degree of hydration,

w/cm = water-cementitious material ratio by weight,

p_{FA} = weight ratio of fly ash in terms of total cementitious content, and

p_{SLAG} = weight ratio of GGBF slag in terms of total cementitious content.

The model developed by Schindler and Folliard was found to accurately predict the measured degree of hydration results from their calibration database. The coefficient of determination (r^2) and mean square of the error (s^2) were calculated to be 0.988 and 0.01%, respectively. A plot of measured versus predicted degree of hydration values for this model is presented in Figure 5.3.

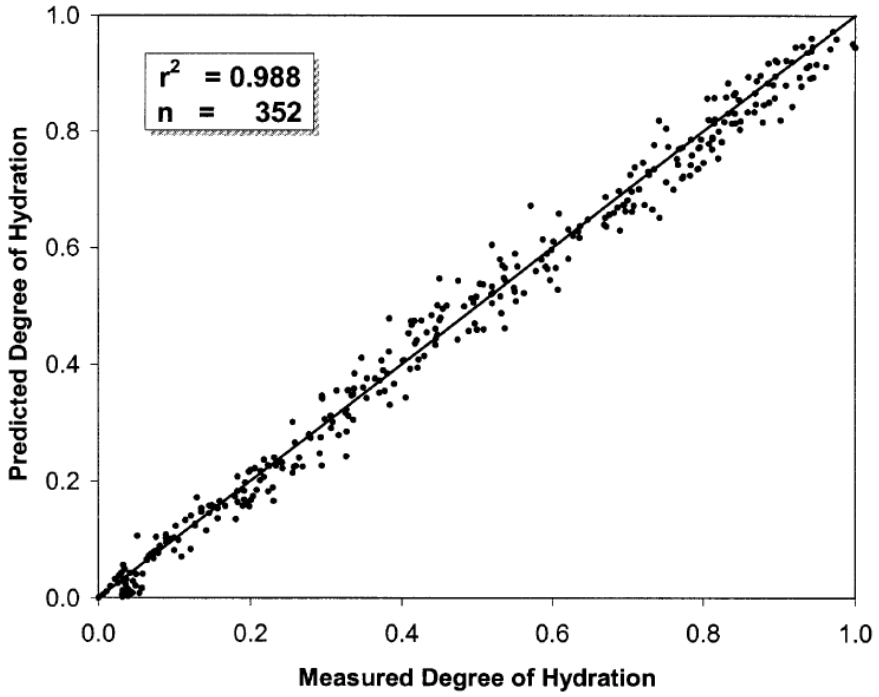

Figure 5.3: Plot of measured versus predicted degree of hydration for model developed by Schindler and Folliard (2005)

The model presented by Schindler and Folliard (2005) was developed with only two fly ash sources and does not account for the effect of chemical admixtures on hydration. Before developing a new hydration model for HVFA concrete, the model from Schindler and Folliard was applied to the calibration database described in Section 5.2, and the goodness of fit was evaluated. The β, τ, and α_u were calculated for each mixture using Equations 5.7 through 5.9. A plot of measured versus predicted degree of hydration values for this exercise is presented in Figure 5.4.

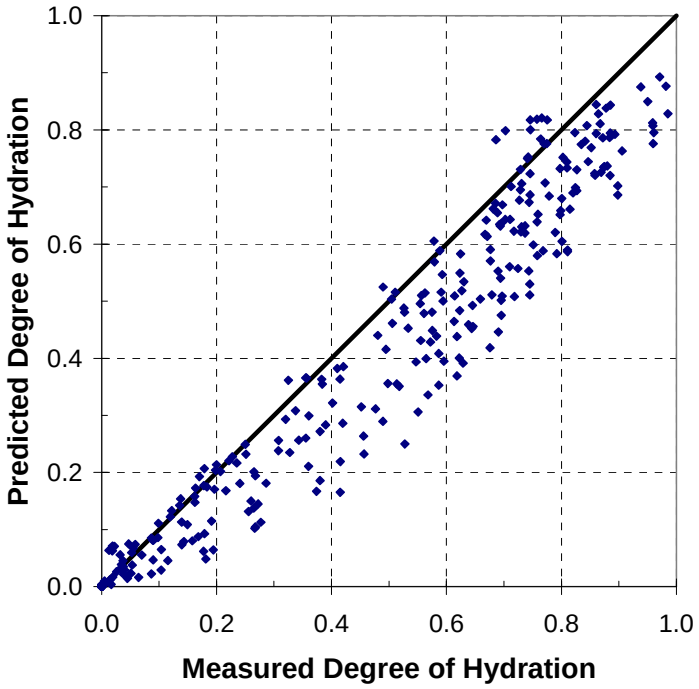

Figure 5.4: Plot of measured versus predicted degree of hydration for Schindler and Folliard (2005) model with calibration database from Section 5.2

Based on Figure 5.5, it is shown that the model developed by Schindler and Folliard (2005) provides a low estimate of the degree of hydration when compared to the measured results. The coefficient of determination (r^2) and standard deviation of the absolute error (S_j) were calculated to be 0.963 and 0.225, respectively. Based on these results, a new hydration model for HVFA concrete was developed to provide a more accurate estimate of hydration development.

5.3.2 Portland Cement Hydration Evaluation

In the model proposed by Schindler and Folliard (2005), each of the hydration parameters (τ and β) is composed of a "cement-only" expression and a modifier to

account for the behavior of SCMs. When no SCMs are used, the exponential portions of the τ and β expressions are equal to one, leaving the "cement-only" portion of the expression. Schindler and Folliard's model was developed based in part on the Lerch and Ford data set from the 1950s. Modifications to the cement manufacturing process have resulted in changes to both cement chemical composition and fineness. Therefore, a portland cement hydration study was conducted to identify the most significant variables for the development of the "cement-only" portions of the β and τ expressions to be used in the final HVFA concrete hydration model.

The portland cement study was completed based on the four control concrete mixtures from this project and the three cement-only mixtures from Schindler and Folliard's (2005) research. The database for this study included five Type I cement sources with varying chemical compositions, as identified in Tables 3.3 and 5.2. To identify the statistically significant variables, a regression model was developed to predict the degree of hydration parameters for each mixture. The chemical and physical properties of the cements were taken as explanatory variables and the hydration parameters (β and τ) were the response variables. With the use of SAS software, the RSQUARE (R^2) selection method was employed to evaluate the significance of both individual explanatory variables and combinations of explanatory variables. The SAS program file and output for the RSQUARE selection procedure is presented in Appendix E. The following sets of explanatory variables were found to provide the best statistical fit to the measured hydration parameters for the selected cement-only mixtures:

Hydration Shape parameter (β): 3 parameters, $r^2 = 0.9986$

$\beta = f(C_3A, SO_3, \text{Blaine})$

Hydration Time Parameter (τ): 3 parameters, $r^2 = 0.9846$

$\tau = f(C_2S, Blaine, NaEqu)$

Hydration Time Parameter (τ): 3 parameters, $r^2 = 0.9808$

$\tau = f(C_3S, C_3A, Blaine)$

where:

p_{C3A} = weight ratio of C_3A in terms of total cement content,

p_{SO3} = weight ratio of SO_3 in terms of total cement content,

Blaine = cement Blaine value (m^2/kg),

p_{C2S} = weight ratio of C_2S in terms of total cement content,

p_{C3S} = weight ratio of C_3S in terms of total cement content, and

NaEqu = cement equivalent alkali content in terms of total cement content.

Based on the seven concrete mixtures for this study, it is shown that the statistically significant variables for the prediction of β and τ differ slightly from those used in the model developed by Schindler and Folliard. From this study, it was determined that β could be accurately modeled by considering the cement tricalcium aluminate content (C_3A), the cement sulfate content (SO_3), and the cement fineness (Blaine). Two sets of variables for predicting τ were selected from this study. The first set of explanatory variables does not agree with what was used by Schindler and Folliard. It was found that τ could be accurately modeled by considering the cement dicalcium silicate content (C_2S), the cement fineness (Blaine) and the cement equivalent alkali content (NaEqu). The second set of variables, however, coincides with the model proposed by Schindler and Folliard. The statistically significant variables for β and τ

determined from this study were used to help select the explanatory variables to be used in the final HVFA concrete hydration model.

5.3.3 Development of Final Hydration Model

To develop the final hydration model, the modeling approach outlined in Section 5.1 was used to analyze the calibration database presented in Section 5.2. The SAS program outputs for each step of the modeling process are presented in Appendix E.

First, the explanatory variables to be used in the nonlinear analysis were selected. To do this, a regression model was developed to predict the degree of hydration parameters (β and τ) for each of the thirty-one concrete mixtures. The chemical and physical properties of the cements, fly ash chemical compositions and fly ash dosages were taken as explanatory variables. With SAS software, the RSQUARE selection method was used to evaluate the significance of individual and combinations of explanatory variables. The results from the portland cement hydration study were also used to help identify the significant variables. Based on the R^2 selection procedure and the portland cement hydration study, the following variables were found to provide the best statistical fit to the measured hydration parameters:

Hydration slope parameter (β): 4 parameters, $r^2 = 0.9530$

$$\beta = f\ (C_3A,\ NaEqu,\ Blaine,\ p_{FA},\ p_{FA\text{-}SiO2})$$

Hydration Time Parameter (τ): 4 parameters, $r^2 = 0.8473$

$$\tau = f\ (C_3A,\ C_2S,\ Blaine,\ p_{FA},\ p_{FA\text{-}CaO})$$

where:

p_{C3A} = weight ratio of C_3A in terms of total cement content,

p_{C2S} = weight ratio of C_2S in terms of total cement content,

NaEqu = cement equivalent alkali content in terms of total cement content,

Blaine = cement Blaine value (m^2/kg),

p_{FA} = fly ash volume ratio in terms of total cementitious content,

$p_{FA\text{-}SiO2}$ = fly ash SiO_2 weight ratio in terms of total fly ash content, and

$p_{FA\text{-}CaO}$ = fly ash CaO weight ratio in terms of total fly ash content.

The ultimate degree of hydration model developed by Mills (1966) was used successfully by Schindler and Folliard (2005) in the development of their hydration model for cementitious materials. Therefore, this ultimate degree of hydration model was used for development of the HVFA concrete hydration model. Similar to the approach taken by Schindler and Folliard, an increase in the ultimate degree of hydration due to the presence of fly ash was modeled as shown in Equation 5.10. The increase in ultimate degree of hydration, $\Delta\alpha_u$, was found to be a function of the fly ash dosage, p_{FA}.

$$\alpha_u = \frac{1.031 \cdot w/cm}{0.194 + w/cm} + \Delta\alpha_u \qquad \textbf{Equation 5.10}$$

where:

α_u = ultimate degree of hydration

w/cm = water-cementitious material ratio by weight

$\Delta\alpha_u$ = increase in ultimate degree of hydration due to presence of fly ash.

The variables selected to model the hydration parameters are suitable based on engineering judgment. Cements with high C_3A and Blaine values have high early-age strength gains due to an increased rate of hydration at early ages. As discussed in Section

2.3.1, C_3A begins to hydrate immediately when mixing water is added, liberating a significant amount of heat (1350 J/g). The hydration of the calcium silicates (C_3S and C_2S) occurs at a much slower rate than the C_3A hydration reaction, but still releases a considerable amount of heat. Schindler and Folliard (2005) used C_3S in their final hydration model. For the development of this model, C_2S replaced C_3S due to the discovery of a correlation between C_3S and C_3A during the RSQUARE selection procedure. Also, the cement sulfate content, SO_3, was not used for the HVFA concrete model due to a high correlation with C_3A. Finally, the cement equivalent alkali content was included in the development of the expression for β.

Parameters other than those selected for the final model may be used to effectively predict hydration development. When considering contributions of many variables simultaneously, however, the statistical best-fit regression model may not include these single most significant parameters.

After selecting the independent variables for β and τ, initial values for the regression model were determined by performing multivariate linear regression analysis. This analysis was completed with use of the SAS GLM procedure. The analysis of variance (ANOVA) results from the GLM procedure are presented in Appendix E.

After determining initial values for the regression model, the final hydration model could be developed. For development of the final model, the response variables were the degree of hydration values versus concrete equivalent age for each mixture. The degree of hydration values used for modeling corresponded to equivalent ages of 1, 4, 8, 12, 24, 48, 72, 168, 672, and 2160 hours. A total of 299 observations were used for development of the final model. The final nonlinear regression analysis was performed

with the SAS NLIN procedure. The NLIN procedure is an iterative method that requires that initial estimates of the regression coefficients be given and the nonlinear regression model be defined.

The results from the NLIN procedure are presented in Appendix E. From the results, it is shown that convergence was achieved. The best-fit models for β, τ, and α_u are presented in Equations 5.11 to 5.13.

$$\beta = p_{C3A}^{0.670} \cdot NaEqu^{0.080} \cdot Blaine^{2.55} \cdot \exp(-1.37 \cdot p_{FA} \cdot p_{FA\text{-}SiO2} - 12.9) \quad \textbf{Equation 5.11}$$

$$\tau = p_{C3A}^{-1.42} \cdot p_{C2S}^{0.556} \cdot Blaine^{-7.32} \cdot \exp(6.12 \cdot p_{FA} \cdot p_{FA\text{-}CaO} + 43.5) \quad \textbf{Equation 5.12}$$

$$\alpha_u = \frac{1.031 \cdot w/cm}{0.194 + w/cm} + 0.428 \cdot p_{FA} \leq 1.0 \quad \textbf{Equation 5.13}$$

where:

p_{C3A} = weight ratio of C_3A in terms of total cement content,

p_{C3S} = weight ratio of C_3S in terms of total cement content,

NaEqu = cement equivalent alkali content in terms of total cement content,

Blaine = cement Blaine value (m^2/kg),

p_{FA} = weight ratio of fly ash in terms of total cementitious content,

$p_{FA\text{-}SiO2}$ = fly ash SiO_2 weight ratio in terms of total fly ash content,

p_{FACaO} = weight ratio of fly ash CaO in terms of total fly ash content, and

w/cm = water-cementitious material ratio by weight.

A scatter plot of the measured degree of hydration values from SAC testing versus the predicted values from the final model (Equations 5.11 to 5.13) is presented in Figure 5.5. This figure illustrates that the model accurately predicts the hydration

development for concrete containing high fly ash dosages based on cement chemical composition, cement fineness, fly ash chemical composition, fly ash dosage and w/cm ratio.

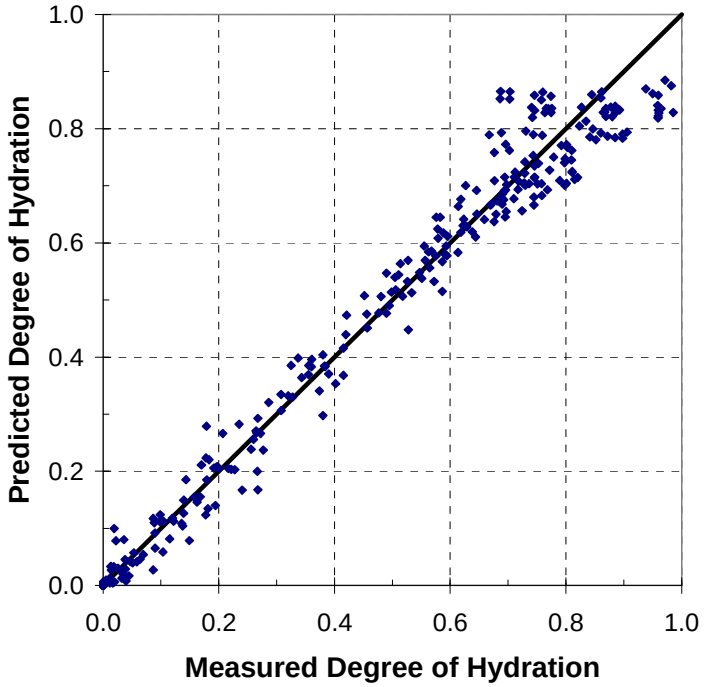

Figure 5.5: Plot of measured versus predicted degree of hydration for final model

The goodness of fit of the final model was evaluated by calculating the coefficient of determination (r^2) and the standard deviation of the absolute error (S_j). The r^2 for the final model was calculated to be 0.991. This r^2 indicates that 99.1% of the experimental variation of the response variable is explained by the final model. The standard deviation of the absolute error (S_j) for the final model was calculated to be 0.104. For the final model, a random distribution of the unexplained error is desired. Therefore, residual plots were constructed to evaluate the homogeneity of variance. The residual plot for the final model is presented in Figure 5.6. Residual plots for each of the explanatory

variables used in the final model are presented in Appendix E along with the SAS program outputs for each step in the modeling process.

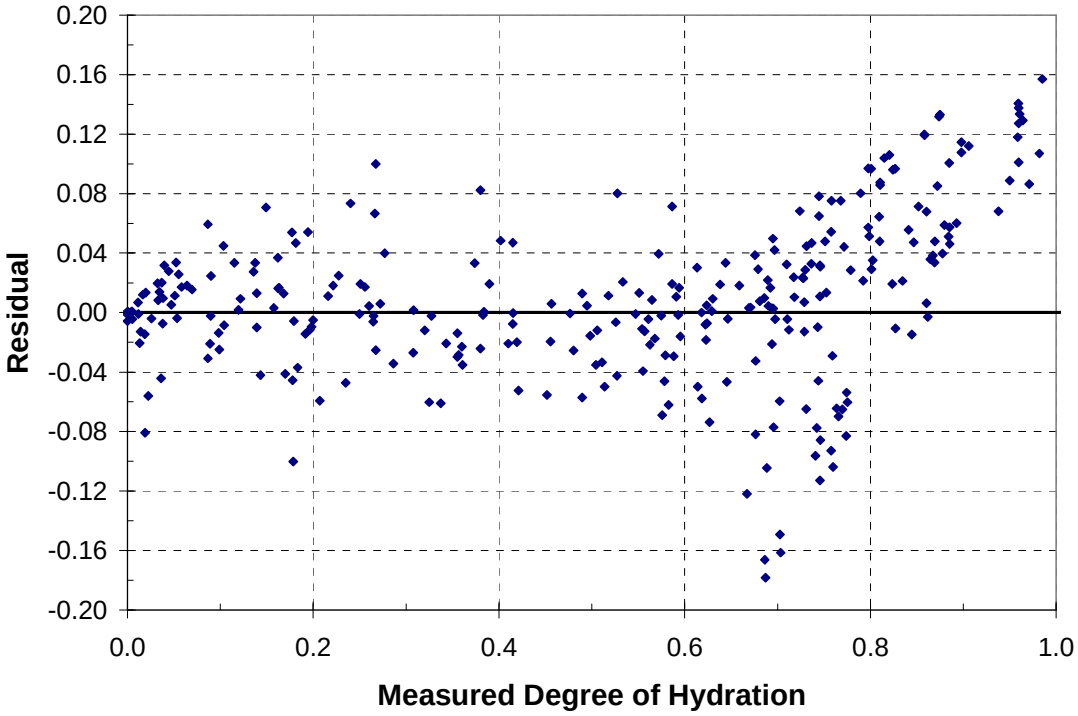

Figure 5.6: Plot of measured degree of hydration versus residual

5.4 Summary

Typically, SAC testing is used to characterize the hydration development of concrete mixtures. As discussed in Section 2.4.2, the true adiabatic temperature profile may be determined for any concrete mixture by correcting the semi-adiabatic profile for the device-specific heat losses. After calculating the true adiabatic temperature profile, the degree of hydration at any time may be computed based on the heat generated at that given time versus the total heat of hydration of the cementitious system (Equations 2.4 and 2.5). Finally, the hydration parameters (β, τ, α_u) may be calculated by fitting Equation 2.13 to the experimentally determined degree of hydration curve.

A nonlinear regression analysis was used to develop a model to predict the hydration development of HVFA concrete mixtures. The calibration database used to develop this hydration model included SAC testing results obtained from both the laboratory testing portion of this project and Schindler and Folliard's (2005) research. Using this model, the hydration shape parameter (β), hydration time parameter (τ) and ultimate degree of hydration (α_u) for HVFA concrete mixtures may be computed independently based on the chemical composition of the cementitious materials and the mixture proportions of the HVFA concrete mixture. With the use of this model, the SAC testing procedure outlined above is not required. Therefore, the hydration parameters may be calculated quickly without the time or cost associated with SAC testing. This HVFA concrete hydration model was used to develop design aids to predict the maximum in-place concrete temperature, time to initial set, and compressive strength development of HVFA concrete placed in selected transportation structures. This process is described in the following chapter.

Chapter 6

Evaluation of the Modeled In-Place Performance of HVFA Concrete

After completing all laboratory testing and developing the HVFA concrete hydration model, the modeled in-place performance of HVFA concrete was evaluated. The results from this analysis are intended to aid contractors and transportation agencies in estimating the maximum in-place concrete temperature, initial setting times, and compressive strength development for HVFA concrete when used in various transportation structures. In the following sections, the analysis approach and baseline conditions that were used to complete this analysis are introduced. Also, sample in-place temperature profiles are presented. Finally, a review of the modeled in-place performance of HVFA concrete as it relates to maximum in-place concrete temperature, time to initial set, and compressive strength development is presented.

6.1 Analysis Approach

The final stage of this research consisted of evaluating the in-place performance of HVFA concrete to provide guidance to contractors and transportation agencies. The goal of this research was to ultimately increase the use of HVFA concrete by providing a reliable means to estimate the in-place performance of HVFA concrete mixtures. Specifically, the maximum in-place concrete temperature, setting times, and compressive strength development were investigated for HVFA concrete placed in varying conditions.

When HVFA concrete is used in mass concrete applications, a reduction in maximum in-place concrete temperature can reduce the susceptibility of the concrete to

delayed ettringite formation (DEF). DEF is defined as the "formation of ettringite in a cementitious material by a process that begins after hardening is substantially complete and in which none of the sulfate comes from outside the cement paste (Taylor et al. 2001)." For DEF to occur, the concrete must be subjected to high temperatures early in the curing process. Taylor et al. (2001) reported that the critical temperature for portland cement concrete is 158 °F. Folliard et al. (2008) recommend a maximum in-place concrete temperature of 185 °F when at least 25% Class F or 35% Class C fly ash dosages are specified. When the in-place concrete temperature exceeds these limits, the formation of ettringite is inhibited and the formation of calcium silicate hydrate (C-S-H) is accelerated. The sulfates which form ettringite at normal curing temperatures are trapped in the C-S-H. At later ages, the sulfate ions are released from the C-S-H and react with available monosulfate hydrate (MSH) to form ettringite (Folliard et al. 2008). The formation of ettringite exerts pressure on the surrounding hardened concrete, causing expansion and cracking (Folliard et al. 2008). In this chapter, the maximum in-place concrete temperatures are estimated for HVFA concrete mixtures under varying placement conditions.

One of the main barriers to the increased use of HVFA concrete is the concern over retarded set times, especially when high fly ash dosages are specified or cold curing conditions are encountered. Retarded set times can cause delays to concrete finishing operations, causing HVFA concrete to be undesirable. Similarly, there are concerns over low early-age compressive strength development for HVFA concrete. Low early-age compressive strength development can require extended curing, which can delay formwork removal times and negatively impact construction sequencing. In this chapter,

in-place setting and compressive strength development are estimated for HVFA concrete mixtures under varying placement conditions.

To evaluate the performance of HVFA concrete for each of the properties identified above, the ConcreteWorks software program was used to estimate in-place temperature profiles for HVFA concrete placed under various placement conditions. Multiple iterations were performed with the ConcreteWorks software to examine the effect of fly ash type, fly ash dosage, concrete member type, and placement temperature on the in-place temperature development, time to initial set, and compressive strength development of HVFA concrete.

The ConcreteWorks software program was developed at the Concrete Durability Center at the University of Texas. This software may be used to calculate mass concrete temperature development, thermal stress development, alkali-silica reaction (ASR) susceptibility, and delayed ettringite formation (DEF) susceptibility of user-defined concrete mixtures under various placement conditions. The software is available for free download to the public at http://www.texasconcreteworks.com.

To evaluate the in-place performance of HVFA concrete, the temperature prediction feature of the ConcreteWorks software program was used. The temperature prediction calculations performed by ConcreteWorks are based on heat transfer modeling. Detailed information on the heat transfer analysis method, concrete thermal properties, and concrete element models used by the ConcreteWorks software may be found in the ConcreteWorks User Manual (Riding 2007).

For the ConcreteWorks analysis, various HVFA concrete mixtures were investigated to quantify the effect of fly ash type and dosage on the in-place performance.

The HVFA concrete mixtures that were used for the ConcreteWorks analysis are introduced in Section 6.2.3. After selecting the database of HVFA concrete mixtures to be used for the analysis, iterations were performed to evaluate the effect of various placement conditions and element types on the development of the in-place concrete temperature for each mixture.

6.2 Baseline Conditions for ConcreteWorks Analysis

In the following sections, the baseline conditions that were used to complete the ConcreteWorks analysis are detailed. First, an overview of the HVFA concrete mixtures that were used to develop the in-place temperature profiles is presented. Next, the concrete placement temperature and ambient weather conditions are defined. Finally, each of the concrete element types and their corresponding modeling inputs are presented.

6.2.1 HVFA Concrete Mixtures

To evaluate the in-place performance of HVFA concrete, a database of HVFA concrete mixtures with varying fly ash dosages and fly ash types were analyzed with the ConcreteWorks software program. Simulations were completed for each concrete mixture to develop in-place concrete temperature profiles based on varying placement conditions. In the following section, the HVFA concrete mixtures used for this analysis are detailed.

The HVFA concrete mixtures for the ConcreteWorks analysis were varied based on the fly ash dosage and fly ash type. Iterations were completed at fly ash dosages of 0,

35%, and 50% by volume of cementitious materials. For each fly ash dosage investigated, iterations were completed using two Class F and two Class C fly ash sources, each with varying chemical compositions. The four fly ash sources used for the ConcreteWorks analysis correspond to the four sources used for the laboratory testing phase of this research. The chemical composition for each source is defined in Table 3.5.

The ConcreteWorks software program accommodates user-defined inputs for all materials defined in the concrete mixture proportioning stage. To eliminate unwanted variability in the ConcreteWorks results due to changes in materials, a single cement source and single aggregate source were used for all ConcreteWorks simulations. The "low-alkali" (LA) cement source from W.R. Grace was selected. The chemical composition of this cement is presented in Table 3.3. As discussed in Chapter 3, this cement source was received in two shipments, LA Cement (1) and LA Cement (2), each with slightly different chemical compositions. For the ConcreteWorks simulations, the hydration parameters for each concrete mixture were computed using the chemical composition of LA Cement (1). The coarse aggregate and fine aggregate used for all simulations were a siliceous river gravel and siliceous river sand, respectively.

The mixture proportions for the 35% and 50% fly ash dosage mixtures correspond to the LA-35FA and LA-50FA concrete mixture proportions presented in Table 3.2. For each concrete mixture, the hydration parameters (E, β, τ, α_u, and H_u) were required to develop the in-place concrete temperature profiles. The HVFA concrete hydration model developed in Chapter 5 was used to estimate the hydration time parameter (τ), hydration shape parameter (β), and ultimate degree of hydration (α_u) for each concrete mixture. The activation energy (E) for the 35% and 50% fly ash dosage mixtures were determined

from isothermal calorimetry. For all mixtures, the total heat of hydration (H_u) was calculated based on the chemical composition of the cement and fly ash sources according to Equations 2.7, 2.8, and 5.6. A summary of the hydration parameter inputs for each of the concrete mixtures is presented in Table 6.1.

Table 6.1: ConcreteWorks hydration parameter inputs

Mix	Hydration Parameters				
	E (J/mol)	**β**	**τ (hours)**	**α_u**	**Hu (J/kg)**
CTRL44-LA	33,500	1.199	9.544	0.716	478,880
LA-35-1	28,300	0.901	9.753	0.838	369,511
LA-35-15	36,300	0.936	13.26		426,143
LA-35-24	32,600	0.994	15.65		469,017
LA-35-28	35,700	1.027	17.37		489,333
LA-50-1	29,600	0.798	9.844	0.870	314,697
LA-50-15	30,300	0.842	15.26		401,086
LA-50-24	29,900	0.917	19.34		464,285
LA-50-28	33,700	0.962	22.45		494,019

6.2.2 Placement Conditions and Concrete Temperature

The ConcreteWorks software program includes a database of environmental conditions (temperature, wind speed, percent cloud cover, solar radiation, atmospheric pressure, and relative humidity) based on thirty-year average data for 239 U.S. cities. At least one city is included for each of the 50 states, as well as the U.S. territories of Guam and Puerto Rico. When defining the placement conditions for ConcreteWorks analysis, the placement time, placement date, and project location must be selected (Riding et al. 2007).

In addition to the placement time, date, and location, the fresh concrete temperature must also be specified. The fresh concrete temperature is the temperature of the concrete when it is placed at the jobsite. The ConcreteWorks software program allows for the fresh concrete temperature to be defined in one of three ways. First, the fresh concrete temperature may be calculated based on the concrete mixture proportions according to ACI 305R (1999). Second, the fresh concrete temperature can be estimated to be equal to the ambient temperature at the time of placement. Finally, the fresh concrete temperature may be entered manually (Riding 2007).

To evaluate the in-place performance of HVFA concrete, the fresh concrete temperature (T_{c0}) was assumed to be equal to the ambient air temperature (T_{air}) from the ConcreteWorks historical database ($T_{c0} = T_{air}$). Using this assumption, iterations were completed for fresh concrete temperatures equal to 40, 50, 60, 70, 80, 90 and 95 °F. The upper and lower bounds for the fresh concrete temperatures were selected to reflect the conventional limits on concrete placement temperature.

Since the fresh concrete temperature was taken to be equal to the ambient air temperature, multiple project locations, placement times, and placement dates could be used to complete the analysis for each placement temperature that was investigated. To complete the ConcreteWorks analysis, two project locations were investigated: Chicago, Illinois and Phoenix, Arizona. These two cities were selected to allow the full range of placement temperatures to be evaluated. No one city in the United States could be found that reached the average temperature extremes of 40 and 95 °F.

For the ConcreteWorks analysis, column elements and flatwork elements were modeled for in-place temperature development. A description of the modeling

considerations for each element type is presented in the following section. The placement conditions for each fresh concrete temperature are defined in Tables 6.2 and 6.3 for the column elements and flatwork elements, respectively. A 12:00 PM (noon) time of placement was used for all column element simulations. For the flatwork elements, an earlier placement time was selected in an effort to ensure that the peak heat of hydration and solar radiation peak both occur within the first 24 hours. A preliminary analysis was conducted, and it was found that noon placement time for the flatwork elements resulted in an offset in the heat of hydration and solar radiation peaks for the HVFA mixtures due to their retarded rate of hydration. In Tables 6.2 and 6.3, a range of placement dates is given for each fresh concrete temperature. For each range of placement dates, the ambient air temperature, T_{air}, is equal to the specified concrete temperature, $T_{concrete}$, plus/minus 2 °F. In the final column of both tables, the placement date that was used to complete the iterations at the specified fresh concrete temperature is given.

Table 6.2: Placement conditions for Column Elements

T_{c0}	Project Location	Time of Placement	Range of Placement Dates	Placement Date
40 °F	Chicago, IL	12:00 PM (noon)	November 20–27	November 24
			March 19–21	
50 °F			November 4–9	November 7
			April 6–11	
60 °F			October 7–17	October 12
			April 29-May 3	
70 °F			September 13–22	September 17
			May 18-June 3	
80 °F			June 30-August 31	July 15
90 °F	Phoenix, AZ		May 15-June 2	May 22
			September 17-October 2	
95 °F			June 7–16	June 13
			August 11-September 10	

Table 6.3: Placement conditions for Flatwork Elements

T_{c0}	Project Location	Time of Placement	Range of Placement Dates	Placement Date
40 °F	Chicago, IL	9:00 AM	November 10–19	November 12
			March 23–28	
50 °F			October 23–30	October 27
			April 12–17	
60 °F			September 23-October 2	September 29
			May 8–15	
70 °F			September 4–11	September 10
			June 4–6	
80 °F	Phoenix, AZ		September 17–30	September 25
			May 16–31	
90 °F			June 22-July 8	June 24
			July 15-August 10	
95 °F		10:00 AM	June 27-July 15	July 2

6.2.3 Concrete Element Types

The ConcreteWorks software program has built-in concrete member models for mass concrete elements (columns, footings, bent caps), concrete bridge decks, precast concrete beams, and concrete pavements. Each member type has different formwork, boundary conditions, curing methods, and geometry considerations defined within the ConcreteWorks software that are used to generate in-place temperature profiles. To evaluate the in-place performance of HVFA concrete, three element types were

investigated: columns, bridge decks, and pavements. In the following sections, the inputs and modeling considerations used for each of the three element types are detailed.

6.2.3.1 Mass Concrete – Square Column

To evaluate the in-place performance of HVFA concrete for mass concrete applications, three square column sizes were analyzed. The ConcreteWorks software program models a two-dimensional horizontal cross section for column members and assumes heat transfer in the vertical direction to be zero (Riding 2007). Therefore, the columns were defined based on their plan dimensions. To reduce the computational time required to generate the in-place temperature profiles, the ConcreteWorks software program models column elements by considering symmetry in both directions (Riding 2007). The rectangular column model used by the ConcreteWorks software is presented in Figure 6.1. The plan dimensions analyzed for the three column sizes were: 3 ft x 3 ft, 6 ft x 6 ft, and 10 ft x 10 ft. These three column sizes were selected to bracket typical sizes used for transportation structures.

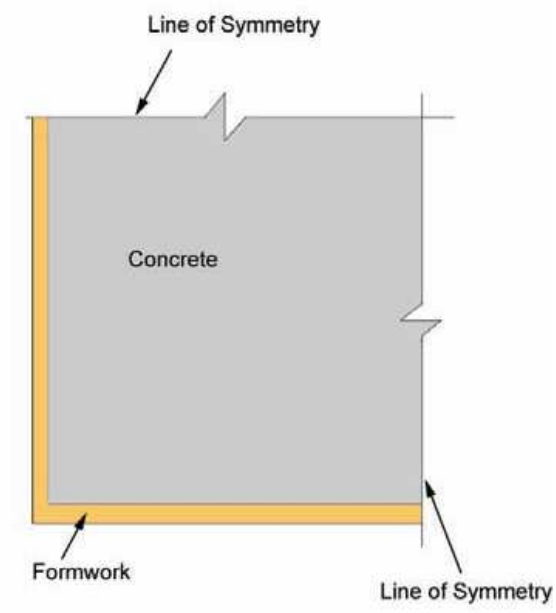

Figure 6.1: Square column model used by ConcreteWorks (Riding 2007)

The ConcreteWorks software program considers three separate construction phases to develop the in-place temperature profiles for column elements. The three phases are based on user-defined inputs for formwork removal times and curing techniques. Three construction phases are considered for simulating concrete column temperature development (Riding 2007):

1. concrete placement and curing before form removal,
2. after form removal and before curing techniques are applied, and
3. concrete curing.

For this project, all concrete columns were modeled according to the conditions defined in Table 6.4.

Table 6.4: Concrete column modeling inputs

Construction Phase	Parameter	Modeling Input
1	Formwork	Steel (red) without form liners
	Concrete age at form removal	96 hours
2	Time between form removal and curing	1 hour
3	Curing method	Wet curing blanket with clear plastic sheeting

6.2.3.2 Concrete Bridge Deck

A concrete bridge deck element was also analyzed. Bridge deck in-place temperature profiles are generated by ConcreteWorks assuming one-dimensional heat transfer through a vertical cross section of the deck (Riding 2007). The bridge deck model used by the ConcreteWorks software program is presented in Figure 6.2. ConcreteWorks may be used to model the temperature development of bridge decks cast on prestressed panels, metal pans, or removable wood forms. For this analysis, a bridge deck with metal pan formwork was used for all simulations. The overall deck thickness was selected to be 8 in., with a 2 in. cover for the top mat of steel. An 8 in. thick bridge deck is used for many full-depth bridge decks built in the United States.

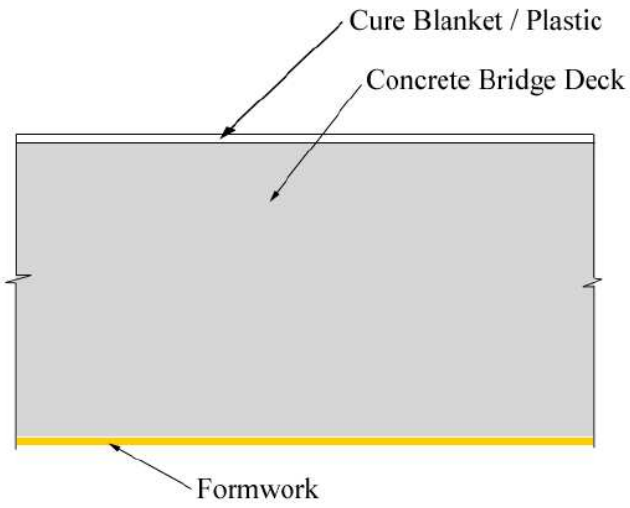

Figure 6.2: Bridge deck model used by ConcreteWorks (Riding 2007)

To develop the in-place temperature profile for the bridge deck elements, the ConcreteWorks software program considers four construction phases based on user-defined inputs for formwork removal times and curing techniques (Riding 2007):

1. after placement and before selected curing method is applied to top surface,
2. curing method is applied to top surface, but before form removal (if applicable) and curing method removal,
3. curing method removed from top surface, and
4. form removal, if applicable.

For this project, the concrete bridge deck was modeled according to the conditions defined in Table 6.5.

Table 6.5: Concrete bridge deck modeling inputs

Construction Phase	Parameter	Modeling Input
1	Formwork	Steel (red) without form liners
2	Cure method	Curing blanket with clear plastic sheeting
	Concrete age when curing is applied	1 hour
3	Concrete age at curing removal	168 hours

6.2.3.3 Concrete Pavement

The final type of concrete member considered for evaluation of the in-place performance of HVFA concrete was a concrete pavement. Concrete pavement temperature profiles are generated by ConcreteWorks assuming one-dimensional heat transfer through a vertical cross section (Riding et al. 2007). The pavement cross section is composed of five layers: curing blanket, concrete pavement, subbase 1, subbase 2, and subgrade. The pavement model used by the ConcreteWorks software is presented in Figure 6.3.

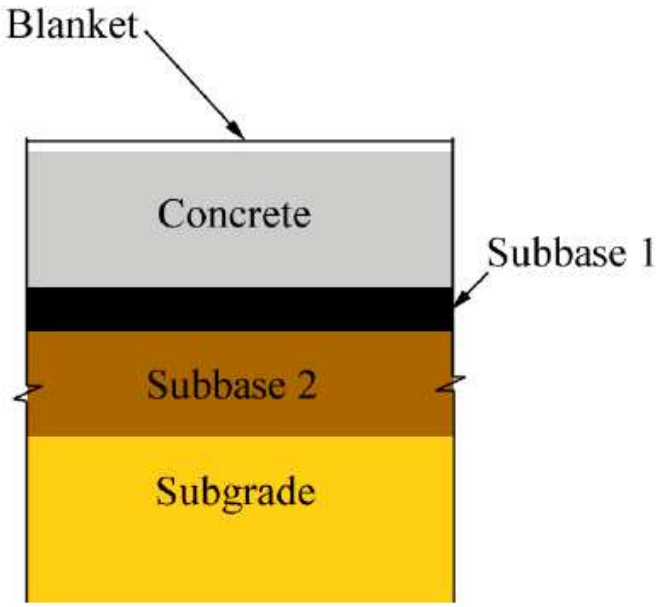

Figure 6.3: Pavement model used by ConcreteWorks (Riding 2007)

The subbase and subgrade types are selected by the user, and ConcreteWorks generates the corresponding material properties (thermal conductivity, specific heat, density, solar absorptivity, and emissivity). The material properties used for each subbase type are defined in the ConcreteWorks user manual. A concrete pavement with the following dimensions was used for all simulations:

pavement thickness	=	14 inches,
subbase 1	=	asphalt concrete (3 inch thickness),
subbase 2	=	granular (12 inch thickness), and
subgrade	=	clay.

To develop the in-place temperature profile for the concrete pavement, the ConcreteWorks software program considers three construction phases (Riding 2007):

1. before selected curing method is applied,
2. curing method is applied, and
3. curing method removed.

For all concrete pavement simulations, a white curing compound was selected as the curing method. The curing compound was applied one hour after paving was completed.

6.3 Sample In-Place Temperature Profiles from ConcreteWorks Analysis

In this section, the effect of fly ash dosage, fly ash CaO content, placement temperature, and element type on the in-place temperature development of HVFA concrete is reviewed. All in-place temperature profiles presented in this chapter were generated using the baseline conditions presented in Section 6.2. Iterations were completed for each combination of concrete element type, concrete mixture, and placement temperature, leading to a total of 315 in-place temperature profiles. Due to the large number of iterations, representative results are presented in this section to identify the effect of each variable (fly ash dosage, fly ash type, placement temperature, and element type) on the in-place temperature development of HVFA concrete. After reviewing the effect of each variable separately, an overall evaluation of the in-place performance of HVFA concrete is described in Section 6.4. Sample in-place temperature profile data from ConcreteWorks are presented in Appendix F.

6.3.1 Effect of Fly Ash Dosage on In-Place Temperature Development

The general effect of fly ash dosage on the in-place temperature development of HVFA concrete is presented in Figure 6.4. In this figure, the temperature profiles are presented for the concrete mixtures proportioned with the 1% CaO Class F fly ash and the 24% CaO Class C fly ash at both the 35% and 50% dosages. The temperature profile for the CTRL44-LA mixture is also presented. The temperature profiles presented correspond to the 6 ft x 6 ft column element placed at 70 °F. In each plot, temperature profiles are presented for nodes located at both the center and the edge of the column elements.

In Figure 6.4, it is shown that the effect of fly ash dosage on the in-place temperature development is dependent on both the chemical composition of the fly ash and mixture proportions of the concrete. For the 1% CaO Class F fly ash mixtures, an increase in fly ash dosage from 35% to 50% resulted in a decrease in the maximum in-place concrete temperature (measured at the center of the member) from approximately 140 °F to 132 °F. Both of the Class F fly ash mixtures generated less heat than the control mixture (CTRL44-LA). For the 24% CaO Class C fly ash mixtures, however, the same increase in dosage resulted in no change in the maximum in-place concrete temperature. Also, the Class C fly ash mixtures reached a higher maximum in-place concrete temperature than the control mixture. The results obtained for the Class C fly ash mixtures are attributed to the combined effect of the increased fly ash heat of hydration and the low w/cm ratio of the mixture. The effect of fly ash CaO content on the in-place temperature development will be discussed in the following section.

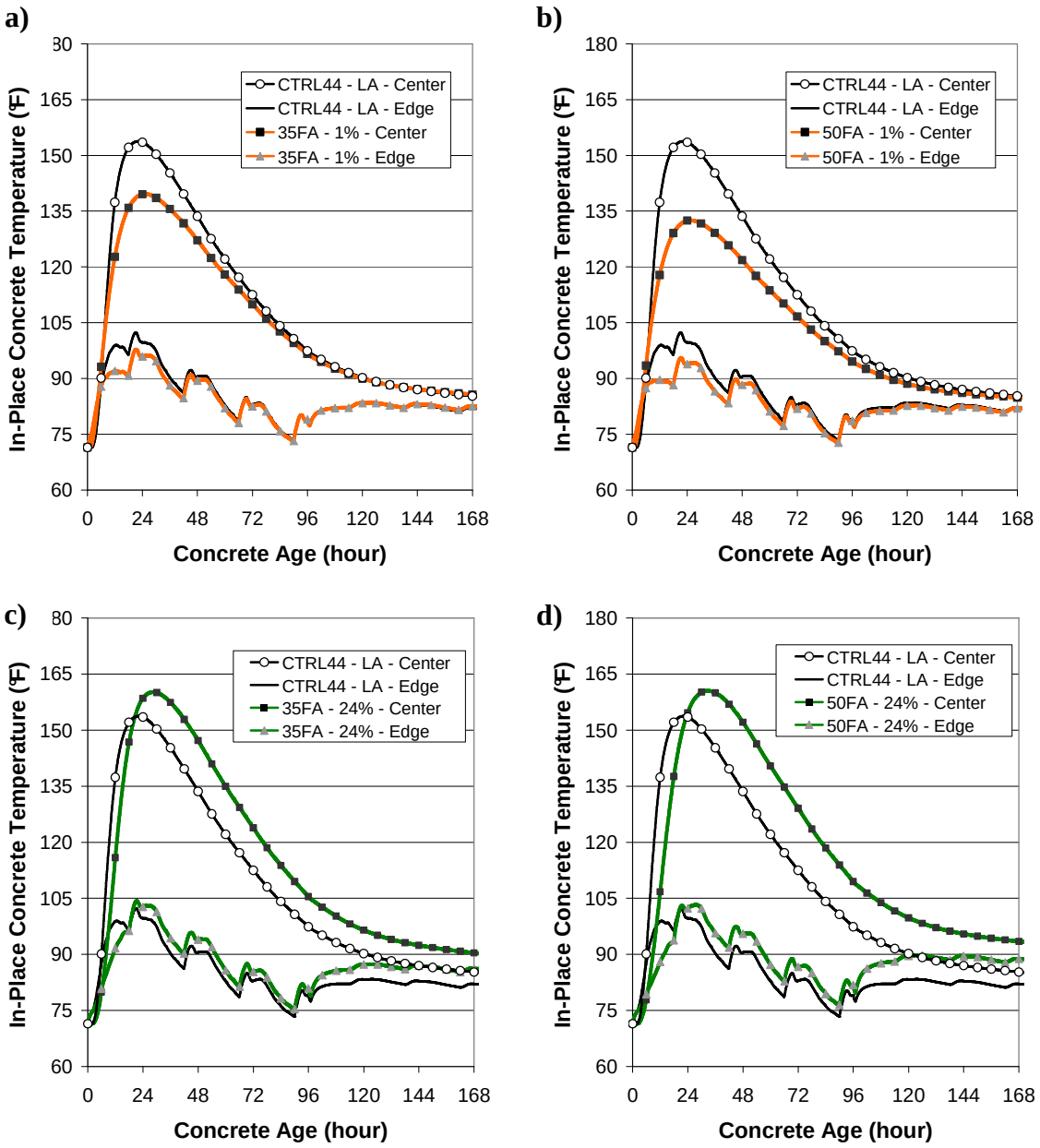

Figure 6.4: In-place temperature profiles for 6 ft x 6 ft columns placed at 70 °F for the following mixtures: a) 35FA-1%, b) 50FA-1%, c) 35FA-24%, and d) 50FA-24%

6.3.2 Effect of Fly Ash Type on In-Place Temperature Development

The general effect of fly ash type on the maximum in-place temperature development for the 6 ft x 6 ft columns is presented in Figure 6.5. The results presented

in this figure represent the estimated temperature development at the center node of the column element. The results were generated with a concrete placement temperature of 70 °F.

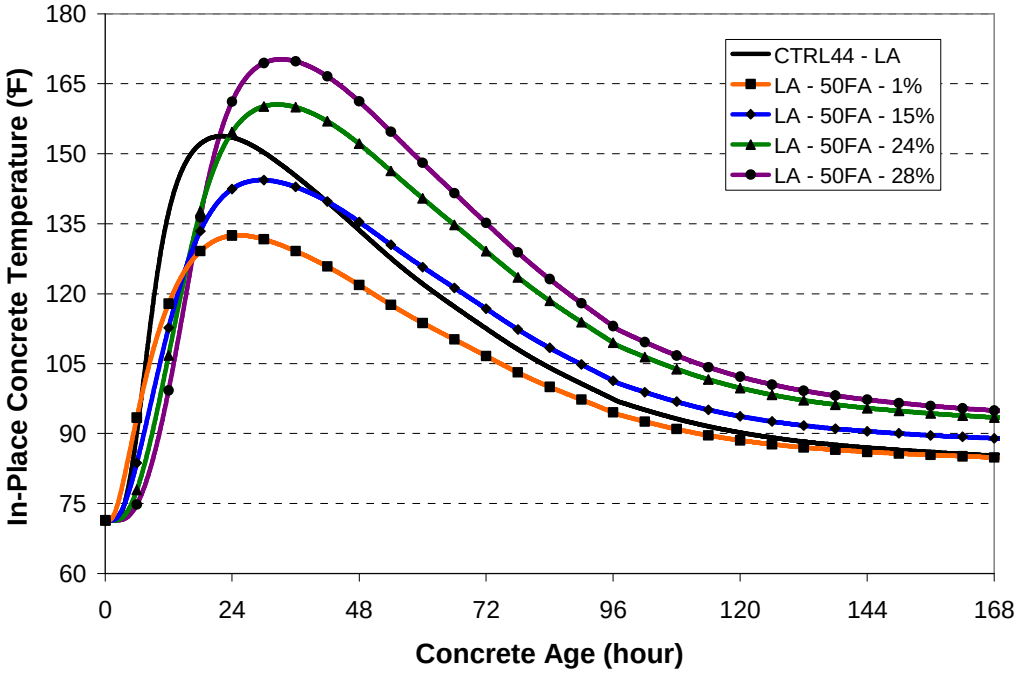

Figure 6.5: In-place temperature profiles for HVFA concrete proportioned with 50% fly ash dosage placed in 6 ft x 6 ft columns at 70 °F

In Figure 6.5, it is shown that as the fly ash CaO content increases, for a given fly ash dosage, the maximum in-place concrete temperature also increases. In Equation 5.6, it was shown that the heat contribution of fly ash increases based on the CaO content of the ash. For the 6 ft x 6 ft columns placed at 70 °F, an increase in fly ash CaO content from 1% to 28% resulted in an increase in the maximum in-place concrete temperature of 37 °F. Also, the HVFA concrete mixtures proportioned with a 50% dosage of the Class C fly ashes reached a higher in-place concrete temperature than the control mixture. The same trend was observed for the 10 ft x 10 ft columns; however, the maximum in-place

concrete temperature increased by 45 °F as the fly ash CaO content increased from 1% to 28%.

The results presented in Figure 6.5 agree with past research conducted by Langley et al. (1992), as described in Section 2.5.2.5. Langley et al. (1992) reported that the temperature rise caused by the hydration of concrete proportioned with high dosages of Class F fly ashes can be significantly lower than the temperature rise of a control concrete with no fly ash replacement. For their study, the maximum temperature rise for a 10 ft x 10 ft x 10 ft meter concrete block was reduced by 52 °F when a 55% dosage of a Class F fly ash was used.

6.3.3 Effect of Curing Conditions on In-Place Temperature Development

The effect of concrete placement temperature on the in-place temperature development of HVFA concrete is illustrated in Figure 6.6. In this figure, the in-place temperature profiles at the center of the 6 ft x 6 ft column are presented when placed at 40 °F and 95 °F. Similar temperature profiles for 6 ft x 6 ft columns placed at 70 °F were presented in Figure 6.5.

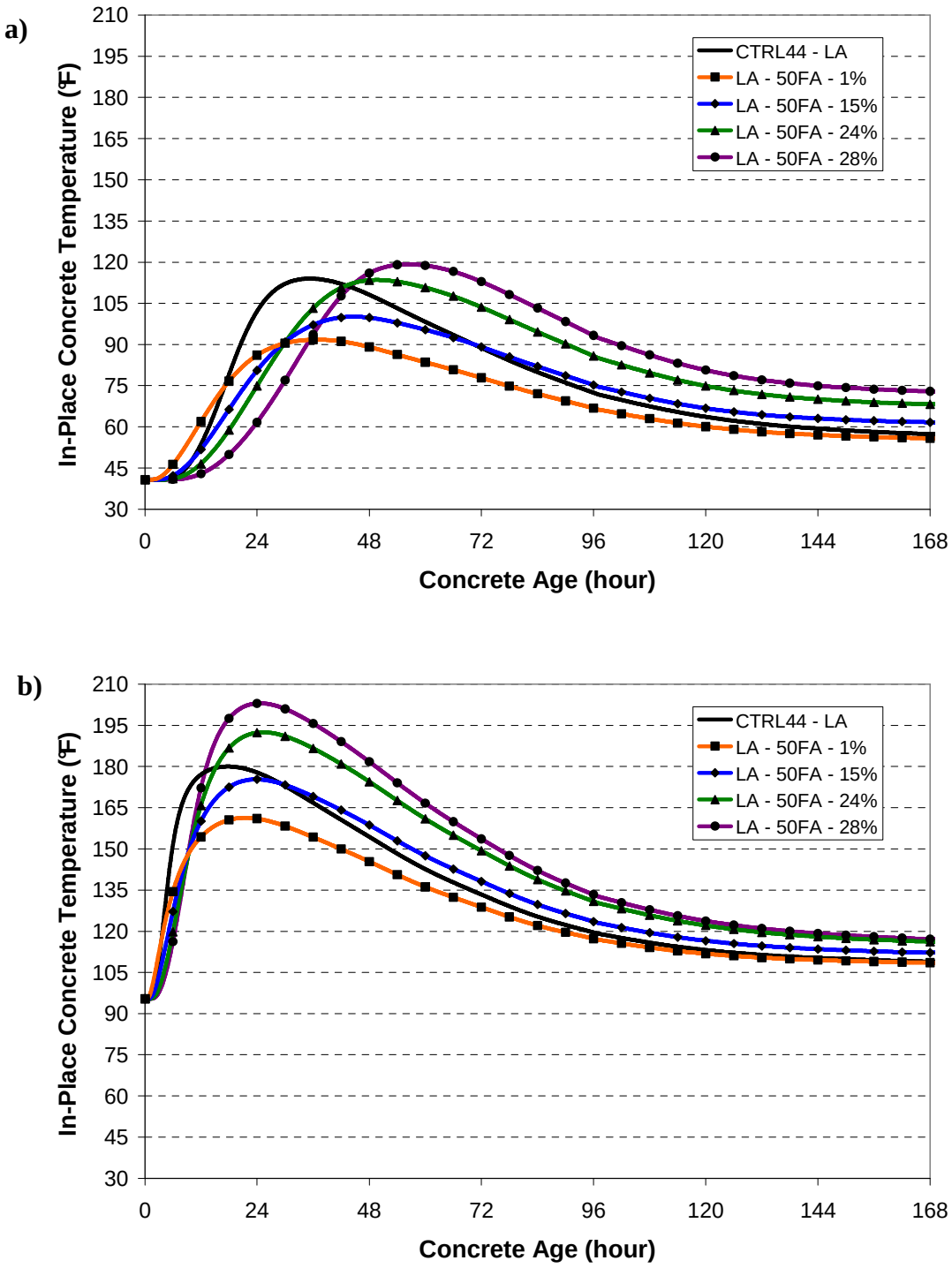

Figure 6.6: In-place temperature profiles for HVFA concrete proportioned with 50% fly ash dosage placed in 6 ft x 6 ft columns at a) 40 °F and b) 95 °F

The results presented in Figure 6.6 indicate that the in-place temperature development of HVFA concrete is dependent on the concrete placement temperature and curing conditions. An increase in placement temperature from 40 °F to 95 °F resulted in a 69 °F increase in maximum in-place temperature from 92 °F to 161 °F for the 1% CaO Class F fly ash mixture and 78 °F increase from 114 °F to 192 °F for the 24% CaO Class C fly ash mixture. The results also illustrate that the rate of temperature development is significantly affected by the concrete placement temperature. For example, when the concrete placement temperature is decreased from 95 °F to 40 °F for the 6 ft x 6 ft columns, the time required to reach the maximum in-place temperature for the 50FA-1% mixture increases from approximately 22 hours to 36 hours. Similarly, the time required to reach the maximum in-place concrete temperature for the 50FA-28% concrete mixture increases from 24 hours to 57 hours. The results presented in Figures 6.5 and 6.6 illustrate that the in-place temperature development of HVFA concrete mixtures varies according to curing conditions.

6.3.4 Effect of Concrete Element Type on In-Place Temperature Development

The general effect of element type on the in-place temperature development of HVFA concrete is presented in Figure 6.7. In this figure, in-place temperature profiles from the center of the element are presented for the 50% fly ash dosage concrete mixtures when placed in the 10 ft x 10 ft column and 8 in. bridge deck elements. The profiles presented in this figure were generated using a placement temperature of 70 °F. Results for the 6 ft x 6 ft columns placed at 70 °F are shown previously in Figure 6.5.

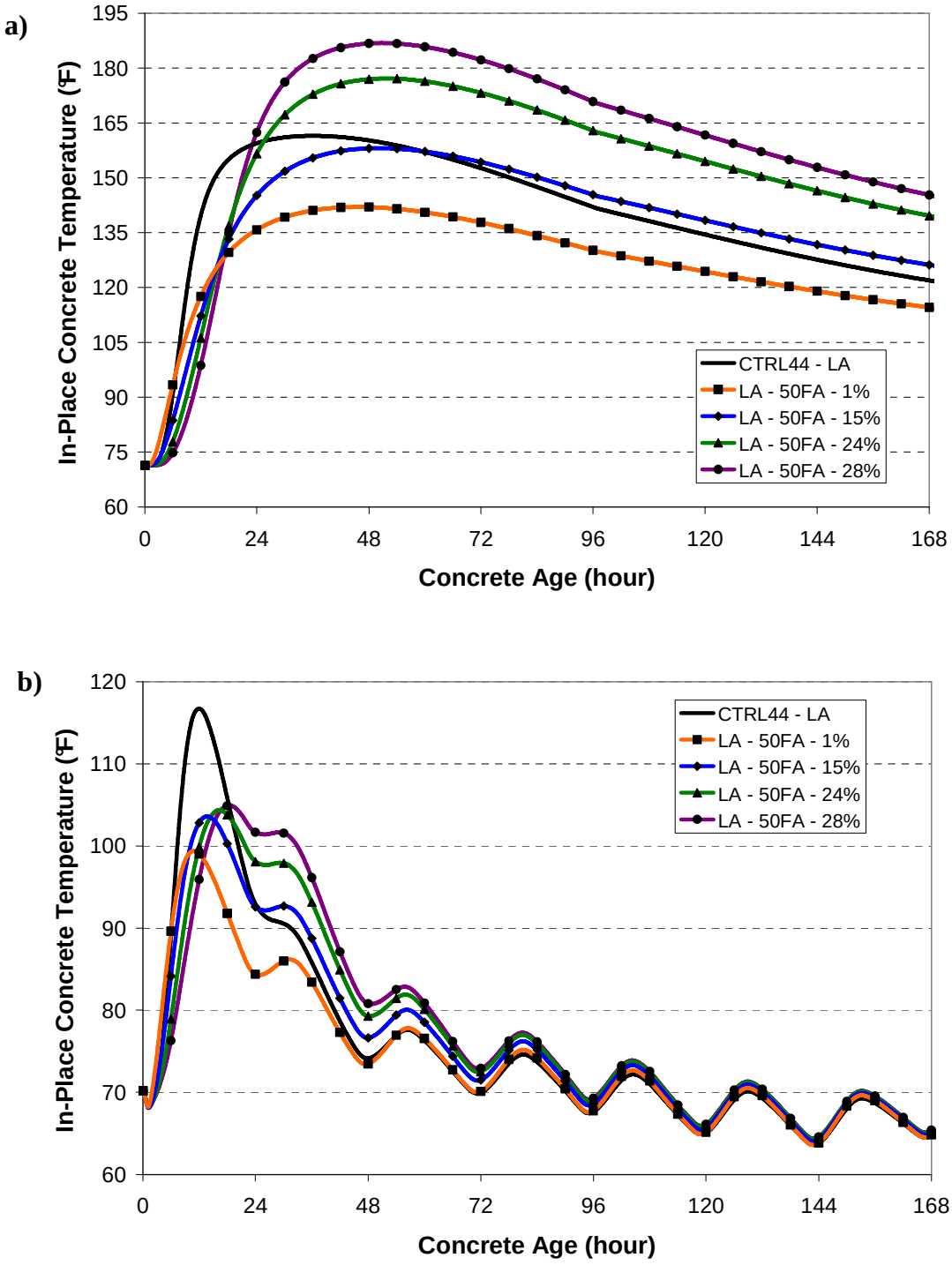

Figure 6.7: In-place temperature profiles for HVFA concrete proportioned with 50% fly ash dosage placed in: a) 10 ft x 10 ft column and b) 8 in. bridge deck elements at 70 °F

From Figures 6.5 and 6.7, it is shown that as the concrete element size increases, for a given placement temperature and concrete mixture, the maximum in-place concrete temperature also increases. Also, the time required for the center of the concrete element to return to the ambient temperature conditions increases with an increase in element size. In Figure 6.7b, it is shown that the temperature development of the 8 in. bridge deck element is more susceptible to changes in ambient temperature conditions than the column elements. At 48 hours and beyond, the in-place concrete temperature for the bridge deck is shown to vary according to the diurnal temperature cycle. Also, it is shown that after 4 days, the average ambient temperature begins to decrease below the selected placement temperature of 70 °F. Similar results were obtained for the 14 in. pavement element. The results presented in this section illustrate that the in-place temperature development of HVFA concrete varies according to concrete element type.

6.4 Evaluation of In-Place Performance of HVFA Concrete

In the previous section, the general effects of fly ash dosage, fly ash type, placement temperature, and element type on the in-place temperature development of HVFA concrete were each examined individually. In this section, the combined effect of the four variables on the in-place performance of HVFA concrete is examined. The results presented in this section are designed to provide guidance on the estimation of the maximum in-place concrete temperature, initial set times, and compressive strength development of HVFA concrete mixtures placed in selected transportation structures.

6.4.1 Maximum In-Place Concrete Temperature

In the following sections, the ConcreteWorks analysis results for maximum in-place concrete temperature are summarized for each element that was investigated. After reviewing all results, it was determined that the HVFA concrete mixtures proportioned with the 24% and 28% CaO Class C fly ashes had similar maximum in-place temperature development results. Therefore, only the results for the 28% CaO Class C fly ash concrete mixtures are presented in this section.

6.4.1.1 Column Elements

Maximum in-place concrete temperature versus concrete placement temperature plots for the 3 ft x 3 ft, 6 ft x 6 ft, and 10 ft x 10 ft columns are presented in Figures 6.8, 6.9, and 6.10, respectively. In these figures, the results for the control concrete mixture (CTRL44 – LA) and HVFA concrete mixtures proportioned with the 1%, 15% and 28% CaO content fly ashes are presented. All results presented in Figures 6.8 through 6.10 correspond to the maximum temperature generated at the center node of the column elements. Also, the DEF temperature limits for concrete proportioned with portland cement (PC) and supplementary cementitious materials (SCMs) are marked in each figure.

In Figure 6.8, it is shown that the maximum in-place concrete temperature increases linearly according to an increase in the concrete placement temperature. Also, the maximum in-place concrete temperature for the HVFA concrete mixtures proportioned with 50% fly ash dosages were consistently lower than those proportioned with the 35% dosage of the same ash.

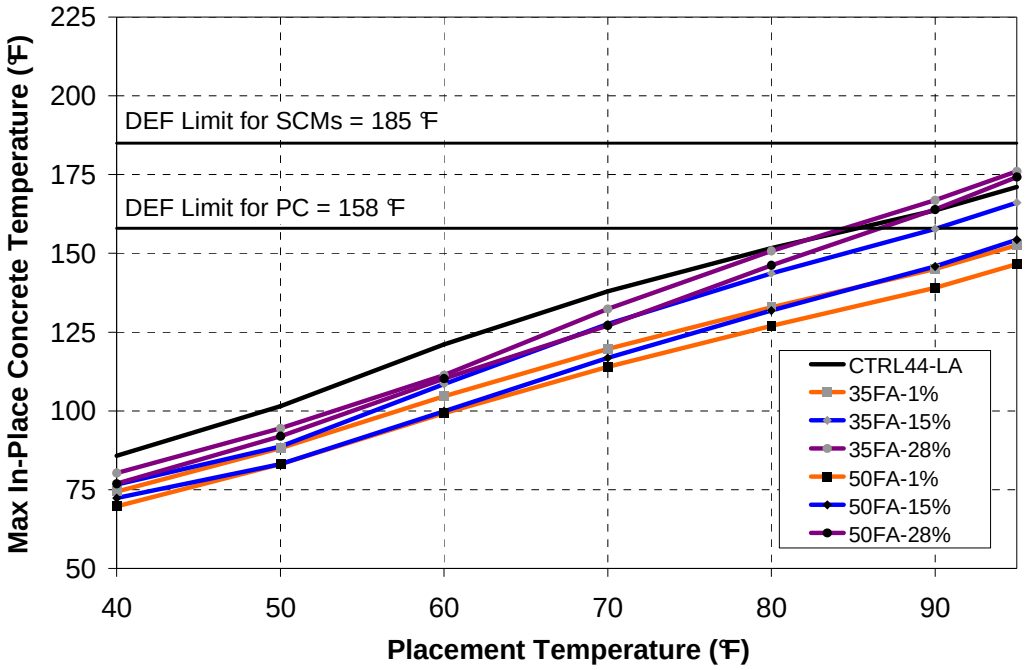

Figure 6.8: Maximum in-place concrete temperature versus concrete placement temperature for 3 ft x 3 ft columns

The HVFA concrete mixtures proportioned with the Class F fly ash sources (1% and 15% CaO content) generated less heat than the control mixture at all placement temperatures. The only HVFA mixtures with a maximum in-place concrete temperature greater than the control mixture were the 35FA-28% and 50FA-28% mixtures placed at 90 and 95 °F. For these cases, however, the in-place concrete temperature of the HVFA mixtures only exceeded the control concrete mixture results by a maximum of 5 °F. The results presented in Figure 6.8 indicate that when HVFA concrete is used for 3 ft x 3 ft or smaller columns, the mixtures may be proportioned with high dosages of both Class F and Class C fly ashes without running the risk of exceeding the threshold for the formation of DEF.

The maximum in-place concrete temperature results for the 6 ft x 6 ft columns are presented in Figure 6.9.

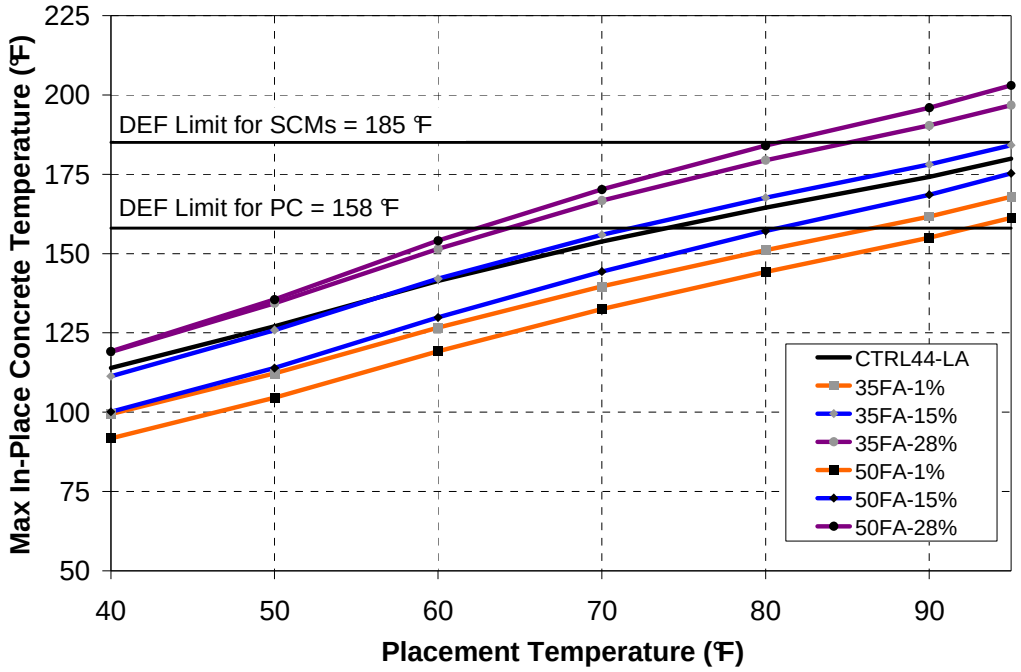

Figure 6.9: Maximum in-place concrete temperature versus concrete placement temperature for 6 ft x 6 ft columns

In Figure 6.9, the same linear relationship between maximum in-place concrete temperature and placement temperature is observed. For the 6 ft x 6 ft columns however, there is a larger range of maximum in-place temperature results for the HVFA concrete mixtures at each placement temperature. It is also shown that the maximum in-place concrete temperature for the Class C fly ash concrete mixtures exceeded the maximum in-place temperature for the control concrete mixture at all placement temperatures. Also, the results for the 35FA-15% mixture were nearly identical to the results for the control concrete mixture at all placement temperatures.

For the HVFA concrete mixtures proportioned with the Class F fly ashes, the maximum in-place concrete temperature for the 50% dosages were lower than the results for the mixtures proportioned with 35% fly ash at all placement temperatures. These results are similar to those obtained for the 3 ft x 3 ft columns. The same trend was not observed for the Class C fly ash mixtures, however. The results presented in Figure 6.9 illustrate that an increase in fly ash dosage does not translate to reduced maximum in-place temperature development when high-calcium Class C fly ashes are used for large concrete elements.

Finally, the maximum in-place temperature results for the 10 ft x 10 ft columns are presented in Figure 6.10.

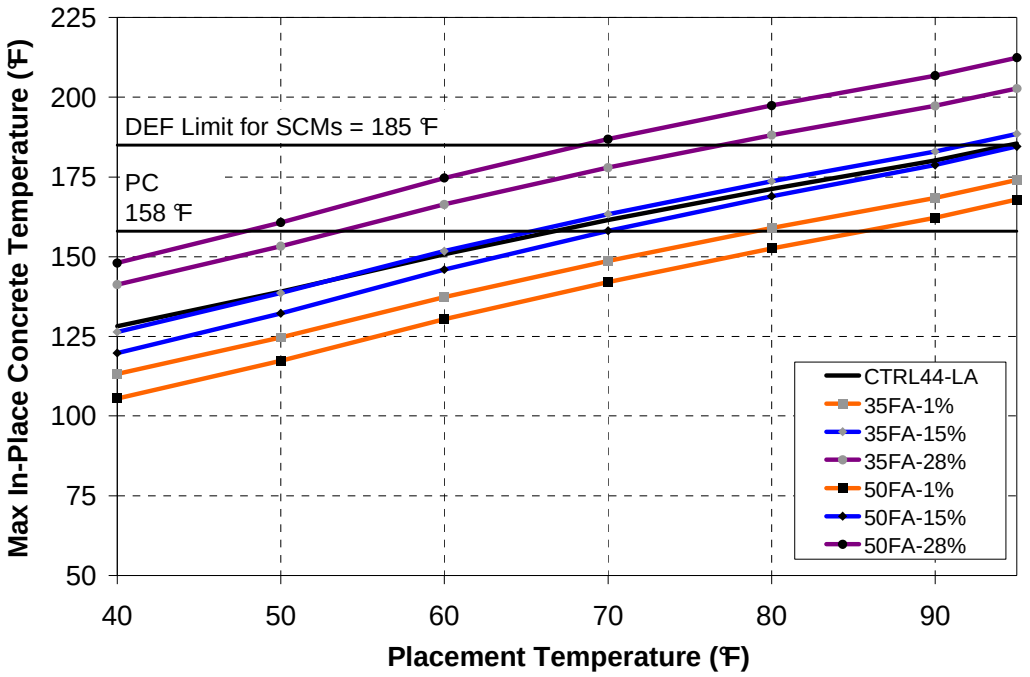

Figure 6.10: Maximum in-place concrete temperature versus concrete placement temperature for 10 ft x 10 ft columns

The results obtained for the 10 ft x 10 ft columns are similar to those obtained for the 3 ft x 3 ft and 6 ft x 6 ft columns. At the 10 ft x 10 ft column size, the low-calcium Class F fly ash mixtures (CaO = 1%) are still shown to generate less heat than the control concrete. At all placement temperatures, the maximum in-place temperature for the 50FA-1% mixture is approximately 20 °F less than the control mixture temperature. The results for the 50FA-28% mixture, however, range from 20 to 27 °F higher than the control concrete results when the placement temperature is increased from 40 °F to 95 °F.

The key findings from the results presented in Figures 6.8 through 6.10 may be summarized as follows:

- There is an aproximatly linear relationship between maximum in-place concrete temperature and concrete placement temperature for all HVFA concrete mixtures and column sizes that were investigated.
- For all column sizes investigated, the HVFA concrete produced with the 1% CaO Class F fly ash generated less heat than the control concrete mixture.
- For both Class F fly ash mixtures, an increase in fly ash dosage from 35% to 50% resulted in a decreased maximum in-place temperature, despite the lowered w/cm ratio.
- The results from the 6 ft x 6 ft and 10 ft x 10 ft columns indicate that an increase in fly ash dosage does not translate to reduced maximum in-place temperature development when high-calcium Class C fly ashes are used for large mass concrete elements.

6.4.1.2 Flatwork

Maximum in-place concrete temperature results for the 8 in. bridge deck and 14 in. pavement elements are presented in Figures 6.11 and 6.12. The results represent the maximum temperature generated at mid-depth of the members. The placement conditions for all flatwork element iterations are presented in Table 6.3.

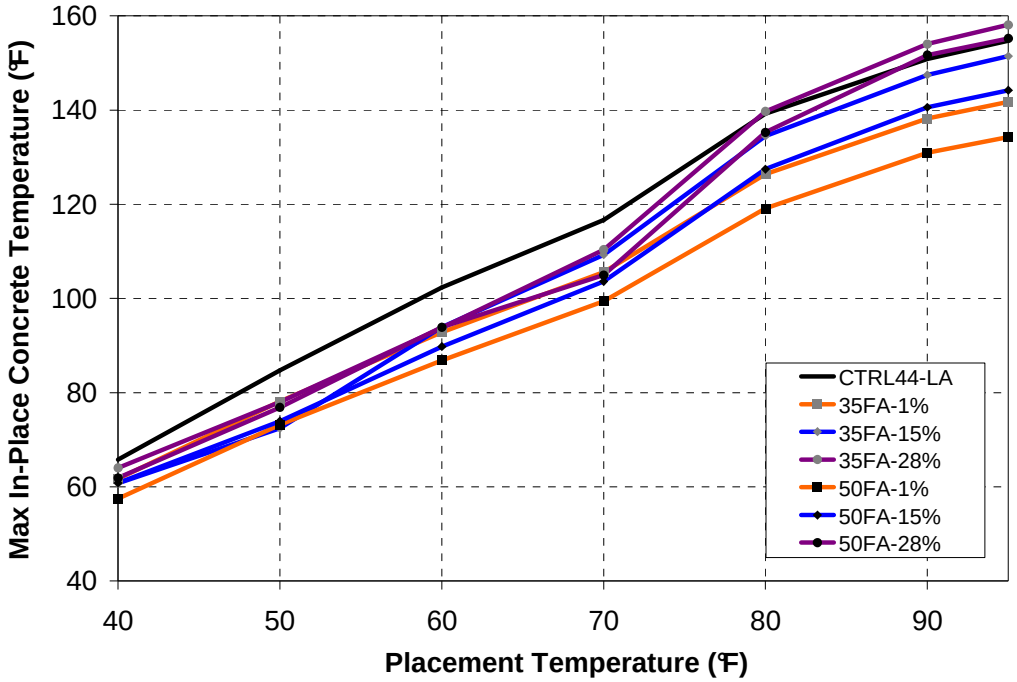

Figure 6.11: Maximum in-place concrete temperature versus concrete placement temperature for 8 in. bridge deck element

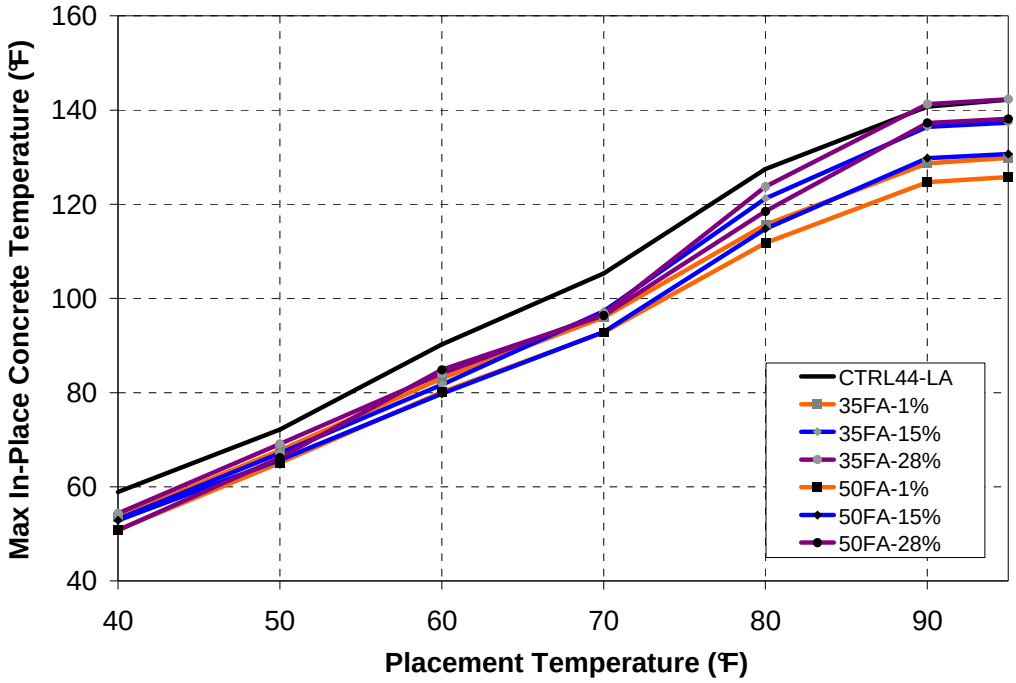

Figure 6.12: Maximum in-place concrete temperature versus concrete placement temperature for 14 in. pavement element

The results presented in Figures 6.11 and 6.12 show that both flatwork elements had very similar in-place temperature development results. At the 40 to 70 °F placement temperatures there is very little separation between the maximum in-place temperature results for all HVFA concrete mixtures. At the 80 to 95 °F placement temperatures, there is increased separation between the HVFA concrete temperature results. These results indicate that the in-place temperature development for HVFA concrete placed in flatwork elements is most influenced by element size, curing method, and placement conditions rather than the fly ash dosage and fly ash CaO content at low placement temperatures. At all placement temperatures, the 50% fly ash dosage mixtures generated less heat than the 35% fly ash dosages for each fly ash source.

When comparing the 8 in. bridge deck and 14 in. pavement results, it is shown that the pavement element had lower maximum in-place concrete temperatures at all placement temperatures, despite having a greater thickness. The maximum difference in the in-place temperature results between the two elements was 10 °F at the 40 °F placement temperature and 17 °F at the 95 °F placement temperature. The higher in-place temperature results for the 8 in. bridge deck element can be attributed to the curing method. The bridge deck element was cured with a blanket, whereas a white curing compound was used for the pavement element.

The results for the bridge deck and pavement elements are similar to the results presented in Figure 6.8 for the 3 ft x 3 ft column element, except that higher temperatures are reached in the thicker concrete column. For all three elements, the HVFA concrete mixtures generated less heat than the control mixture at all placement temperatures, regardless of fly ash dosage and CaO content. The only exception to this trend were the 28% CaO Class C fly ash mixtures at the 90 and 95 °F placement temperatures. The key findings from the results presented in Figures 6.11 and 6.12 may be summarized as follows:

- For the flatwork elements at low placement temperatures (40 to 70 °F) the temperature development of HVFA concrete is most influenced by the element size, curing method, and placement conditions rather than the fly ash dosage and fly ash CaO content.
- For small columns (3 ft x 3 ft or smaller) and flatwork elements, high-calcium Class C fly ash sources may be used at high dosages without

high in-place concrete temperatures, even at placement temperatures exceeding 80 °F.

6.4.2 Initial Set Time

The in-place temperature profiles from the ConcreteWorks analysis were used to estimate the time required to reach initial set for each of the HVFA concrete mixtures. During the laboratory testing phase of this project, the equivalent age at initial and final set were calculated for each room temperature batch. The equivalent ages at initial set are summarized in Table 6.6 for the HVFA concrete mixtures used for the ConcreteWorks analysis. Since the equivalent age at initial set was known for each mixture, the time required to reach initial set could be calculated based on the equivalent age maturity method and in-place concrete temperature profiles generated using ConcreteWorks.

Table 6.6: Equivalent age at initial set for LA cement mixtures

Mix Description	Equivalent Age at Initial Set (hours)
CTRL44-LA	4.38
LA-35-1	3.54
LA-35-15	4.57
LA-35-24	5.15
LA-35-28	4.73
LA-50-1	3.61
LA-50-15	4.12
LA-50-24	5.78
LA-50-28	5.73

Initial set is typically used for timing of finishing operations. Therefore, to estimate the time required to reach initial set, the temperature profile at the *surface* of each element was used. This location was used because the maturity of the concrete at the surface of the element will drive finishing operations. After reviewing the ConcreteWorks results, it was found that the temperature profiles at the surface of the elements were affected by the element type, time of placement, and curing method. Example temperature profiles are shown in Figure 6.13 for the 50FA-15% concrete mixture placed in the 6 ft x 6 ft column, 10 ft x 10 ft column, 8 in. bridge deck, and 14 in. pavement at placement temperatures of 40 and 95 °F.

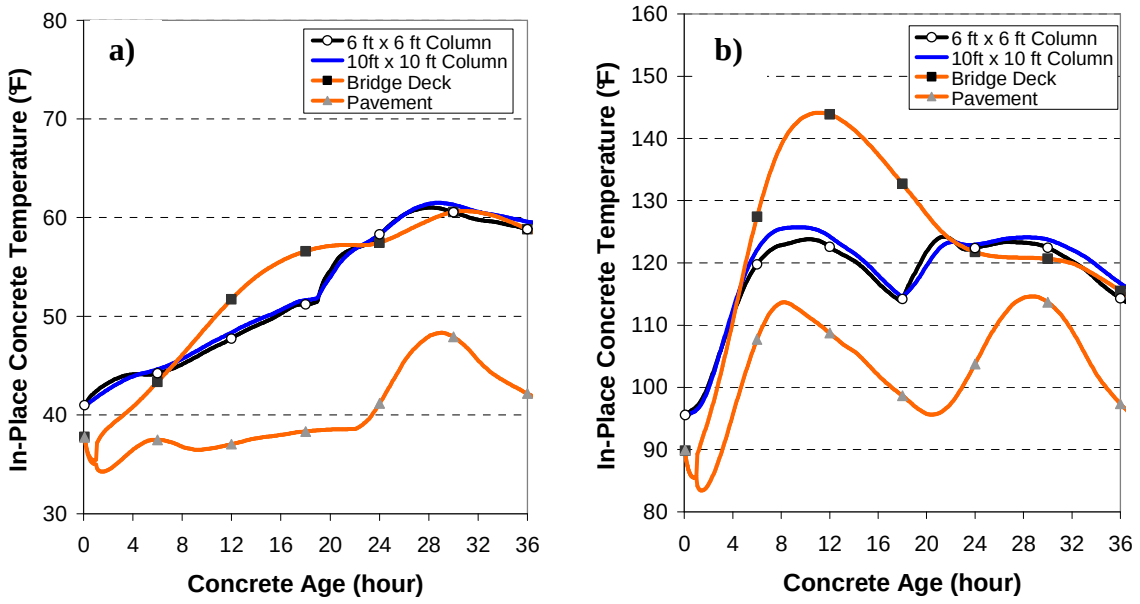

Figure 6.13: Surface temperature profiles for the 50FA-15% concrete mixture placed in the 8 in. bridge deck, 14 in. pavement, 6 ft x 6 ft column and 10 ft x 10 ft column elements at a) 40 °F and b) 95 °F

In Figure 6.13, it is shown that the in-place temperature profiles at the surfaces of the elements vary according to element type. For the 40 °F placement temperature, the in-place temperature profiles for the 6 ft x 6 ft column, 10 ft x 10 ft column, and bridge deck elements do not differ significantly within the first 36 hours. Similarly, the temperature profiles generated at the 95 °F placement temperature for these elements do not differ significantly within the first 8 hours of placement. The temperature profile for the pavement element, however, varies significantly from the temperature profiles for all other elements at both placement temperatures. Based on these results, it can be concluded that the time required to reach initial set for the column and bridge deck elements will be similar at all placement temperatures for the same mixture. After reviewing all initial set times results, it was found that the maximum difference in initial setting times among all 3 column sizes and the bridge deck element was 0.7 hours. The time required to reach initial set for the pavement elements, however, will be delayed, especially at low placement temperatures.

In Figure 6.13, it is shown that the temperature development at the surface of the concrete pavement is lower than all other elements at both placement temperatures. At the 40 °F placement temperature, there is little temperature rise within the first 20 hours. When placed at 95 °F, the first peak in the temperature profile at the pavement surface occurs approximately 8 hours after placement. Similarly, the bridge deck element, reaches a maximum temperature at the surface at approximately 12 hours for the same placement conditions.

The delayed temperature development and low temperature rise at the surface of the concrete pavement placed at low temperatures are the result of the curing method and

placement time. For the ConcreteWorks analysis, a placement time of 9 A.M. was selected for all flatwork elements. This placement time was selected to ensure that the peak heat of hydration and solar radiation peak would not be offset. At the low placement temperatures (40 to 50 °F), however, this could not be achieved for all HVFA mixtures due to the slow rate of hydration under these conditions. In Figure 6.13a, it is shown that the offset in heat of hydration and solar radiation peaks had a significant effect on the temperature development of the 50FA – 15% mixture when placed at 40 °F HVFA concretes. The temperature rise within the first 12 hours to 24 hours is much lower than other concrete element types.

In Figure 6.14, the time required to reach initial set versus concrete placement temperature for the HVFA concrete mixtures proportioned with the 1, 15, and 28% CaO fly ash sources are presented. Two plots are presented, one for the 35% fly ash dosage mixtures and one for the 50% fly ash dosage mixtures. The results presented in this figure represent the setting times of the column and bridge deck elements. The results for the pavement element are presented in Figure 6.14.

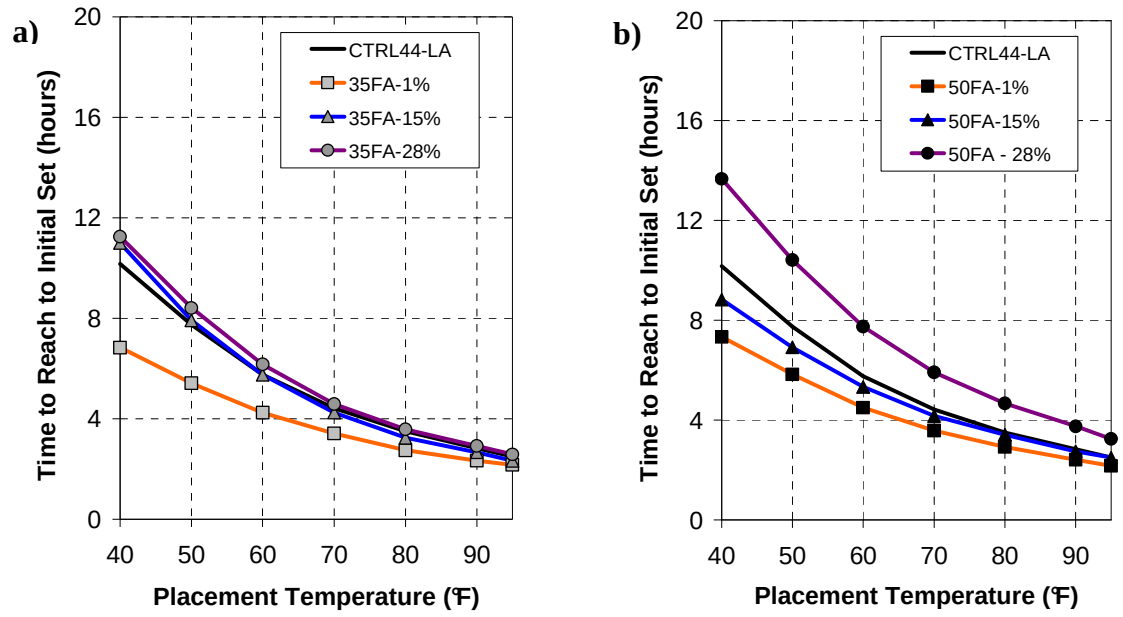

Figure 6.14: Time to reach initial for the a) 35% fly ash dosage and b) 50% fly ash dosage concrete mixtures when placed in the column or bridge deck elements

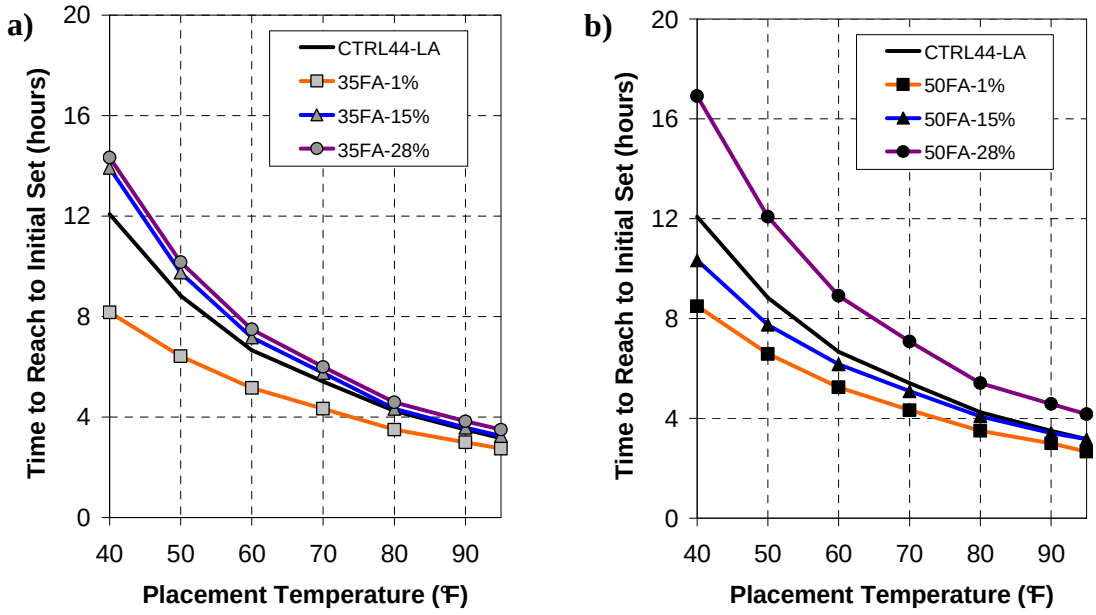

Figure 6.15: Time to reach initial set for the a) 35% fly ash dosage and b) 50% fly ash dosage concrete mixtures when placed in the pavement element

The results presented in Figures 6.14 and 6.15 illustrate that, unlike the results obtained for maximum in-place concrete temperature, a linear relationship between initial setting time and concrete placement temperature does not exist. For all concrete elements investigated, the range in initial setting times was largest at the 40 °F placement temperature and smallest at the 95 °F placement temperature.

In Figure 6.13, it was shown that the in-place temperature development of the pavement element was affected by the environmental conditions and time of placement. The initial setting times for the pavement elements were delayed when compared to the results for the column and bridge deck elements at all placement temperatures. The maximum difference in initial setting times for the pavement elements and column and bridge deck elements ranged from approximately 3.5 hours at the 40 °F placement temperature to 1 hour at the 95 °F placement temperature.

Initial set times for the HVFA concrete mixtures were delayed with increases in the fly ash CaO content. The HVFA concrete mixtures proportioned with the high-calcium Class C fly ashes exhibit the longest initial set times at all placement temperatures. At the 40 °F placement temperature, the initial set time for the 50FA-28% mixture placed in the pavement element was 4.8 hours greater than the control mixture set time under the same conditions. The initial set times for the 1% CaO Class F fly ash mixtures, however, were shorter than the control mixture set times for all elements and environmental conditions.

Based on the results presented in this section, the following conclusions can be made concerning the in-place set time development of HVFA concrete:

- HVFA concrete may be proportioned to have similar, if not reduced, initial set times than conventional portland cement concrete when low-calcium Class F fly ashes are used with high dosages of accelerating admixtures.
- Unless very low concrete placement temperatures (40 to 50 °F) are expected, HVFA concrete may be used for both mass concrete elements and flatwork without encountering excessive delays in initial set times, regardless of the fly ash CaO content.
- An increase in fly ash dosage did not severely affect setting time results for the concrete mixtures investigated due to the use of an accelerating admixture and low w/cm ratios.

6.4.3 Compressive Strength Development

In this section, the results from the evaluation of the in-place compressive strength development of HVFA concrete are presented. One of the main limitations to the increased use of HVFA concrete is the concern that high fly ash dosages can result in low early-age compressive strengths when compared to conventional portland cement concrete. Low early-age compressive strengths are a problem because they have the potential to negatively impact construction efficiency. The results presented in this section are designed to aid in the estimation of compressive strength development of HVFA concrete mixtures when placed in transportation structures under varying environmental conditions.

Formwork removal times are often based on the requirement of reaching 70% of the design compressive strength, f'_c. For this project, the control concrete mixture (CTRL44 – LA) had a 28-day compressive strength of 7,100 psi. Therefore, the results in this section correspond to the time required to reach 5,000 psi (70% of 7,100 psi) for each concrete mixture. For pavements, 70% of the specified design strength may be required for tie bar insertion or opening to traffic.

To complete this analysis, the temperature profile from the surface of the concrete element was used. As reported in the previous section, the temperature development at the concrete surface varies according to element type, placement conditions, and curing method. The flatwork elements are more susceptible to changes in environmental conditions due to their geometry and boundary conditions. The temperature development at the surface of the pavement elements is also affected by the placement time. To estimate the initial set times, the bridge deck and column elements are analyzed together because they share very similar temperature profiles within the first few hours after concrete placement. Because the time required to reach 5,000 psi is considerably longer than the time required to reach initial set, the bridge deck and column elements must be analyzed separately when the in-place compressive strength development is considered. The data for the bridge deck are analyzed even though stay-in-place forms are used, as these results may resemble other flatwork such as elevated slabs.

The in-place compressive strength development was estimated for each HVFA concrete mixture by using the temperature profiles generated with the ConcreteWorks software. For each HVFA concrete mixture, the time required to reach 5,000 psi was calculated using the strength-maturity parameters determined during laboratory testing.

The strength-maturity parameters for all LA cement concrete mixtures are presented in Table D.5. The strength-maturity plots for each mixture are also presented in Appendix D. The results for the time to reach 5,000 psi versus concrete placement temperature for the 6 ft x 6 ft column, 10 ft x 10 ft column, bridge deck, and pavement elements are presented in Figures 6.16, 6.17, 6.18 and 6.19.

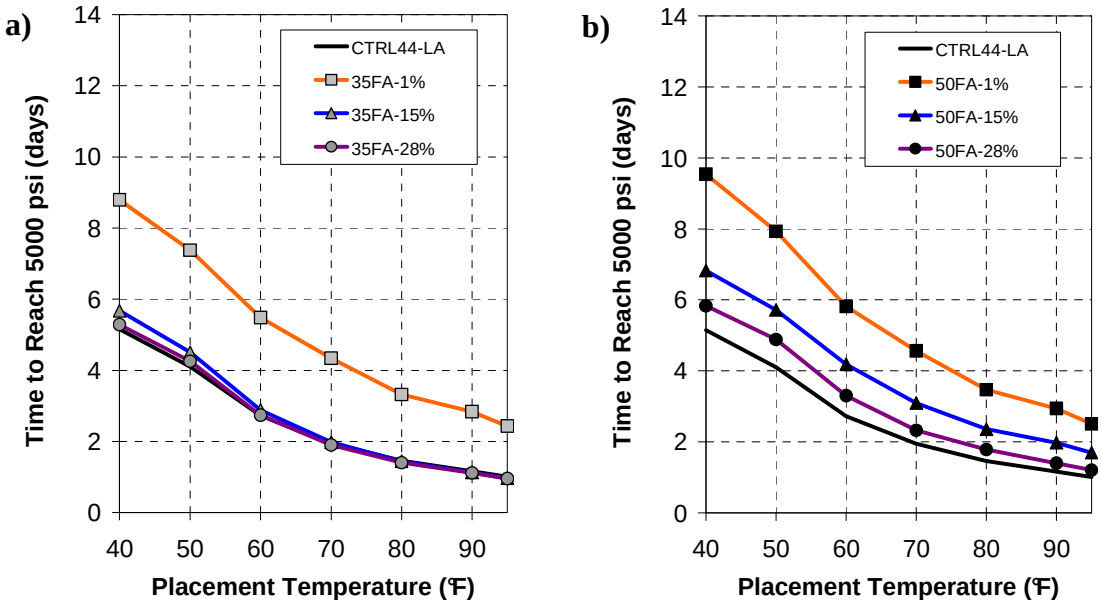

Figure 6.16: Time to reach 5,000 psi for the a) 35% fly ash dosage and b) 50% fly ash dosage concrete mixtures when placed in the 6 ft x 6 ft column

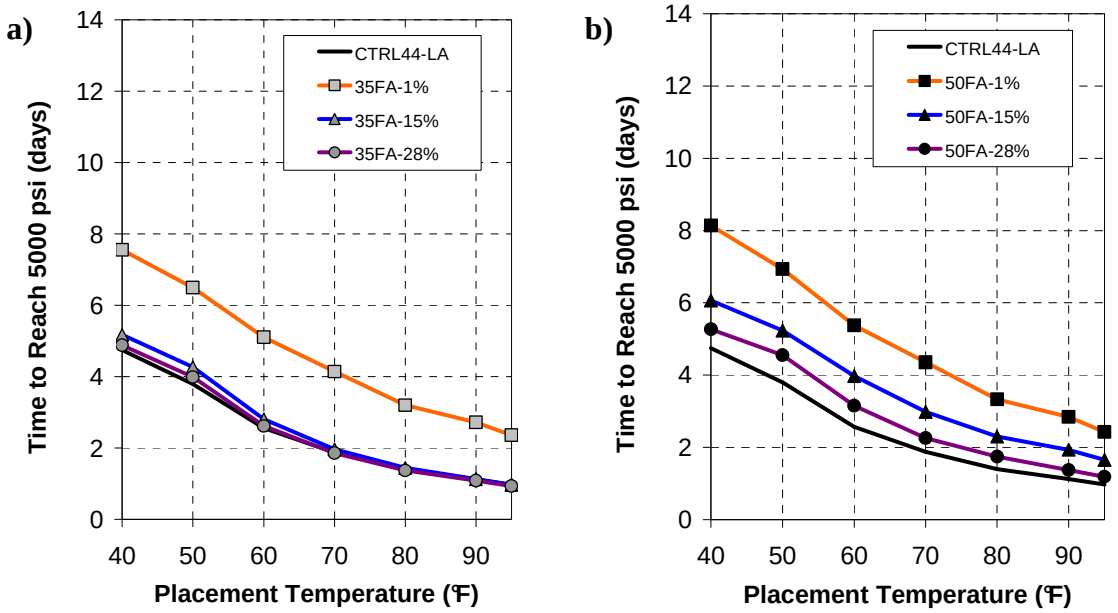

Figure 6.17: Time to reach 5,000 psi for the a) 35% fly ash dosage and b) 50% fly ash dosage concrete mixtures when placed in the 10 ft x 10 ft column

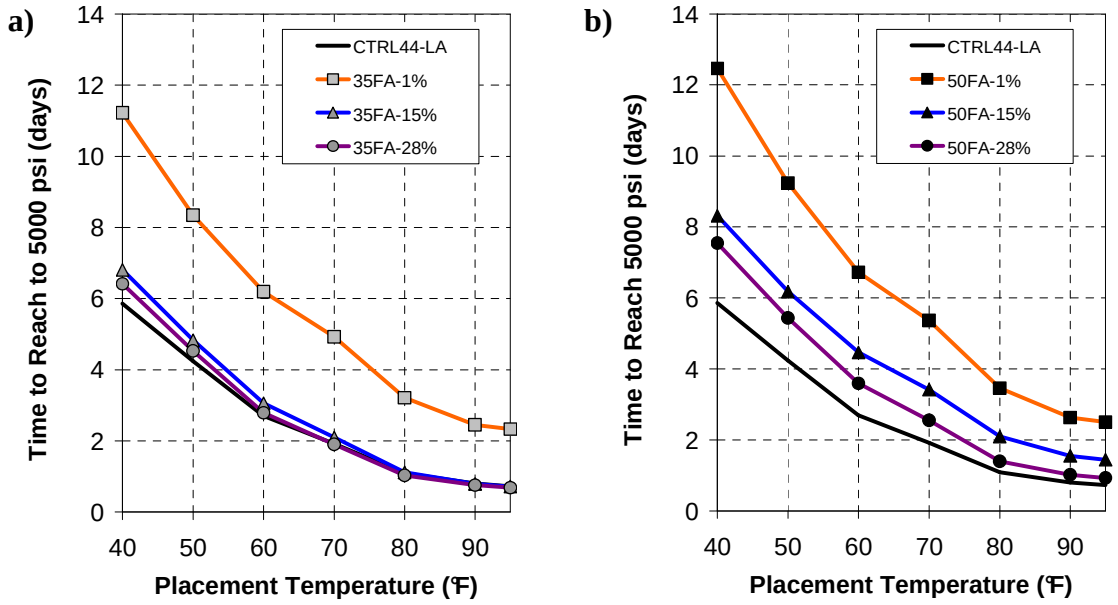

Figure 6.18: Time to reach 5,000 psi for the a) 35% fly ash dosage and b) 50% fly ash dosage concrete mixtures when placed in the bridge deck element

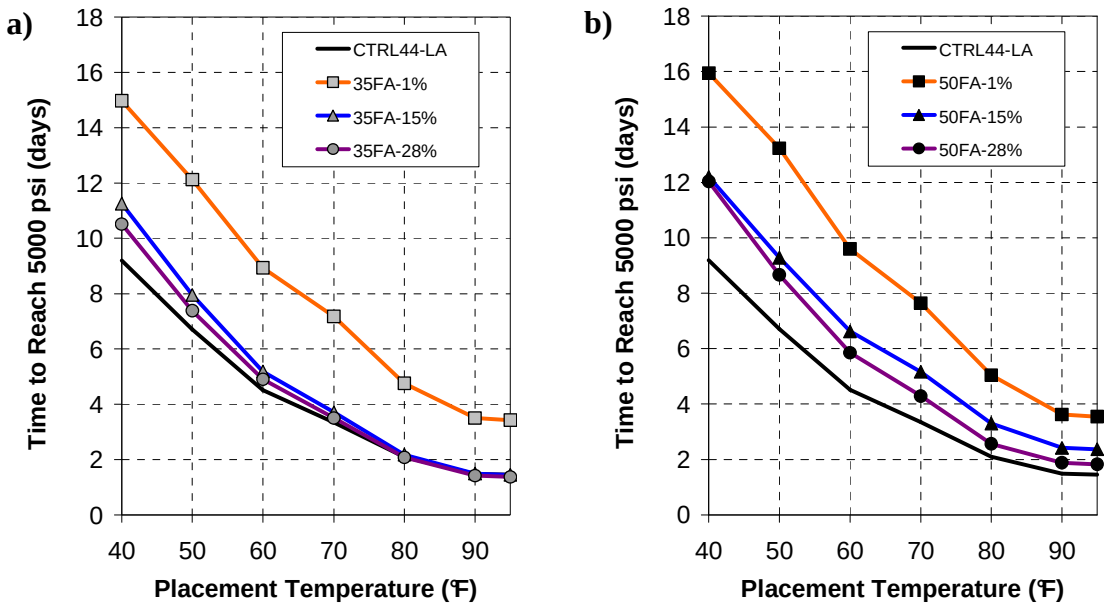

Figure 6.19: Time to reach 5,000 psi for the a) 35% fly ash dosage and b) 50% fly ash dosage concrete mixtures when placed in the pavement element

The results for the compressive strength development are similar in form to the initial setting results presented in the previous section. As the placement temperature was increased, the results converged, for all element types. Also, as the fly ash dosage was decreased, the time required to reach 5,000 psi decreased for each mixture.

From the results presented in Figures 6.16 through 6.19, it is shown that an increase in fly ash CaO content resulted in less time required to reach a compressive strength of 5,000 psi. Typically, HVFA concretes proportioned with Class C fly ashes exhibit increased early-age compressive strengths when compared to similar Class F fly ash mixtures due to an increased rate of reaction at early ages (Smith et al. 1982). The 28% CaO fly ash concrete mixtures required less time to reach 5,000 psi than all other HVFA mixtures at both the 35% and 50% fly ash dosages. The 35FA-15% and 35FA-28% concrete mixtures performed well when compared to the control when placed in all

elements. Also, the 50FA-28% concrete mixture performed well when placed in the column elements. For example, the average delay in time required to reach 5,000 psi for this mixture when placed in the 6 ft x 6 ft column elements was 11 hours.

The largest delays in compressive strength development were associated with the 1% CaO Class F fly ash concrete mixtures. For example, the average delay in compressive strength development for the 50FA-1% mixture when compared to the control ranged from 2.4 days for the 10 ft x 10 ft column elements to 4.3 days for the pavement element. These results indicate that high dosages of low-calcium Class F fly ashes should not be used when early-age compressive strength development is a concern.

The results presented in Figures 6.16 through 6.19 also illustrate that the compressive strength development of HVFA concrete is affected by the element type and placement temperature. The compressive strength development for the pavement element was shown to be significantly affected by cold curing conditions, especially when high dosages of Class F fly ashes were used. For the pavement element, longer curing times were required at all temperatures to reach the 5,000 psi compressive strength for the HVFA concrete mixtures and the control concrete mixture. The extended curing times required for the pavement element at cold placement temperatures may be attributed to its curing method. The pavement element was modeled with a white curing compound for all placement temperatures. The delay in compressive strength development at cold temperatures for the concrete pavement may be offset by either heating the concrete before placement or applying cotton mats to help the pavement retain heat.

Based on the results presented in this section, it may be concluded that HVFA concrete may be proportioned to have similar compressive strength development to that of conventional portland cement concrete. The 35% fly ash mixtures proportioned with the 15% and 28% CaO fly ash sources were shown to perform well when compared to the control concrete. Finally, the results indicate that HVFA concrete mixtures proportioned with low-calcium Class F fly ashes should be avoided when early-age compressive strength development is a concern.

6.5 Final Comments

The results presented in this section are designed to provide guidance on the maximum in-place temperature development, time to reach initial set, and compressive strength development of HVFA concrete placed in transportation structures. The results presented in Sections 6.3 and 6.4 are only valid for the baseline conditions described at the beginning of the chapter. If the concrete mixture proportions, material properties, element geometry, or placement conditions are substantially different than what is outlined in this chapter, a separate analysis should be completed with ConcreteWorks. To generate in-place temperature profiles with the ConcreteWorks software, inputs for the mixture-specific activation energy, hydration parameters, and mixture proportions are required. Also, to accurately estimate the in-place setting time and compressive strength development from the ConcreteWorks temperature profiles, the equivalent age at initial set and strength-maturity parameters are required. Therefore, supplemental laboratory testing may be needed. The results presented in this chapter should be used as a

reference to estimate the in-place performance of HVFA concrete mixtures in transportation structures.

Chapter 7

Summary, Conclusions, and Recommendations

7.1 Summary

Fly ash is a by-product of the combustion of coal in electric power generating plants, and it is often specified as a supplementary cementitious material (SCM) in the production of portland cement concrete. Concrete produced with high fly ash replacement levels is referred to as high volume fly ash (HVFA) concrete. There are many benefits associated with the use of HVFA concrete that make it desirable for transportation infrastructure.

One of the main barriers to the increased use of HVFA concrete is the concern about retarded set times, especially when high fly ash dosages are specified or cold curing conditions are encountered. Retarded set times can cause delays to concrete finishing operations, causing HVFA concrete to be undesirable. Similarly, there are concerns about low early-age compressive strength development of HVFA concrete. Low early-age compressive strengths can require extended curing times, which can negatively impact construction sequencing. Finally, there are concerns that material incompatibilities may arise when fly ash is specified in high dosages. Contractors and transportation agencies are often reluctant to use HVFA concrete due to these concerns.

A laboratory testing program was developed to investigate the effect of fly ash dosage, fly ash chemical composition, cement chemical composition, and environmental conditions on the hydration development, setting times, and compressive strength

development of HVFA concrete. Concrete mixtures with 35% and 50% fly ash replacement levels were investigated. Also four fly ash sources, two Class C and two Class F, were selected for testing to represent the range of fly ash chemical compositions available across the United States. Each concrete mixture was batched at 40 °F, 73 °F, and 105 °F. Compressive strength testing and semi-adiabatic calorimetry were conducted on all 73 °F batches to develop strength-maturity relationships and characterize the hydration development for the HVFA concrete mixtures. Penetration resistance testing and isothermal calorimetry were conducted on all concrete batches. Results from isothermal calorimetry were used to calculate the temperature sensitivity of each HVFA concrete mixture.

The main goal of this research was to evaluate the in-place performance of HVFA concrete. The results from this research are aimed at providing guidance to contractors, concrete producers, and transportation agencies when specifying HVFA concrete for use in transportation infrastructure. A hydration model for HVFA concrete was developed to provide an efficient and reliable means of determining the hydration parameters (β, τ, and α_u) for HVFA concrete mixtures. After developing the hydration model, the ConcreteWorks software program was used to generate in-place temperature profiles for selected HVFA concrete mixtures from the laboratory testing program. Temperature profiles were generated for each concrete mixture based on varying curing conditions and concrete element types. Results from laboratory testing program (activation energies, setting data, and strength-maturity parameters) were used alongside the ConcreteWorks temperature profiles to complete an evaluation of the in-place performance of HVFA concrete. The three topics of investigation were the maximum in-place concrete

temperature, initial set time, and compressive strength. The final results from this analysis are intended to provide guidance to contractors, concrete producers, and transportation agencies on estimating the in-place concrete temperatures, finishing times, and form stripping times that are expected when HVFA concrete is used for transportation infrastructure.

7.2 Conclusions

7.2.1 Laboratory Testing Program

In this section, the conclusions corresponding to the testing and analysis conducted for each phase of the laboratory testing procedure are presented. Fly ash dosage, fly ash CaO content, cement chemical composition, and curing temperature were all found to affect the hydration development, time of setting, and compressive strength development for HVFA concrete mixtures. The general effect of each variable on the selected concrete properties may be summarized as follows:

- Setting times are delayed with an increase in fly ash dosage.
- Initial and final setting times are delayed when the fly ash CaO content is increased for a given fly ash dosage.
- Setting times for HVFA concrete are temperature dependent. As the curing temperature is decreased, set times are delayed; especially when high-calcium, Class C fly ashes are used at high dosages.
- Generally, as the fly ash dosage is increased, the heat generated per volume of concrete decreases.

- An increase in the fly ash CaO content (for a given fly ash dosage), results in more heat generated per volume of concrete.
- Generally, an increase in fly ash dosage results in lowered early age compressive strengths. This effect can be offset by lowering the w/cm ratio of the mixture.
- HVFA concrete mixtures continue to gain strength at late ages due to extended moist-curing.
- Compressive strengths are decreased at most test ages for HVFA concrete mixtures proportioned with the high-alkali cement source when compared to the results for the low-alkali cement source mixtures.

7.2.2 Evaluation of the In-Place Performance of HVFA Concrete

The conclusions relating to the in-place performance of HVFA concrete are summarized as follows:

- The effect of fly ash dosage on the in-place temperature development of HVFA concrete is dependent on the chemical composition of the fly ash and the mixture proportions of the concrete.
- An increase in fly ash CaO content, for a given fly ash dosage, results in an increase in the maximum in-place concrete temperature, regardless of the curing conditions or element type.
- The maximum in-place concrete temperature and rate of temperature development is dependent on the concrete placement temperature and element

type. At high placement temperatures, the rate of hydration is increased. This effect is amplified for large concrete elements.

- An increase in fly ash dosage does not translate to reduced maximum in-place concrete temperatures when high-calcium Class C fly ashes are used for mass concrete elements.
- When HVFA concrete is used for flatwork elements at low placement temperatures (40 to 60 °F), the in-place temperature development is controlled by the element size and boundary conditions, rather than the fly ash dosage and CaO content.
- For small columns (3 ft x 3 ft or smaller) and flatwork elements, high-calcium Class C fly ash sources may be used at high dosages without high in-place concrete temperatures, even at placement temperatures exceeding 80 °F.
- HVFA concrete may be proportioned to have similar, if not reduced, initial set times than conventional portland cement concrete when low-calcium Class F fly ashes are used with high dosages of accelerating admixtures.
- Unless very low concrete placement temperatures (40 to 50 °F) are expected, HVFA concrete may be used for both mass concrete elements and flatwork without encountering excessive delays in initial set times, regardless of the fly ash CaO content.
- When high-calcium Class C fly ash mixtures are used for flatwork, the time of placement affects the temperature development at the concrete surface. Delays in initial set times may be experienced if the peak heat of hydration is offset with the solar radiation peak.

- Low-calcium Class F fly ashes should not be used in high dosages if early-age compressive strength is a concern, especially for flatwork and small concrete elements.
- The in-place compressive strength development of the HVFA concrete mixtures proportioned with the 15% and 28% CaO fly ash sources are comparable to that of the control concrete mixture.

7.3 Recommendations for Future Work

After completing the laboratory testing, data analysis, and modeling required for this research, there are a number of recommendations that can be made for future work. To gain further knowledge on the hydration development, setting characteristics and compressive strength development of HVFA concrete, additional fly ash dosages (possibly 20% and 60%) should be investigated.

It is recommended that the HVFA concrete hydration model be calibrated whenever additional SAC testing results for HVFA concrete mixtures become available. The goodness of fit of the HVFA concrete hydration model should be evaluated for a wider range of fly ash dosages, w/cm ratios, and cement chemical compositions. The model was developed based on all SAC testing results that were available to the author.

Finally, it is recommended that additional ConcreteWorks analysis be performed to develop comprehensive design aids for estimating the maximum in-place concrete temperature, initial set times, and compressive strength development of HVFA concrete used for transportation structures. The laboratory testing results, HVFA concrete hydration model, and ConcreteWorks analysis completed for this project are all intended

to provide a foundation for the development of these design aids. Additional simulations should be completed with the ConcreteWorks software for mixtures with fly ash dosages other than those already investigated.

References

Abrams, D. 1919. Design of Concrete Mixtures. *Bulletin* No. 1. Structural Materials Research Laboratory. Lewis Institute. Chicago, IL. 1-20.

ACI Committee 116. 2000. Cement and Concrete Terminology (ACI 116R-00). Farmington Hills, MI. American Concrete Institute.

ACI Committee 211. 1991. Standard Practice for Selecting Proportions for Normal, Heavyweight, and Mass Concrete (ACI 211.1R-91). Farmington Hills, MI. American Concrete Institute.

ACI Committee 232. 2003. Use of Fly Ash in Concrete (ACI 232.2R-03). Farmington Hills, MI. American Concrete Institute.

ACI Committee 305. 1999. Hot Weather Concreting (ACI 305R-99). Farmington Hills, MI. American Concrete Institute.

ACI Committee 318. 2008. Building Code Requireements for Structural Concrete (ACI 318-08) and Commentary. Farmington Hills, MI. American Concrete Institute.

American Coal Ash Association (ACAA). 2011. *Corrected 2009 Coal Combustion Product (CCP) Production and Use Survey*. Aurora, Colorado.

American Coal Ash Association (ACAA). 2009. *Coal Combustion Products: Beneficial Use – Simply Recycling by Another Name*. Aurora, Colorado.

ASTM C 33. 2003. *Standard Specification for Coarse Aggregates*. ASTM International. West Conshocken, PA.

ASTM C 109. 2007. *Standard Test Method for Compressive Strength of Hydraulic Cement Mortars (Using 2-in. or [50-mm] Cube Specimens).* ASTM International. West Conshocken, PA.

ASTM C 114. 2006. *Standard Test Methods for Chemical Analysis of Hydraulic Cement*. ASTM International. West Conshocken, PA.

ASTM C 128. 2007. *Standard Test Method for Density, Relative Density (Specific Gravity), and Absorption of Fine Aggregate*. ASTM International. West Conshocken, PA.

ASTM C 136. 2006. *Standard Test Method for Sieve Analysis of Fine and Coarse Aggregates*. ASTM International. West Conshocken, PA.

ASTM C 138. 2008. *Standard Test Method for Density (Unit Weight), Yield, and Air Content (Gravimetric) of Concrete*. ASTM International. West Conshocken, PA.

ASTM C 143. 2005. *Standard Test Method for Slump of Hydraulic-Cement Concrete*. ASTM International. West Conshocken, PA.

ASTM C 192. 2007. *Standard Practice for Making and Curing Concrete Test Specimens in the Laboratory*. ASTM International. West Conshocken, PA.

ASTM C 231. 2004. *Standard Test Methods for Air Content of Freshly Mixed Concrete by the Pressure Method*. ASTM International. West Conshocken, PA.

ASTM C 232. 2007. *Standard Test Methods for Bleeding of Concrete*. ASTM International. West Conshocken, PA.

ASTM C 311. 2005. *Standard Test Methods for Sampling and Testing Fly Ash or Natural Pozzolans for Use in Portland-Cement Concrete*. ASTM International. West Conshocken, PA.

ASTM C 403. 2006. *Standard Test Method for Time of Setting of Concrete Mixtures by Penetration Resistance*. ASTM International. West Conshocken, PA.

ASTM C 494. 2005. *Standard Specification for Chemical Admixtures for Concrete*. ASTM International. West Conshocken, PA.

ASTM C 566. 1997. *Standard Test Method for Total Evaporable Moisture Content of Aggregate by Drying*. ASTM International, West Conshocken, PA.

ASTM C 618. 2005. *Standard Specification for Coal Fly Ash and Raw Calcined Natural Pozzolan for Use in Concrete*. ASTM International, West Conshocken, PA.

ASTM C 1064. 2008. *Standard Test Method for Temperature of Freshly Mixed Hydraulic-Cement Conrete*. ASTM International, West Conshocken, PA.

ASTM C 1074. 2004. *Standard Practice for Estimating Concrete Strength by the Maturity Method*. ASTM International, West Conshocken, PA.

Barnes, J. 1994. *Statistical Analysis for Engineers and Scientists: A Computer Based Approach*. New York: McGraw-Hill, Inc. 396 pages.

Berry, E.E. and V.M. Malhotra. 1980. Fly Ash for Use in Concrete – A Critical Review. ACI Journal, *Proceedings*, Vol. 77, NO. 2, March-April, 59-73.

Bilodeau, A., V.M. Malhotra, and P.T. Seabrook. 2001. Use of High-Volume Fly Ash Concrete at the Liu Centre. International Centre for Sustainable Development of Cement and Concrete (ICON), Materials and Research Laboratory, CANMET. Natural Resources Canada. Ottawa, Canada, 21 pages.

Bisaillon, A., M. Rivest, and V.M. Malhotra. 1994. Performance of High Volume Fly Ash Concrete in Large Experimental Monoliths. *ACI Materials Journal*, Vol. 91, No. 2, 178-187.

Bogue, R.H. 1947. *The Chemistry of Portland Cement*. Reinhold Publishing Corporation, New York, 572 pages.

Byfors, J. 1980. Plain Concrete at Early Ages. Research 3:80. Swedish Cement and Concrete Institute, Stockholm.

Carino, N.J. 2004. The Maturity Method. In *Handbook on Nondestructive Testing of Concrete*. 2nd. ed. V.M. Malhotra and N.J Carino. 5.1–5.47. West Conshocken, Pennsylvannia: ASTM International.

Chen, I.A., and M.C.G. Juenger. 2009. Incorporation of Waste Materials into Portland Cement Clinker Synthesized from Natural Raw Materials. *Journal of Materials Science* 44, no. 10:2617-2627.

Eren, O., J. Brooks, and T. Celik. 1995. Setting Times of Fly Ash and Slag-Cement Concretes as Affected by Curing Temperature. *Cement, Concrete, and Aggregates*, Vol. 17, No. 1, 11-17.

Folliard, K.J., M.T. Ley, N.J. Harris, and K.C. Hover. 2007. Investigation of Air-Entraining Admixture Dosage in Fly Ash Concrete. *ACI Materials Journal*, Vol. 105, No. 5, 494-498.

Friesleben, P. Hansen, and J. Pederson. 1977. Maturity Computer for Controlled Curing and Hardening of Concrete. *Nordisk Betong,* Vol. 1, No. 19, 19-34.

Friesleben, P. Hansen, and J. Pederson. 1985. Curing of Concrete Structures. *CEB Inf. Bull.* 166, May 1985.

Folliard, K.J, M. Juenger, A.K. Schindler, K. Riding, J. Poole, L. Kallivokas, S. Slatnick, J. Whigham, J.L. Meadows. 2008. Prediction Model for Concrete Behavior – Final Report. Research Report No. 0-4563-1. Center for Transportation Research, The University of Texas at Austin. 65 pages.

Ge, Z. and K. Wang. 2009. Modified Heat of Hydration and Strength Models for Concrete Contaiing Fly Ash and Slag. *Computers and Concrete,* Vol. 6, No. 1, 19-40.

Greer, W. L., G. J. Hawkins, and T. B. Carter. 2004. Air Emissions and Control Measures. Chap. 6.1 in *Innovations in Portland Cement Manufacturing*. Skokie, Illinois: Portland Cement Association.

Gebler, S.H., and P. Klieger. 1983. Effect of Fly Ash on the Air-Void Stability of Concrete. *Fly Ash, Silica Fume, Slag, and other Mineral By-Products in Concrete.* ACI SP-79, Vol. 1, American Concrete Institute, Farmington Hills, MI, 103-142.

Gebler, S.H., and P. Klieger. 1986. Effect of Fly Ash on the Durability of Air-Entrained Concrete. *Proceedings of the 2nd International Conference on Fly Ash, Silica Fume, Slag, and other Natural Pozzolans in Concrete.* ACI SP-91, Vol.1, American Concrete Institute, Farmington Hills, MI, 483-519.

Jawed, L. and J. Skalney. 1978. Alkalis in Cement: A Review: II. Effects of Alkalis on Hydration and Performance of Portland Cement. *Cement and Concrete Research*, Vol. 8, 37-52

Kishi, T. and K. Maekawa. 1995. Thermal and Mechanical Modeling of Young Concrete Based on Hydration Process of Multi-Component Cement Minerals. *Proceedings of the International RILEM Symposium on Thermal Cracking in Concrete at Early Ages*, ed. R. Springenschmid, E & FN Spon, London. 11-18.

Kjellsen, K.O., and R.J. Detwiler. 1992. Reaction Kinetics of Portland Cement Mortars Hydrated at Different Temperatures. *Cement and Concrete Research*, Vol. 22, No. 1, 112-120.

Langley, W.S., G.G. Carette, and V.M. Malhotra. 1989. Structural Concrete Incorporating High Volumes of ASTM Class F Fly Ash. *ACI Materials Journal*, Vol. 86, No. 5, 507-514.

Langley, W.S., G.G. Carette, and V.M. Malhotra. 1992. Strength Development and Temperature Rise in Large Concrete Blocks Containing High Volumes of Low-Calcium (ASTM Class F) Fly Ash. *ACI Materials Journal*, Vol. 89, No. 4, 362-368.

Lerch, W., and C.L. Ford. 1948. Long-Term Study of Cement Performance in Concrete: Chapter 2. Chemical and Physical Tests of Cements. ACI Journal, *Proceedings*, V. 19, No. 8, August, 1948, 745 to 795.

Luke, W. I. 1961. Nature and Distribution of Particles of Various Sizes in Fly Ash. *Technical Report* No. 6-583. U.S. Army Engineer Waterways Experiment Station. Vicksburg, Mississippi. November, 21 pages.

Malhotra, V.M. and L.H. Jiang. 2000. Reduction in Water Demand of Non-Air-Entrained Concrete Incorporating Large Volumes of Fly Ash. *Cement and Concrete Research*, Vol. 30, 1785-1789

Malhotra, V.M. and P.K. Mehta. *High Performance, High-Volume Fly Ash Concrete*. Supplementary Cementing Materials for Sustainable Development, Inc., Ottawa, Canada, 2002, 101 pages.

Mehta, P.K. 1984. Testing and Correlation of Fly Ash Properties with Respect to Pozzolanic Behavior. EPRI Report No. CS 3314. 59 pages.

Mehta, P. K. 2004. High-Performance, High-Volume Fly Ash Concrete for Sustainable Development. *Proceedings of the International Workshop on Sustainable Development and Concrete Technology*. ed. Kejin Wang. 3-14. Center for Transportation Research and Education, Iowa State University.

Mehta, K. and P. Monteiro. 2006. *Concrete: Microstructure, Properties and Materials*. 3d. ed. New York: McGraw Hill.

Mills, R.H. 1966. Factors Influencing Cessation of Hydration in Water-Cured Cement Pastes. *Special Report No. 90, Proceedings of the Symposium on the Structure of Portland Cement Paste and Concrete*. Highway Research Board, Washington, D.C., 406-424.

Mindess, S., J.F. Young, and D. Darwin. 2003. *Concrete*. 2nd ed. New Jersey: Prentice Hall Inc.

Muench, S.T., J.L Anderson, J.P Hatfield, J.R. Koester, and M. Soderlund et al. 2011. *Greenroads Manual v1.5*. ed. J.L Anderson, C.D. Weiland and S.T. Muench. University of Washington, Seattle, WA, 488 pages.

NRMCA Publication 2PE004. 2009. *Thermal Measurements of Hydrating Concrete Mixtures*. Prepared by Tim Cost. NRMCA Engineering Division. 10 pages.

Obla, K., R. Hill, and R. Martin. 2003. HVFA Concrete – An Industry Perspective. *Concrete International*, 29-33.

Owens, P.L. 1979. Fly Ash and Its Usage in Concrete. *Concrete Magazine*, July, pages 22-26.

Philleo, R. E. 1991. Concrete Science and Reality. *Materials Science of Concrete II*, American Ceramic Society, Westerville, Ohio, 1-8.

Pinto, R. and A.K. Schindler. 2010. Unified Modeling of Setting and Strength Development. *Cement and Concrete Research*, Vol. 40, No. 1, 58-65.

Pinto, R. and K.C. Hover. 1999. Application of Maturity Approach to Setting Times. *ACI Materials Journal*, Vol. 96, No. 6, 686-691.

Pistilli, M.F. Air-Void Parameters Developed by Air-Entraining Admixtures as Influenced by Soluble Alkalis from Fly Ash and Portland Cement. ACI Journal, *Proceedings*, V. 80, No. 3, May-June, 1983, 217-222.

Poole, J., K. Riding, K. Folliard, M. Juenger and A. Schindler. 2007. Methods for Calculating Activation Energy for Portland Cement. *ACI Materials Journal*, Vol. 104, No. 1, 303-311.

Popovics, S. 1986. What Do We Know About the Contribution of Fly Ash to the Strength of Concrete? *Proceedings of Second International Conference on Fly Ash, Silica Fume, Slag and Natural Pozzolans in Concrete*. ACI SP-91, ed. V.M. Malhotra, American Concrete Institute, Farmington Hills, MI, 313-331.

Popovics, S. 1993. Portland Cement – Fly Ash – Silica Fume Systems in Concrete. *Advanced Cement Based Materials*, Vol. 1, No. 2, 93-91.

Powers, T.C. and T.L. Brownyard. 1948. Studies of the Physical Properties of Hardened Portland Cement Paste. *Bulletin No. 22*, Research and Development Laboratories of the Portland Cement Association.

Prusinski, J.R., F.H. Fouad, and M.J. Donovan. 1993. Plant Performance of High Strength Prestressed Concrete Made With Class C Fly Ash. *Paper 41*, Document TR-101774, *EPRI: Proceedings; 10th International Ash Use Symposium*, 15 pages.

Ravina, D, and P.K. Mehta. 1986. Properties of Fresh Concrete Containing Large Amounts of Fly Ash. *Cement and Concrete Research*, Vol. 16, No. 6, 227-238.

Riding, K.A., Poole, J.L., Schindler, A.K., Juenger, M.C.G. and K.J. Folliard. 2007. Temperature Boundary Condition Models for Concrete Bridge Members. *ACI Materials Journal*, Vol.104, No. 4, 379-387.

Riding, K. 2007. Early Age Concrete Thermal Stress Measurement and Modeling. PhD Dissertation. The University of Texas at Austin. Austin, TX.

RILEM CEA 42. 1981. Properties of Concrete at Early Ages State-of-the-Art Report. *Materials and Structures*, Vol. 14, No. 84, 400-450.

RILEM TC 119. 1997. TCE1: Adiabatic and Semi-Adiabatic Calorimetry to Determine the Temperature Increase in Concrete Due to the Hydration Heat of the Cement. In *Prevention of Thermal Cracking in Concrete at Early Ages*. RILEM Report 15, ed. R. Springenschmid, 315-346. London: E&FN Spon.

Schindler, A.K. 2004. Effect of Temperature on Hydration of Cementitious Materials. *ACI Materials Journal*, Vol.101, No. 1, 72-81.

Schindler, A.K. and K.J Folliard. 2005. Heat of Hydration Models for Cementitious Materials. *ACI Materials Journal*, Vol. 102, No. 1, 24-33.

Sear, L.K.A. 2001. *The Properties and Use of Coal Fly Ash*. London: Thomas Telford.

Smith, R.L, Raba, C.F. and M.A. Mearing. 1982. Utilization of Class C Fly Ash in Concrete. *Sixth International Fly Ash Utilization Symposium*. Reno, NV. March, 31 pages.

Spiratos, N, M. Page, N. Milvaganam, V.M Malhotra, and C. Jolicoeur. 2003. *Superplasticizers for Concrete: Fundamentals, Technology, and Practice*. Supplementary Cementing Materials for Sustainable Development, Inc., Ottawa, Canada, 322 pages.

Taylor, H.F.W., C. Famy, and K.L.Scrivener. 2001. Review: Delayed Ettringite Formation. *Cement and Concrete Research*, Vol. 31, 683-693.

Thomas, M. 2007. *Optimizing the Use of Fly Ash in Concrete*. Portland Cement Association. Skokie, IL. 24 pages.

Thomas, M.D.A, P.K. Mukherjee, J.A. Sato, and M.F. Everitt. 1995. Effect of Fly Ash Compsotion on the Thermal Cracking of Concrete. *Proceedings of the Fifth CANMET/ACI International Conference on Fly Ash, Silica Fume, Slag and Natural Pozzolans in Concrete*, ACI SP-153. American Concrete Institute, Farmington Hills, MI.

Wade, S.A., J.M. Nixon, A.K.Schindler and R.W. Barnes. 2010. Effect of Temperature on the Setting Behavior of Concrete. *Journal of Materials in Civil Engineering*. Vol. 22, No. 3, March, 214-222.

Weakley, Richard. 2010. Evaluation of Semi-Adiabatic Calorimetry to Quantify Concrete Setting. M.S. Thesis, Auburn University.

Appendix A

Fresh Concrete Properties Summary

A summary of the fresh concrete properties (slump, air content, and unit weight) tested for each batch is presented in Appendix A. All results in Appendix A are presented in U.S. units.

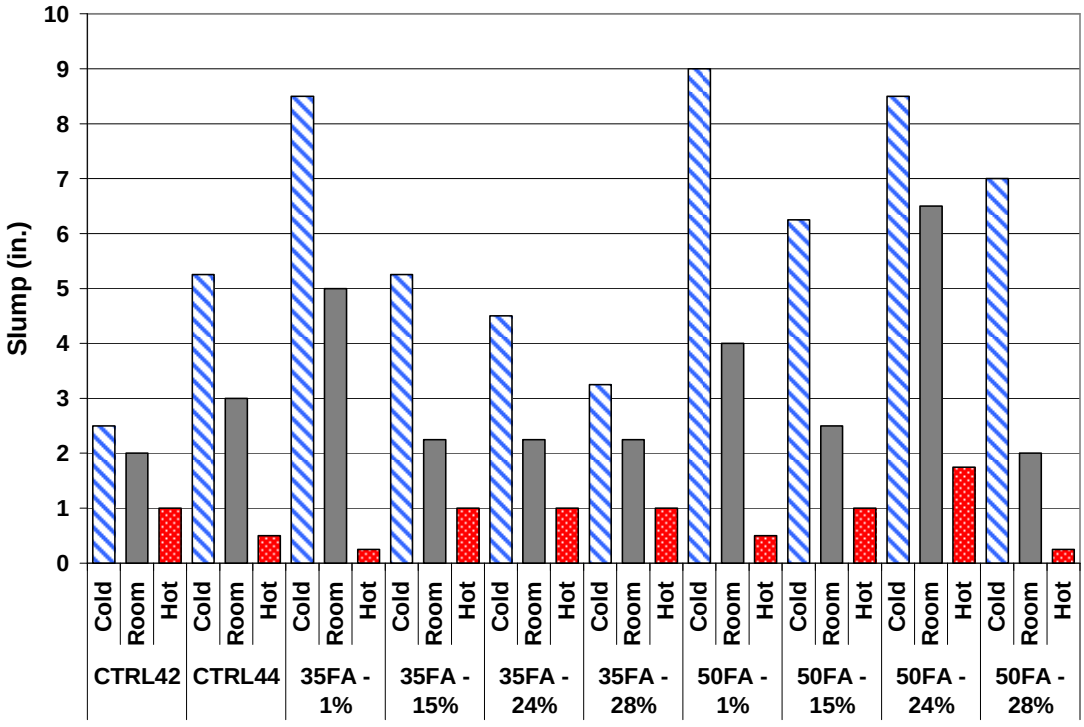

Figure A.1: Slump results for LA cement batches

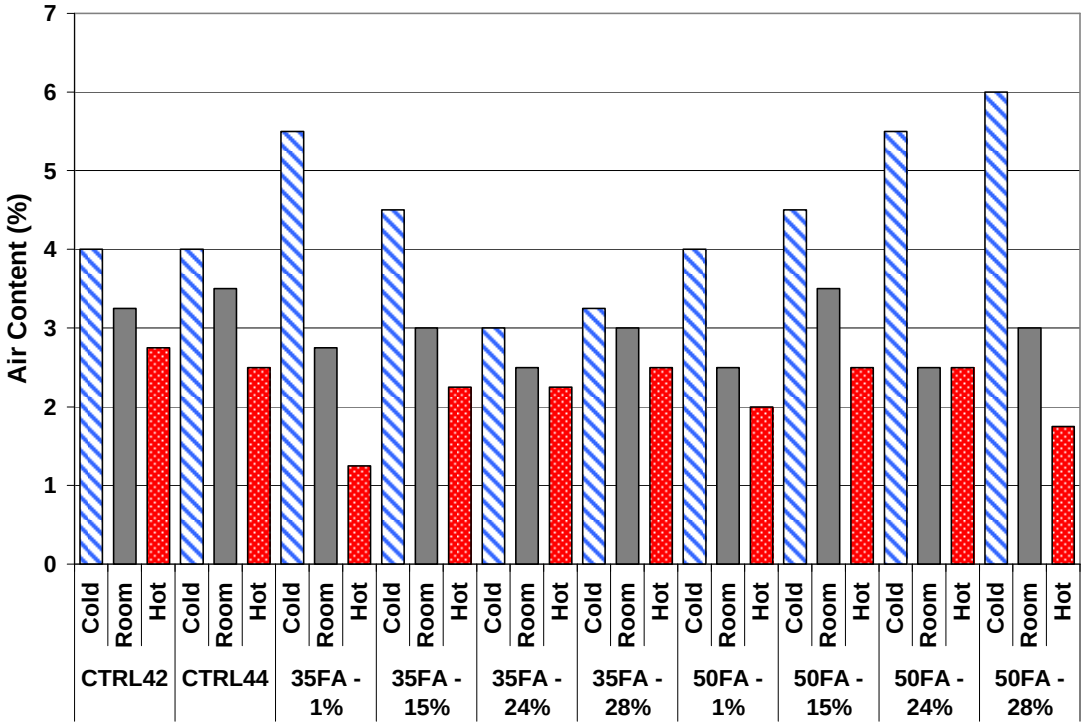

Figure A.2: Air content results for LA cement batches

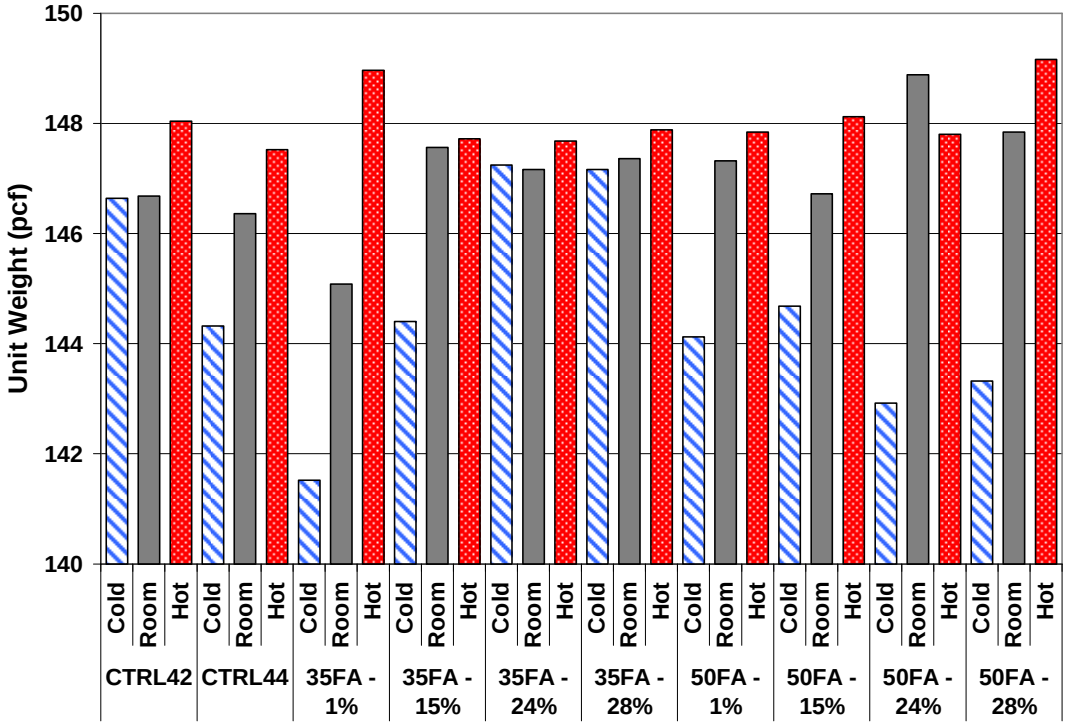

Figure A.3: Unit weight results for LA cement batches

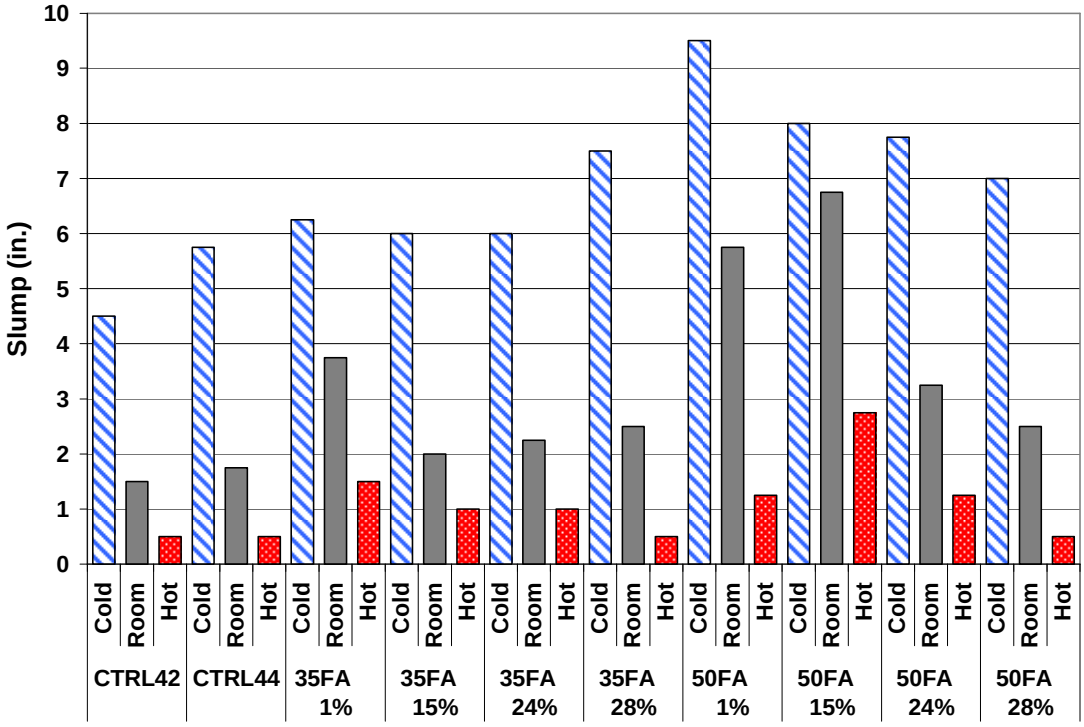

Figure A.4: Slump results for HA cement batches

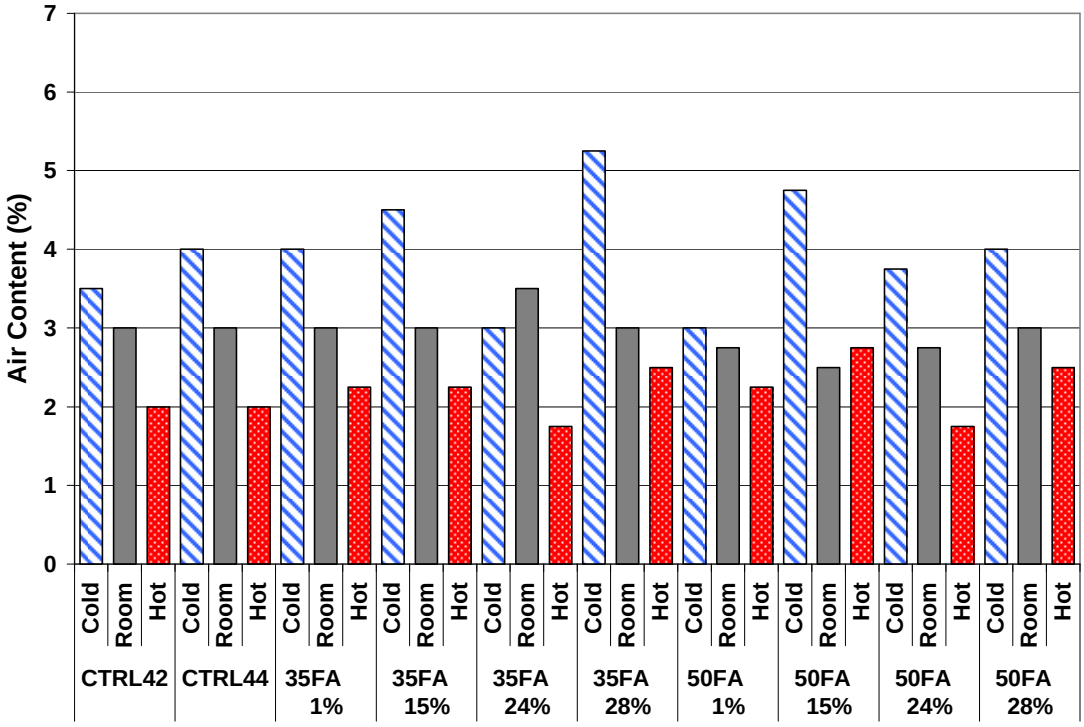

Figure A.5: Air content results for HA cement batches

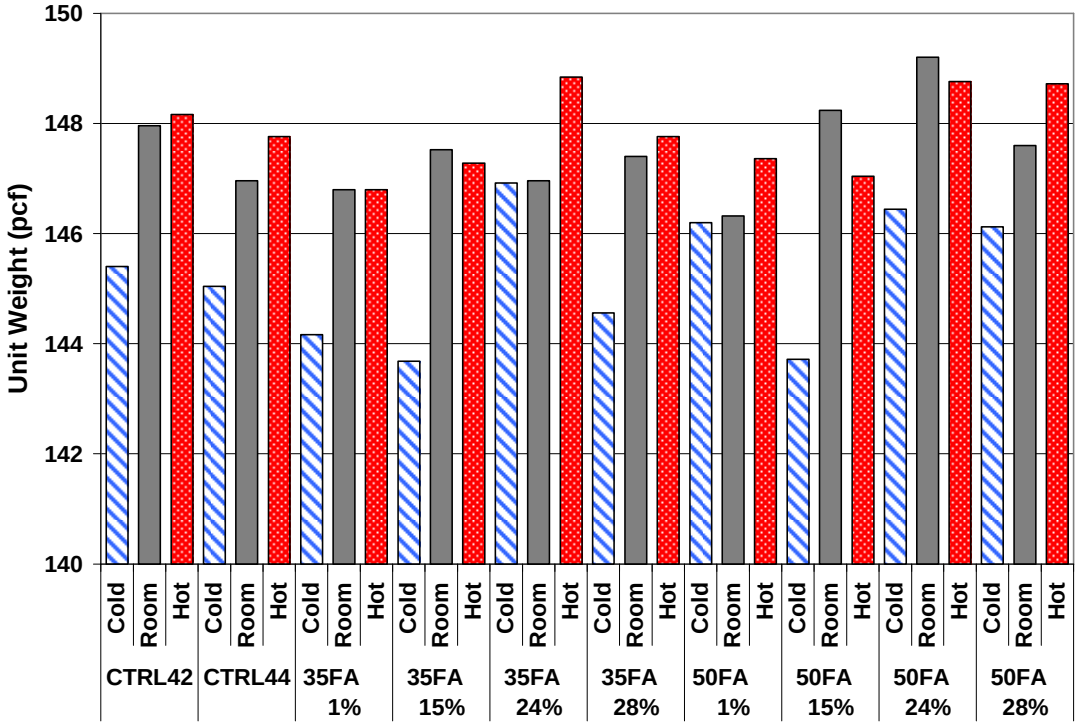

Figure A.6: Unit weight results for HA cement batches

Appendix B

Penetration Resistance Testing Results

Penetration resistance testing results are presented in Appendix B for all concrete batches. For each concrete mixture, the penetration resistance plots from each of the three batching temperatures (room, hot and cold) are presented. All penetration resistance testing was conducted in accordance with ASTM C 403 (2006).

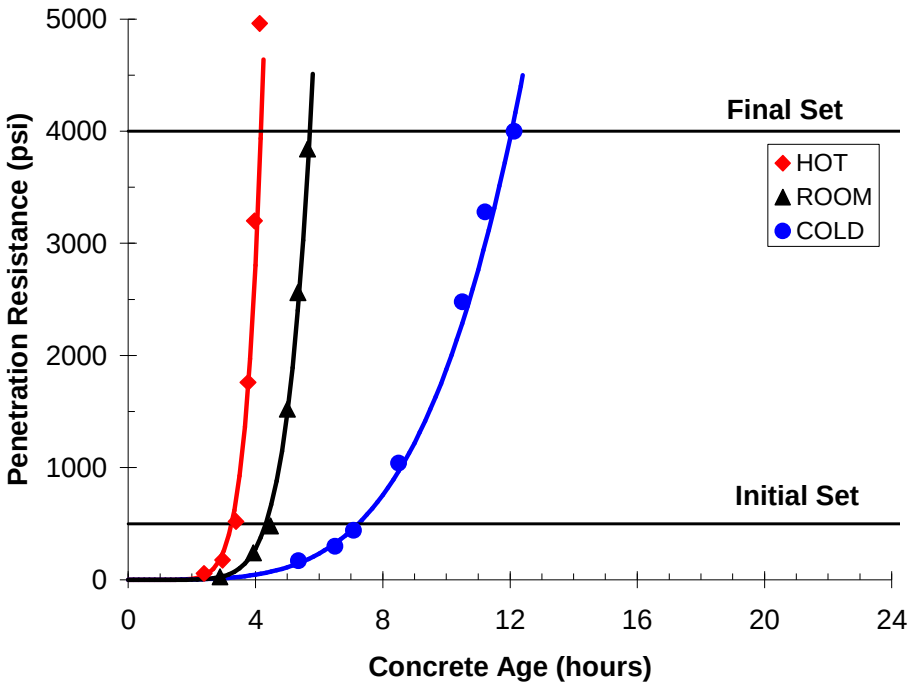

Figure B.1: Penetration resistance testing results for CTRL42-LA

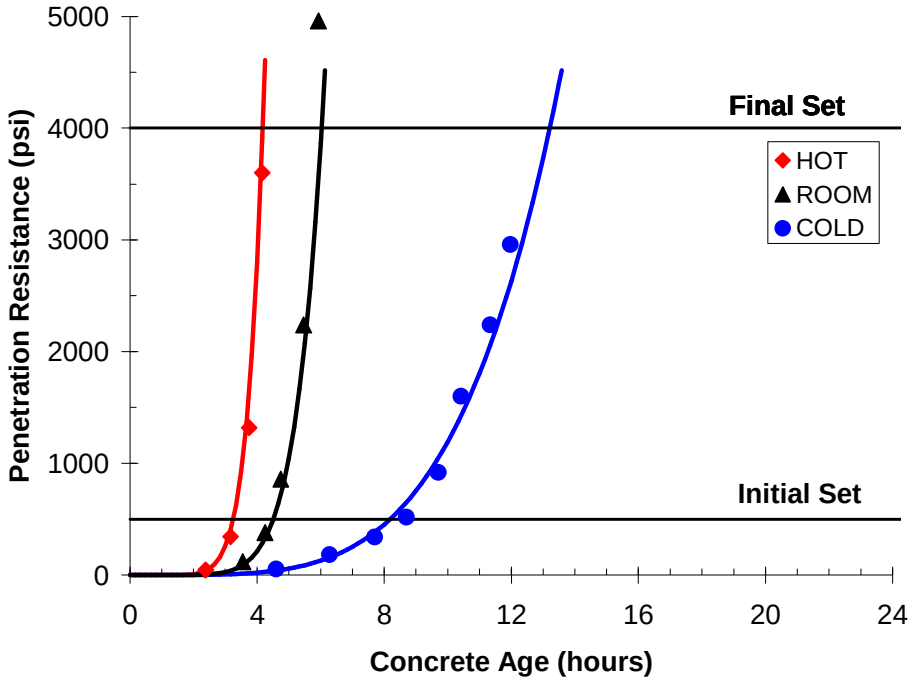

Figure B.2: Penetration resistance testing results for CTRL44-LA

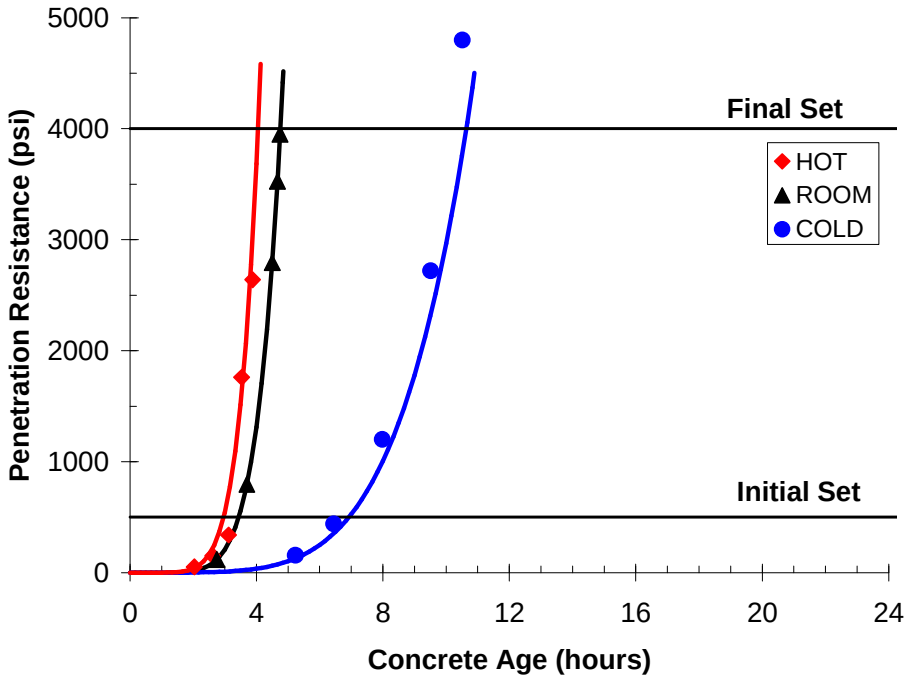

Figure B.3: Penetration resistance testing results for LA-35FA-1%

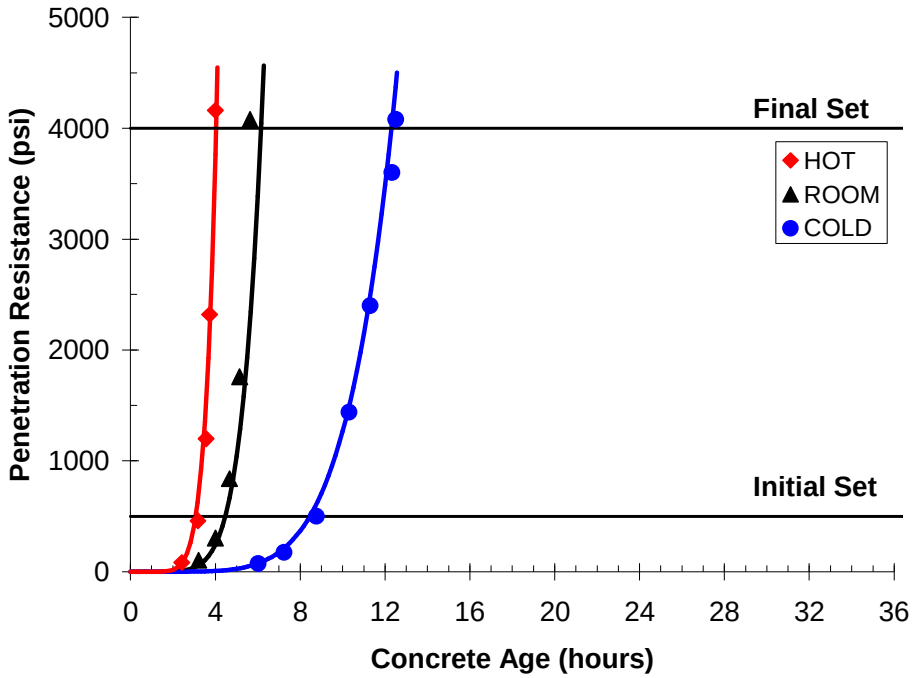

Figure B.4: Penetration resistance testing results for LA-35FA-15%

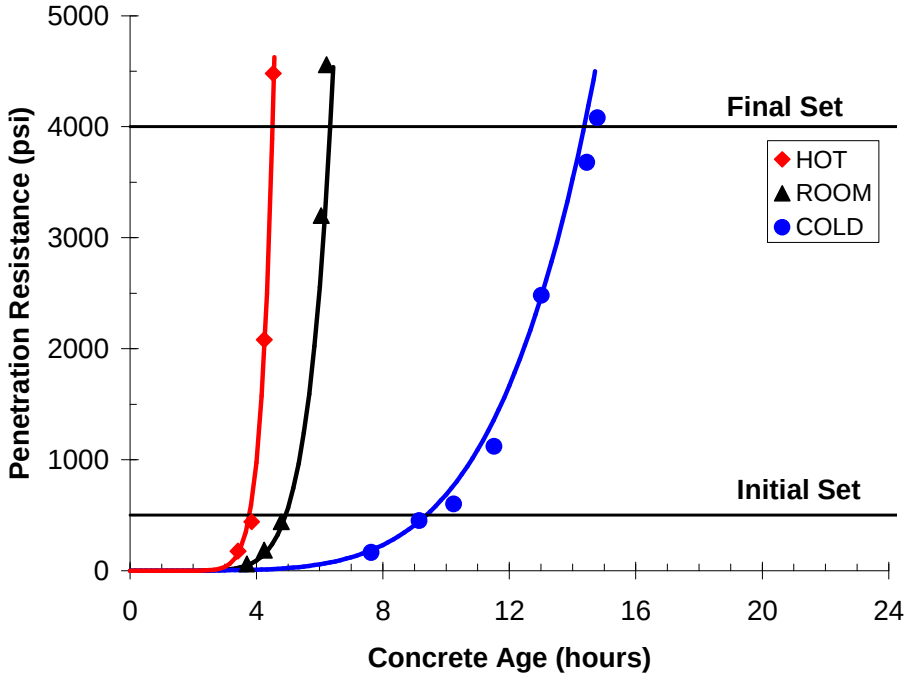

Figure B.5: Penetration resistance testing results for LA-35FA-24%

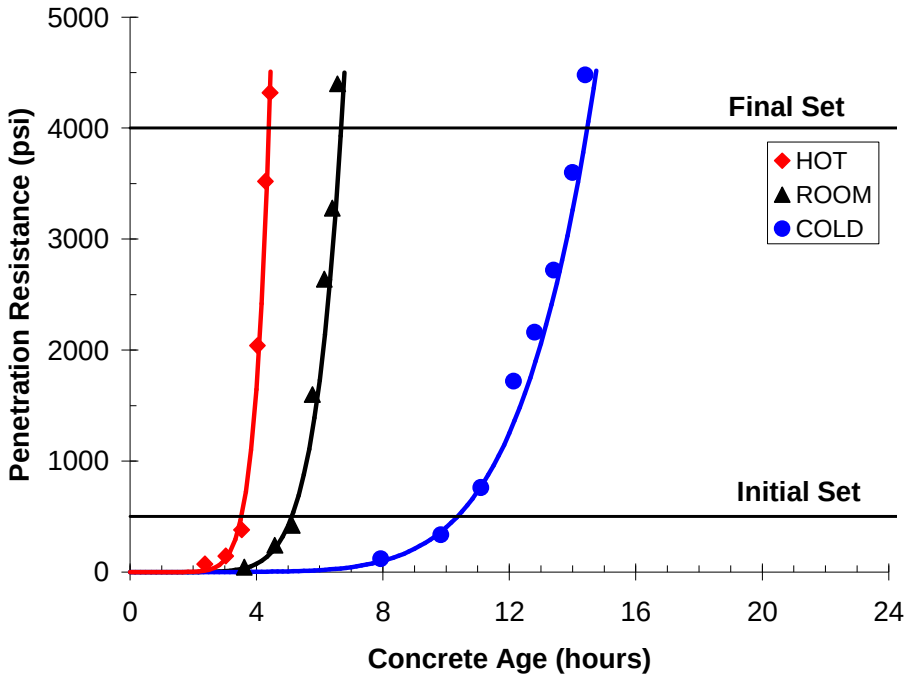

Figure B.6: Penetration resistance testing results for LA-35FA-28%

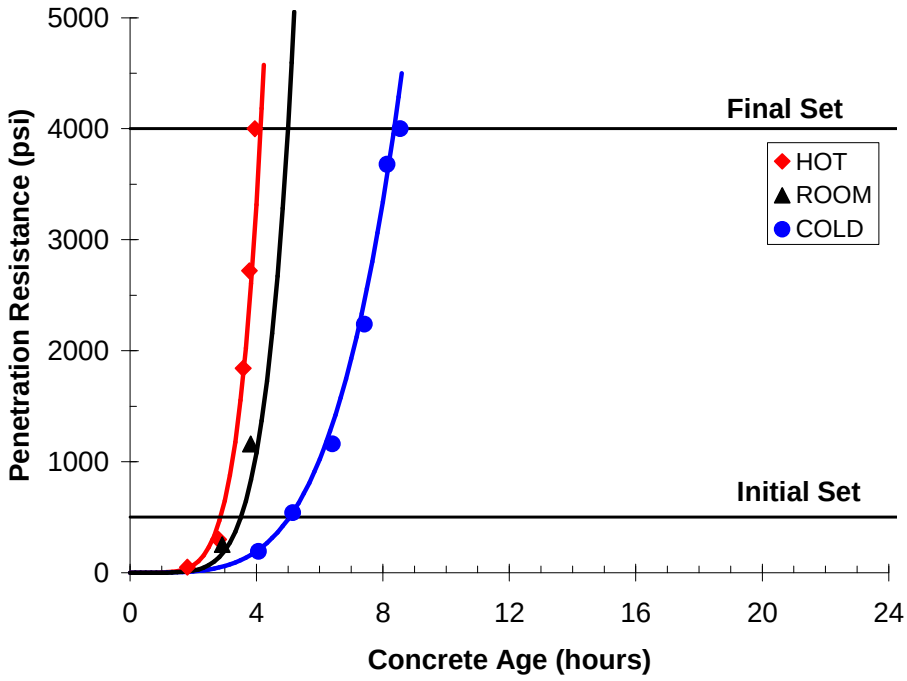

Figure B.7: Penetration resistance testing results for LA-50FA-1%

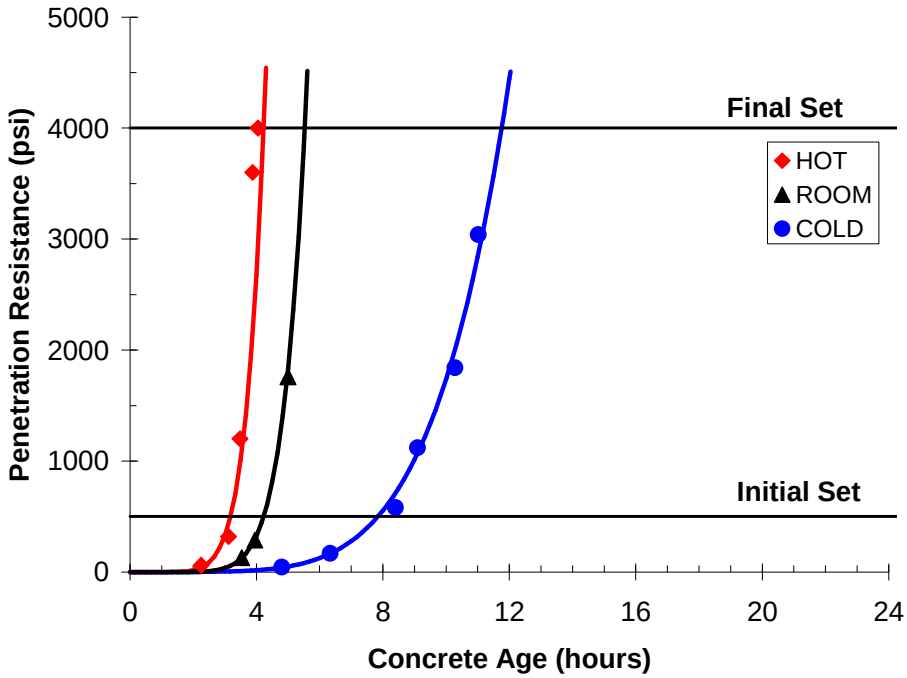

Figure B.8: Penetration resistance testing results for LA-50FA-15%

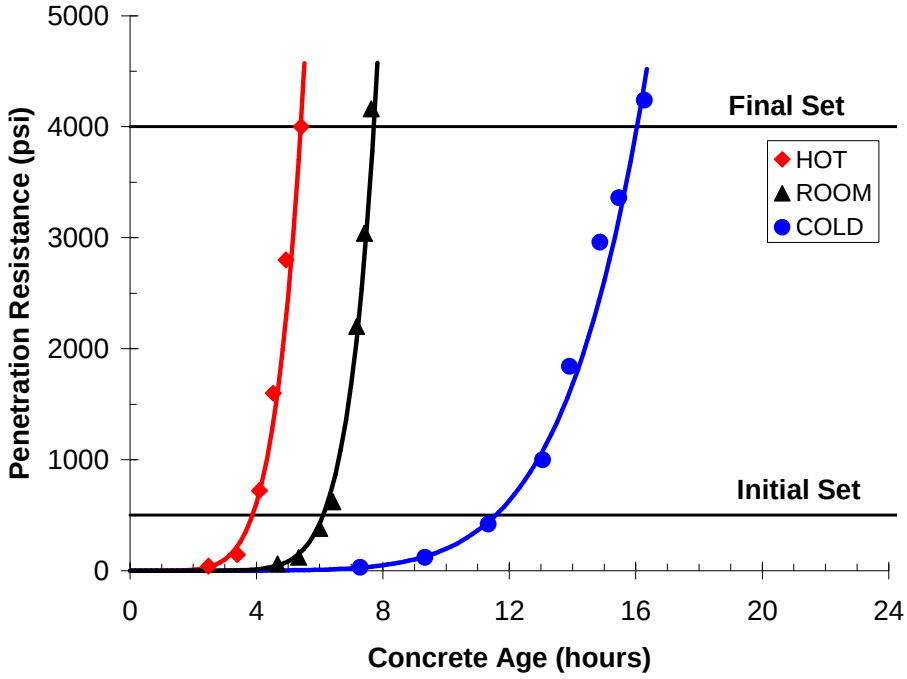

Figure B.9: Penetration resistance testing results for LA-50FA-24%

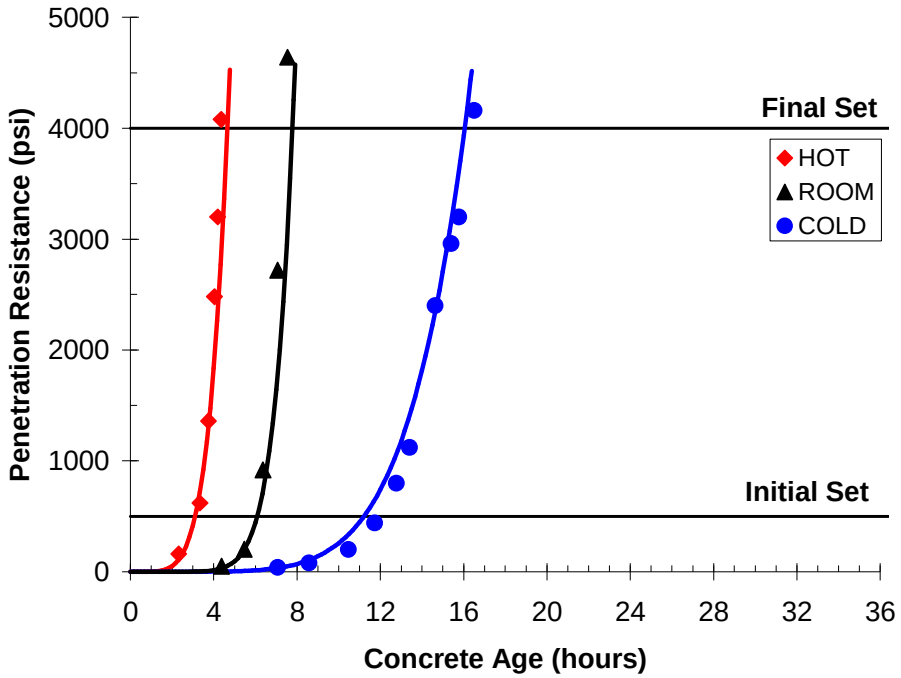

Figure B.10: Penetration resistance testing results for LA-50FA-28%

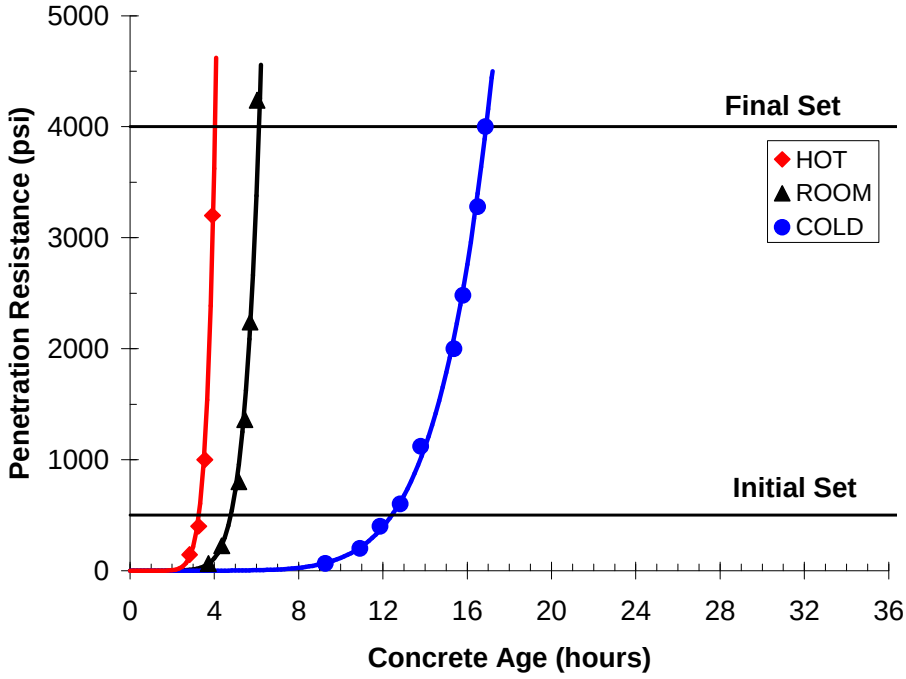

Figure B.11: Penetration resistance testing results for CTRL42-HA

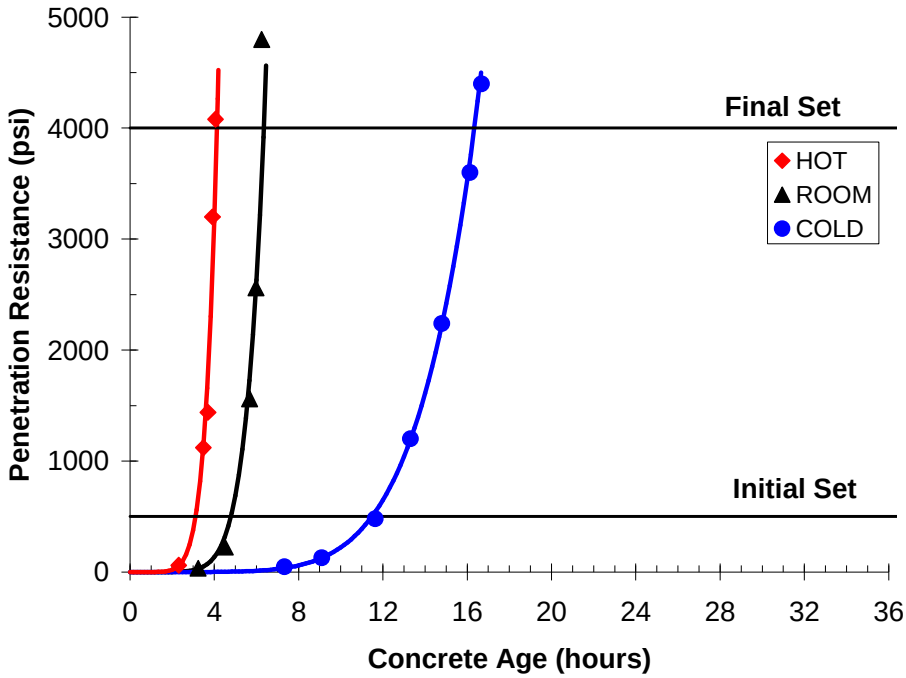

Figure B.12: Penetration resistance testing results for CTRL44-HA

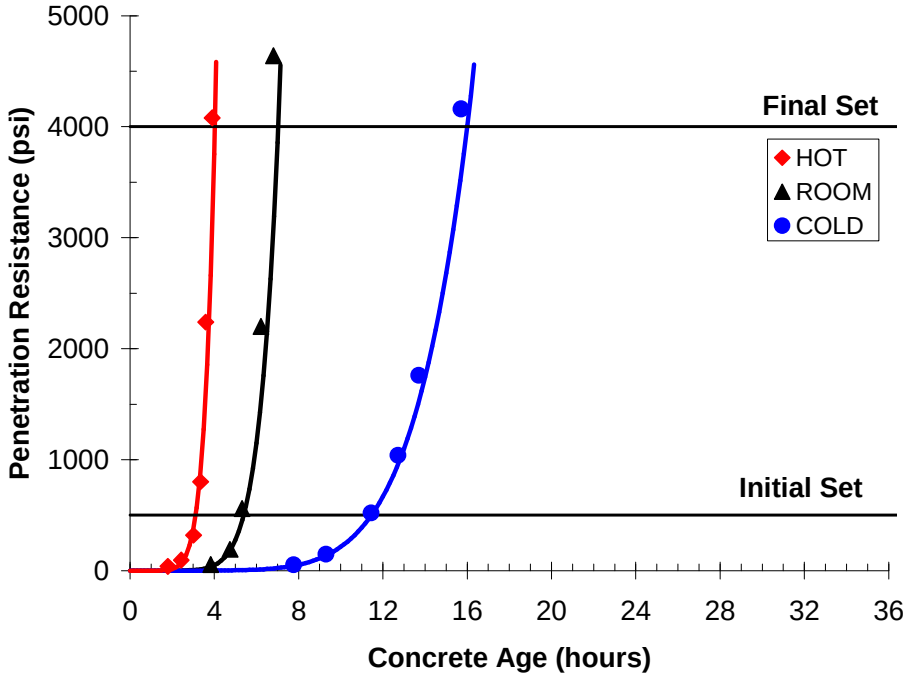

Figure B.13: Penetration resistance testing results for HA-35FA-1%

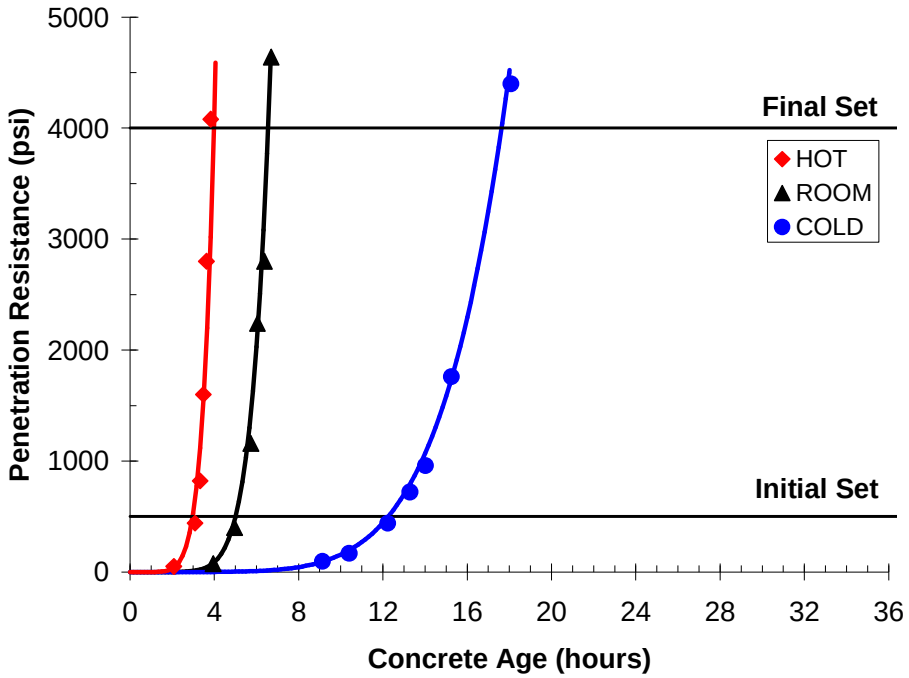

Figure B.14: Penetration resistance testing results for HA-35FA-15%

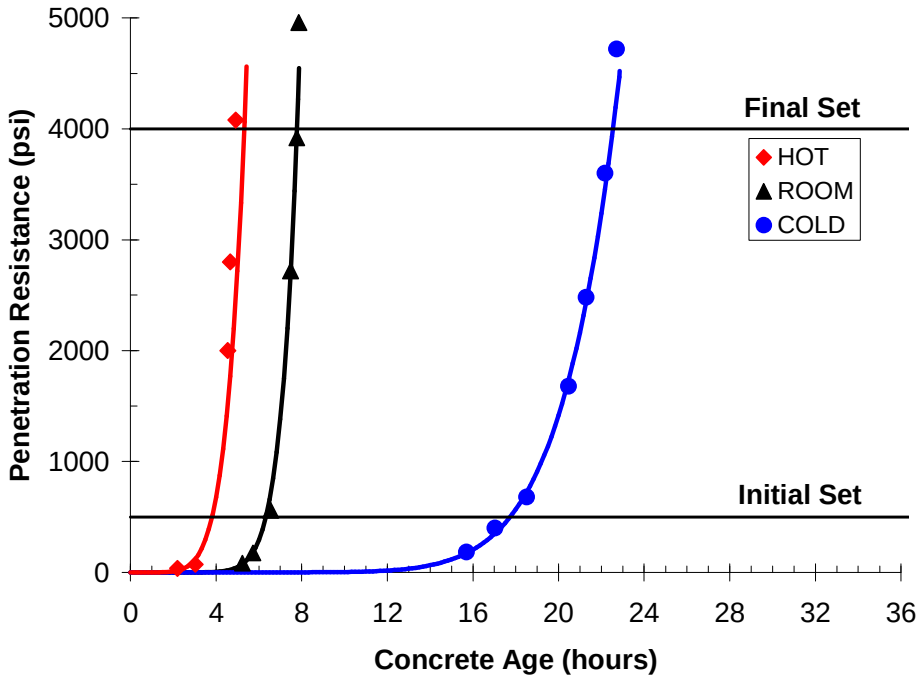

Figure B.15: Penetration resistance testing results for HA-35FA-24%

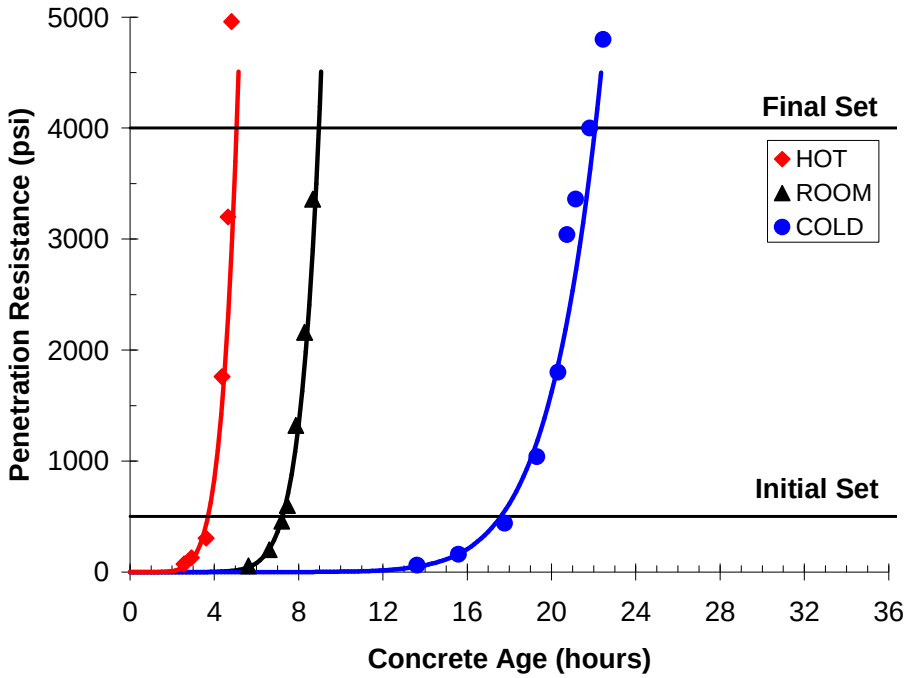

Figure B.16: Penetration resistance testing results for HA-35FA-28%

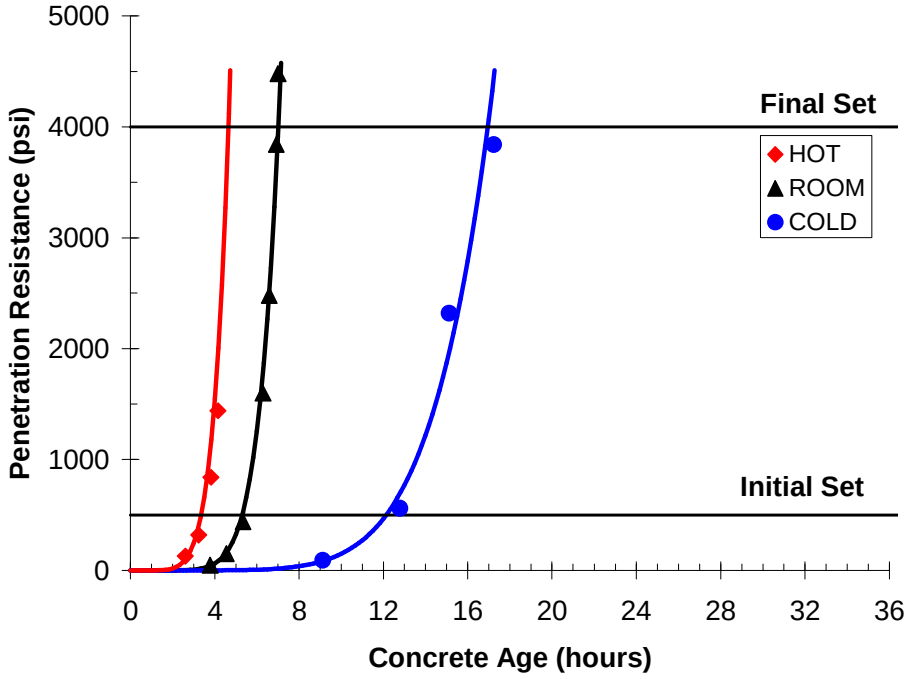

Figure B.17: Penetration resistance testing results for HA-50FA-1%

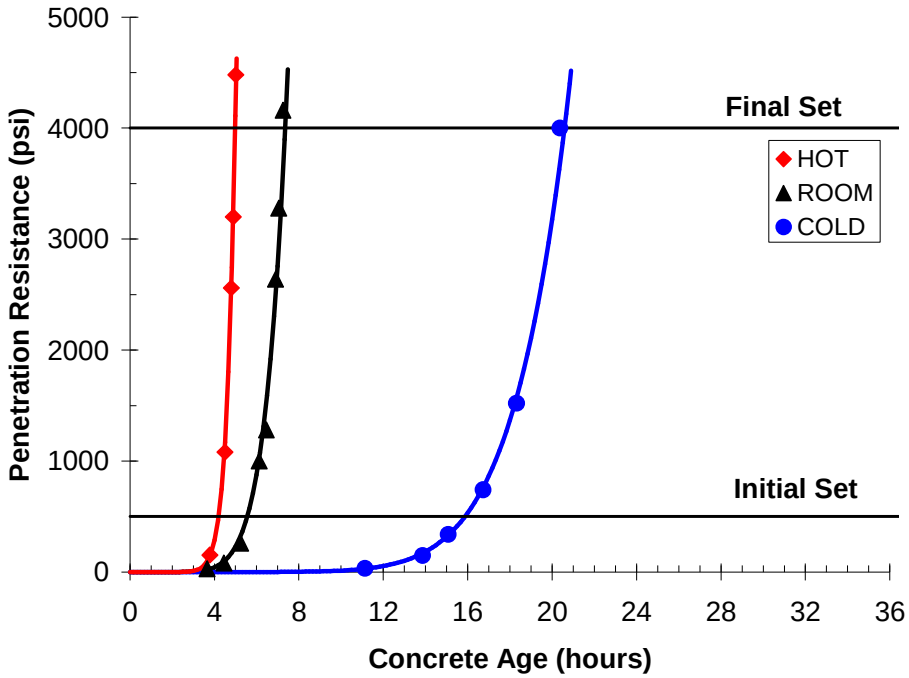

Figure B.18: Penetration resistance testing results for HA-50FA-15%

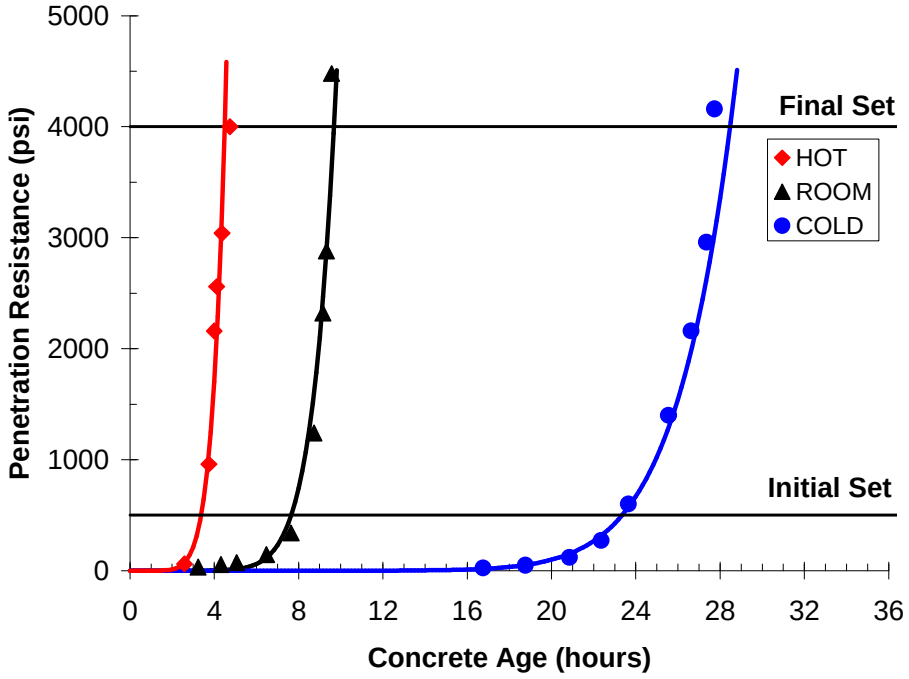

Figure B.19: Penetration resistance testing results for HA-50FA-24%

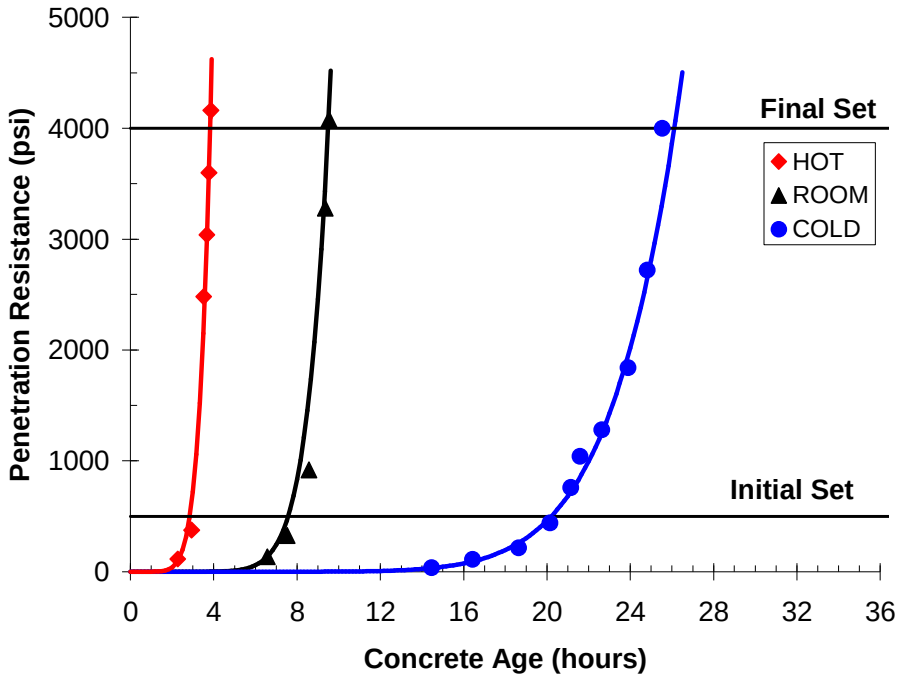

Figure B.20: Penetration resistance testing results for HA-50FA-28%

Appendix C

Calorimetry Testing Results

Appendix C contains results from isothermal and semi-adiabatic calorimetry for each concrete mixture. First, the isothermal curves are presented for each concrete mixture at each batching temperature. The activation energies presented in Section 4.2.2 were calculated from the isothermal calorimetry data presented in Appendix C. Also, the semi-adiabatic temperature curves are presented for each room temperature concrete batch. The time of initial and final set is indicated on each SAC temperature curve. All calorimetry testing was conducted with the equipment detailed in Chapter 3.

C.1 Isothermal Calorimetry Results

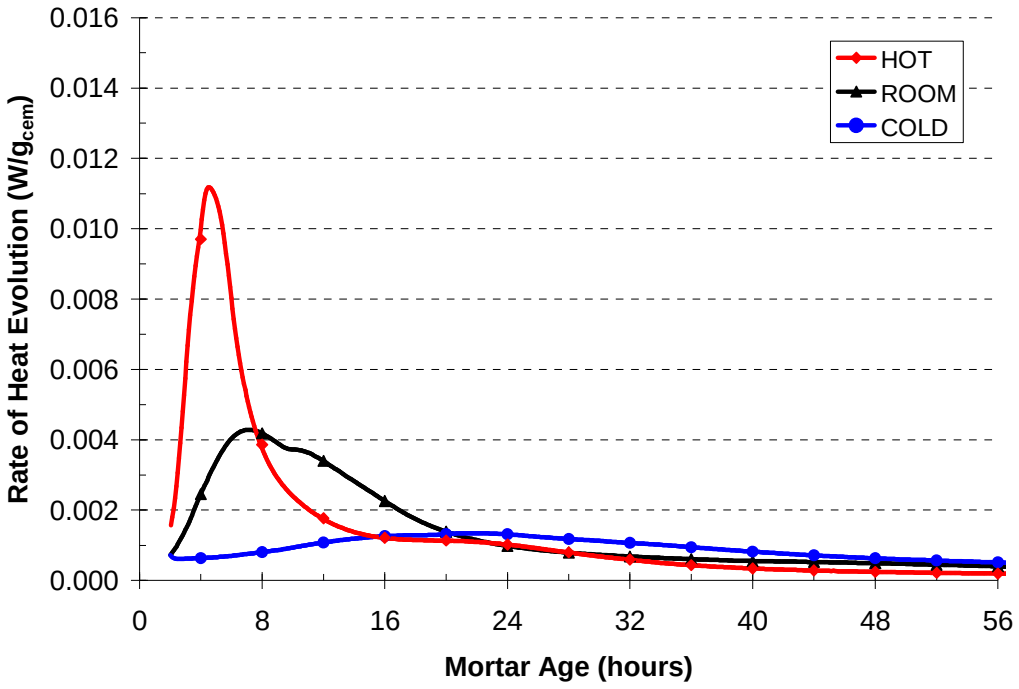

Figure C.1: Isothermal calorimetry results for CTRL42-LA

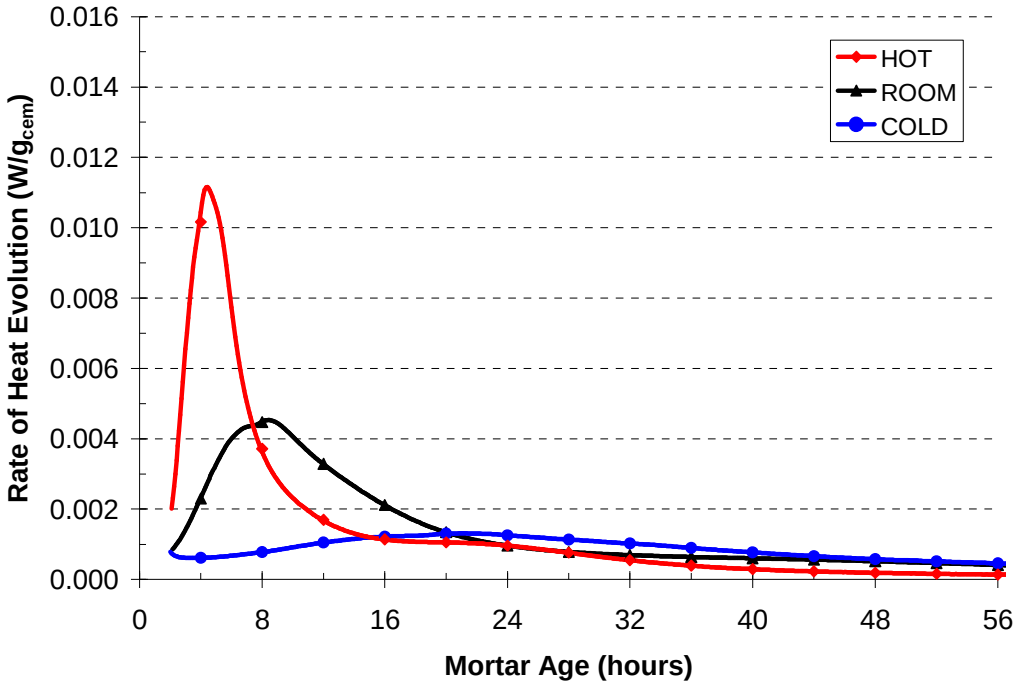

Figure C.2: Isothermal calorimetry results for CTRL44-LA

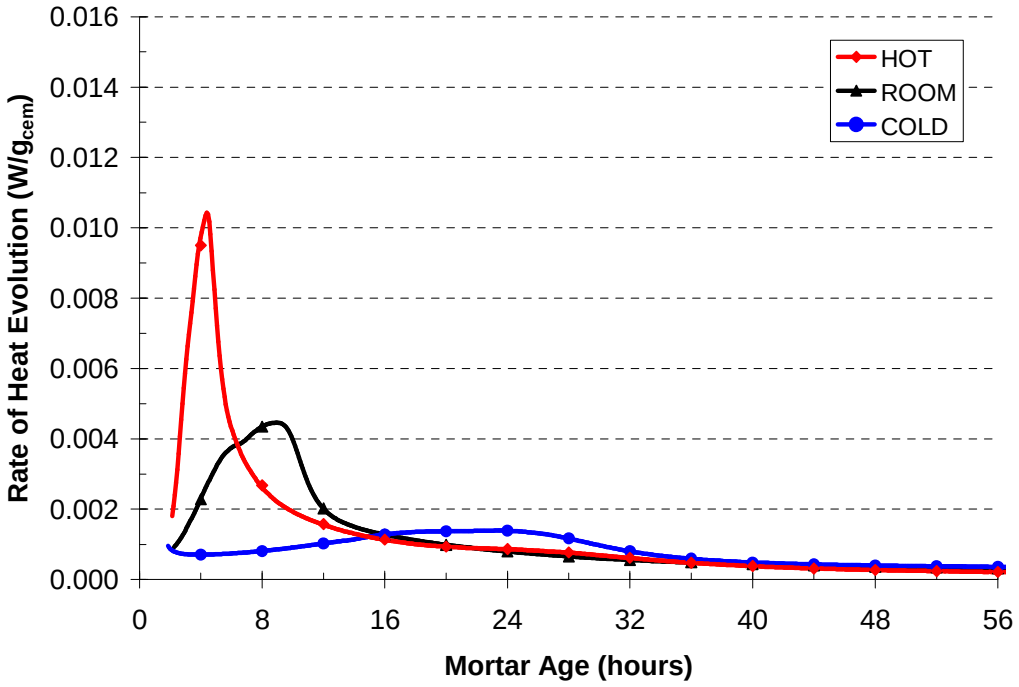

Figure C.3: Isothermal calorimetry results for LA-35FA-1%

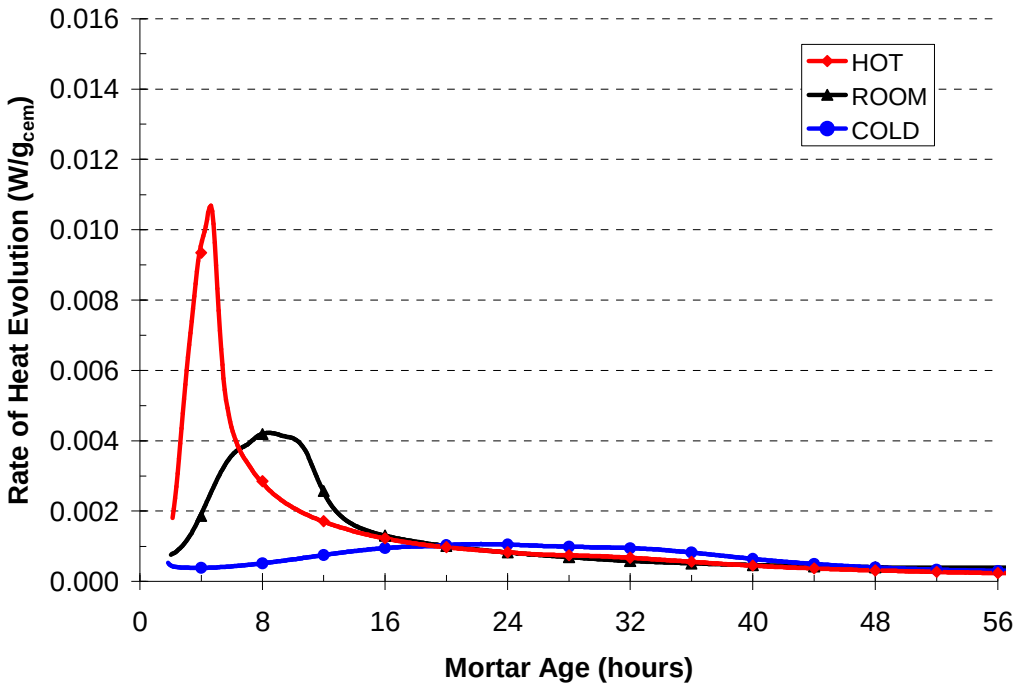

Figure C.4: Isothermal calorimetry results for LA-35FA-15%

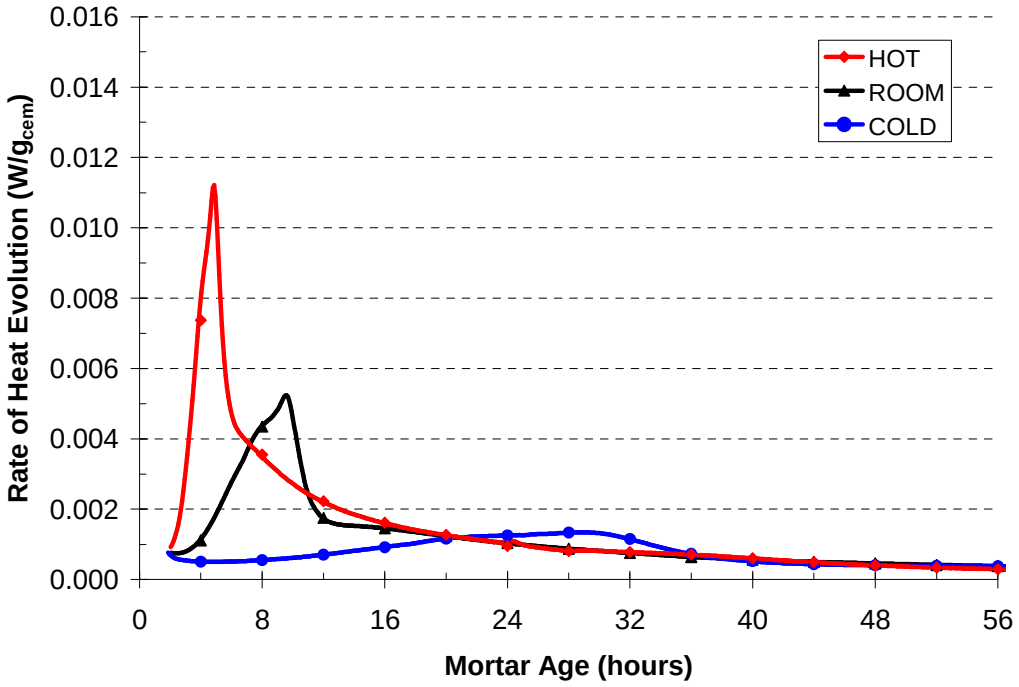

Figure C.5: Isothermal calorimetry results for LA-35FA-24%

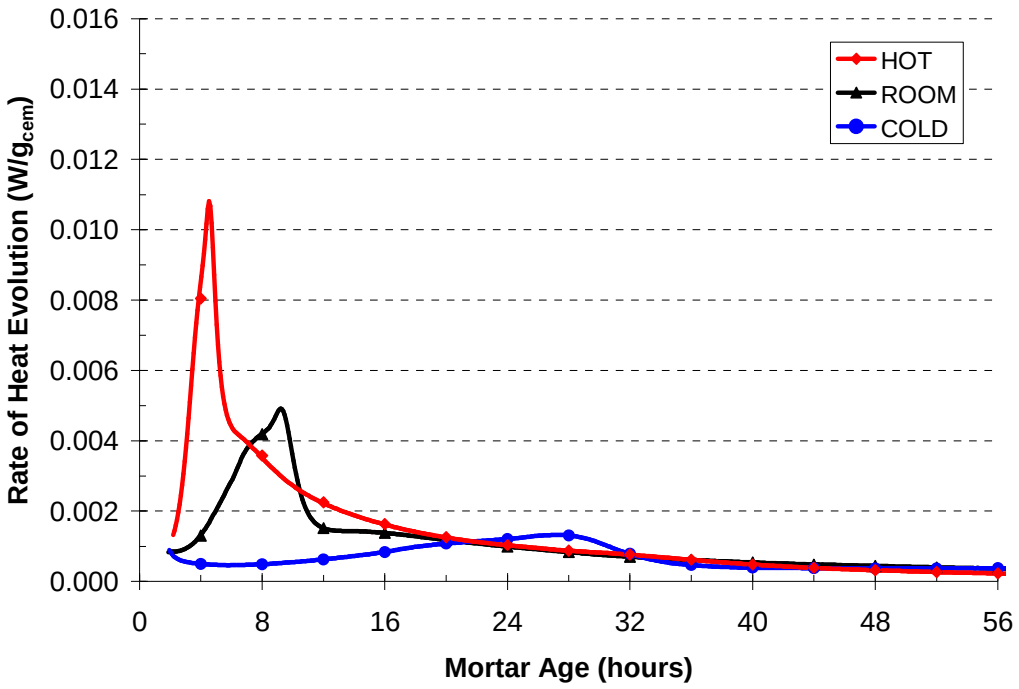

Figure C.6: Isothermal calorimetry results for LA-35FA-28%

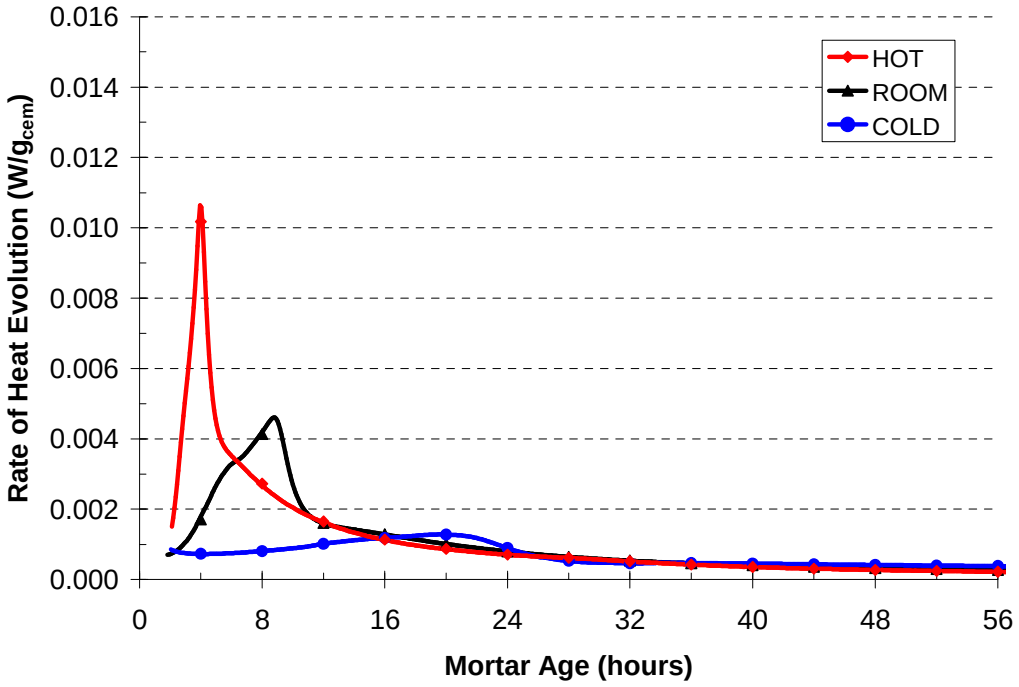

Figure C.7: Isothermal calorimetry results for LA-50FA-1%

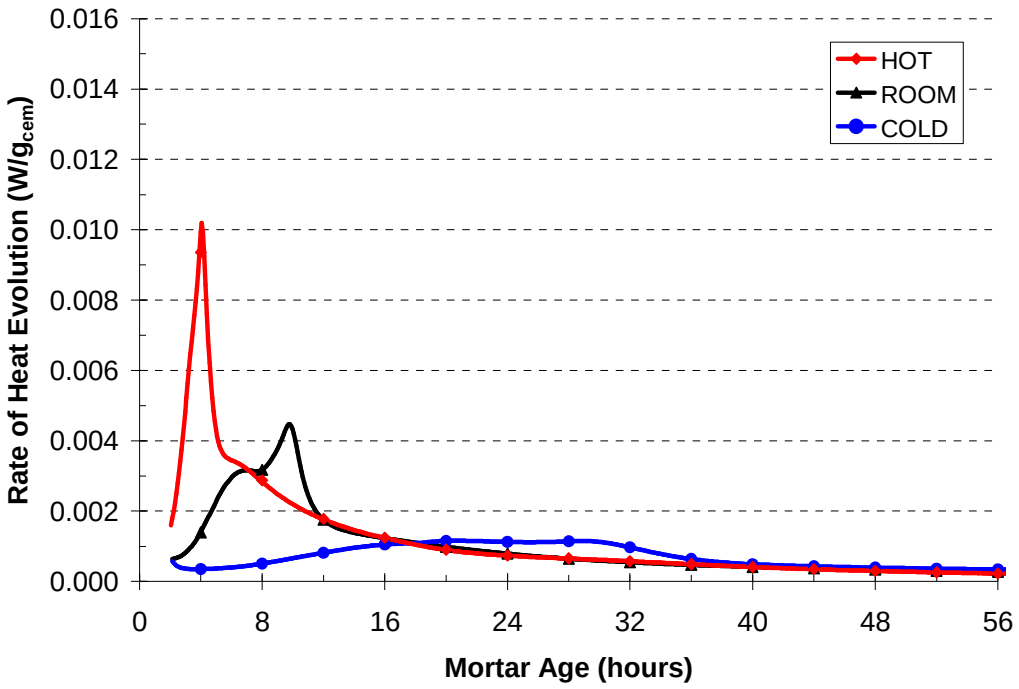

Figure C.8: Isothermal calorimetry results for LA-50FA-15%

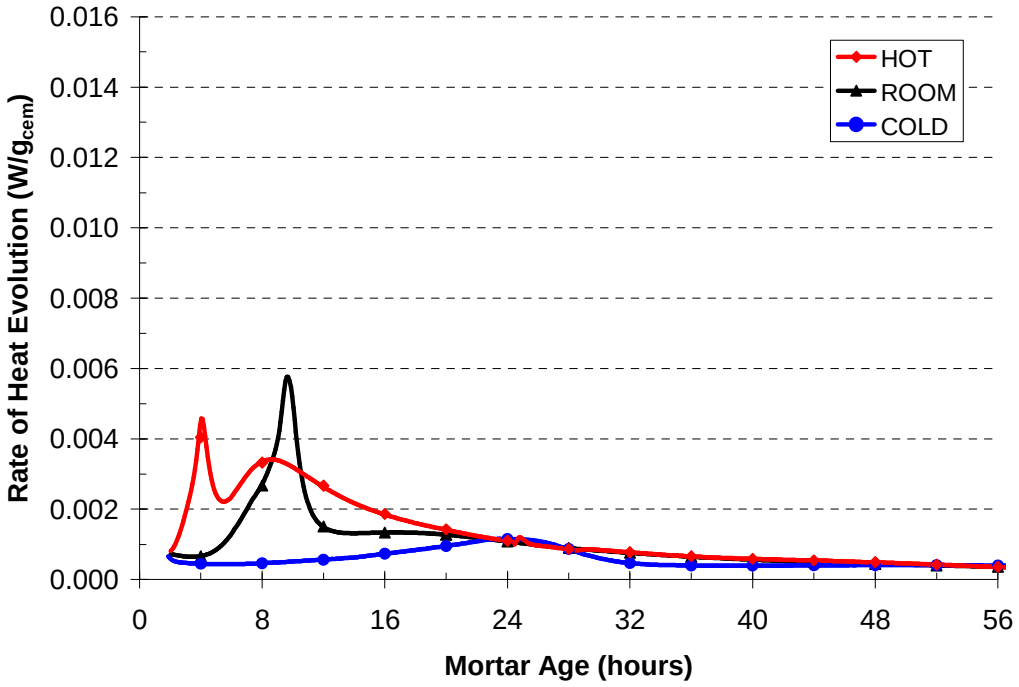

Figure C.9: Isothermal calorimetry results for LA-50FA-24%

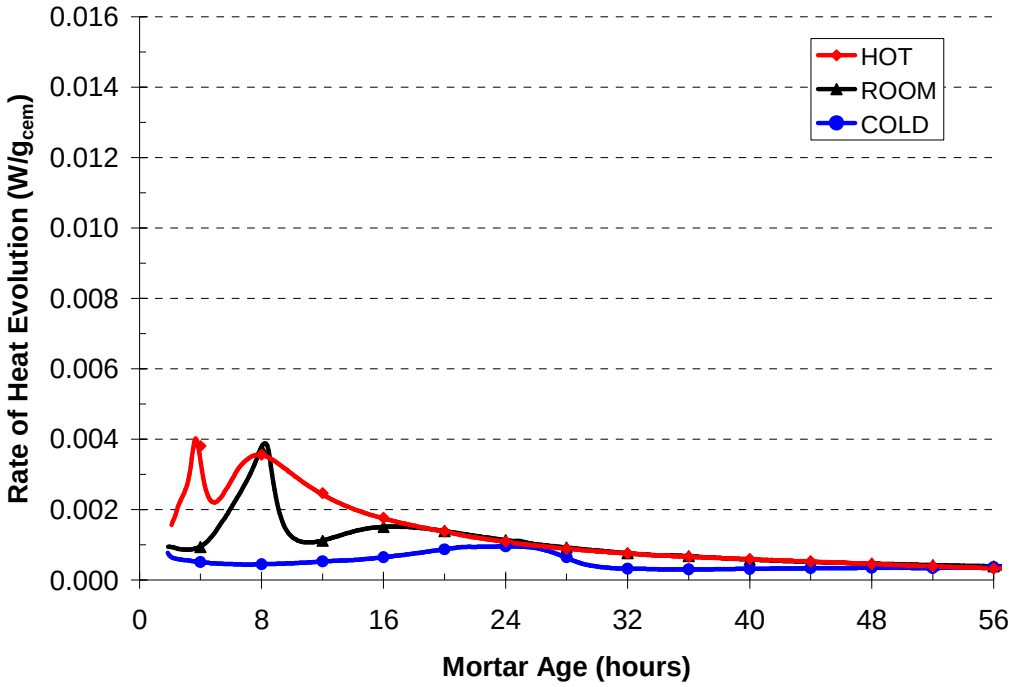

Figure C.10: Isothermal calorimetry results for LA-50FA-28%

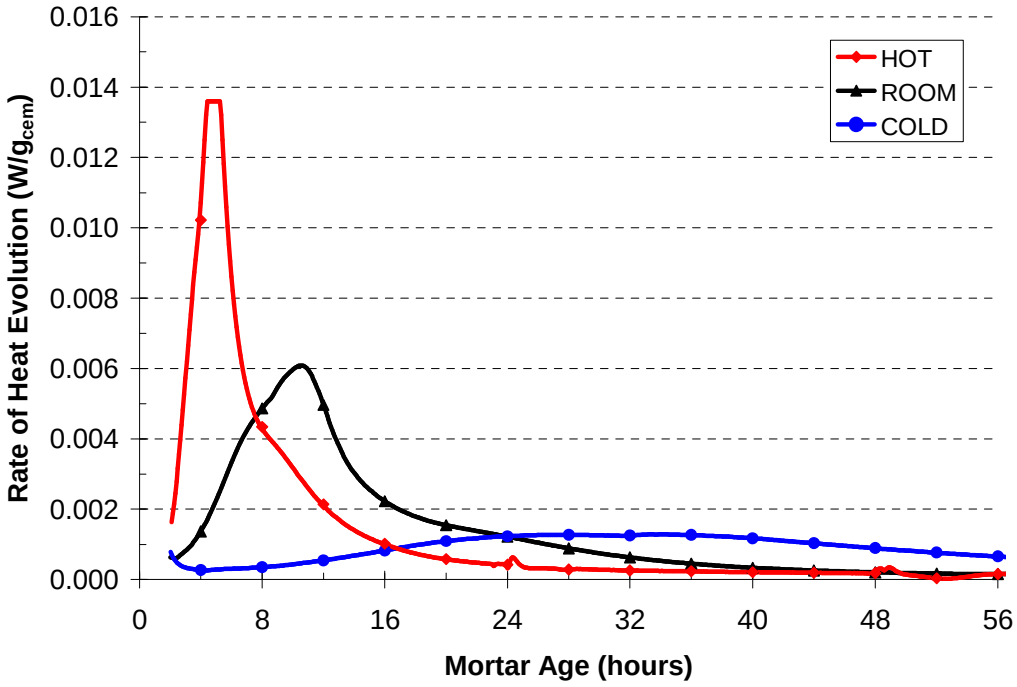

Figure C.11: Isothermal calorimetry results for CTRL42-HA

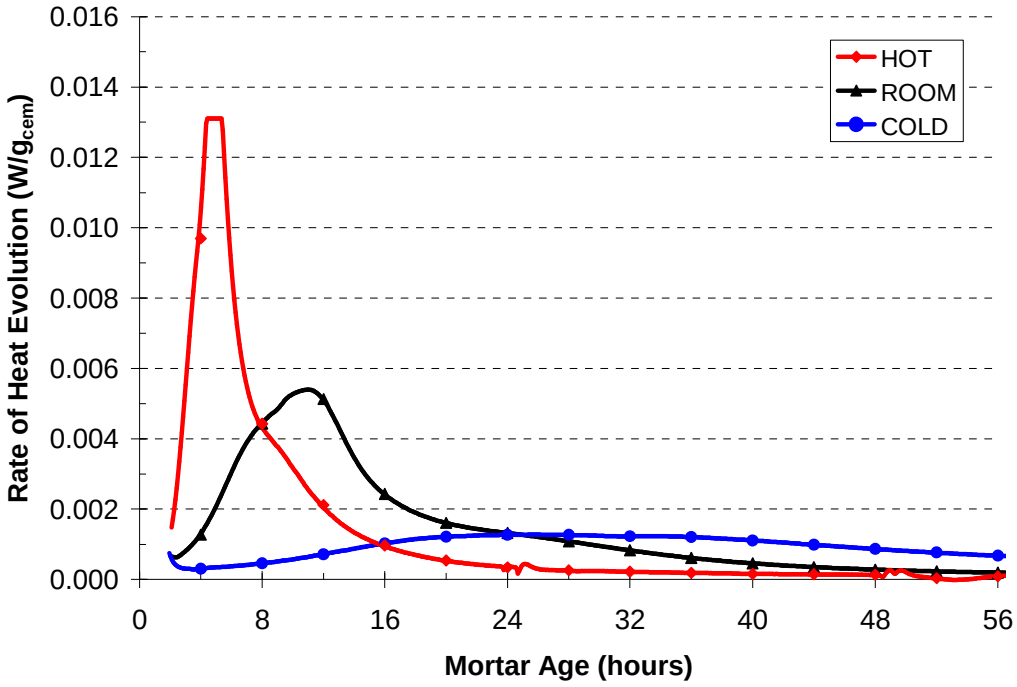

Figure C.12: Isothermal calorimetry results for CTRL44-HA

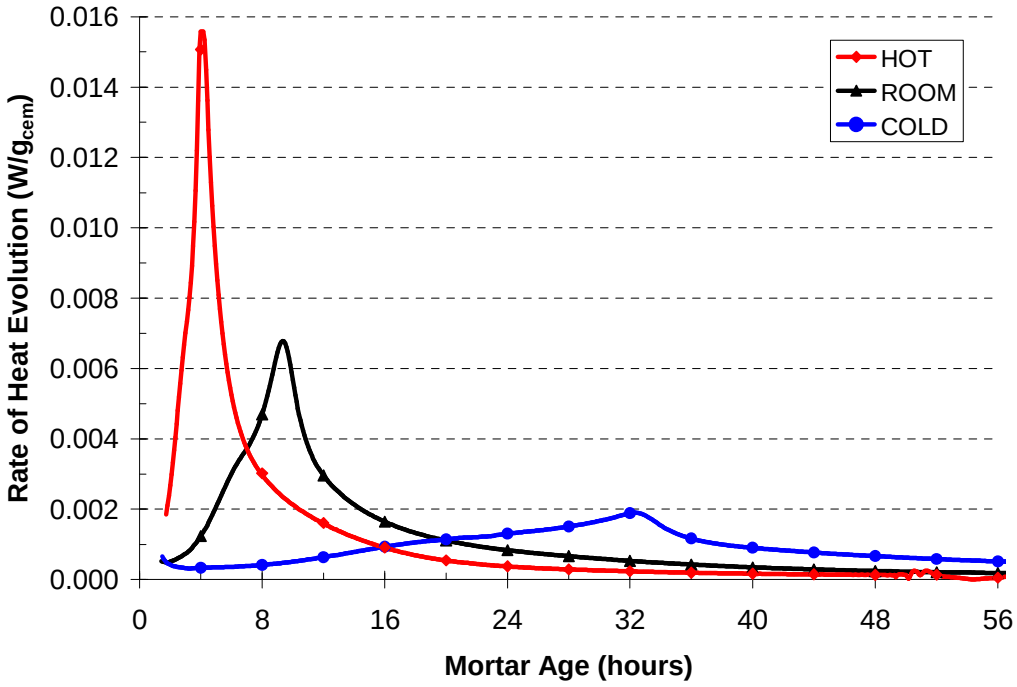

Figure C.13: Isothermal calorimetry results for HA-35FA-1%

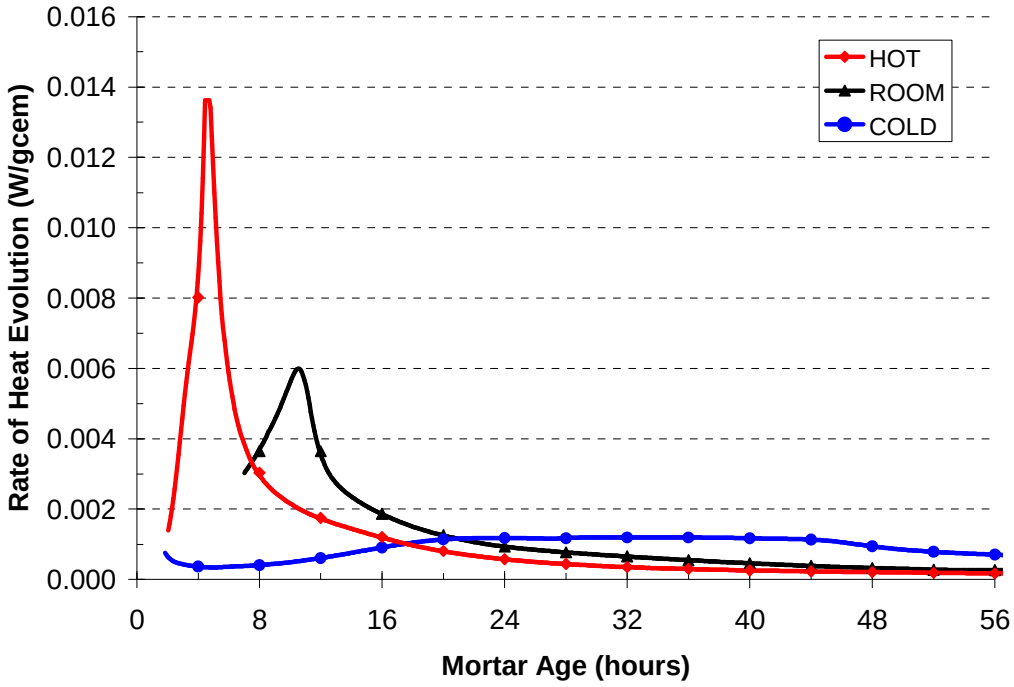

Figure C.14: Isothermal calorimetry results for HA-35FA-15%

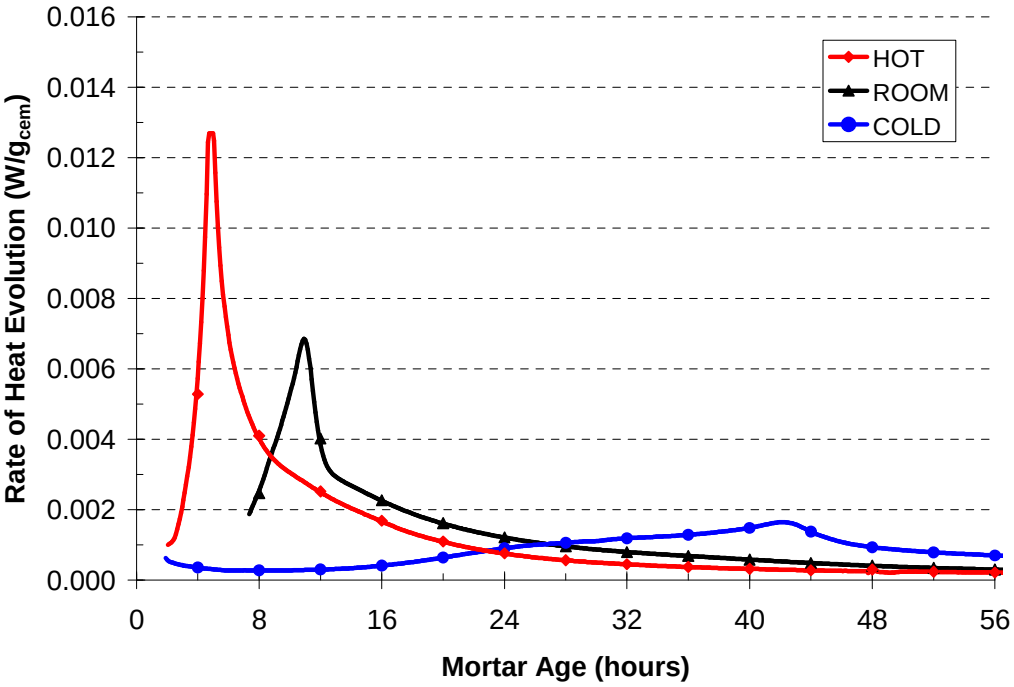

Figure C.15: Isothermal calorimetry results for HA-35FA-24%

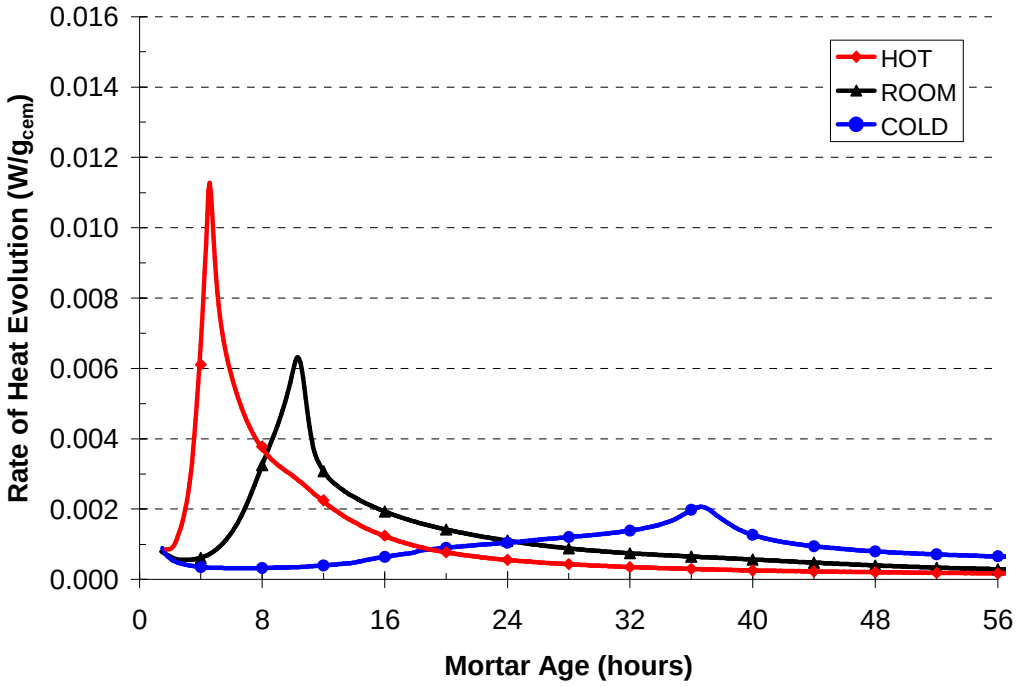

Figure C.16: Isothermal calorimetry results for HA-35FA-28%

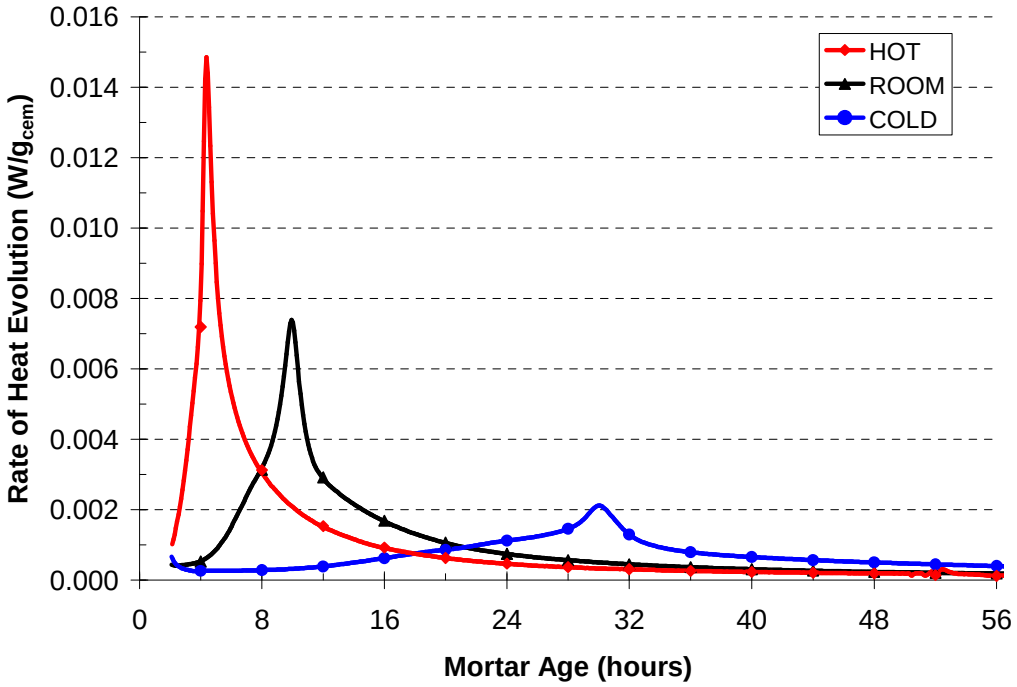

Figure C.17: Isothermal calorimetry results for HA-50FA-1%

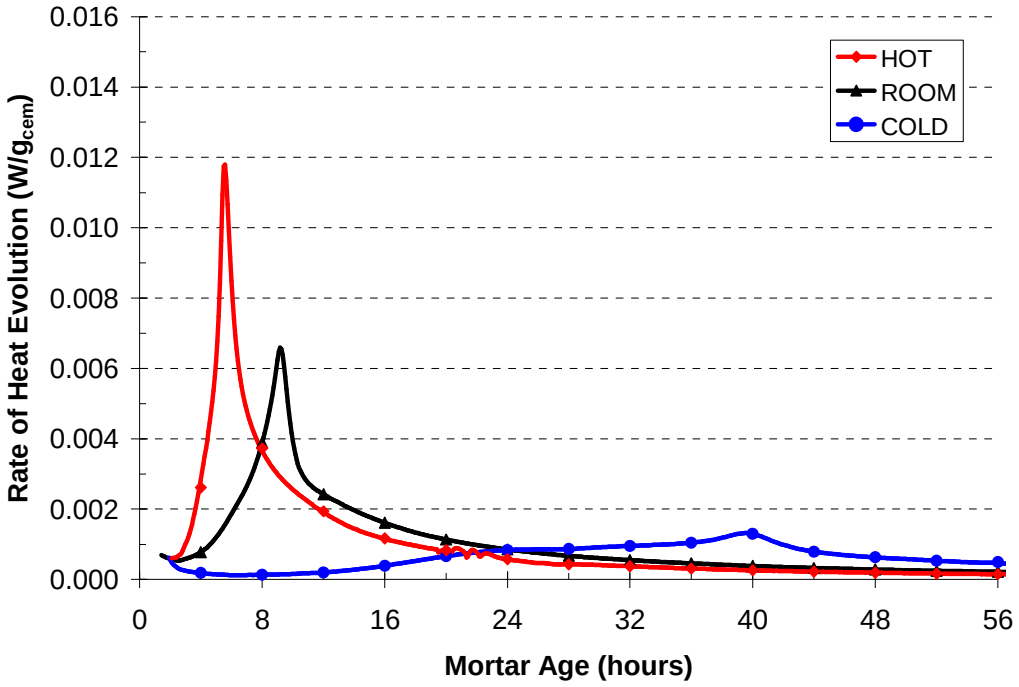

Figure C.18: Isothermal calorimetry results for HA-50FA-15%

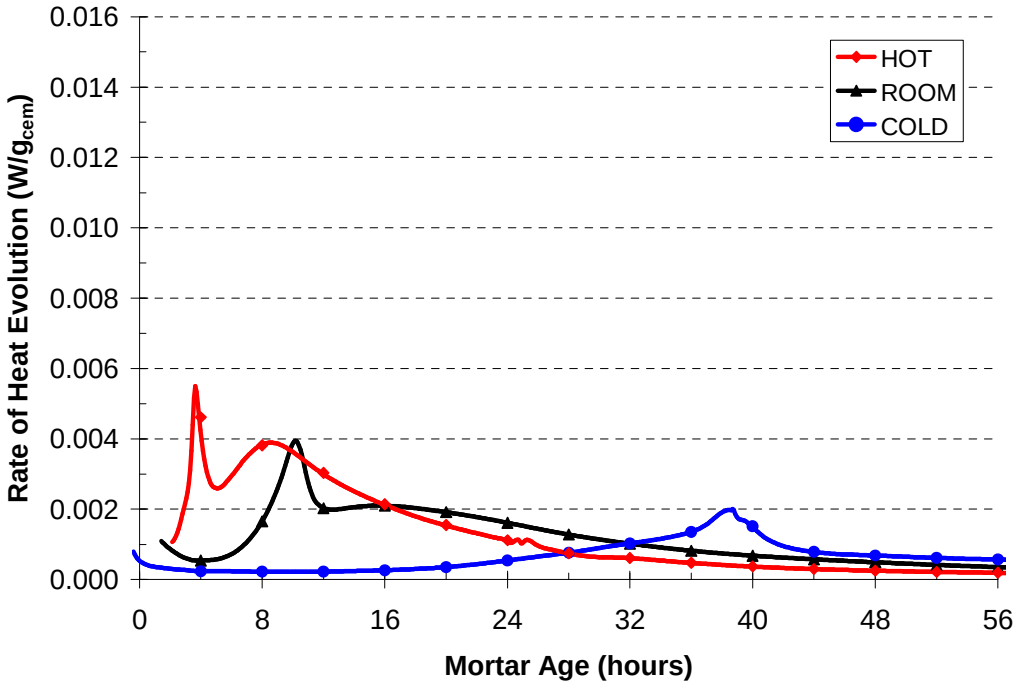

Figure C.19: Isothermal calorimetry results for HA-50FA-24%

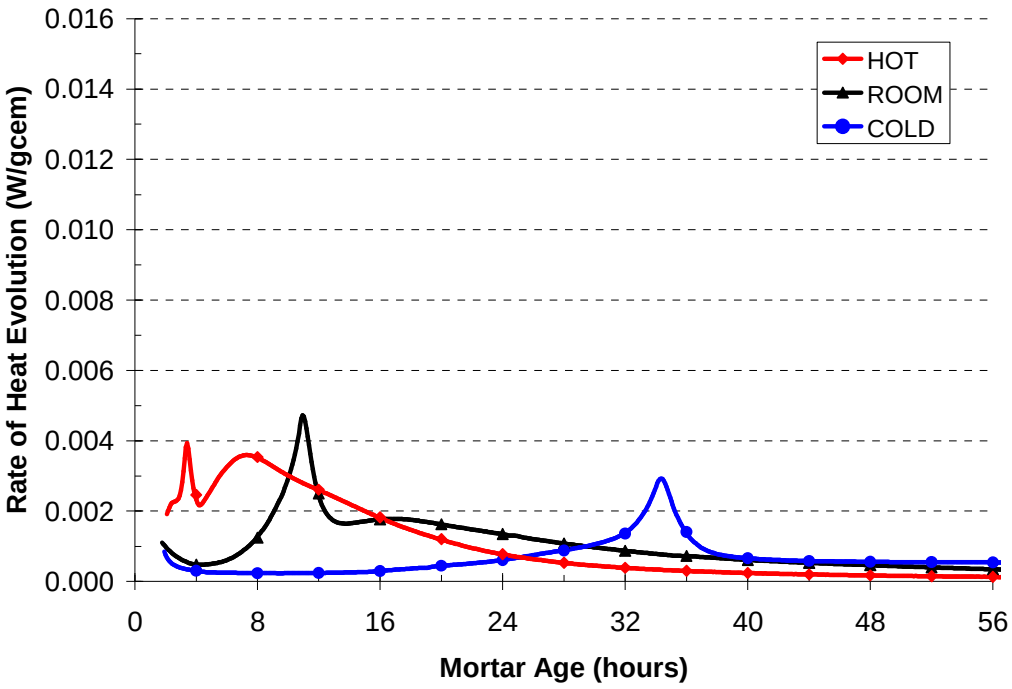

Figure C.20: Isothermal calorimetry results for HA-50FA-28%

C.2 Semi-Adiabatic Calorimetry Results

C.2.1 Best-Fit Hydration Parameters from SAC Testing

Table C.1: Best-fit hydration parameters for LA cement concrete mixtures

Mixture Description	E_A (J/mol)	Hydration Parameters			H_u (J/g)
		β	τ	α_u	
CTRL42-LA	32,500	0.966	10.442	0.812	466
CTRL44-LA	33,500	0.937	11.410	0.833	479
LA-35-1	28,300	0.856	10.944	0.990	377
LA-35-15	36,300	0.895	11.435	0.762	433
LA-35-24	32,600	0.844	15.530	0.917	476
LA-35-28	35,700	0.814	14.603	0.874	496
LA-50-1	29,600	0.778	11.057	0.990	314
LA-50-15	30,300	0.803	13.959	0.805	401
LA-50-24	29,900	0.925	17.679	0.767	464
LA-50-28	33,700	0.870	19.002	0.849	494

Table C.2: Best-fit hydration parameters for HA cement concrete mixtures

Mixture Description	E_A (J/mol)	Hydration Parameters			H_u (J/g)
		β	τ	α_u	
CTRL42-HA	38,000	1.468	9.678	0.728	462
CTRL44-HA	35,600	1.500	9.657	0.747	491
HA-35-1	34,800	1.272	10.423	0.872	379
HA-35-15	32,000	1.281	10.430	0.769	435
HA-35-24	34,200	1.355	12.844	0.767	478
HA-35-28	28,400	1.431	12.054	0.777	498
HA-50-1	34,700	1.230	11.434	0.866	322
HA-50-15	33,500	1.193	12.305	0.764	408
HA-50-24	30,800	1.590	15.554	0.705	471
HA-50-28	28,400	1.403	14.598	0.689	501

C.2.2 SAC Temperature Curves

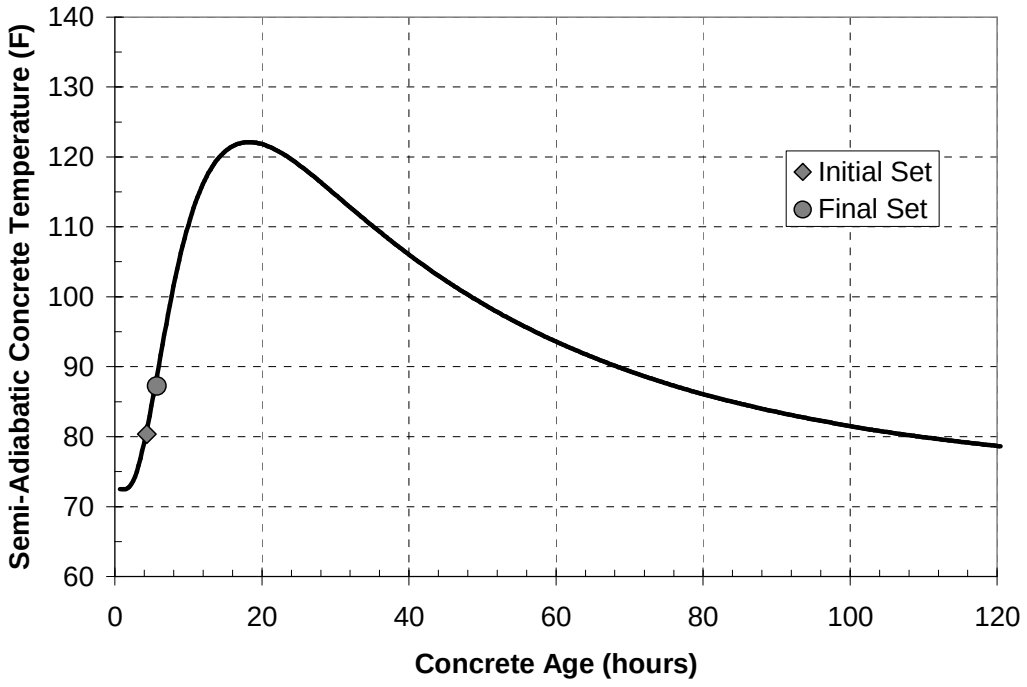

Figure C.21: Semi-adiabatic concrete temperature curve for CTRL42-LA

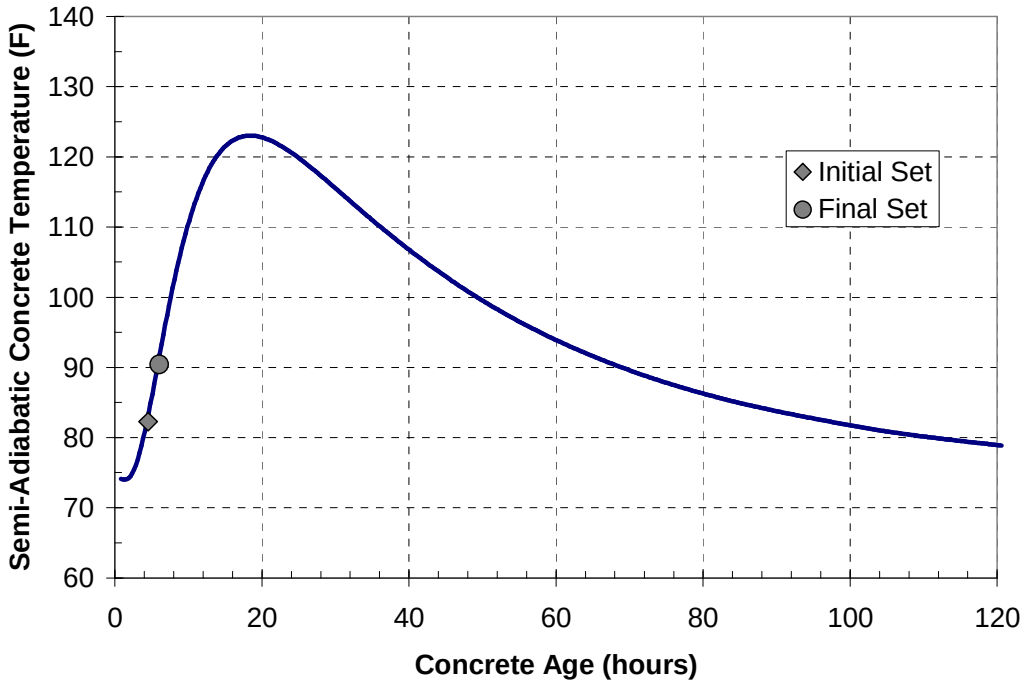

Figure C.22: Semi-adiabatic concrete temperature curve for CTRL44-LA

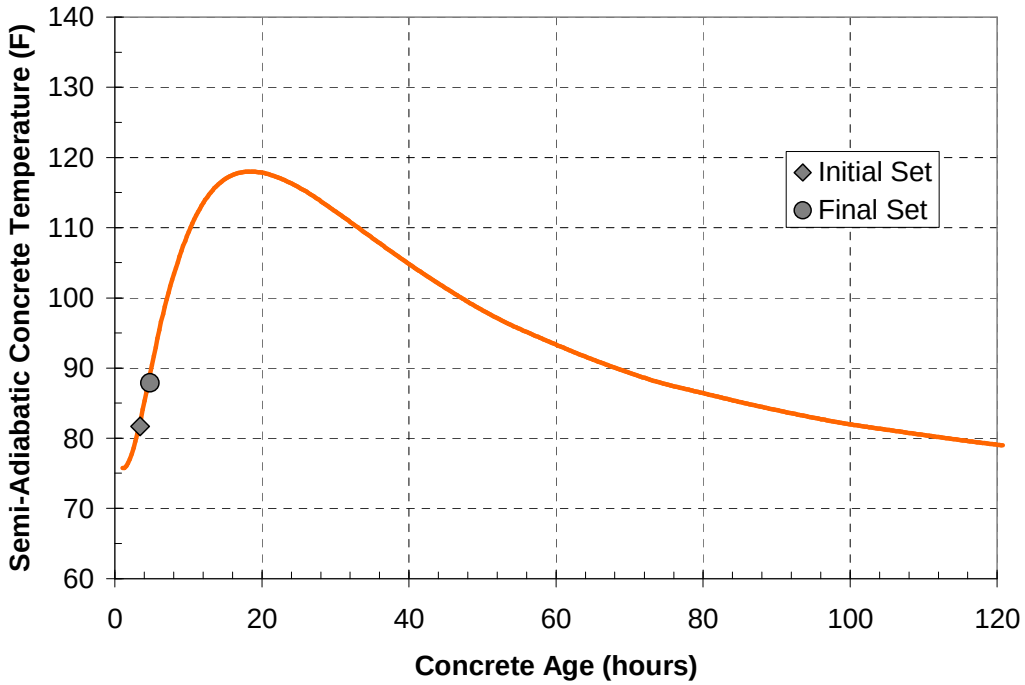

Figure C.23: Semi-adiabatic concrete temperature curve for LA-35FA-1%

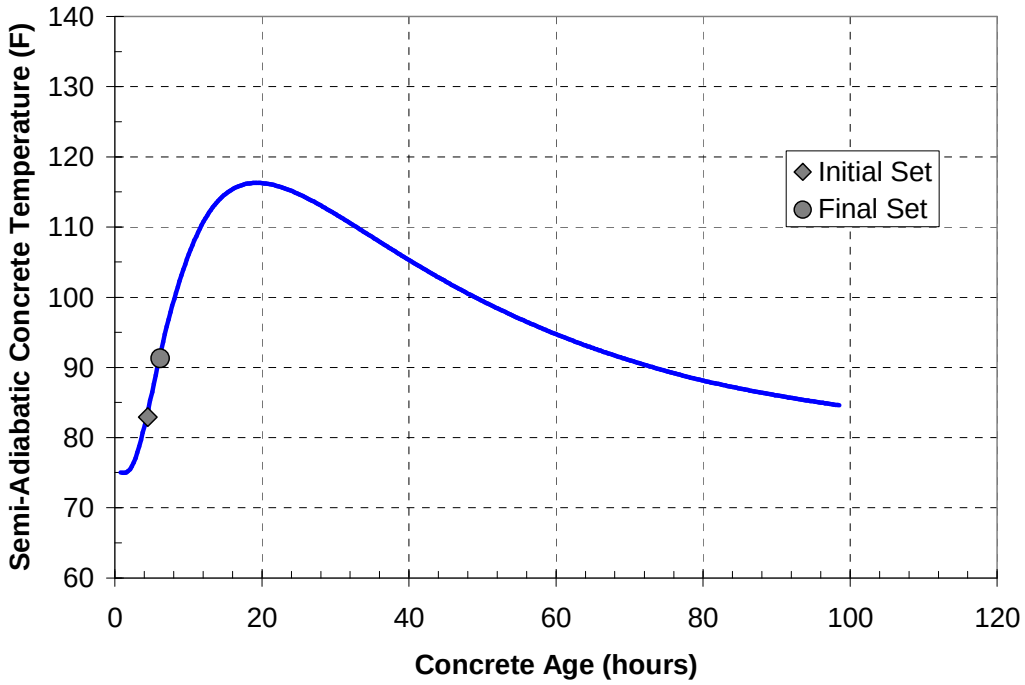

Figure C.24: Semi-adiabatic concrete temperature curve for LA-35FA-15%

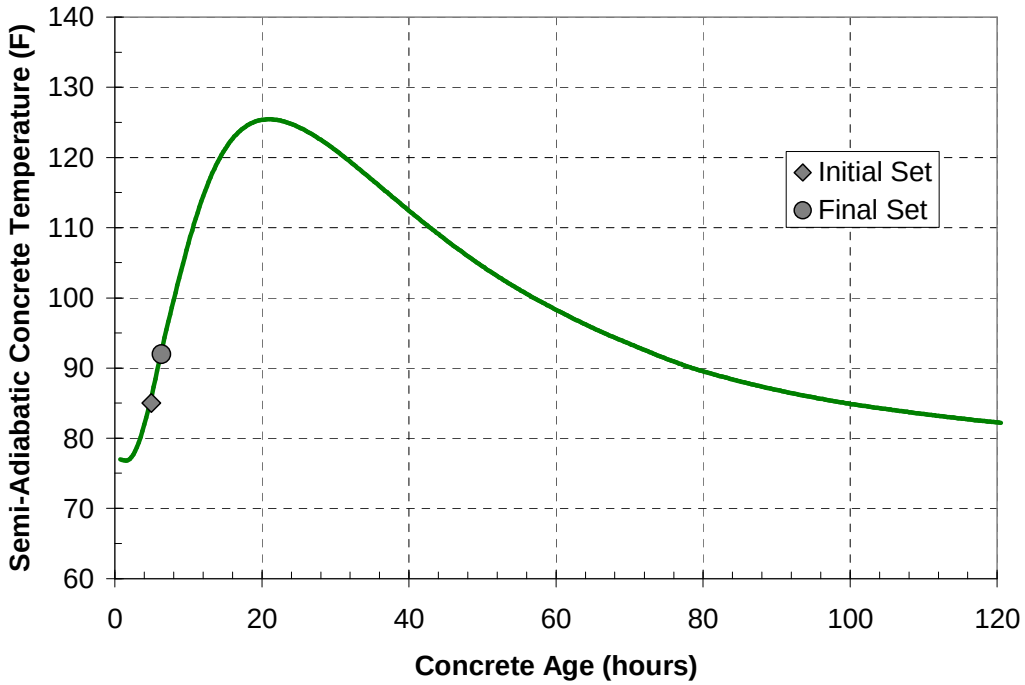

Figure C.25: Semi-adiabatic concrete temperature curve for LA-35FA-24%

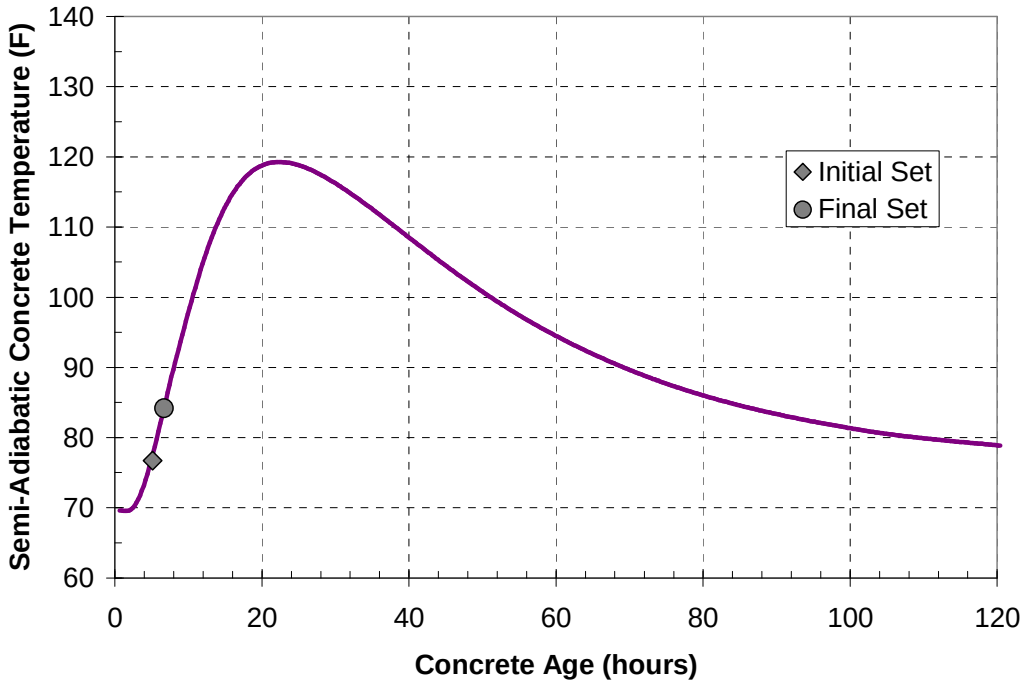

Figure C.26: Semi-adiabatic concrete temperature curve for LA-35FA-28%

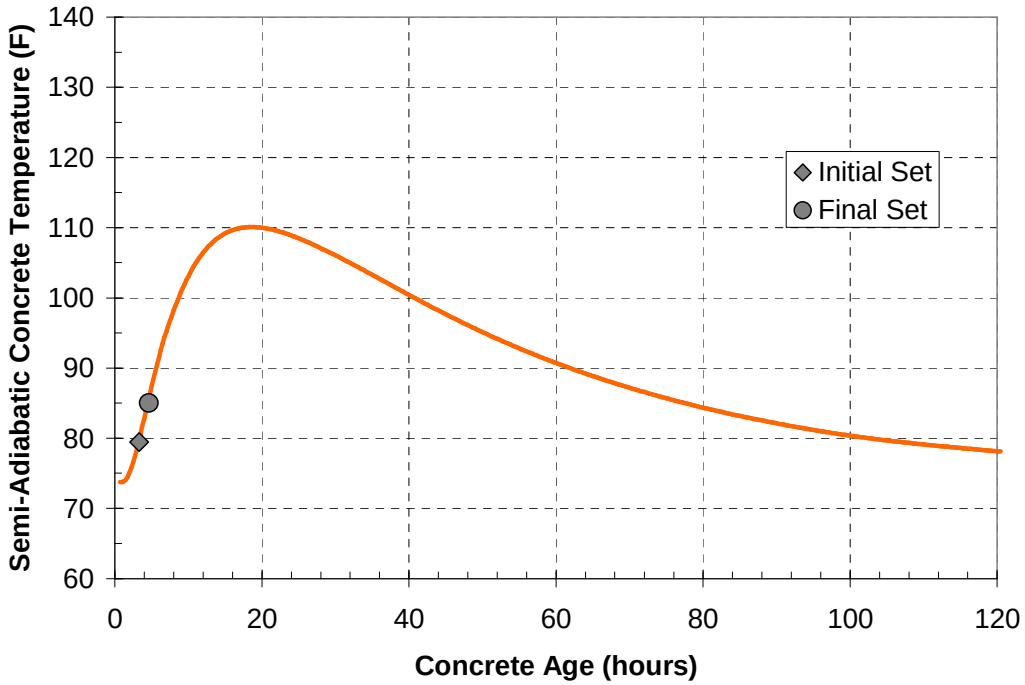

Figure C.27: Semi-adiabatic concrete temperature curve for LA-50FA-1%

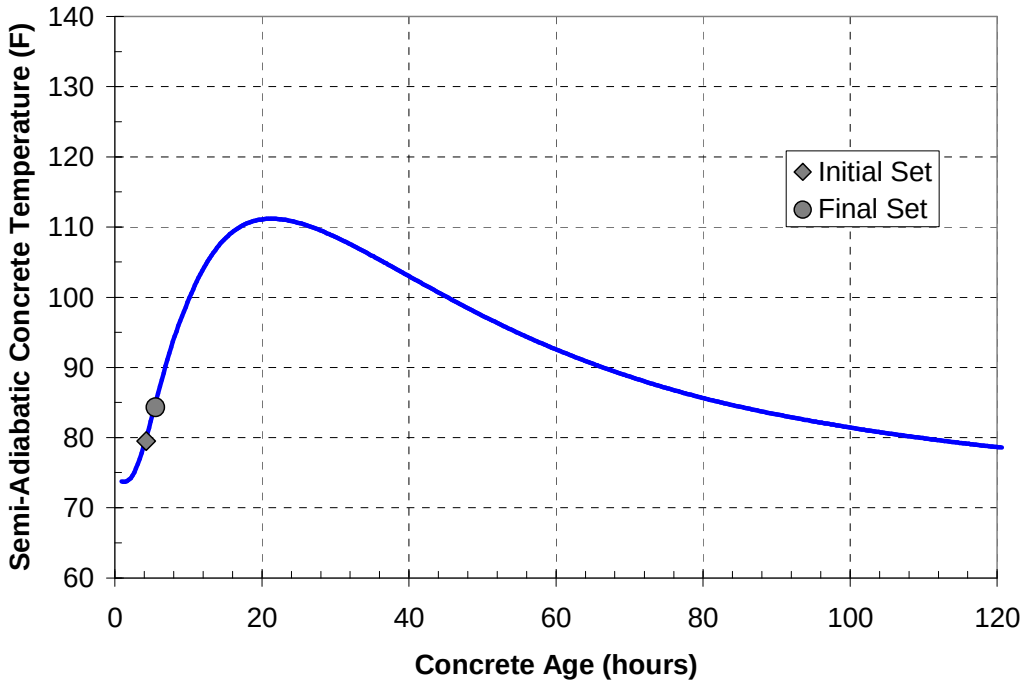

Figure C.28: Semi-adiabatic concrete temperature curve for LA-50FA-15%

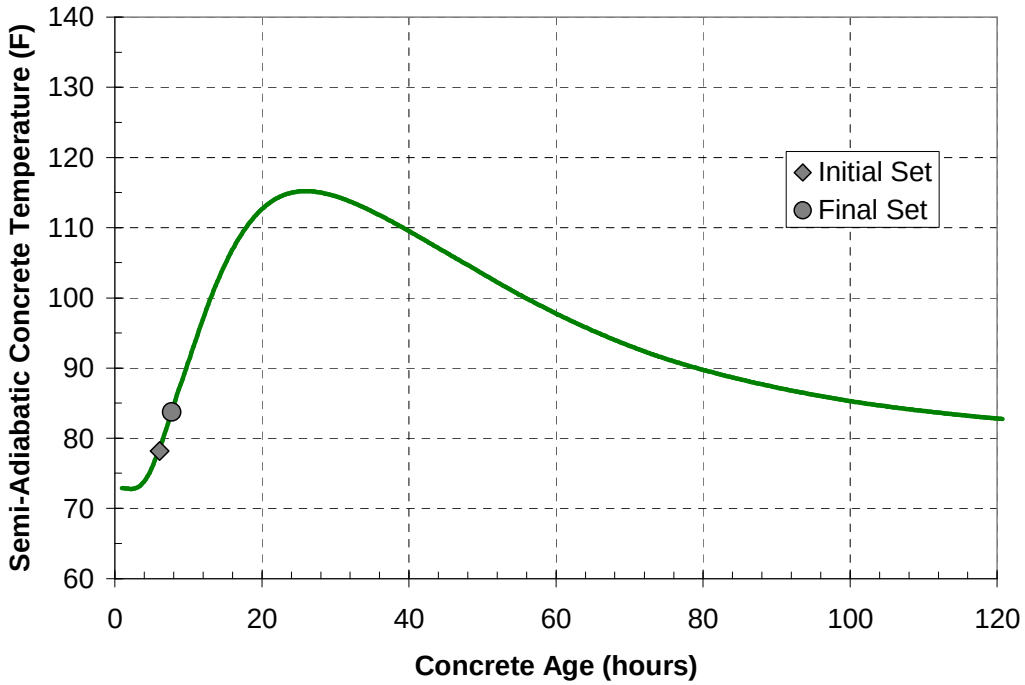

Figure C.29: Semi-adiabatic concrete temperature curve for LA-50FA-24%

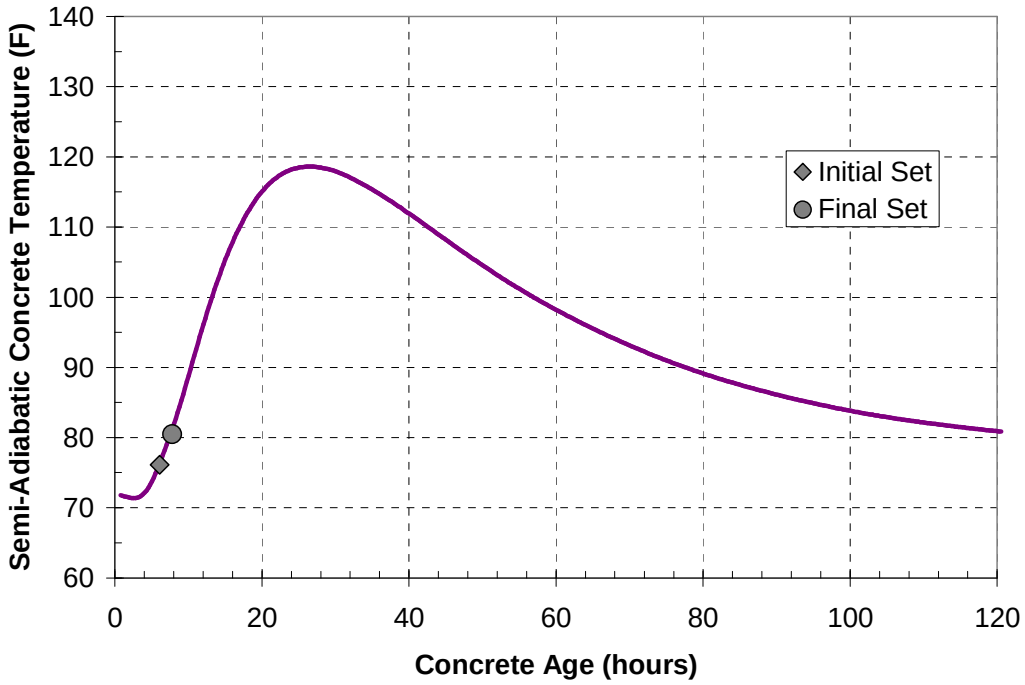

Figure C.30: Semi-adiabatic concrete temperature curve for LA-50FA-28%

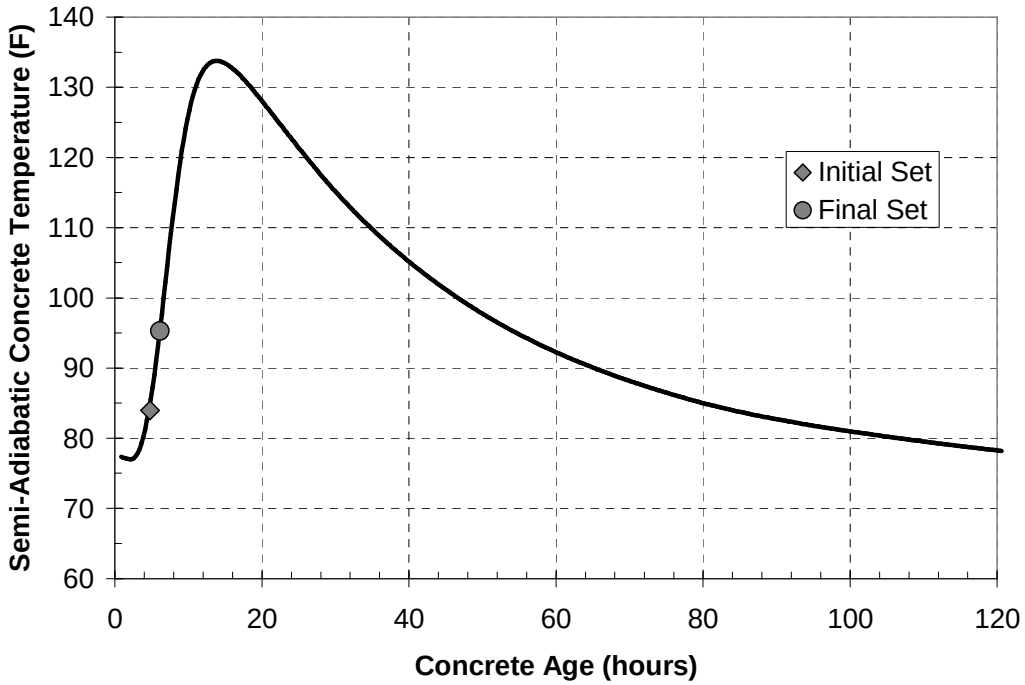

Figure C.31: Semi-adiabatic concrete temperature curve for CTRL42 - HA

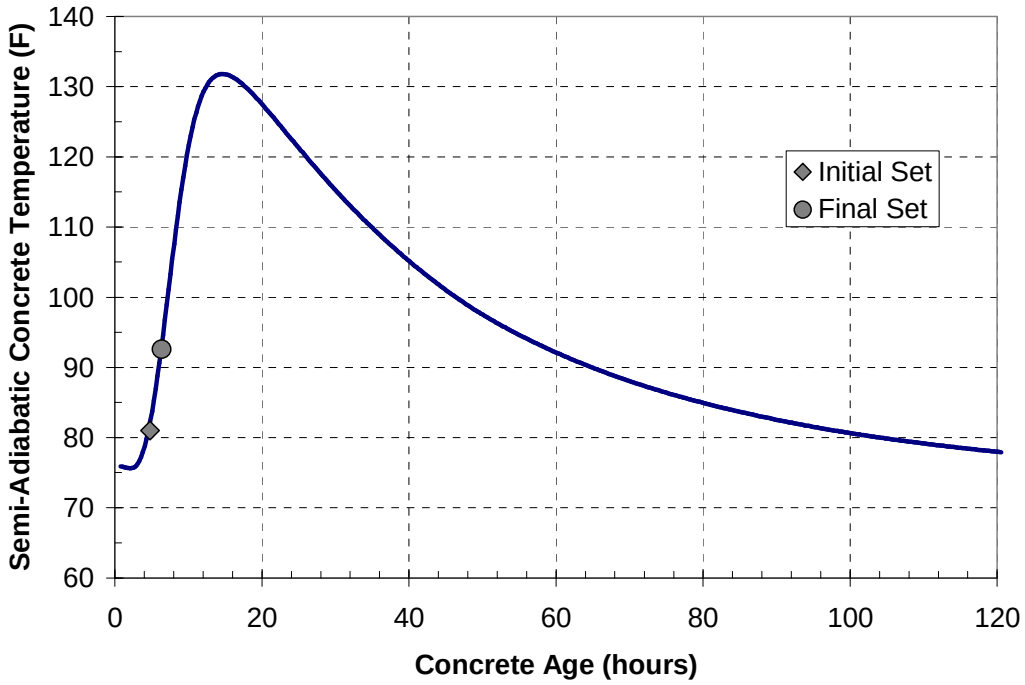

Figure C.32: Semi-adiabatic concrete temperature curve for CTRL44 - HA

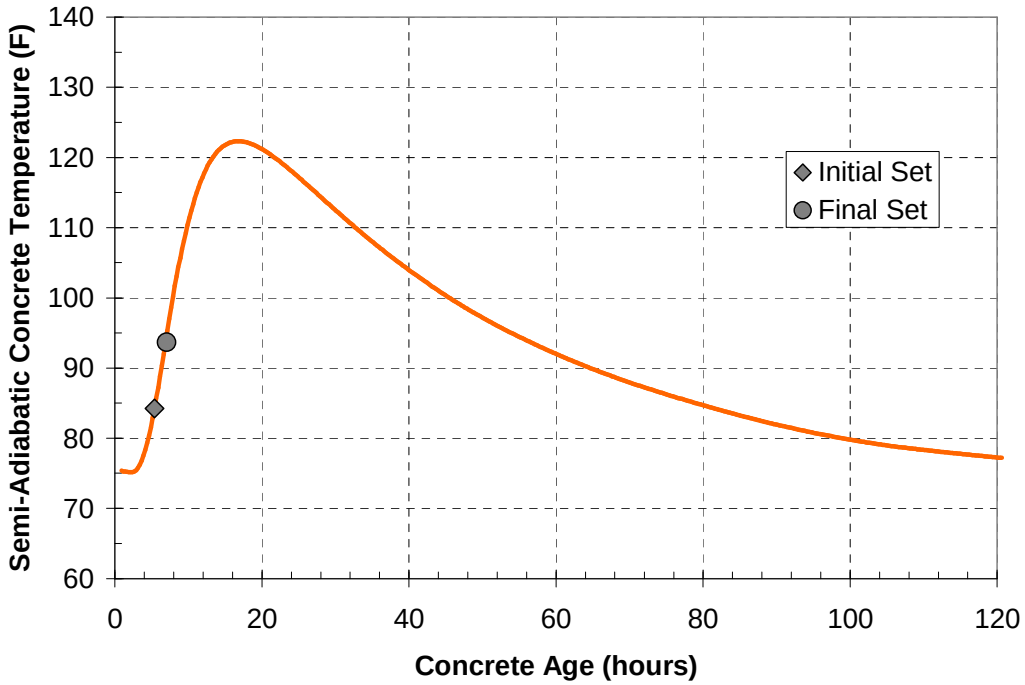

Figure C.33: Semi-adiabatic concrete temperature curve for HA-35FA-1%

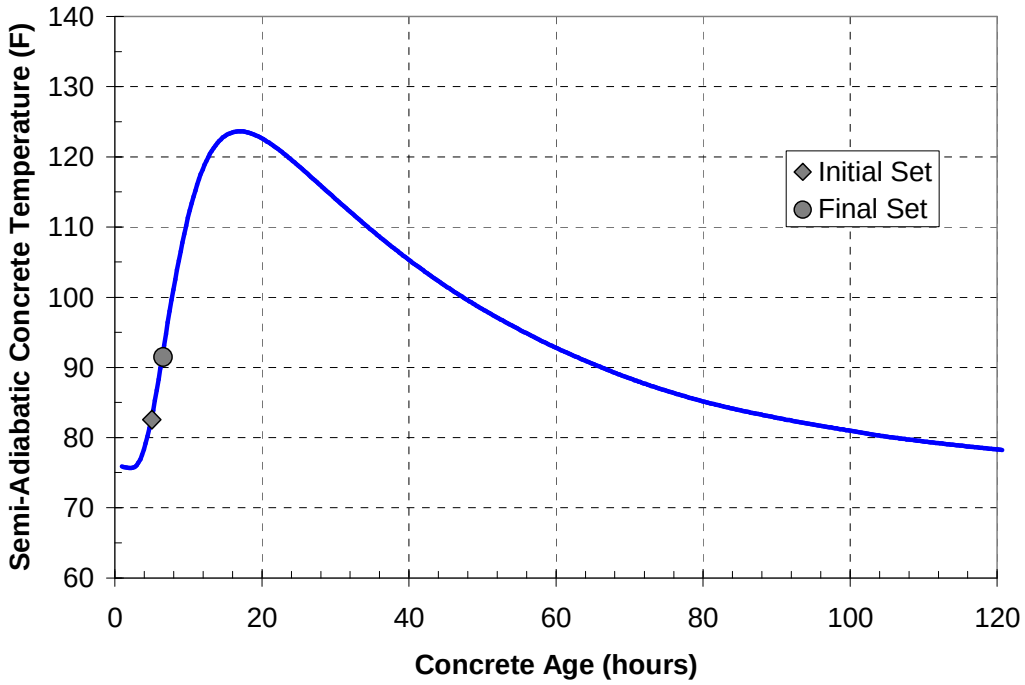

Figure C.34: Semi-adiabatic concrete temperature curve for HA-35FA-15%

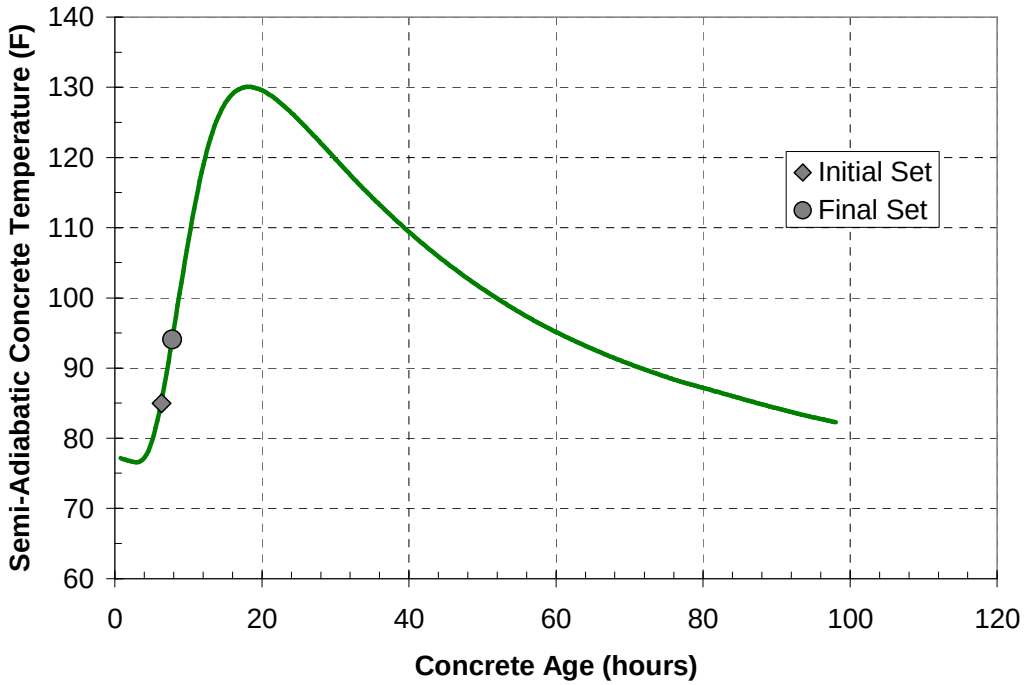

Figure C.35: Semi-adiabatic concrete temperature curve for HA-35FA-24%

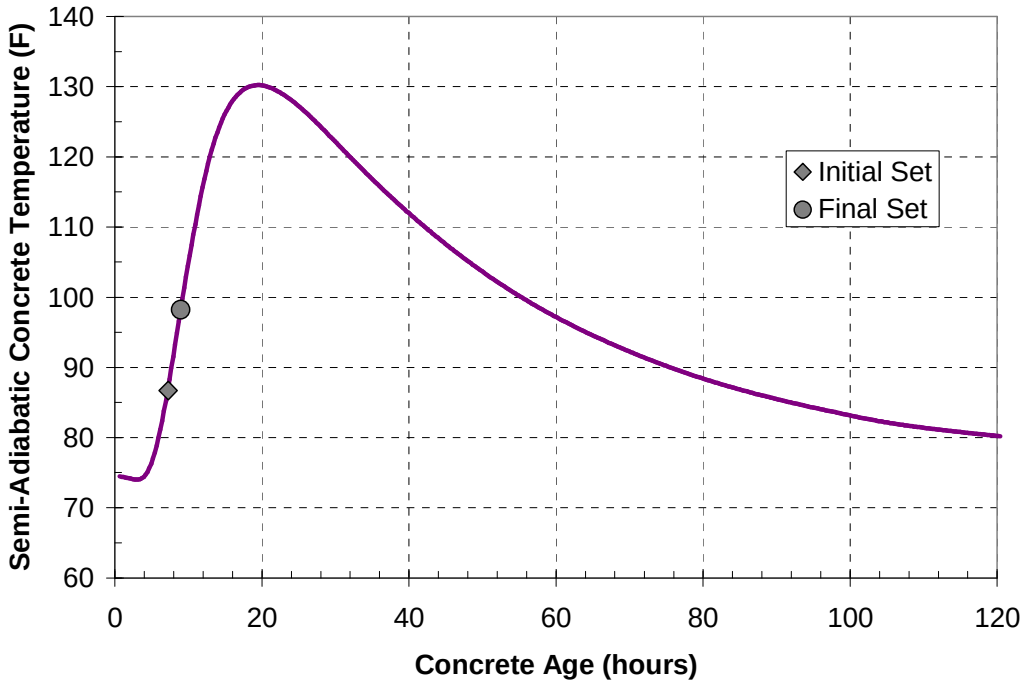

Figure C.36: Semi-adiabatic concrete temperature curve for HA-35FA-28%

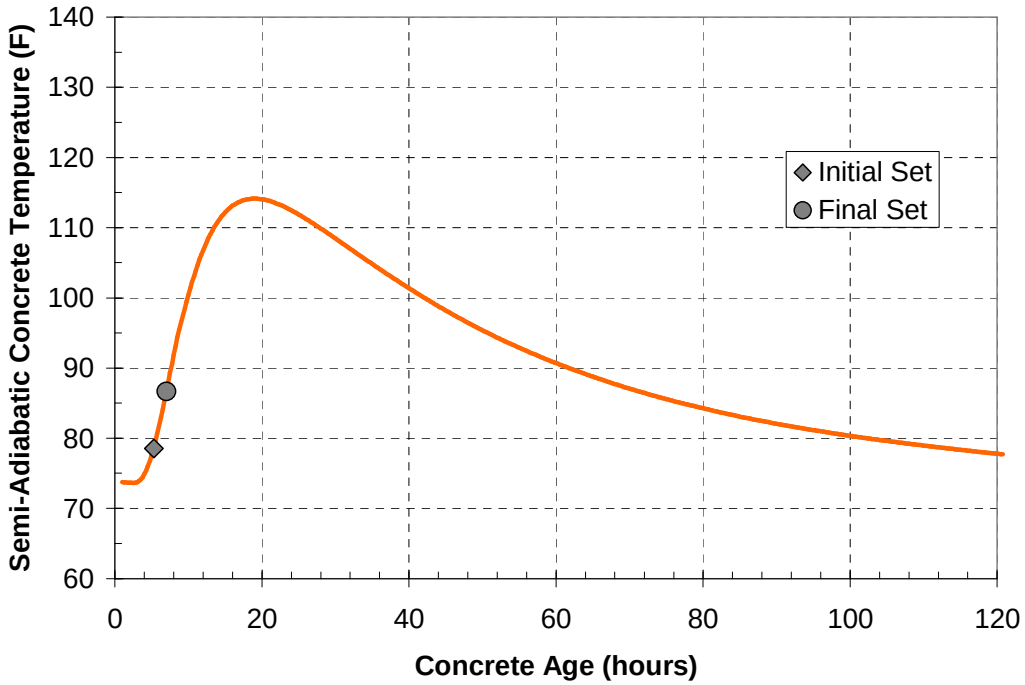

Figure C.37: Semi-adiabatic concrete temperature curve for HA-50FA-1%

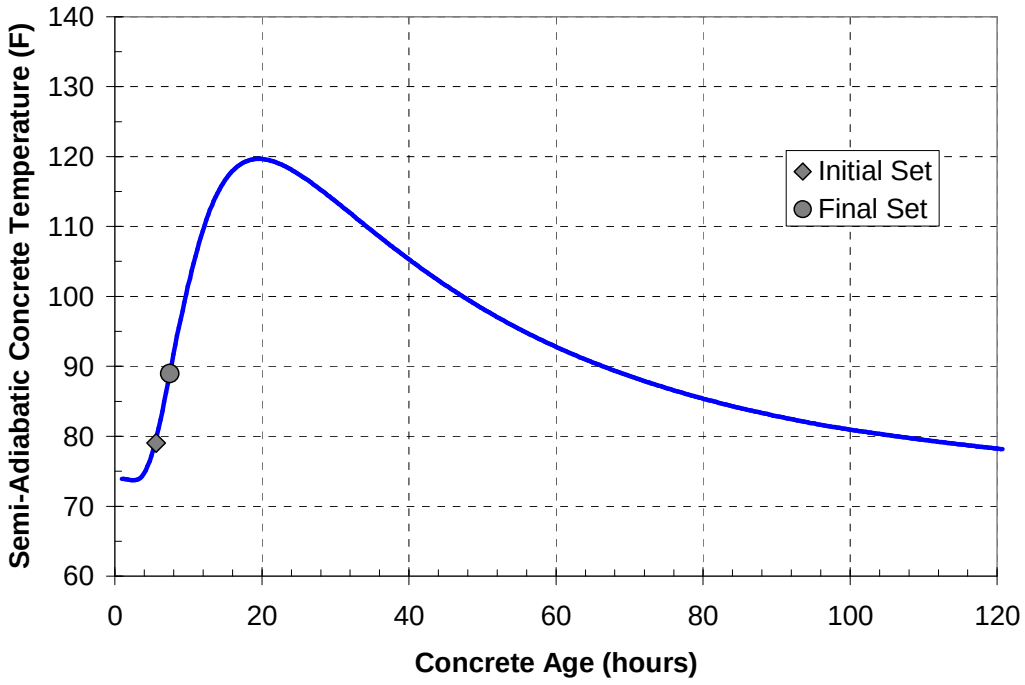

Figure C.38: Semi-adiabatic concrete temperature curve for HA-50FA-15%

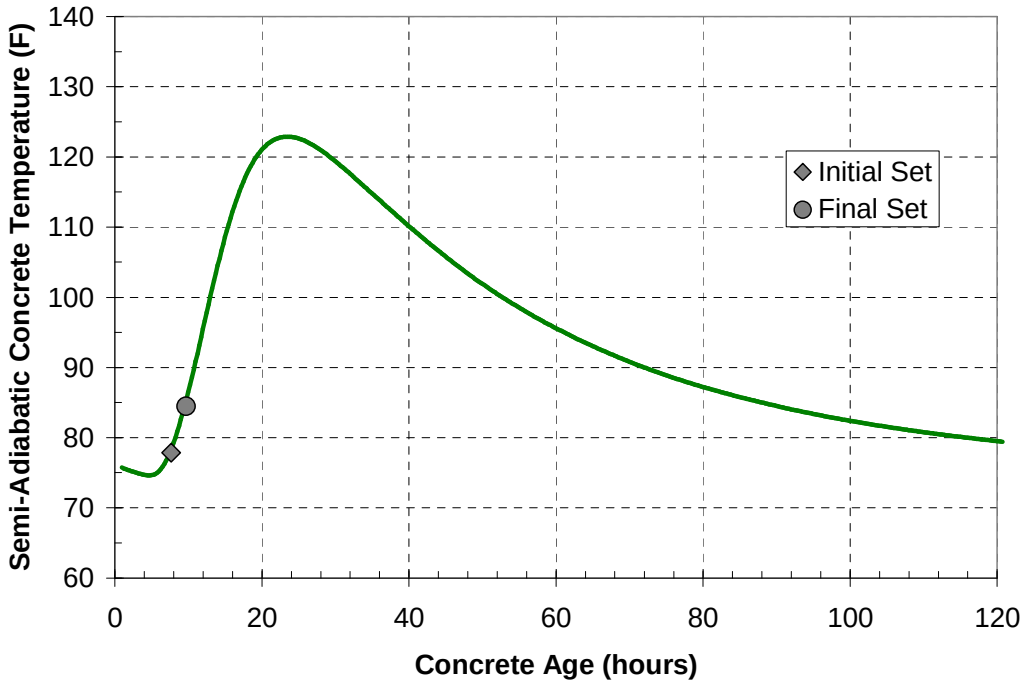

Figure C.39: Semi-adiabatic concrete temperature curve for HA-50FA-24%

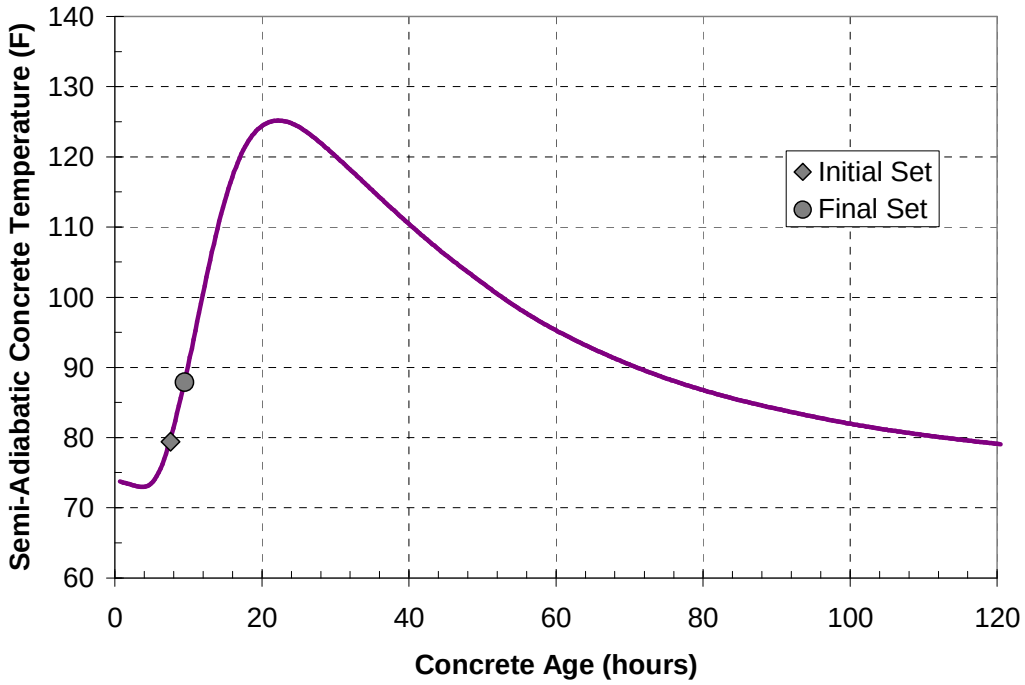

Figure C.40: Semi-adiabatic concrete temperature curve for HA-50FA-28%

Appendix D

Compressive Strength Testing Summary

Appendix D contains all compressive strength testing results for each concrete mixture. Also, the exponential strength-maturity curve for each concrete mixture is presented. The strength-maturity curves were calculated based on the measured compressive strengths and the recorded temperature history of the concrete samples. The strength-maturity relationships presented for each concrete mixture in Appendix D were used to complete the ConcreteWorks analysis described in Chapter 6. All compressive strength testing was conducted in accordance with ASTM C 39 (2004).

D.1 Compressive Strength Testing Results

In Tables D.1 and D.2, the compressive strength testing results from all room temperature batches are presented for each cement source. Next, the results from compressive strength testing for the 28-day quality-control cylinders for the hot and cold batches are presented for each mixture. The results presented in this section represent the average compressive strength of three 4x4 cylinders.

Table D.1: Compressive strength testing results for LA cement mixtures (73 °F)

Mixture Description	Average Moist-Cured Compressive Strength (psi)							
	12 hours	1 day	2 days	4 days	7 days	14 days	28 days	56 days
CTRL42-LA	1030	3150	4380	5140	5940	6830	7370	7420
CTRL44-LA	1150	2590	3720	4670	5530	6250	6820	6860
LA-35FA-1%	1240	2350	3430	4240	4870	5700	6790	7670
LA-35FA-15%	990	2630	3610	4970	5740	6460	7180	8220
LA-35FA-24%	910	2510	3900	4950	5660	6300	7160	8050
LA-35FA-28%	600	2000	3510	4520	5580	6130	7000	7380
LA-50FA-1%	1460	2660	3560	4070	4640	6090	7010	7900
LA-50FA-15%	1220	2650	3660	4550	5220	6410	7380	8720
LA-50FA-24%	560	2260	3560	4660	5440	6610	7750	8630
LA-50FA-28%	250	1110	3090	4620	5460	6560	7620	8590

Table D.2: Compressive strength testing results for HA cement mixtures (73 °F)

Mixture Description	Average Moist-Cured Compressive Strength (psi)							
	12 hours	1 day	2 days	4 days	7 days	14 days	28 days	56 days
CTRL42-HA	700	3230	4070	4710	5000	5250	5600	5890
CTRL44-HA	1080	3240	3710	4290	4710	4950	5280	5650
HA-35FA-1%	1300	2680	3240	3640	4260	4820	5660	6530
HA-35FA-15%	1180	2670	3410	3980	4370	4850	5680	6350
HA-35FA-24%	570	2320	3490	4130	4420	5170	5690	6420
HA-35FA-28%	650	2570	3640	4440	4890	5530	5980	6620
HA-50FA-1%	1690	2810	3450	4150	4590	5360	6360	7680
HA-50FA-15%	1160	2640	3380	4110	4640	5340	6610	7550
HA-50FA-24%	160	2050	3590	4280	5040	6100	6730	7060
HA-50FA-28%	190	1890	3290	4050	4540	5080	5790	6480

Table D.3: Quality-control compressive strength results for LA cement mixtures

Mixture Description	28-Day Compressive Strength (psi)	
	Cold (40 °F)	Hot (105 °F)
CTRL42-LA	6010	6920
CTRL44-LA	5230	6900
LA-35FA-1%	6020	6880
LA-35FA-15%	6720	6910
LA-35FA-24%	6770	7090
LA-35FA-28%	7360	7220
LA-50FA-1%	7080	6850
LA-50FA-15%	6680	7990
LA-50FA-24%	6840	7870
LA-50FA-28%	5980	8300

Table D.4: Quality-control compressive strength results for HA cement mixtures

Mixture Description	28-Day Compressive Strength (psi)	
	Cold (40 °F)	Hot (105 °F)
CTRL42-HA	5290	5340
CTRL44-HA	4940	5320
HA-35FA-1%	5660	5210
HA-35FA-15%	6260	5410
HA-35FA-24%	6340	5530
HA-35FA-28%	5700	5690
HA-50FA-1%	6750	6050
HA-50FA-15%	5840	6160
HA-50FA-24%	6030	6460
HA-50FA-28%	5670	6110

D.2 Strength-Maturity Parameters and Plots

Table D.5: Strength-maturity parameters for LA cement mixtures

Mixture Description	Strength-Maturity Parameters		
	β_s	τ_s (hours)	$f'c_{ult}$ (psi)
CTRL42-LA	0.720	25.24	7910
CTRL44-LA	0.845	22.43	7110
LA-35-1	0.431	49.49	9540
LA-35-15	0.496	31.63	9320
LA-35-24	0.735	29.36	8100
LA-35-28	0.839	29.17	7480
LA-50-1	0.330	89.08	11820
LA-50-15	0.392	68.03	11570
LA-50-24	0.590	44.09	9590
LA-50-28	0.763	46.67	8890

Table D.6: Strength-maturity parameters for HA cement mixtures

Mixture Description	Strength-Maturity Parameters		
	β_s	τ_s (hours)	$f'c_{ult}$ (psi)
CTRL42-HA	1.734	19.53	5480
CTRL44-HA	1.290	17.00	5300
HA-35-1	0.347	47.33	8680
HA-35-15	0.555	24.62	6750
HA-35-24	0.851	25.08	6170
HA-35-28	0.930	22.26	6330
HA-50-1	0.223	336.8	16030
HA-50-15	0.366	67.14	10300
HA-50-24	0.975	29.33	7100
HA-50-28	0.918	27.51	6170

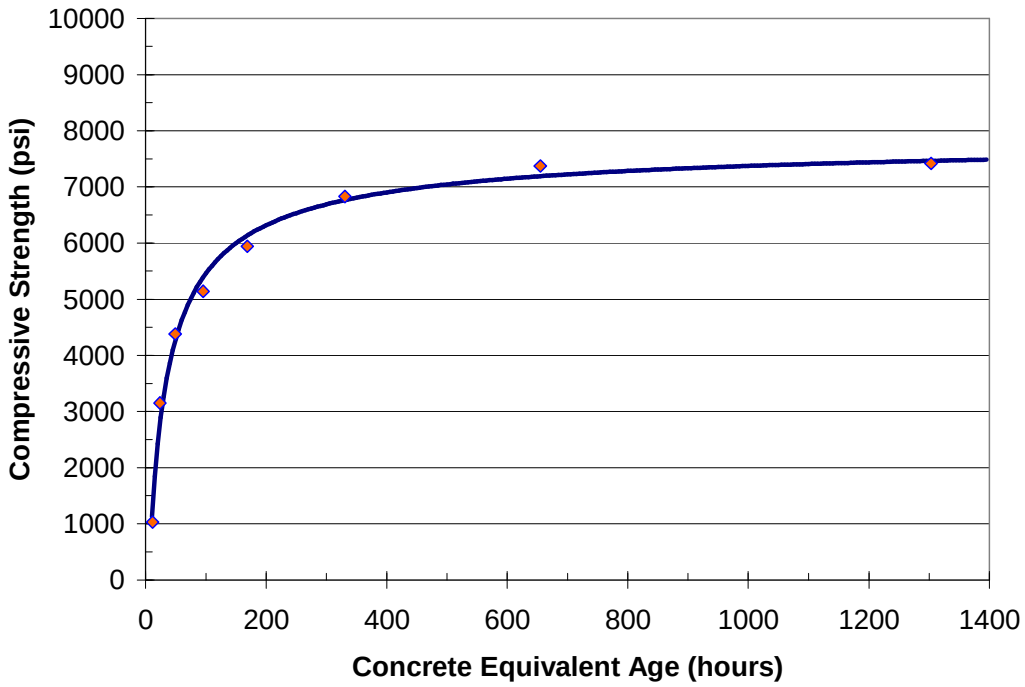

Figure D.1: Strength-maturity curve for CTRL42 - LA

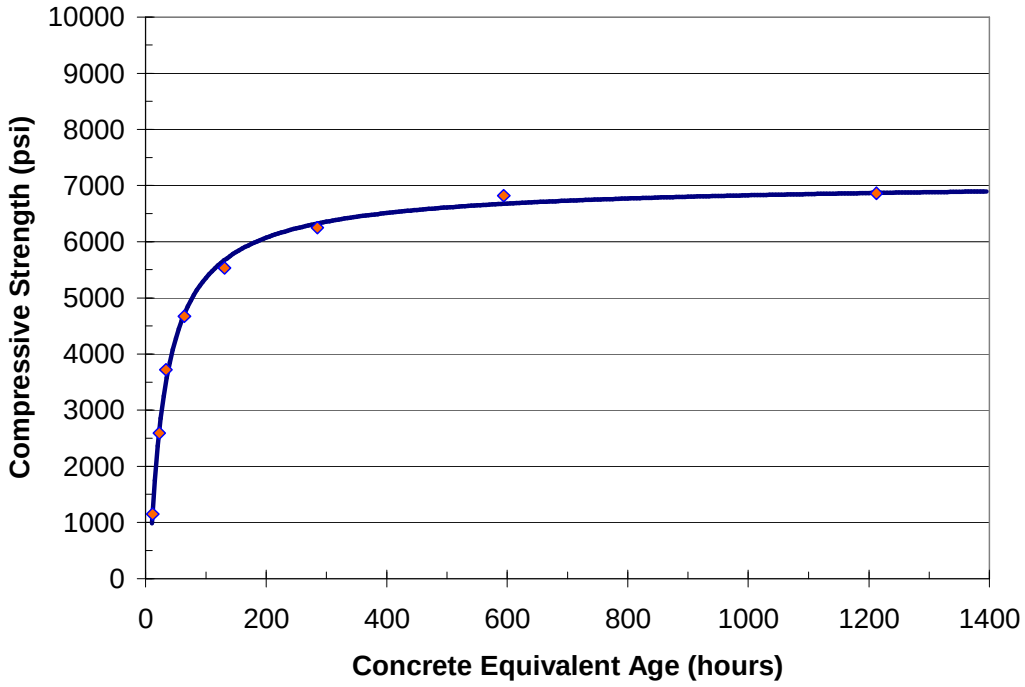

Figure D.2: Strength-maturity curve for CTRL44 - LA

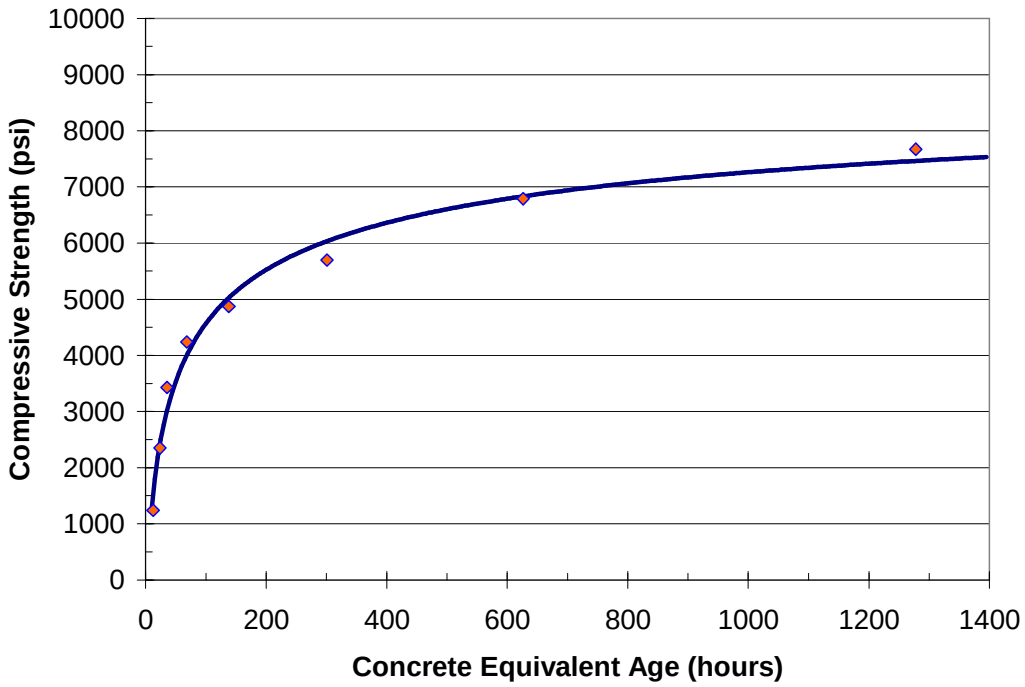

Figure D.3: Strength-maturity curve for LA-35FA-1%

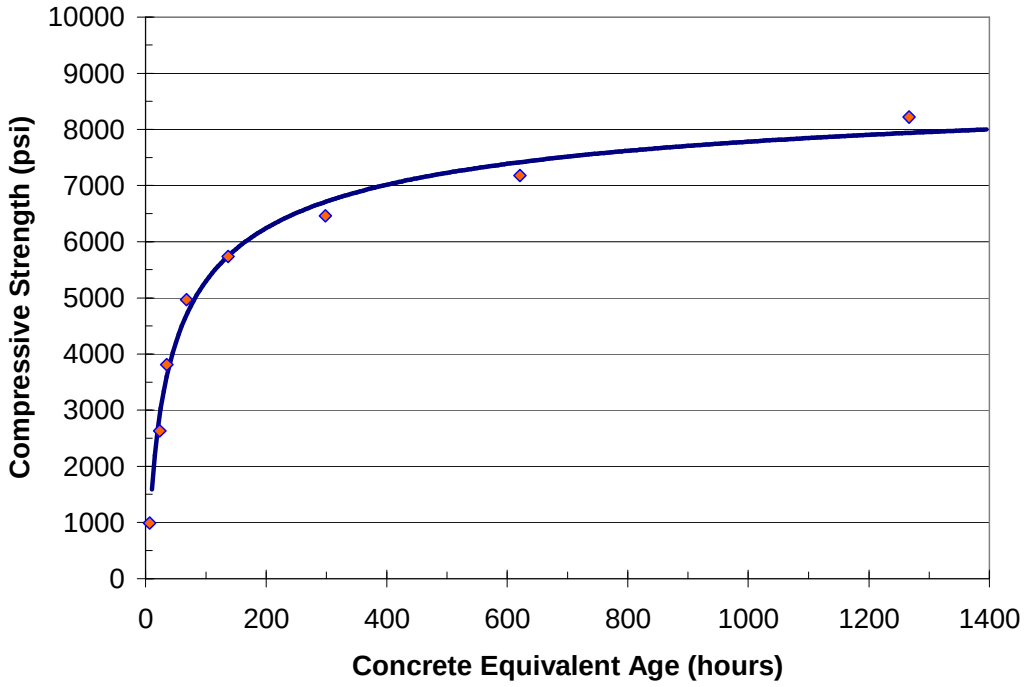

Figure D.4: Strength-maturity curve for LA-35FA-15%

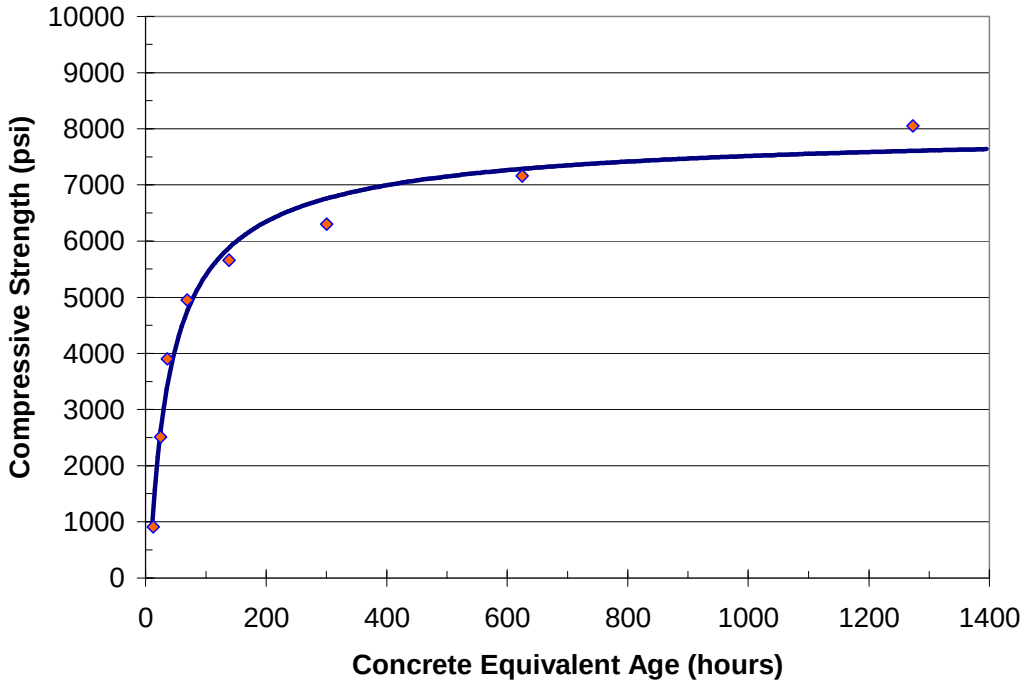

Figure D.5: Strength-maturity curve for LA-35FA-24%

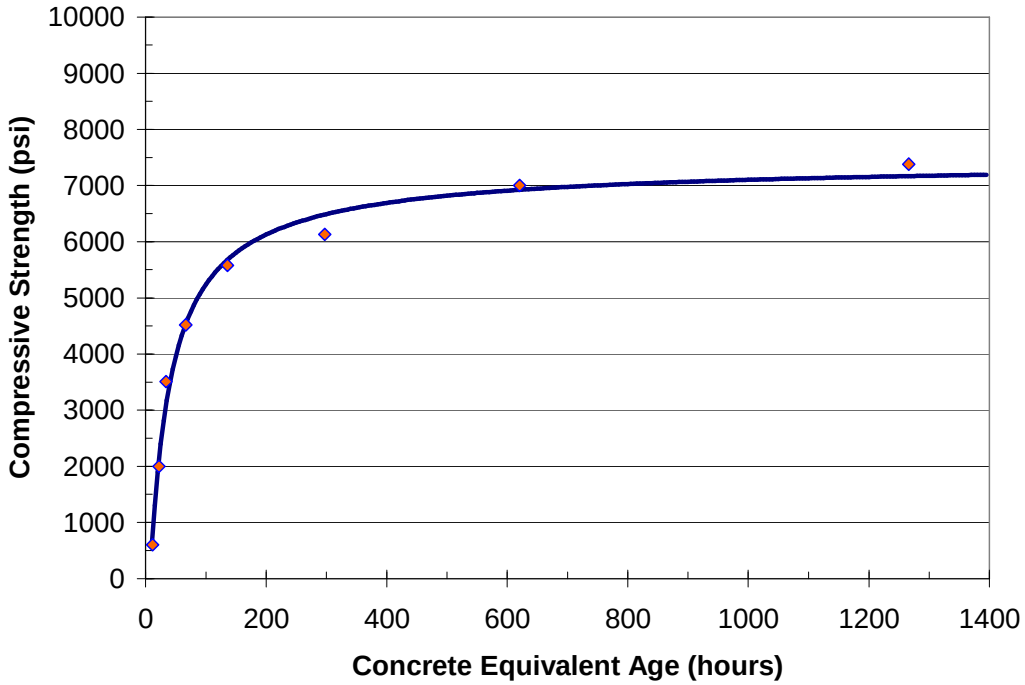

Figure D.6: Strength-maturity curve for LA-35FA-28%

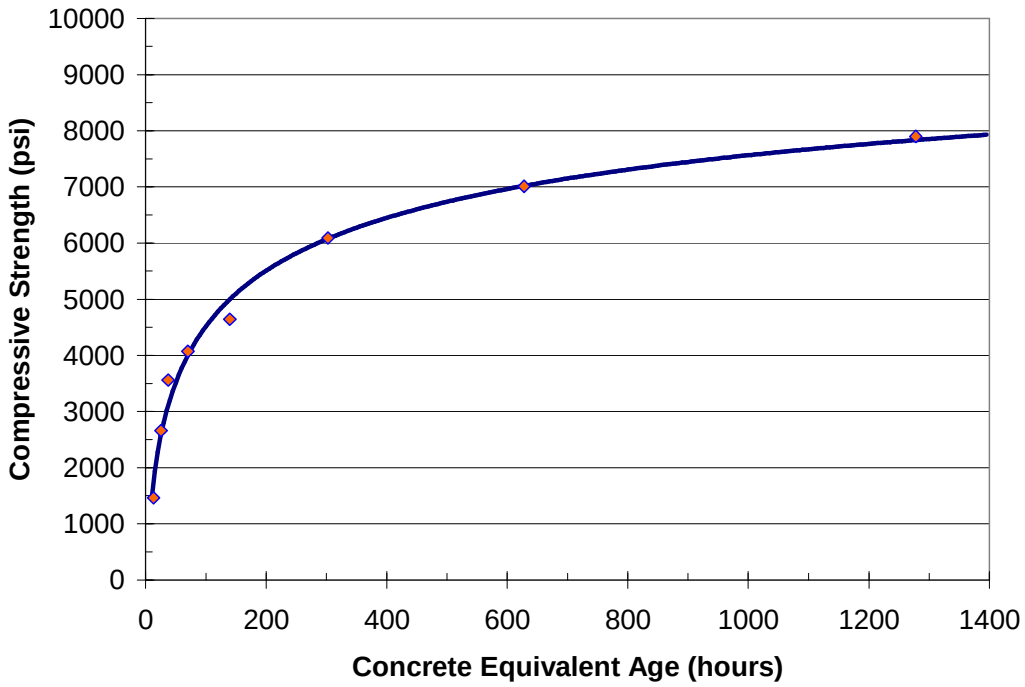

Figure D.7: Strength-maturity curve for LA-50FA-1%

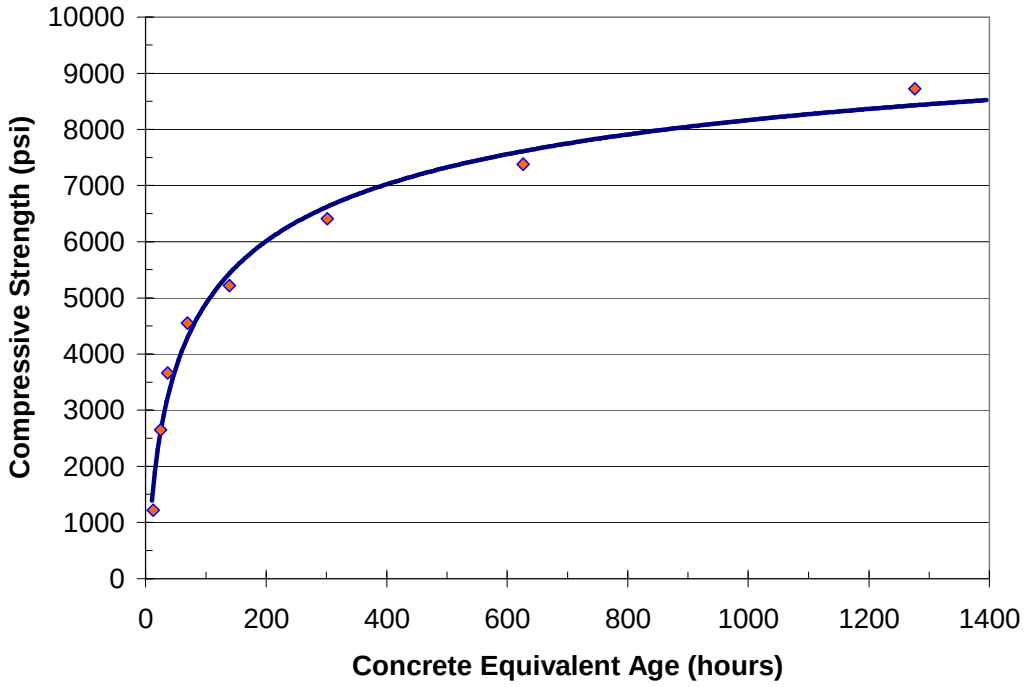

Figure D.8: Strength-maturity curve for LA-50FA-15%

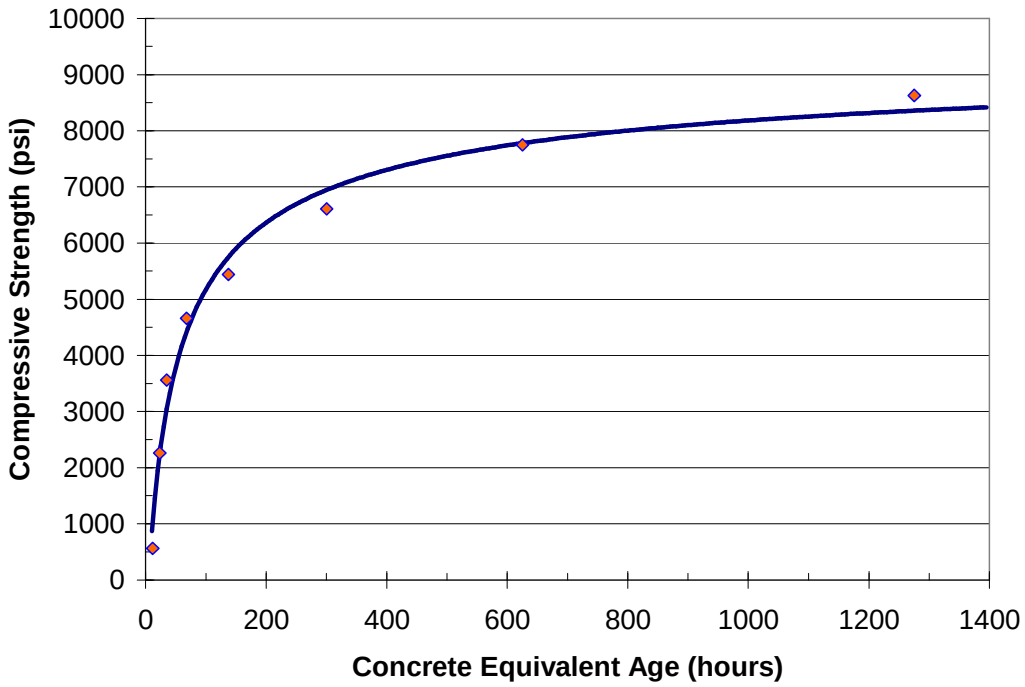

Figure D.9: Strength-maturity curve for LA-50FA-24%

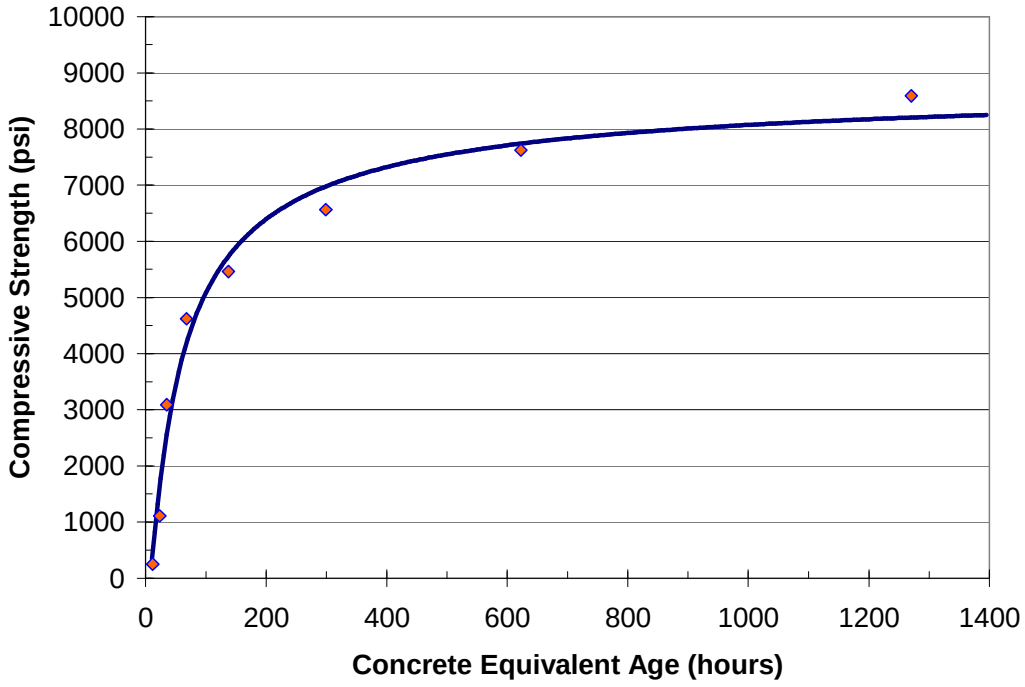

Figure D.10: Strength-maturity curve for LA-50FA-28%

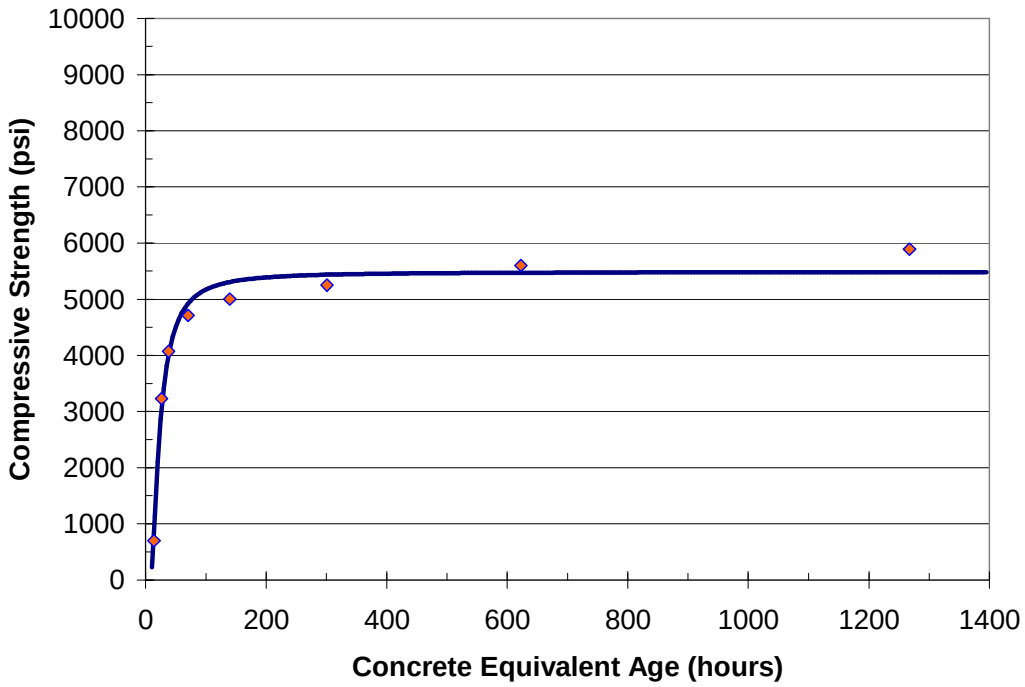

Figure D.11: Strength-maturity curve for CTRL42-HA

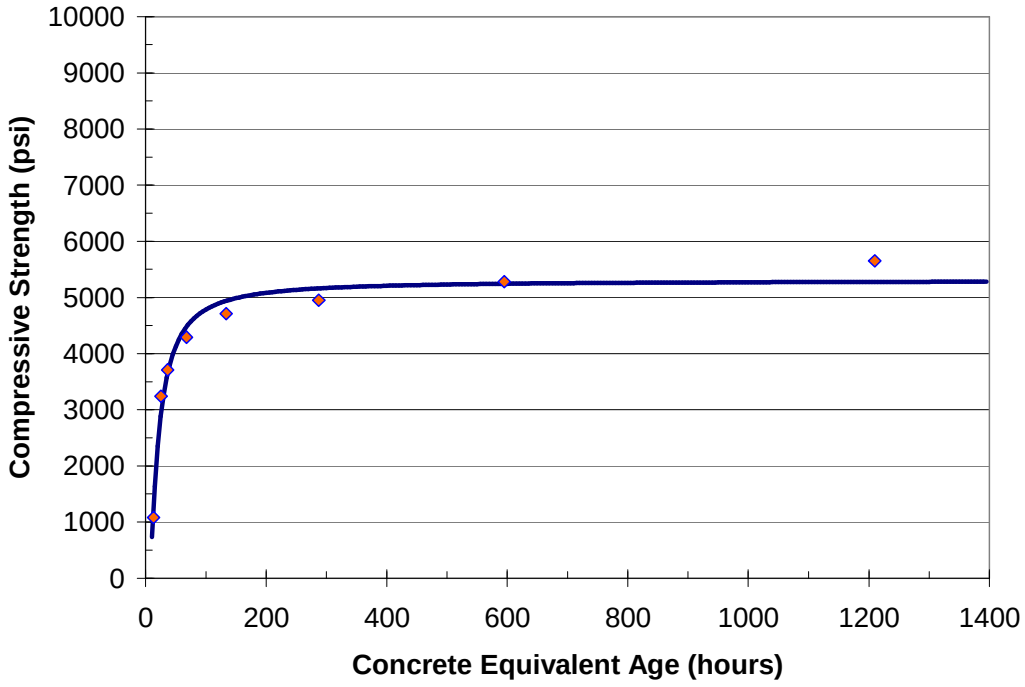

Figure D.12: Strength-maturity curve for CTRL44-HA

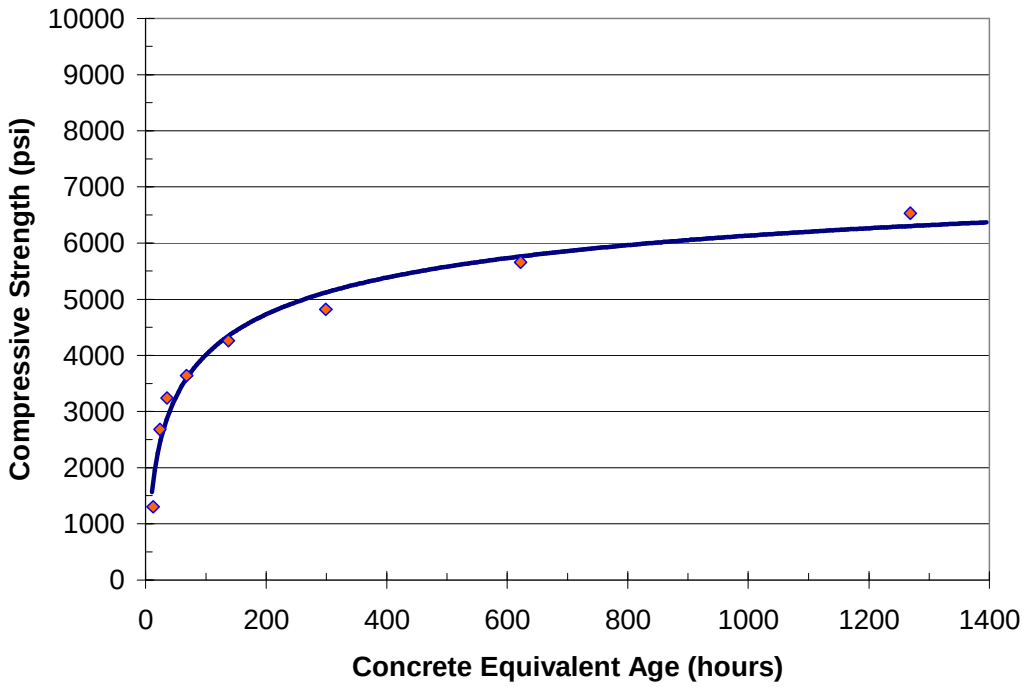

Figure D.13: Strength-maturity curve for HA-35FA-1%

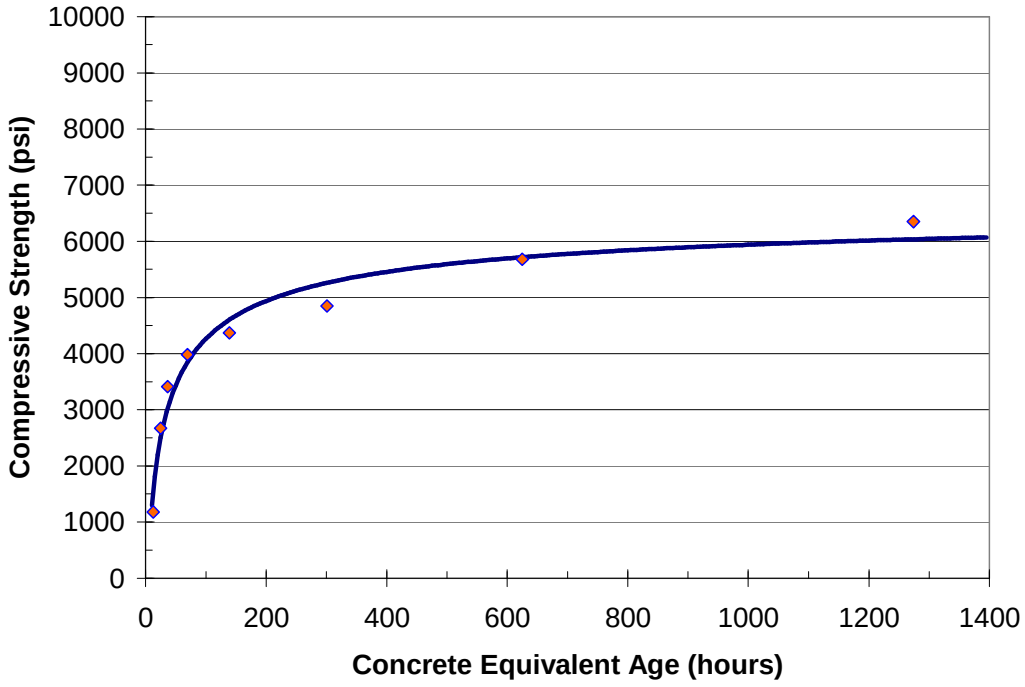

Figure D.14: Strength-maturity curve for HA-35FA-15%

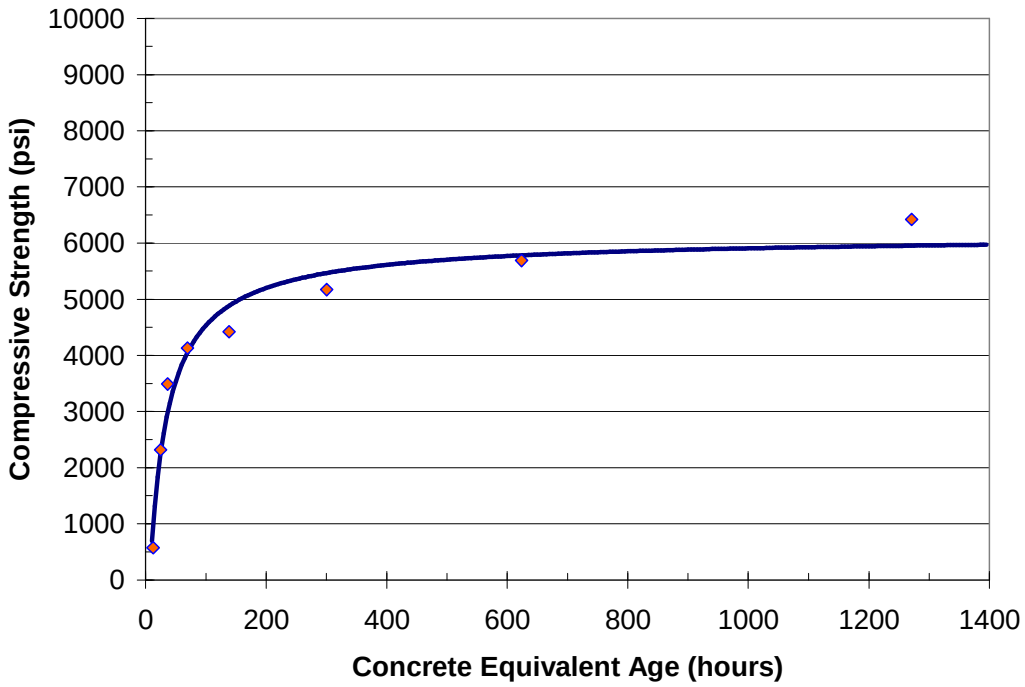

Figure D.15: Strength-maturity curve for HA-35FA-24%

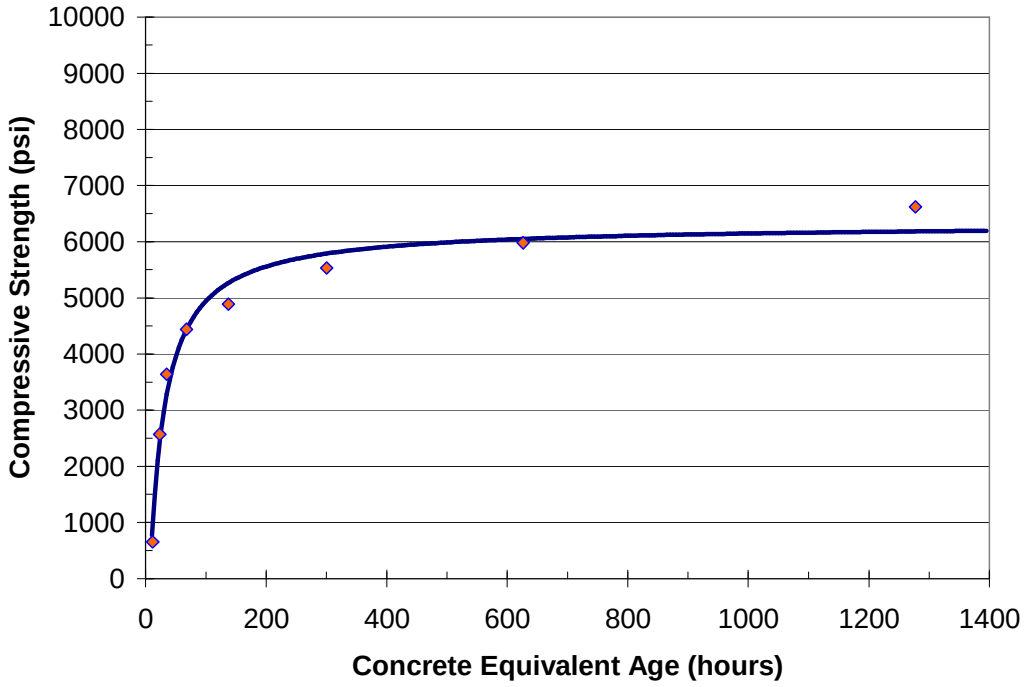

Figure D.16: Strength-maturity curve for HA-35FA-28%

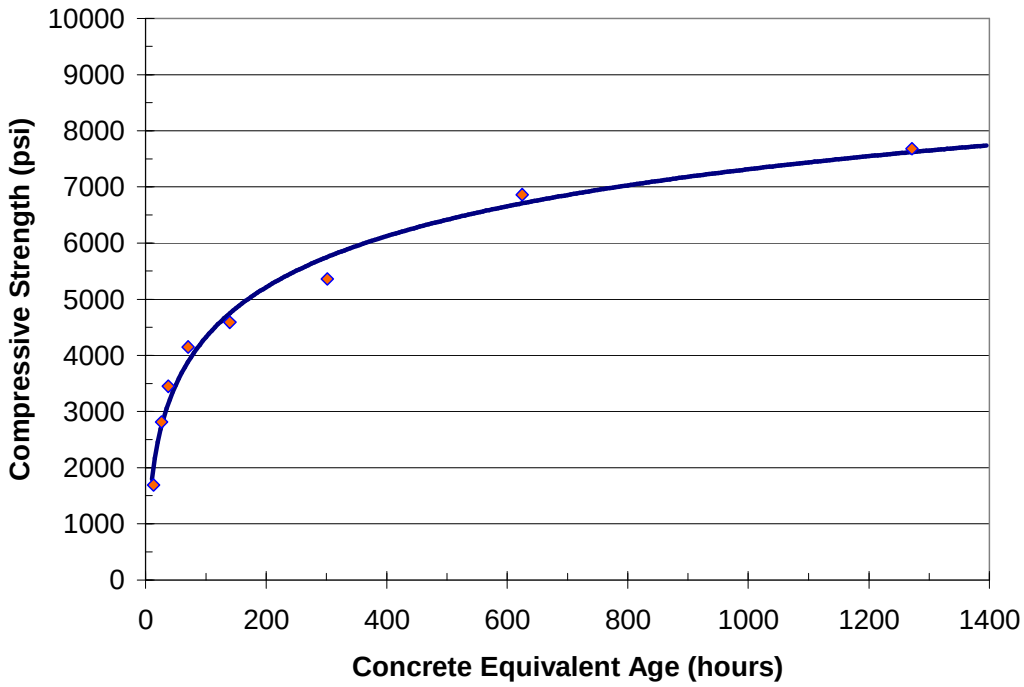

Figure D.17: Strength-maturity curve for HA-50FA-1%

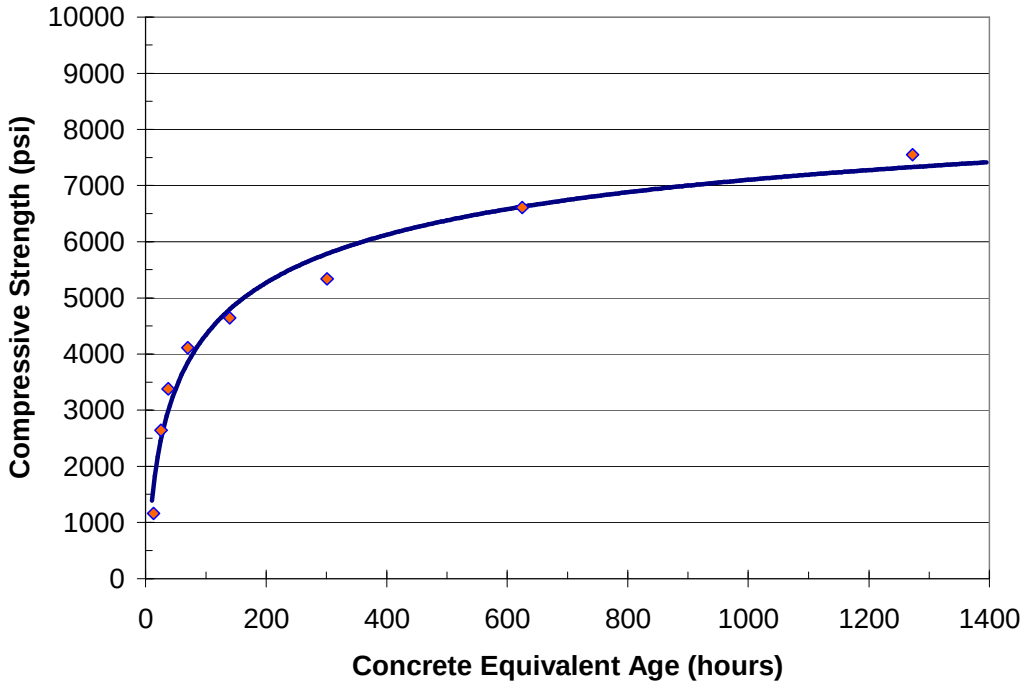

Figure D.18: Strength-maturity curve for HA-50FA-15%

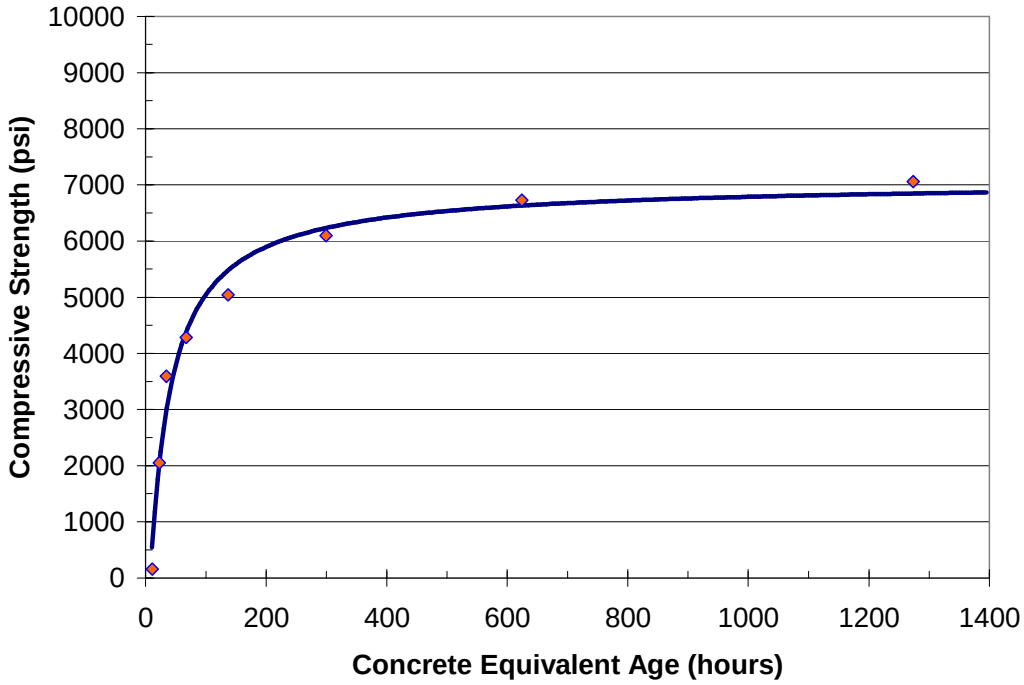

Figure D.19: Strength-maturity curve for HA-50FA-24%

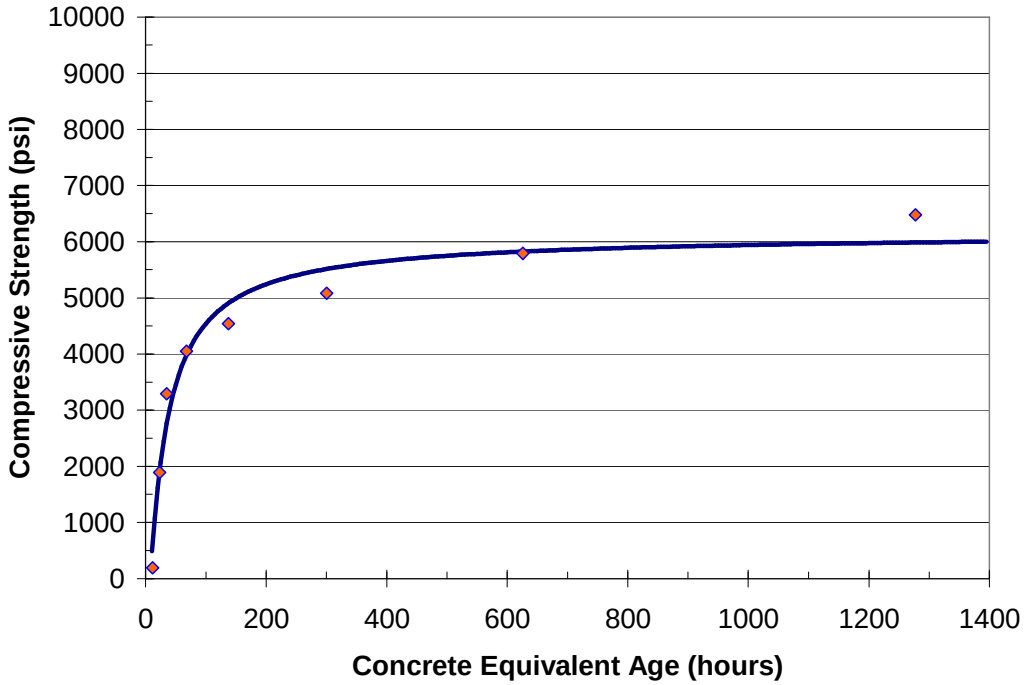

Figure D.20: Strength-maturity curve for HA-50FA-28%

Appendix E

SAS Inputs and Outputs from Degree of Hydration Modeling

Portland Cement Hydration Study

1. ANOVA Analysis for Hydration Parameters β and τ (R^2 Procedure)

a. SAS Program:

```
data temp; set Cementrsq;

lc3s=log(c3s); lc3a=log(c3a); lcao=log(cao); lc2s=log(c2s);
lc4af=log(c4af); lso3=log(so3); lmgo=log(mgo); lnaequ=log(naequ);
lblaine=log(blaine);
lbeta=log(beta);
ltau=log(tau);

i1=c3s*c3a; i2=c3s*blaine; i3=c3s*so3; i4= c3s*naequ; i5=c3a*blaine;
i6=c3a*so3; i7=c3a*naequ; i8=blaine*so3; i9=blaine*naequ; i10=c2s*c4af;
i11=c2s*so3; i12=c2s*naequ; i13=c4af*so3; i14=so3*mgo; i15=so3*naequ;
i16=mgo*naequ;
run;

proc rsquare c;
model lbeta ltau = lc3s lc3a lcao lc2s lc4af lso3 lmgo lnaequ lblaine
/select=10 stop=10;
run;
```

b. Analysis Results:

R^2 Procedure Correlation Matrix:

Variable	lc3s	lc3a	lcao	lc2s	lc4af	lso3
lc3s	1.0000	-0.5862	0.1676	-0.8954	0.2312	-0.7539
lc3a	-0.5862	1.0000	-0.4553	0.4469	-0.8107	0.6992
lcao	0.1676	-0.4553	1.0000	0.0332	0.3396	-0.3764
lc2s	-0.8954	0.4469	0.0332	1.0000	-0.3395	0.3975
lc4af	0.2312	-0.8107	0.3396	-0.3395	1.0000	-0.1509
lso3	-0.7539	0.6992	-0.3764	0.3975	-0.1509	1.0000
lmgo	-0.8607	0.7243	-0.3047	0.9103	-0.6341	0.5003
lnaequ	-0.6178	0.7909	-0.5448	0.2497	-0.3021	0.9618
lblaine	-0.3072	-0.5160	0.0505	0.4138	0.5384	-0.1494
lbeta	-0.9364	0.7369	-0.4805	0.7472	-0.3556	0.8509
ltau	0.9428	-0.4111	0.2981	-0.8589	0.0995	-0.6343

Variable	lmgo	lnaequ	lblaine	lbeta	ltau
lc3s	-0.8607	-0.6178	-0.3072	-0.9364	0.9428
lc3a	0.7243	0.7909	-0.5160	0.7369	-0.4111
lcao	-0.3047	-0.5448	0.0505	-0.4805	0.2981
lc2s	0.9103	0.2497	0.4138	0.7472	-0.8589
lc4af	-0.6341	-0.3021	0.5384	-0.3556	0.0995
lso3	0.5003	0.9618	-0.1494	0.8509	-0.6343
lmgo	1.0000	0.4585	0.1584	0.8500	-0.8149
lnaequ	0.4585	1.0000	-0.3303	0.7984	-0.4992
lblaine	0.1584	-0.3303	1.0000	0.1484	-0.5412
lbeta	0.8500	0.7984	0.1484	1.0000	-0.9007
ltau	-0.8149	-0.4992	-0.5412	-0.9007	1.0000

R^2 Selection Method (β):

Number in Model	R-Square	Variables in Model
1	0.8768	lc3s
1	0.7241	lso3
1	0.7225	lmgo
1	0.6374	lnaequ
1	0.5583	lc2s
1	0.5430	lc3a
1	0.2309	lcao
1	0.1264	lc4af
1	0.0220	lblaine
2	0.9846	lc3s lcao
2	0.9642	lso3 lmgo
2	0.9576	lc2s lnaequ
2	0.9550	lc3s lnaequ
2	0.9339	lmgo lnaequ
2	0.9306	lc3s lc3a
2	0.9255	lc3s lso3
2	0.9239	lc3a lblaine
2	0.9227	lc2s lso3
2	0.9188	lc3s lc2s
3	0.9986	lc4af lso3 lblaine
3	0.9986	lc3a lso3 lblaine
3	0.9985	lc3a lmgo lnaequ
3	0.9985	lc3a lc4af lblaine
3	0.9985	lcao lc2s lso3
3	0.9982	lmgo lnaequ lblaine
3	0.9978	lc3a lc4af lso3
3	0.9973	lc3s lcao lnaequ
3	0.9969	lc3s lcao lblaine
3	0.9949	lc3s lcao lso3
4	0.9987	lc3s lc2s lc4af lnaequ
4	0.9987	lc3s lc3a lc2s lnaequ
4	0.9987	lc3s lc3a lc2s lso3

4	0.9987	lc3s lc2s lc4af lso3
4	0.9987	lc3s lc3a lc2s lc4af
4	0.9987	lc3s lso3 lmgo lnaequ
4	0.9987	lc3s lc2s lso3 lnaequ
4	0.9987	lc3s lc2s lso3 lmgo
4	0.9987	lc3s lc2s lmgo lnaequ
4	0.9987	lc3s lc2s lc4af lblaine

R^2 Selection Method (τ):

Number in Model	R-Square	Variables in Model
1	0.8888	lc3s
1	0.7376	lc2s
1	0.6640	lmgo
1	0.4024	lso3
1	0.2929	lblaine
1	0.2492	lnaequ
1	0.1690	lc3a
1	0.0889	lcao
1	0.0099	lc4af
2	0.9587	lc3s lblaine
2	0.9553	lc4af lmgo
2	0.9424	lc3a lblaine
2	0.9193	lc3s lc3a
2	0.9090	lc3s lcao
2	0.9036	lc3s lc4af
2	0.9023	lc3s lso3
2	0.9000	lc3s lnaequ
2	0.8899	lc3s lc2s
2	0.8888	lc3s lmgo
3	0.9884	lso3 lmgo lblaine
3	0.9882	lc3s lcao lblaine
3	0.9881	lc3a lmgo lnaequ
3	0.9865	lc2s lc4af lmgo
3	0.9846	lc2s lnaequ lblaine
3	0.9818	lcao lc4af lmgo
3	0.9808	lc3s lc3a lblaine
3	0.9803	lc3a lc4af lblaine
3	0.9800	lc3s lc3a lcao
3	0.9799	lc3a lso3 lblaine
4	0.9884	lc3s lc2s lc4af lnaequ
4	0.9884	lc3s lc3a lc2s lnaequ
4	0.9884	lc3s lc2s lc4af lso3
4	0.9884	lc3s lc3a lc2s lc4af
4	0.9884	lc3s lc2s lmgo lnaequ
4	0.9884	lc3s lc4af lso3 lnaequ
4	0.9884	lc3s lc3a lc4af lnaequ
4	0.9884	lc3s lcao lc2s lnaequ
4	0.9884	lc3s lcao lmgo lnaequ
4	0.9884	lc3s lc3a lc4af lmgo

HVFA Concrete Hydration Model

1. ANOVA Analysis for Hydration Parameters β and τ (R^2 Procedure)

a. SAS Program

data temp; set Hvfarsq;

lc3s=log(c3s); lc3a=log(c3a); lcao=log(cao); lc2s=log(c2s); lc4af=log(c4af);
lso3=log(so3); lmgo=log(mgo); lnaequ=log(naequ); lblaine=log(blaine);

lbeta=log(beta);
ltau=log(tau);

i1=c3s*c3a; i2=c3s*blaine; i3=c3s*so3; i4= c3s*naequ; i5=c3a*blaine;
i6=c3a*so3; i7=c3a*naequ; i8=blaine*so3; i9=blaine*naequ; i10=c2s*c4af;
i11=c2s*so3; i12=c2s*naequ; i13=c4af*so3; i14=so3*mgo; i15=so3*naequ;
i16=mgo*naequ; i17=pfa*FACaO; i18=pfa*FASiO2; i19=pfa*FANaEqu;
i20=pfa*FACaO*FASiO2; i21=pfa*FACaO*FASiO2*FANaEqu; i22=FACaO*naequ;
run;

proc rsquare c;
model lbeta ltau = lc3s lc3a lcao lc2s lc4af lso3 lmgo lnaequ lblaine pfa i17-i22
/select=**10** stop=**10**;
run;

b. Analysis Results

R^2 Procedure Correlation Matrix:

Variable	lc3s	lc3a	lcao	lc2s	lc4af
lc3s	1.0000	-0.7790	0.4490	-0.9084	0.6162
lc3a	-0.7790	1.0000	-0.5020	0.5657	-0.9108
lcao	0.4490	-0.5020	1.0000	-0.2836	0.5565
lc2s	-0.9084	0.5657	-0.2836	1.0000	-0.5121
lc4af	0.6162	-0.9108	0.5565	-0.5121	1.0000
lso3	-0.8353	0.9124	-0.4217	0.5513	-0.6662
lmgo	-0.7994	0.6860	-0.7202	0.7270	-0.7126
lnaequ	-0.7932	0.9505	-0.5326	0.5041	-0.7548
lblaine	0.2080	-0.6273	-0.1996	-0.0601	0.5268
pFA	-0.2740	0.0662	-0.0896	0.2742	-0.0129
i17	-0.1851	0.0452	-0.0452	0.1856	-0.0059
i18	-0.2534	0.0609	-0.0915	0.2534	-0.0136
i19	-0.2818	0.0588	-0.3565	0.2767	-0.0620
i20	-0.1982	0.0491	-0.0290	0.1990	-0.0028
i21	-0.2101	0.0453	-0.2239	0.2071	-0.0385
i22	-0.3214	0.3032	-0.0608	0.2342	-0.2085
lbeta	-0.8010	0.7552	-0.8002	0.6140	-0.6802
ltau	0.2905	-0.1802	0.6402	-0.2294	0.2273

Variable	lso3	lmgo	lnaequ	lblaine	pFA
lc3s	-0.8353	-0.7994	-0.7932	0.2080	-0.2740
lc3a	0.9124	0.6860	0.9505	-0.6273	0.0662
lcao	-0.4217	-0.7202	-0.5326	-0.1996	-0.0896
lc2s	0.5513	0.7270	0.5041	-0.0601	0.2742
lc4af	-0.6662	-0.7126	-0.7548	0.5268	-0.0129
lso3	1.0000	0.6002	0.9815	-0.5462	0.1363
lmgo	0.6002	1.0000	0.6163	0.1097	0.3044
lnaequ	0.9815	0.6163	1.0000	-0.5706	0.0825
lblaine	-0.5462	0.1097	-0.5706	1.0000	0.2170
pFA	0.1363	0.3044	0.0825	0.2170	1.0000
i17	0.0946	0.1980	0.0560	0.1358	0.6846
i18	0.1246	0.2858	0.0761	0.2067	0.9195
i19	0.0968	0.4460	0.0800	0.4098	0.8720
i20	0.1044	0.2022	0.0603	0.1317	0.7443
i21	0.0791	0.3114	0.0604	0.2759	0.6749
i22	0.3485	0.2644	0.3109	-0.1444	0.5361
lbeta	0.7487	0.8774	0.7796	-0.0332	0.0676
ltau	-0.1615	-0.5428	-0.2042	-0.3925	0.2491

Variable	i17	i18	i19	i20	i21
lc3s	-0.1851	-0.2534	-0.2818	-0.1982	-0.2101
lc3a	0.0452	0.0609	0.0588	0.0491	0.0453
lcao	-0.0452	-0.0915	-0.3565	-0.0290	-0.2239
lc2s	0.1856	0.2534	0.2767	0.1990	0.2071
lc4af	-0.0059	-0.0136	-0.0620	-0.0028	-0.0385
lso3	0.0946	0.1246	0.0968	0.1044	0.0791
lmgo	0.1980	0.2858	0.4460	0.2022	0.3114
lnaequ	0.0560	0.0761	0.0800	0.0603	0.0604
lblaine	0.1358	0.2067	0.4098	0.1317	0.2759
pFA	0.6846	0.9195	0.8720	0.7443	0.6749
i17	1.0000	0.3523	0.6107	0.9658	0.9533
i18	0.3523	1.0000	0.7700	0.4684	0.3703
i19	0.6107	0.7700	1.0000	0.6002	0.7038
i20	0.9658	0.4684	0.6002	1.0000	0.9390
i21	0.9533	0.3703	0.7038	0.9390	1.0000
i22	0.8706	0.2284	0.4610	0.8310	0.8105
lbeta	0.1061	0.0312	0.2438	0.0873	0.2273
ltau	0.4607	0.0645	-0.0019	0.4379	0.2700

Variable	i22	lbeta	ltau
lc3s	-0.3214	-0.8010	0.2905
lc3a	0.3032	0.7552	-0.1802
lcao	-0.0608	-0.8002	0.6402
lc2s	0.2342	0.6140	-0.2294
lc4af	-0.2085	-0.6802	0.2273
lso3	0.3485	0.7487	-0.1615
lmgo	0.2644	0.8774	-0.5428
lnaequ	0.3109	0.7796	-0.2042
lblaine	-0.1444	-0.0332	-0.3925
pFA	0.5361	0.0676	0.2491
i17	0.8706	0.1061	0.4607

i18	0.2284	0.0312	0.0645
i19	0.4610	0.2438	-0.0019
i20	0.8310	0.0873	0.4379
i21	0.8105	0.2273	0.2700
i22	1.0000	0.2388	0.3714
lbeta	0.2388	1.0000	-0.5942
ltau	0.3714	-0.5942	1.0000

R^2 Selection Method (β):

Number in Model	R-Square	Variables in Model
1	0.7698	lmgo
1	0.6416	lc3s
1	0.6404	lcao
1	0.6078	lnaequ
1	0.5704	lc3a
1	0.5605	lso3
1	0.4626	lc4af
1	0.3770	lc2s
1	0.0594	i19
1	0.0570	i22
2	0.8905	lc3a lblaine
2	0.8848	lc3s lcao
2	0.8618	lmgo lnaequ
2	0.8591	lnaequ lblaine
2	0.8469	lso3 lmgo
2	0.8461	lcao lso3
2	0.8287	lcao lmgo
2	0.8223	lmgo i18
2	0.8148	lcao lnaequ
2	0.8143	lc3a lmgo
3	0.9319	lc3a lblaine i18
3	0.9232	lc3a lblaine pFA
3	0.9140	lc3a lblaine i19
3	0.9134	lc4af lnaequ lblaine
3	0.9130	lc3a lmgo lblaine
3	0.9120	lc3s lcao i18
3	0.9100	lc3a lnaequ lblaine
3	0.9084	lcao lso3 lmgo
3	0.9067	lc3a lc4af lso3
3	0.9040	lc3s lcao pFA
4	0.9530	lc3a lnaequ lblaine i18
4	0.9523	lc3a lc4af lso3 i18
4	0.9508	lmgo lnaequ lblaine i18
4	0.9496	lc4af lso3 lblaine i18
4	0.9493	lc3a lso3 lblaine i18
4	0.9491	lc3a lc4af lblaine i18
4	0.9485	lc4af lnaequ lblaine i18
4	0.9477	lc3a lmgo lblaine i18

4	0.9444	lc3a lmgo lnaequ i18
4	0.9443	lc3a lnaequ lblaine pFA
5	0.9557	lc3a lnaequ lblaine pFA i21
5	0.9556	lc3a lc4af lso3 pFA i21
5	0.9548	lmgo lnaequ lblaine pFA i21
5	0.9537	lc4af lso3 lblaine pFA i21
5	0.9537	lc3a lnaequ lblaine i18 i21
5	0.9535	lc3a lnaequ lblaine pFA i17
5	0.9535	lc3a lc2s lnaequ lblaine i18
5	0.9534	lc3a lso3 lblaine pFA i21
5	0.9534	lc3s lc3a lnaequ lblaine i18
5	0.9533	lc3a lnaequ lblaine i18 i20
6	0.9620	lc3a lc4af lso3 i19 i20 i21
6	0.9618	lmgo lnaequ lblaine i19 i20 i21
6	0.9615	lc3a lnaequ lblaine i19 i20 i21
6	0.9610	lc4af lso3 lblaine i19 i20 i21
6	0.9609	lc3a lso3 lblaine i19 i20 i21
6	0.9607	lc3a lc4af lblaine i19 i20 i21
6	0.9595	lc3a lmgo lnaequ i19 i20 i21
6	0.9566	lc3a lc4af lso3 i17 i18 i21
6	0.9565	lc3a lc4af lso3 pFA i20 i21
6	0.9565	lc3s lc3a lnaequ lblaine pFA i21
7	0.9742	lc3a lc4af lso3 pFA i19 i20 i21
7	0.9740	lmgo lnaequ lblaine pFA i19 i20 i21
7	0.9734	lc4af lso3 lblaine pFA i19 i20 i21
7	0.9733	lc3a lnaequ lblaine pFA i19 i20 i21
7	0.9732	lc3a lso3 lblaine pFA i19 i20 i21
7	0.9731	lc3a lc4af lblaine pFA i19 i20 i21
7	0.9723	lc3a lmgo lnaequ pFA i19 i20 i21
7	0.9667	lc4af lnaequ lblaine pFA i19 i20 i21
7	0.9662	lmgo lnaequ lblaine i18 i19 i20 i21
7	0.9661	lc3a lc4af lso3 i18 i19 i20 i21

R^2 Selection Method (τ):

Number in Model	R-Square	Variables in Model
1	0.4099	lcao
1	0.2947	lmgo
1	0.2123	i17
1	0.1917	i20
1	0.1541	lblaine
1	0.1380	i22
1	0.0844	lc3s
1	0.0729	i21
1	0.0621	pFA
1	0.0526	lc2s
2	0.6502	lcao i17
2	0.6307	lmgo i17
2	0.6185	lcao i20

2	0.6073	lmgo i20
2	0.5897	lcao i21
2	0.5798	lmgo i22
2	0.5789	lcao i22
2	0.5265	i17 i21
2	0.5081	lmgo i21
2	0.5046	lcao pFA
3	0.8388	lc3a lblaine i17
3	0.8092	lc3a lblaine i20
3	0.8011	lnaequ lblaine i17
3	0.7952	lmgo lblaine i17
3	0.7886	lc3a lblaine i21
3	0.7724	lnaequ lblaine i20
3	0.7676	lmgo lblaine i20
3	0.7634	lcao lblaine i17
3	0.7518	lc4af lmgo i17
3	0.7465	lc3a lmgo i17
4	0.8720	lc3a lblaine i17 i22
4	0.8699	lc3a lblaine pFA i18
4	0.8545	lc3a lblaine pFA i17
4	0.8510	lc3a lblaine i17 i19
4	0.8510	lc3a lblaine i17 i18
4	0.8473	lc3a lc2s lblaine i17
4	0.8468	lc4af lnaequ lblaine i17
4	0.8464	lc3a lblaine i17 i21
4	0.8461	lc3a lcao lblaine i17
4	0.8454	lc3a lmgo lblaine i17
5	0.8980	lc3a lblaine pFA i18 i22
5	0.8840	lc3a lcao lblaine i17 i22
5	0.8818	lc4af lnaequ lblaine i17 i22
5	0.8814	lc3a lblaine pFA i17 i22
5	0.8811	lc3a lblaine i17 i19 i22
5	0.8807	lcao lmgo lblaine i17 i22
5	0.8804	lc3a lc4af lso3 i17 i22
5	0.8787	lc3a lblaine i17 i18 i22
5	0.8782	lc3a lblaine i17 i21 i22
5	0.8778	lc3a lmgo lblaine i17 i22
6	0.9088	lc3a lblaine pFA i17 i18 i20
6	0.9053	lc3a lcao lblaine pFA i18 i22
6	0.9050	lc3a lblaine pFA i18 i19 i22
6	0.9050	lc4af lnaequ lblaine pFA i18 i22
6	0.9039	lc3a lc4af lso3 pFA i18 i22
6	0.9035	lmgo pFA i17 i18 i20 i21
6	0.9032	lc3a lblaine pFA i18 i20 i22
6	0.9024	lc3a lmgo lblaine pFA i18 i22
6	0.9022	lc3a lc2s lblaine pFA i18 i22
6	0.9012	lc3s lc3a lblaine pFA i18 i22
7	0.9400	lc4af lmgo pFA i17 i18 i20 i21
7	0.9398	lc3a lblaine pFA i17 i18 i20 i22
7	0.9323	lc3a lblaine pFA i17 i18 i20 i21
7	0.9257	lso3 lblaine pFA i17 i18 i20 i21

7	0.9254	lc4af lmgo pFA i17 i18 i19 i20
7	0.9239	lc3a lblaine pFA i17 i18 i19 i20
7	0.9211	lmgo lblaine pFA i17 i18 i20 i21
7	0.9200	lnaequ lblaine pFA i17 i18 i20 i21
7	0.9146	lmgo lblaine pFA i17 i18 i20 i22
7	0.9135	lc3a lmgo pFA i17 i18 i20 i21

---

2. General Linear Model Development (GLM)

a. SAS Program

```
data temp; set Hvfarsq;

lc3s=log(c3s); lc3a=log(c3a); lcao=log(cao); lc2s=log(c2s); lc4af=log(c4af);
lso3=log(so3); lmgo=log(mgo); lnaequ=log(naequ); lblaine=log(blaine);

lbeta=log(beta);
ltau=log(tau);

i17=pfa*FACaO;
i18=pfa*FASiO2;
i19=pfa*FANaEqu;
i20=pfa*FACaO*FASiO2;
i21=pfa*FACaO*FASiO2*FANaEqu;
i22=FACaO*naequ;
run;

proc glm;
model lbeta = lc3a lnaequ lblaine i18 /solution ;
output out=plotit p=pred; run;
proc gplot; plot pred*lbeta; run;

proc glm;
model ltau = lc3a lso3 lblaine i17 /solution ;
output out=plotit p=pred; run;
proc gplot; plot pred*ltau; run;
```

b. Analysis Results

GLM Procedure (β):

Source	DF	Sum of Squares	Mean Square	F Value	Pr > F
Model	4	1.90582815	0.47645704	131.69	<.0001
Error	26	0.09406913	0.00361804		
Corrected Total	30	1.99989728			

R-Square	Coeff Var	Root MSE	lbeta Mean
0.952963	-185.1543	0.060150	-0.032487

Source	DF	Type I SS	Mean Square	F Value	Pr > F
lc3a	1	1.14073016	1.14073016	315.29	<.0001
lnaequ	1	0.07906253	0.07906253	21.85	<.0001
lblaine	1	0.60010151	0.60010151	165.86	<.0001

i18	1	0.08593395	0.08593395	23.75	<.0001
Source	**DF**	**Type III SS**	**Mean Square**	**F Value**	**Pr > F**
lc3a	1	0.11519995	0.11519995	31.84	<.0001
lnaequ	1	0.04211878	0.04211878	11.64	0.0021
lblaine	1	0.68462234	0.68462234	189.22	<.0001
i18	1	0.08593395	0.08593395	23.75	<.0001

Parameter	**Estimate**	**Standard Error**	**t Value**	**Pr > |t|**
Intercept	-23.08338907	1.98958971	-11.60	<.0001
lc3a	1.19189803	0.21122720	5.64	<.0001
lnaequ	0.50463744	0.14790351	3.41	0.0021
lblaine	4.79260161	0.34840364	13.76	<.0001
i18	-0.60393988	0.12392194	-4.87	<.0001

GLM Procedure (τ):

Source	**DF**	**Sum of Squares**	**Mean Square**	**F Value**	**Pr > F**
Model	4	2.63000419	0.65750105	36.08	<.0001
Error	26	0.47380825	0.01822339		
Corrected Total	30	3.10381244			

R-Square	**Coeff Var**	**Root MSE**	**ltau Mean**
0.847346	5.028101	0.134994	2.684792

Source	**DF**	**Type I SS**	**Mean Square**	**F Value**	**Pr > F**
lc3a	1	0.10083893	0.10083893	5.53	0.0265
lc2s	1	0.07412665	0.07412665	4.07	0.0541
lblaine	1	1.31503359	1.31503359	72.16	<.0001
i17	1	1.14000502	1.14000502	62.56	<.0001

Source	**DF**	**Type III SS**	**Mean Square**	**F Value**	**Pr > F**
lc3a	1	0.90939071	0.90939071	49.90	<.0001
lc2s	1	0.02661075	0.02661075	1.46	0.2378
lblaine	1	1.65067838	1.65067838	90.58	<.0001
i17	1	1.14000502	1.14000502	62.56	<.0001

Parameter	**Estimate**	**Standard Error**	**t Value**	**Pr > |t|**
Intercept	46.50442062	4.81598314	9.66	<.0001
lc3a	-1.71518213	0.24280053	-7.06	<.0001
lc2s	0.32551092	0.26937152	1.21	0.2378
lblaine	-7.99463782	0.84000563	-9.52	<.0001
i17	4.30711730	0.54456278	7.91	<.0001

3. Final Non-Linear Model Development for β, τ and α_u (NLIN Procedure)

a. SAS Program

data temp; set Hvfadb;
proc print; **run**;
proc nlin;

```
parms      f1=0.50
           c1=1.19 c2=0.505 c3=4.79 c4=-0.604 c5=-23.1
           e1=-1.72 e2=0.33 e3=-8.00 e4=4.31 e5=46.50;

beta1 =c3a**c1*naequ**c2*blaine**c3*exp(pFA*FASiO2*c4+c5);
tau1 =c3a**e1*c2s**e2*blaine**e3*exp(pFA*FACaO*e4+e5);
amax1=1.031*wcm/(0.194+wcm);

model alpha =exp(-((tau1/time)**beta1))*(amax1+f1*pFA);
output out=good p=predict r=resid stdr=eresid;
proc gplot; plot alpha*predict resid*predict resid*alpha; run;
```

b. Analysis Results

NLIN Procedure Iterative Phase

Iter	f1	c1	c2	c3	c4	c5
0	0.500	1.190	0.505	4.790	-0.604	-23.100
1	0.4010	0.6831	0.0711	2.4417	-1.3744	-12.3040
2	0.4265	0.7059	0.0891	2.7145	-1.3692	-13.8205
3	0.4267	0.6678	0.0817	2.5330	-1.3632	-12.8668
4	0.4276	0.6713	0.0911	2.5534	-1.3675	-12.9839
5	0.4275	0.6693	0.0810	2.5447	-1.3664	-12.9370
6	0.4275	0.6697	0.0809	2.5460	-1.3668	-12.9444
7	0.4275	0.6695	0.0810	2.5456	-1.3667	-12.9421

Iter	e1	e2	e3	e4	e5
0	-1.720	0.330	-8.000	4.3100	46.5000
1	-1.4466	0.6141	-7.3451	5.7841	43.7200
2	-1.4149	0.5577	-7.2972	6.0582	43.4071
3	-1.4201	0.5566	-7.3158	6.1103	43.5016
4	-1.4209	0.5564	-7.3191	6.1195	43.5186
5	-1.4211	0.5564	-7.3193	6.1209	43.5194
6	-1.4211	0.5564	-7.3194	6.1212	43.5201
7	-1.4211	0.5564	-7.3194	6.1213	43.5201

Iter	Sum of Squares	
0	1.4065	
1	0.9107	
2	0.9007	
3	0.9003	
4	0.9003	
5	0.9003	
6	0.9003	
7	0.9003	**NOTE: Convergence criterion met.**

Estimation Summary	
R	8.604E-6
PPC(c2)	0.000085
RPC(c2)	0.000181
Object	1.191E-9
Objective	0.900327
Observations Read	321
Observations Used	321

Observations Missing 0

Source	DF	Sum of Squares	Mean Square	F Value	Approx Pr > F
Model	11	101.1	9.1922	3165.06	<.0001
Error	310	0.9003	0.00290		
Uncorrected Total	321	102.0			

Parameter	Estimate	Approx Std Error	Approximate	95% Confidence Limits
f1	0.4275	0.0203	0.3876	0.4675
c1	0.6695	0.4985	-0.3114	1.6505
c2	0.0810	0.3489	-0.6055	0.7675
c3	2.5456	0.7953	0.9806	4.1105
c4	-1.3667	0.3078	-1.9724	-0.7610
c5	-12.9421	4.5242	-21.8441	-4.0400
e1	-1.4211	0.1874	-1.7897	-1.0525
e2	0.5564	0.2111	0.1412	0.9717
e3	-7.3194	0.6784	-8.6543	-5.9845
e4	6.1213	0.4157	5.3033	6.9393
e5	43.5201	3.8902	35.8655	51.1746

Approximate Correlation Matrix

	f1	c1	c2	c3	c4	c5
f1	1.0000000	-0.0051867	-0.0043701	-0.0223570	-0.3648591	0.0198678
c1	-0.0051867	1.0000000	-0.9254605	0.3312047	-0.0715470	-0.4449762
c2	-0.0043701	-0.9254605	1.0000000	-0.0822852	-0.0249781	0.2343499
c3	-0.0223570	0.3312047	-0.0822852	1.0000000	-0.3123541	-0.9854486
c4	-0.3648591	-0.0715470	-0.0249781	-0.3123541	1.0000000	0.2886547
c5	0.0198678	-0.4449762	0.2343499	-0.9854486	0.2886547	1.0000000
e1	-0.0261261	0.0409441	0.0396890	0.1308485	-0.0270170	-0.1102611
e2	0.0347034	0.0483709	-0.0560490	-0.0091034	0.0253532	-0.0001285
e3	-0.0014404	0.0346074	0.0230575	0.2328682	-0.0288019	-0.2245138
e4	0.2175530	-0.0176976	0.0064837	-0.0405416	-0.0268276	0.0394675
e5	0.0034101	-0.0259972	-0.0253889	-0.2267540	0.0285916	0.2194395

	e1	e2	e3	e4	e5
f1	-0.0261261	0.0347034	-0.0014404	0.2175530	0.0034101
c1	0.0409441	0.0483709	0.0346074	-0.0176976	-0.0259972
c2	0.0396890	-0.0560490	0.0230575	0.0064837	-0.0253889
c3	0.1308485	-0.0091034	0.2328682	-0.0405416	-0.2267540
c4	-0.0270170	0.0253532	-0.0288019	-0.0268276	0.0285916
c5	-0.1102611	-0.0001285	-0.2245138	0.0394675	0.2194395
e1	1.0000000	-0.6647036	0.7144902	-0.0580861	-0.6976842
e2	-0.6647036	1.0000000	-0.4087685	-0.0909391	0.4550650
e3	0.7144902	-0.4087685	1.0000000	-0.1399219	-0.9966252
e4	-0.0580861	-0.0909391	-0.1399219	1.0000000	0.1233304
e5	-0.6976842	0.4550650	-0.9966252	0.1233304	1.0000000

4. Residual Plots for Explanatory Variables

The following figures present residual plots for all explanatory variables used in the final HVFA concrete degree of hydration model as presented in Chapter 5.

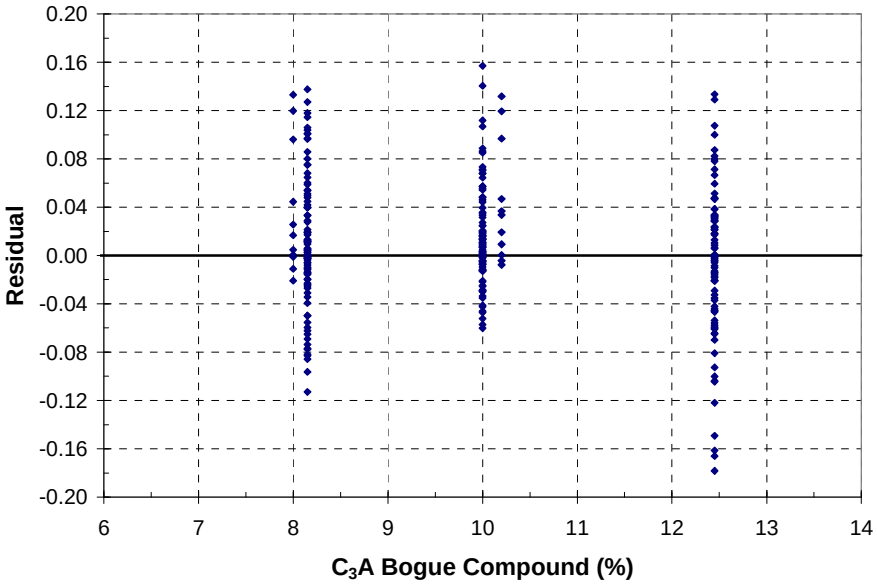

Figure E.1: Plot of residuals against C_3A content

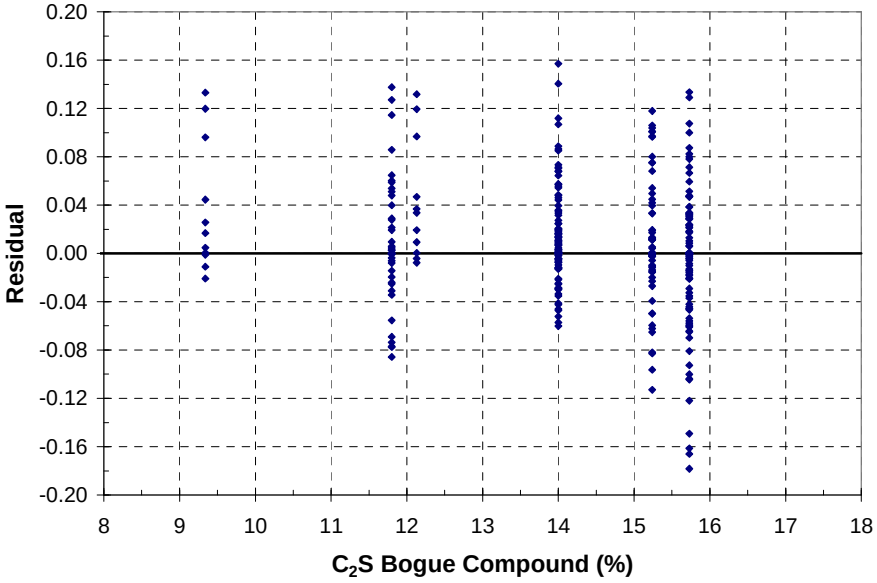

Figure E.2: Plot of residuals against C_2S content

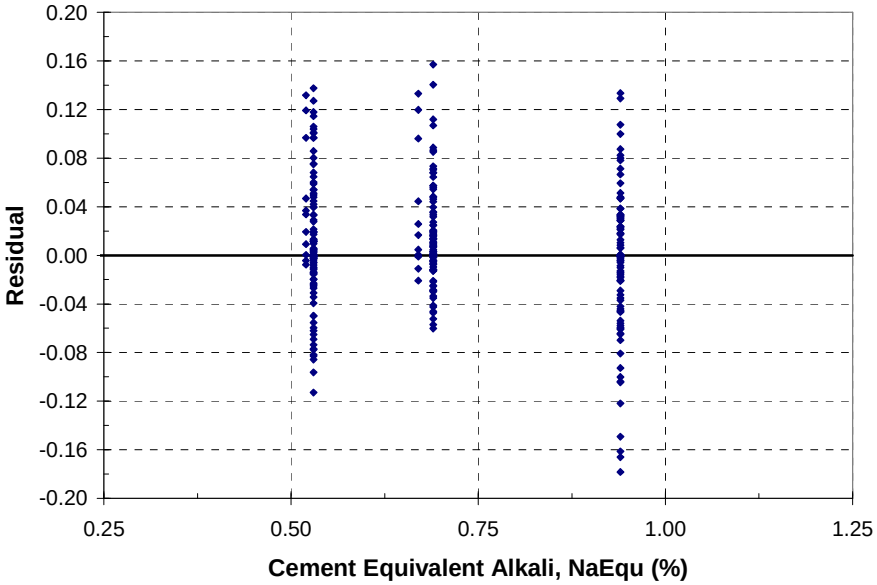

Figure E.3: Plot of residuals against cement equivalent alkali content

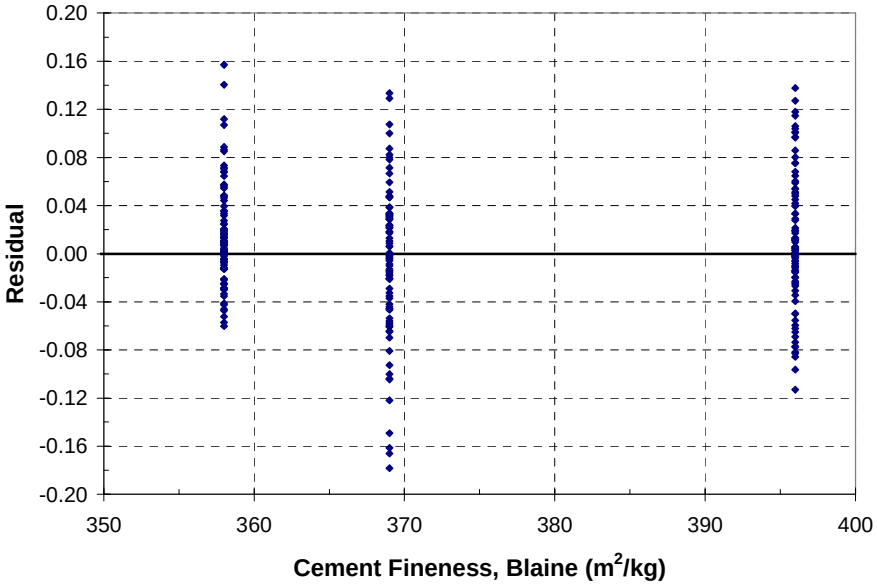

Figure E.4: Plot of residuals against cement fineness

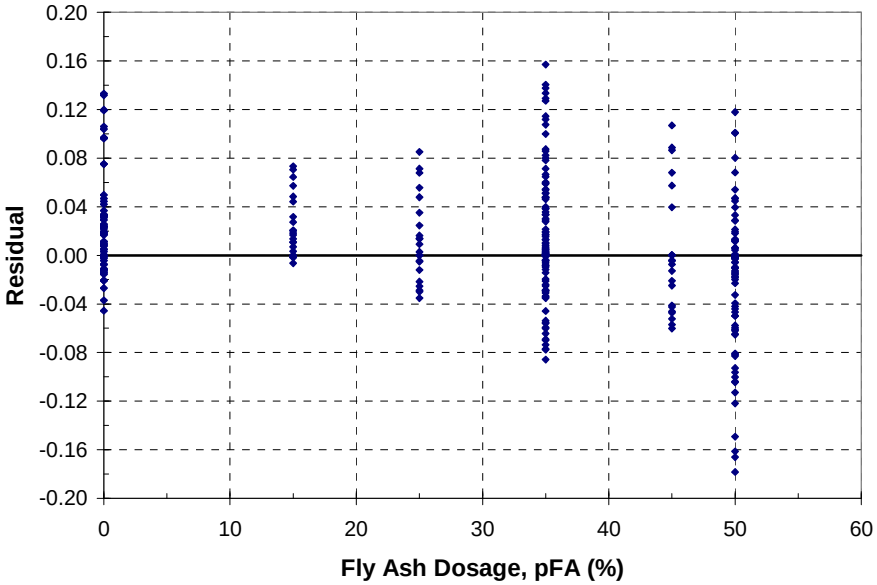

Figure E.5: Plot of residuals against fly ash dosage

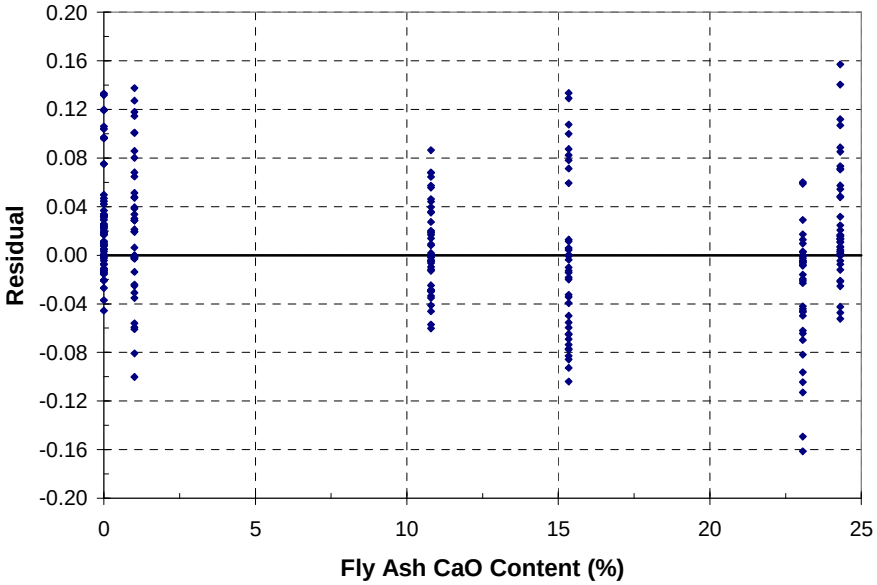

Figure E.6: Plot of residuals against fly ash CaO content

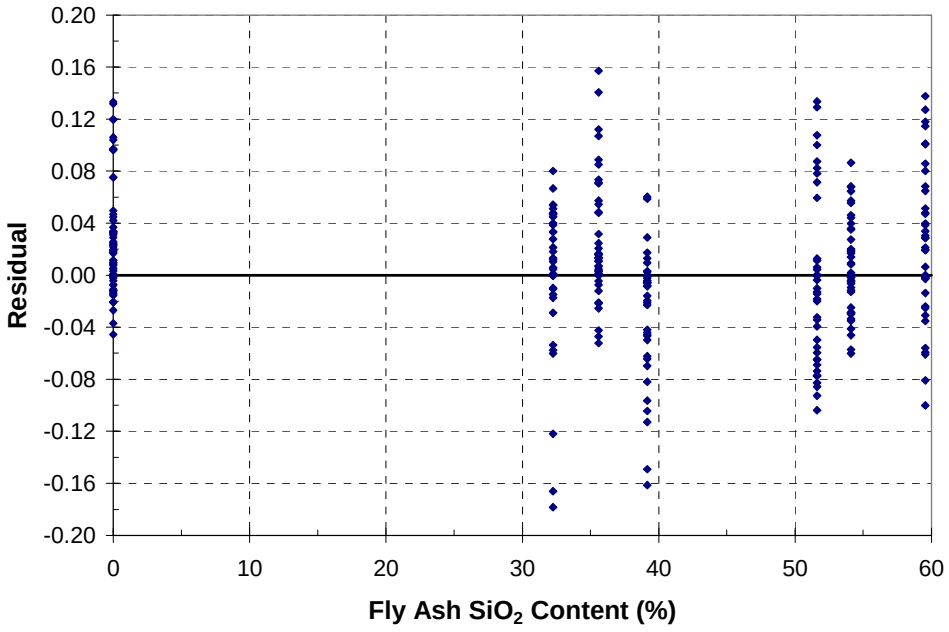

Figure E.7: Plot of residuals against fly ash SiO_2 content

Appendix F

Sample Results from ConcreteWorks Analysis

Appendix F contains sample results that were generated during the ConcreteWorks analysis detailed in Chapter 6. Sample in-place concrete temperature profile data are presented for selected mixtures when placed in the 6 ft x 6 ft column elements at 40 °F, 70 °F, and 95°F.

Table F.1: Sample in-place temperature profiles for CTRL44-LA

Time (hour)	40 °F		70 °F		95 °F	
	Edge (°C)	Center (°C)	Edge (°C)	Center (°C)	Edge (°C)	Center (°C)
0.083	5	4.89	22.05	21.89	35.3	35.22
4	6.6	4.9	26.59	24.68	49.31	51.12
8	7.11	6.44	34.25	42.37	56.16	74.75
12	9.67	12.03	37.15	58.54	53.19	80.59
16	12.57	21.04	36.7	65.3	48.24	82.09
20	16.01	31.1	38.54	67.44	50.05	82.04
24	18.4	38.95	37.58	67.5	49.89	81.02
28	19.62	43.34	37.18	66.47	50.14	79.29
32	18.34	45.19	34.62	64.84	48.39	77.16
36	17.13	45.54	32.36	62.93	45	74.87
40	16.27	44.99	30.72	60.87	41.67	72.57
44	16.67	43.84	33.08	58.7	44.45	70.29
48	17.12	42.29	32.51	56.45	44.93	68
52	17.02	40.49	32.5	54.2	45.8	65.7
56	15.17	38.63	30.26	52.04	44.61	63.48
60	13.63	36.8	28.22	50.06	41.7	61.44
64	12.47	35.03	26.57	48.22	38.42	59.61
68	12.88	33.28	28.69	46.46	41.46	57.93
72	12.4	31.53	28.29	44.73	42	56.31
76	12.25	29.81	28.37	43.05	43.21	54.71
80	11.03	28.16	26.36	41.49	42.4	53.2
84	9.72	26.64	24.53	40.08	39.63	51.85
88	7.9	25.21	23.41	38.79	36.57	50.69
92	7.39	23.83	26.08	37.56	39.93	49.65
96	7.71	22.46	26.18	36.34	40.53	48.64
100	9.73	21.44	27.08	35.44	41.47	47.87
104	10.87	20.55	27.65	34.68	41.93	47.2
108	11.38	19.71	27.82	33.98	41.85	46.58
112	11.62	18.92	27.85	33.36	41.57	46.01
116	11.77	18.21	28.16	32.82	41.76	45.52
120	12.15	17.59	28.52	32.34	42.47	45.09
124	12.33	17.04	28.53	31.93	42.41	44.72
128	12.34	16.56	28.38	31.57	42.4	44.39
132	12.27	16.14	28.11	31.26	42.08	44.11
136	12.18	15.78	27.86	30.99	41.62	43.86
140	12.11	15.47	28	30.76	41.76	43.66
144	12.34	15.2	28.24	30.55	42.43	43.48
148	12.38	14.96	28.15	30.36	42.33	43.31
152	12.27	14.75	27.95	30.18	42.29	43.17
156	12.15	14.55	27.67	30.02	41.94	43.04
160	12.03	14.38	27.42	29.87	41.48	42.92
164	11.92	14.23	27.54	29.73	41.59	42.82
168	12.07	14.09	27.81	29.6	42.27	42.73

Table F.2: Sample in-place temperature profiles for LA-35FA-1%

Time (hour)	40 °F		70 °F		95 °F	
	Edge (°C)	Center (°C)	Edge (°C)	Center (°C)	Edge (°C)	Center (°C)
0.083	5	4.89	22.06	21.89	35.31	35.22
4	7.17	5.5	28.16	27.28	47.24	49.02
8	9.21	10.11	32.4	40.5	51.53	64.56
12	11.38	17.03	33.35	50.39	49.74	71.38
16	12.82	24.05	33.13	56.05	45.82	74.36
20	14.74	29.78	35.82	58.83	48.38	75.42
24	16.1	33.72	35.5	59.76	48.56	75.26
28	16.92	36	35.51	59.57	49.13	74.27
32	15.66	37.1	33.23	58.72	47.56	72.79
36	14.67	37.42	31.19	57.53	44.23	71.08
40	14.07	37.17	29.72	56.14	40.96	69.3
44	14.79	36.47	32.31	54.57	43.95	67.48
48	15.49	35.44	31.87	52.86	44.47	65.59
52	15.6	34.2	31.96	51.08	45.42	63.64
56	13.95	32.9	29.76	49.35	44.28	61.72
60	12.56	31.64	27.78	47.74	41.37	59.95
64	11.54	30.4	26.18	46.23	38.1	58.35
68	12.08	29.14	28.41	44.77	41.28	56.87
72	11.69	27.84	28.04	43.29	41.83	55.43
76	11.62	26.52	28.16	41.83	43.08	53.98
80	10.46	25.26	26.15	40.45	42.29	52.59
84	9.21	24.07	24.33	39.22	39.49	51.36
88	7.45	22.95	23.24	38.08	36.42	50.3
92	7.01	21.85	26	36.97	39.9	49.35
96	7.38	20.72	26.11	35.86	40.49	48.41
100	9.27	19.87	27.01	35.03	41.46	47.69
104	10.35	19.11	27.59	34.33	41.95	47.06
108	10.84	18.39	27.78	33.69	41.88	46.47
112	11.08	17.72	27.82	33.12	41.6	45.94
116	11.25	17.12	28.15	32.63	41.82	45.48
120	11.65	16.59	28.54	32.2	42.56	45.08
124	11.86	16.14	28.57	31.83	42.51	44.74
128	11.9	15.74	28.44	31.51	42.52	44.44
132	11.85	15.4	28.18	31.24	42.2	44.18
136	11.78	15.11	27.95	31	41.75	43.96
140	11.75	14.87	28.11	30.8	41.91	43.77
144	12.01	14.65	28.38	30.62	42.61	43.61
148	12.07	14.47	28.31	30.46	42.52	43.47
152	11.99	14.3	28.12	30.31	42.5	43.34
156	11.89	14.15	27.85	30.18	42.15	43.23
160	11.79	14.03	27.6	30.05	41.68	43.13
164	11.71	13.92	27.74	29.94	41.81	43.05
168	11.89	13.81	28.04	29.83	42.52	42.97

Table F.3: Sample in-place temperature profiles for LA-50FA-1%

Time (hour)	40 °F		70 °F		95 °F	
	Edge (°C)	Center (°C)	Edge (°C)	Center (°C)	Edge (°C)	Center (°C)
0.083	5	4.89	22.06	21.89	35.31	35.22
4	7.49	5.89	28.59	28.15	47.12	49.31
8	9.35	10.61	31.63	39.58	50.14	62.1
12	10.96	16.62	32.01	47.68	48.18	67.97
16	11.93	22.34	31.68	52.47	44.41	70.71
20	13.64	26.91	34.53	54.92	47.22	71.76
24	14.87	30.05	34.34	55.8	47.5	71.67
28	15.69	31.91	34.47	55.66	48.22	70.79
32	14.48	32.86	32.27	54.96	46.75	69.45
36	13.57	33.19	30.31	53.96	43.45	67.91
40	13.04	33.06	28.92	52.77	40.22	66.32
44	13.91	32.54	31.64	51.42	43.34	64.69
48	14.67	31.72	31.26	49.91	43.87	62.98
52	14.86	30.71	31.41	48.33	44.88	61.2
56	13.29	29.64	29.23	46.8	43.79	59.46
60	11.96	28.62	27.29	45.39	40.88	57.85
64	10.99	27.61	25.73	44.07	37.62	56.41
68	11.62	26.57	28.03	42.78	40.92	55.08
72	11.24	25.48	27.68	41.46	41.46	53.77
76	11.2	24.35	27.82	40.13	42.74	52.44
80	10.08	23.26	25.83	38.89	41.97	51.17
84	8.86	22.25	24.02	37.78	39.18	50.04
88	7.13	21.28	22.95	36.77	36.11	49.09
92	6.73	20.32	25.78	35.77	39.68	48.24
96	7.12	19.32	25.89	34.74	40.26	47.38
100	8.88	18.54	26.69	33.98	41.15	46.72
104	9.88	17.86	27.22	33.33	41.59	46.14
108	10.34	17.21	27.38	32.75	41.49	45.6
112	10.55	16.6	27.41	32.23	41.2	45.11
116	10.71	16.07	27.75	31.79	41.42	44.7
120	11.12	15.6	28.13	31.41	42.17	44.34
124	11.33	15.2	28.17	31.09	42.12	44.03
128	11.37	14.85	28.04	30.81	42.13	43.77
132	11.33	14.56	27.79	30.57	41.82	43.54
136	11.27	14.31	27.56	30.37	41.37	43.35
140	11.25	14.1	27.73	30.2	41.54	43.19
144	11.52	13.92	28.01	30.05	42.26	43.06
148	11.59	13.77	27.94	29.91	42.17	42.94
152	11.52	13.63	27.76	29.78	42.15	42.83
156	11.43	13.51	27.5	29.67	41.82	42.74
160	11.34	13.41	27.26	29.56	41.35	42.66
164	11.27	13.32	27.41	29.47	41.49	42.59
168	11.47	13.24	27.71	29.38	42.21	42.53

Table F.4: Sample in-place temperature profiles for LA-35FA-24%

Time (hour)	40 °F		70 °F		95 °F	
	Edge (°C)	Center (°C)	Edge (°C)	Center (°C)	Edge (°C)	Center (°C)
0.083	5	4.89	22.06	21.89	35.3	35.22
4	6.6	4.9	25.09	23.01	43.57	42.72
8	6.39	5.57	29.2	32.22	53.23	65.38
12	7.49	8.25	33.14	46.59	54.12	79.69
16	9.11	12.96	35.48	59.36	50.46	85.52
20	12.1	19.24	39.3	66.92	52.53	87.59
24	14.93	26.28	39.29	70.28	52.48	87.75
28	17.2	33	39.3	71.21	52.55	86.72
32	17.12	38.5	36.87	70.8	50.63	84.97
36	16.93	42.42	34.62	69.67	47.2	82.85
40	16.84	44.79	32.91	68.08	43.77	80.56
44	17.73	45.83	35.14	66.16	46.37	78.17
48	18.5	45.86	34.42	64	46.85	75.69
52	18.6	45.18	34.31	61.7	47.58	73.15
56	16.8	44.09	32.01	59.4	46.25	70.65
60	15.28	42.79	29.86	57.2	43.3	68.29
64	14.11	41.35	28.1	55.09	39.91	66.13
68	14.48	39.77	30.13	53.05	42.82	64.12
72	13.96	38.06	29.64	51.02	43.35	62.17
76	13.79	36.28	29.67	49.03	44.52	60.25
80	12.5	34.52	27.59	47.15	43.59	58.43
84	11.11	32.81	25.69	45.42	40.74	56.77
88	9.18	31.18	24.49	43.83	37.61	55.32
92	8.62	29.56	27.1	42.3	40.91	54
96	8.87	27.95	27.14	40.8	41.51	52.73
100	11.68	26.74	28.58	39.69	42.88	51.77
104	13.26	25.67	29.46	38.76	43.6	50.95
108	14.04	24.65	29.79	37.89	43.64	50.17
112	14.45	23.69	29.92	37.11	43.44	49.45
116	14.73	22.84	30.3	36.42	43.68	48.82
120	15.21	22.08	30.72	35.82	44.44	48.27
124	15.47	21.43	30.76	35.29	44.4	47.79
128	15.55	20.86	30.64	34.84	44.4	47.37
132	15.53	20.38	30.39	34.44	44.09	47.01
136	15.48	19.97	30.15	34.11	43.63	46.69
140	15.45	19.63	30.3	33.81	43.77	46.42
144	15.71	19.33	30.55	33.56	44.45	46.19
148	15.78	19.07	30.47	33.33	44.35	45.98
152	15.7	18.84	30.27	33.11	44.31	45.79
156	15.59	18.65	29.99	32.92	43.96	45.62
160	15.49	18.47	29.73	32.75	43.47	45.47
164	15.4	18.32	29.85	32.59	43.58	45.34
168	15.56	18.19	30.12	32.44	44.26	45.23

Table F.5: Sample in-place temperature profiles for LA-50FA-24%

Time (hour)	40 °F		70 °F		95 °F	
	Edge (°C)	Center (°C)	Edge (°C)	Center (°C)	Edge (°C)	Center (°C)
0.083	5	4.89	22.06	21.89	35.31	35.22
4	6.61	4.9	24.83	22.75	41.71	40.34
8	6.39	5.6	27.81	29.88	50.27	58.34
12	7.35	8.1	31.13	41.52	52.58	74.36
16	8.74	12.3	33.7	53.62	50.32	83.38
20	11.5	17.76	38.31	62.76	53.12	87.61
24	14.15	23.85	39.05	68.13	53.43	89.07
28	16.34	29.88	39.57	70.65	53.6	88.87
32	16.32	35.24	37.45	71.4	51.71	87.66
36	16.29	39.56	35.38	71.1	48.32	85.89
40	16.41	42.64	33.77	70.11	44.89	83.83
44	17.52	44.47	36.02	68.61	47.42	81.57
48	18.49	45.23	35.29	66.73	47.9	79.15
52	18.74	45.18	35.17	64.6	48.57	76.6
56	17.07	44.61	32.88	62.4	47.17	74.06
60	15.63	43.73	30.7	60.24	44.22	71.62
64	14.52	42.62	28.9	58.13	40.78	69.36
68	14.94	41.29	30.89	56.04	43.61	67.24
72	14.44	39.76	30.35	53.94	44.12	65.16
76	14.29	38.11	30.36	51.86	45.28	63.11
80	13	36.42	28.27	49.87	44.28	61.15
84	11.61	34.77	26.34	48.03	41.4	59.36
88	9.66	33.15	25.1	46.32	38.24	57.78
92	9.1	31.53	27.67	44.68	41.5	56.33
96	9.33	29.89	27.68	43.05	42.09	54.94
100	12.48	28.64	29.43	41.86	43.73	53.89
104	14.26	27.54	30.49	40.84	44.59	52.98
108	15.15	26.48	30.92	39.9	44.72	52.13
112	15.65	25.49	31.12	39.05	44.57	51.34
116	16	24.61	31.55	38.3	44.85	50.65
120	16.53	23.84	32	37.65	45.64	50.05
124	16.84	23.18	32.08	37.09	45.62	49.52
128	16.97	22.62	31.98	36.6	45.64	49.06
132	16.99	22.14	31.75	36.19	45.34	48.67
136	16.98	21.75	31.52	35.83	44.89	48.33
140	16.98	21.42	31.69	35.53	45.03	48.04
144	17.27	21.14	31.96	35.26	45.73	47.79
148	17.37	20.9	31.88	35.03	45.63	47.56
152	17.31	20.7	31.69	34.81	45.59	47.37
156	17.23	20.52	31.42	34.62	45.24	47.19
160	17.15	20.37	31.16	34.45	44.76	47.03
164	17.08	20.25	31.29	34.29	44.87	46.9
168	17.26	20.13	31.57	34.14	45.55	46.78